

SYNTHESIS AND CHARACTERIZATION OF WATER SOLUBLE POLYMER
STABILIZED TRANSITION METAL(0) NANOCCLUSERS AS CATALYST IN
HYDROGEN GENERATION FROM THE HYDROLYSIS OF SODIUM
BOROHYDRIDE AND AMMONIA BORANE

A THESIS SUBMITTED TO
THE GRADUATE SCHOOL OF NATURAL AND APPLIED SCIENCES
OF
MIDDLE EAST TECHNICAL UNIVERSITY

BY

ÖNDER METİN

IN PARTIAL FULFILLMENT OF THE REQUIREMENTS
FOR
THE DEGREE OF DOCTOR OF PHILOSOPHY
IN
CHEMISTRY

DECEMBER 2010

Approval of the thesis:

**SYNTHESIS AND CHARACTERIZATION OF WATER SOLUBLE
POLYMER STABILIZED TRANSITION METAL(0) NANOCCLUSERS AS
CATALYST IN HYDROGEN GENERATION FROM THE HYDROLYSIS OF
SODIUM BOROHRIDE AND AMMONIA BORANE**

submitted by **ÖNDER METİN** in partial fulfillment of the requirements for the degree of **Doctor of Philosophy in Chemistry Department, Middle East Technical University** by,

Prof. Dr. Canan Özen
Dean, Graduate School of **Natural and Applied Sciences**

Prof. Dr. İlker Özkan
Head of Department, **Chemistry**

Prof. Dr. Saim Özkaz
Supervisor, **Chemistry Dept., METU**

Examining Committee Members:

Prof. Dr. Ceyhan Kayran
Chemistry Dept., METU

Prof. Dr. Saim Özkaz
Chemistry Dept., METU

Prof. Dr. Gülsün Gökağaç
Chemistry Dept., METU

Assoc. Prof. Dr. Ayşen Yılmaz
Chemistry Dept., METU

Assist. Prof. Dr. Emrah Özensoy
Chemistry Dept., Bilkent University

Date:

I hereby declare that all information in this document has been obtained and presented in accordance with academic rules and ethical conduct. I also declare that, as required by these rules and conduct, I have fully cited and referenced all material and results that are not original to this work.

Name, Last name: Önder Metin

Signature:

ABSTRACT

SYNTHESIS AND CHARACTERIZATION OF WATER SOLUBLE POLYMER STABILIZED TRANSITION METAL(0) NANOCCLUSERS AS CATALYST IN HYDROGEN GENERATION FROM THE HYDROLYSIS OF SODIUM BOROHYDRIDE AND AMMONIA BORANE

Metin, Önder

Ph.D., Department of Chemistry

Supervisor: Prof. Dr. Saim Özkar

December 2010, 158 pages

Metal nanoclusters exhibit unique properties which differ from their bulk materials, owing to the quantum size effects. For example, the catalytic activity of transition metal nanoclusters generally increases with decreasing particle size. However, nanoclusters tend to be fairly unstable with respect to the agglomerate into bulk metal in solution and thus special precautions have to be taken to avoid their aggregation or precipitation during the preparation of such nanoclusters in solution. In order to obtain stable nanoclusters dispersed in solution, a stabilizing agent is usually added into the reaction system. The stabilization of metal nanoclusters in solution can be achieved either by electrostatically by using charged ions such as acetate ion or sterically by long chain molecules such as polymers. Polymers are one of the most widely used steric stabilizers for the preparation of stable metal nanoclusters in solution. The use of polymers as stabilizer for the synthesis of transition metal nanoclusters provides advantageous regarding solubility, conductivity, thermal stability and reusability. The metal nanoclusters stabilized by polymers generally show higher catalytic activity, stability and optical properties. In this dissertation we report the preparation and characterization of water soluble polymer stabilized transition metal(0) (metal= Ni, Co and Ru) nanoclusters and their

catalysis in hydrogen generation from the hydrolysis of sodium borohydride (NaBH_4) and ammonia borane (AB) which are the best candidates as chemical hydrogen storage materials for on-board applications. The water soluble polymer stabilized nickel(0), cobalt(0) and ruthenium(0) nanoclusters were prepared by using two different facile methods; (i) the reduction of metal precursors by sodium borohydride in the presence poly(N-vinyl pyrrolidone) (PVP) in methanol solution after 1h reflux, (ii) the in situ generation during the hydrolysis of ammonia borane in the presence of poly(4-styrene sulfonicacid-co-maleic acid) (PSSA-co-MA). The characterization of both type of polymer stabilized transition metal(0) nanoclusters were done by using UV-Visible electronic absorption spectroscopy (UV-Vis), transmission electron microscopy (TEM), high resolution transmission electron microscopy (HRTEM), X-ray photoelectron spectroscopy (XPS), X-ray diffraction (XRD) and FT-IR techniques. The catalytic activity of PVP stabilized nickel(0), cobalt(0) and ruthenium(0) nanoclusters was tested in the hydrolysis of NaBH_4 and AB. The catalytic activity of PSSA-co-MA stabilized nickel(0), cobalt(0) and ruthenium(0) nanoclusters was tested only in the hydrolysis of AB in which they were in situ generated. The kinetics of hydrogen generation from both hydrolysis reactions in the presence PVP or PSSA-co-MA stabilized nickel(0), cobalt(0) and ruthenium(0) nanoclusters were studied depending on the polymer to metal ratio, catalyst concentration, substrate concentration and temperature as well as the activation parameters (Arrhenius activation energy (E_a), activation enthalpy (ΔH^\ddagger) and activation entropy (ΔS^\ddagger) of both catalytic hydrolysis were calculated from the kinetic data.

Keywords: Nanoclusters, Nickel, Cobalt, Ruthenium, Polymer, Poly(N-vinyl-2-pyrrolidone), Poly(4-styrene sulfonicacid-co-maleic acid), Catalyst, Hydrolysis of Sodium Borohydride, Hydrolysis of Ammonia Borane

ÖZ

SUDA ÇÖZÜNÜR POLİMERLE KARARLILAŞTIRILMIŞ GEÇİŞ METAL(0) NANOKÜMELERİ: HAZIRLANMASI, TANIMLANMASI VE SODYUM BORHİDRÜR VE AMONYAK BORANIN HİDROLİZİNDEN HİDROJEN ELDESİNDE KATALİTİK ETKİNLİKLERİ

Metin, Önder

Doktora, Kimya Bölümü

Tez Yöneticisi: Prof. Dr. Saim Özkar

Aralık 2010, 158 sayfa

Metal nanokümelere parçacık boyutlarının küçük olması nedeniyle külçe metallere çok farklı özellikler gösterirler ve bu özellikler parçacık boyutuna bağlı olarak değişir. Örneğin, geçiş metal nanokümelere katalitik etkinlikleri parçacık boyutunun küçülmesi ile genellikle artmaktadır. Metal nanokümelere katalitik etkinlik gösterebilmeleri için çözelti içerisinde topaklanmaya karşı kararlı hale getirilmesi gerekir. Örneğin, çözelti içerisinde özel kararlılaştırıcı ligantlar eklenilerek belirli büyüklükteki metal nanokümelere kararlılaştırılabilir. Metal nanokümelere çözelti içerisinde kararlılaştırılması HPO_4^{2-} gibi yüklü ligantlar varlığında elektrostatik olarak veya polimerler gibi uzun zincirli moleküller varlığında sterik olarak gerçekleştirilir. Polimerler çözelti içerisinde kararlı metal nanokümelere hazırlanmasında en yaygın olarak kullanılan sterik kararlılaştırıcılardan birisidir. Metal nanokümelere için kararlılaştırıcı olarak kullanılan polimerler, nanokümelere işlenebilirlik, yalıtılabilirlik (izole edilebilirlik), çözünürlük ve ısıya dayanıklılık gibi özellikler de sağlar. Polimer kullanılarak çözelti içerisinde topaklanmaya karşı kararlı hale getirilen nanokümelere genellikle daha etkin katalitik, iletkenlik, manyetik ve optik özellik gösterirler. Bu tezde, suda çözünür polimerle kararlılaştırılmış geçiş metal(0) (metal : Ni, Co ve Ru) nanokümelere hazırlanmasını, tanımlanmasını ve

sodyum borhidrür veya amonyak boranın hidrolizinden hidrojen eldesinde katalik etkinlikleri ile ilgili deneysel bulgular verilmektedir. Polimerle kararlılaştırılmıř nikel(0), kobalt(0) ve rutenyum(0) nanokümeleri suda çözüdür iki farklı polimerle, yeni geliřtirilen farklı iki method kullanılarak; (i) Methanol ierisinde çözünmüř olan metal bařlangı tuzlarının poli(N-vinil-2-pirolidon) (PVP) varlıęında 1 saat refluks dan sonra sodyum borhidrür ile indirgenmesi ile, (ii) bařlangı metal tuzlarının poli(4-sitiren sulfonikasit-co-malevik asit) (PSSA-co-MA) varlıęında sulu çözeltilde amonyak boranın hidrolizinde eř zamanlı olarak indirgenmesi yolu ile hazırlandı. Elde edilen PVP veya PSSA-co-MA ile kararlılaştırılmıř nikel(0), kobalt(0) ve rutenyum(0) nanokümeleri UV-görünür bölge elektronik soęurma spektroskopisi (UV-Vis), geirgenli electron mikroskopisi (TEM), yüksek çözüdürlüklü geirgenli elektron mikroskopisi (HRTEM), X-ıřınları fotoelektron spektroskopisi (XPS), X- ıřınları kırınımı (XRD) ve infrared spektroskopisi (FT-IR) ile tanımlandı. PVP ile kararlılaştırılmıř nikel(0), kobalt(0) and rutenyum(0) nanokümeleri, hem sodyum borhidrürün hem de amonyak boranın hidrolizinden hidrojen eldesinde katalizör olarak kullanıldı. PSSA-co-MA ile kararlılaştırılmıř nikel(0), kobalt(0) and rutenyum(0) nanokümelerinin katalitik etkinlikleri ise eř zamanlı olarak hazırlandıkları amonyak boranın hidrolizinden hidrojen eldesinde test edildi. PVP ya da PSSA-co-MA ile kararlılaştırılmıř nikel(0), kobalt(0) ve rutenyum(0) nanokümeleri ile katalizlenen hidroliz tepkimelerinin detaylı kinetięi polimer deriřimine, katalizör deriřimine, tepken deriřimine ve sıcaklıęa baęlı olarak çalıřıldı. Katalitik tepkimelerin aktivasyon parametreleri (Arrhenius aktivasyon enerjisi (E_a), aktivasyon entalpisi (ΔH^\ddagger) and aktivasyon entropisi (ΔS^\ddagger)) elde edilen kinetik veriler kullanılarak hesaplandı.

Anahtar Kelimeler: Nanokümeler, Nikel, Kobalt, Rutenyum, Polimer, Poli(N-vinil-2-pirolidon), Poli(4-sitiren sulfonikasit-co-malevik asit), Katalizör, Sodyum Borhidrürün Hidrolizi, Amonyak Boranın Hidrolizi.

To my beloved wife Neda Metin and precious family

ACKNOWLEDGEMENT

I would like to express my sincere thanks to Prof. Dr. Saim Özkar for his precious support, guidance and encouragement for the duration of my PhD studies and in the completion of this dissertation. I am profoundly honored to have a chance to work with him, and to be alumni of his highly loved research group.

Thesis examining committee members, Prof. Dr. Ceyhan Kayran and Assist. Prof. Dr. Emrah Özensoy, are also greatly acknowledged for their participation and valuable comments.

My special thanks to Prof. Dr. Shouheng Sun and the members of his Research Group in Department of Chemistry, Brown University in Providence, USA for their host and endless support to make most of the characterization of the catalysts for this dissertation and other studies during my six months visit at Brown University.

Thanks also extended to my laboratory collaborators Huriye Erdoğan and Melek Dinç and all other members in ‘Nanoclusters and Organometallic Research Group’ for their good friendship, scientific collaborations, endless help and motivation.

I would like to thanks to TUBITAK for 2214-Research Fellowship Program and Grant TBAG-108T840 and METU-DPT-OYP program on the behalf of Atatürk University.

The last but not the least, my special appreciation and great thankfulness is dedicated to my wife Neda for her love, patience and moral support during the period of my PhD studies and my family for their endless moral support and encouragement in every moment of my life.

TABLE OF CONTENTS

ABSTRACT.....	iv
ÖZ.....	vi
ACKNOWLEDGMENT.....	ix
TABLE OF CONTENTS.....	x
LIST OF FIGURES.....	xiv
LIST OF TABLES.....	xxiii
LIST OF ABBREVIATIONS.....	xxiv
CHAPTERS	
1. INTRODUCTION.....	1
1.1. Colloidal Transition Metal Nanoclusters.....	1
1.1.1. Stabilization of Transition Metal Nanoclusters.....	3
1.1.2. Preparation of Transition Metal Nanoclusters.....	8
1.1.3. Characterization of Transition Metal(0) Nanoclusters.....	10
1.1.4. Applications of Transition Metal Nanoclusters.....	11
2. CATALYSIS.....	13
2.1. General Principles of Catalysis.....	13
2.2. Key Definitions in Catalysis.....	16
2.3. Enhancement of catalytic activity by decreasing the particle size in heterogeneous catalysis.....	16
3. HYDROGEN ECONOMY.....	19
3.1. Hydrogen as an Energy Carrier.....	19
3.2. Hydrogen Storage: A Big Challenge in Hydrogen Economy.....	20
3.3. The Motivation of Thesis.....	23
4. EXPERIMENTAL.....	26
4.1. Materials.....	26

4.2. Preparation and Characterization of PVP stabilized Transition Metal(0) (Metal: Ni, Co and Ru) Nanoclusters.....	27
4.2.1. Preparation of PVP stabilized Nickel(0), Cobalt(0) and Ruthenium(0) Nanoclusters.....	27
4.2.2. Characterization of PVP stabilized Nickel(0), Cobalt(0) and Ruthenium(0) Nanoclusters.....	28
4.2.3. Method for Testing the Catalytic Activity of PVP stabilized Nickel(0), Cobalt(0) and Ruthenium(0) Nanoclusters in The Hydrolysis of Sodium Borohydride and Ammonia Borane	29
4.2.4. Self Hydrolysis of Sodium Borohydride and Ammonia borane	30
4.2.5. Kinetic Study of Catalytic Hydrolysis Of Sodium Borohydride or Ammonia borane Catalyzed by PVP stabilized Nickel(0), Cobalt(0) and Ruthenium(0) Nanoclusters.....	31
4.2.5.1. Effect of PVP Concentration On The Catalytic Activity Of Nickel(0), Cobalt(0) and Ruthenium(0) Nanoclusters.....	31
4.2.5.2. Kinetics of Hydrolysis of Sodium Borohydride Catalyzed by PVP stabilized Nickel(0), Cobalt(0) and Ruthenium(0) Nanoclusters.....	32
4.2.5.3. Kinetics of Hydrolysis of Ammonia Borane Catalyzed by PVP stabilized Nickel(0), Cobalt(0) and Ruthenium(0) Nanoclusters	32
4.3. PSSA-co-MA stabilized Nickel(0), Cobalt(0) or Ruthenium(0) Nanoclusters.....	33
4.3.1. In Situ Generation of PSSA-co-MA Stabilized Nickel(0), Cobalt(0) or Ruthenium(0) Nanoclusters and Concomitant Hydrogen Generation from the Hydrolysis of Ammonia Borane.....	33
4.3.2. Characterization of In Situ Generated PSSA-co-MA stabilized Nickel(0), Cobalt(0) or Ruthenium(0) Nanoclusters.....	36
4.3.3. Kinetic Study of PSSA-co-MA Stabilized Nickel(0), Cobalt(0) and Ruthenium(0) Nanoclusters in Catalytic Hydrolysis of Ammonia Borane.....	37
4.3.3.1. Effect of PSSA-co-MA Concentration on the Catalytic Activity of Nickel(0), Cobalt(0) and Ruthenium(0) Nanoclusters	37

4.3.3.2. Determination of Rate law and Activation Parameters for Hydrolysis of Ammonia Borane Catalyzed by PSSA-co-MA Stabilized Nickel(0), Cobalt(0) or Ruthenium(0) Nanoclusters.....	38
4.3.3.3. Determination of the Catalytic Lifetime of PSSA-co-MA Stabilized Nickel(0), Cobalt(0) or Ruthenium(0) Nanoclusters in the Hydrolysis of Ammonia Borane	38
4.3.3.4. Quantification of the Liberated NH ₃ Gas	39
4.3.3.5. Mercury Poisoning as Heterogeneity Test for In-situ Prepared PSSA-co-MA Stabilized Nickel(0), Cobalt(0) or Ruthenium(0) Nanoclusters	39
5. RESULTS AND DISCUSSIONS	40
5.1. Preparation and Characterization of PVP stabilized Transition Metal(0) (Metal: Ni, Co and Ru) Nanoclusters.....	40
5.1.1. Characterization of PVP stabilized Nickel(0) Nanoclusters	42
5.1.2. Characterization of PVP stabilized Cobalt(0) Nanoclusters	47
5.1.3. Characterization of PVP stabilized Ruthenium(0) Nanoclusters	52
5.1.4. Integrity of PVP on the stabilization of transition metal(0) nanoclusters ...	57
5.2. Catalytic Activity of PVP Stabilized Nickel(0), Cobalt(0) and Ruthenium(0) Nanoclusters in Hydrogen Generation from the Hydrolysis of Sodium Borohydride and Ammonia Borane	59
5.2.1. Catalytic Activity of PVP stabilized Nickel(0) Nanoclusters in The Hydrolysis of Sodium Borohydride and Ammonia borane.....	59
5.2.1.1. Kinetics of the Hydrolysis of Sodium Borohydride Catalyzed by PVP stabilized Nickel(0) Nanoclusters	59
5.2.1.2. Kinetics of the Hydrolysis of Ammonia Borane Catalyzed by PVP stabilized Nickel(0) Nanoclusters	66
5.2.2. Catalytic Activity of The PVP stabilized Cobalt(0) Nanoclusters in The Hydrolysis of Sodium Borohydride or Ammonia borane	71
5.2.2.1. Kinetics of the hydrolysis of sodium borohydride catalyzed by PVP stabilized cobalt(0) nanoclusters in aqueous medium.....	71
5.2.2.2. Kinetics of the hydrolysis of ammonia borane catalyzed by PVP stabilized cobalt(0) nanoclusters.....	76

5.2.2.3. Catalytic Activity of PVP stabilized Cobalt(0) Nanoclusters in the Hydrolysis of Sodium Borohydride in Basic Medium.....	80
5.2.3. Catalytic Activity of The PVP stabilized Ruthenium(0) Nanoclusters in The Hydrolysis of Sodium Borohydride and Ammonia borane.....	87
5.2.3.1. Kinetics of the hydrolysis of sodium borohydride catalyzed by PVP stabilized ruthenium(0) nanoclusters in aqueous medium	87
5.2.3.2. Kinetics of the hydrolysis of sodium borohydride catalyzed by PVP stabilized ruthenium(0) nanoclusters in basic medium	91
5.2.3.3. Kinetics of the hydrolysis of ammonia borane catalyzed by PVP stabilized ruthenium(0) nanoclusters	98
5.3. PSSA-co-MA Stabilized Nickel(0), Cobalt(0) and Ruthenium(0) Nanoclusters.....	102
5.3.1. In situ generation and characterization of PSSA-co-MA stabilized Nickel(0) or Cobalt(0) Nanoclusters	102
5.3.2. Kinetics of Hydrolysis of Ammonia Borane Catalyzed By PSSA-co-MA stabilized Nickel(0) or Cobalt(0) Nanoclusters.....	108
5.3.3. In situ Generation and Characterization of PSSA-co-MA Stabilized Ruthenium(0) Nanoclusters.....	117
5.3.4. Kinetics of Hydrolysis of Ammonia Borane Catalyzed By PSSA-co-MA Stabilized Ruthenium(0) Nanoclusters.....	120
5.3.5. Mercury Poisoning as Heterogeneity Test for In-situ Prepared PSSA-co-MA Stabilized Nickel(0), Cobalt(0) or Ruthenium(0) Nanoclusters	126
6. CONCLUSIONS.....	128
REFERENCES.....	134
APPENDIX.....	147
A. TABLES.....	147
CURRICULUM VITAE.....	153

LIST OF FIGURES

FIGURES

Figure 1. The effect of particle size on the ratio of the number of surface atoms to the total number of atoms. N = the total number atoms; n = the number of surface atoms. 2	
Figure 2. Formation of discrete electronic energy levels on the way from bulk to molecule..... 3	3
Figure 3. Schematic representation of the electrostatic stabilization of transition metal nanoclusters..... 4	4
Figure 4. The schematic representation of the steric stabilization of transition metal nanoclusters..... 4	4
Figure 5. Structure model of polymer-stabilized metal nanoclusters..... 5	5
Figure 6. Two models suggested for the stabilization of the metal nanocluster by a polymer; (a) the stabilization of each nanoclusters by one polymer chain (the widely accepted one); (b) the stabilization of many nanoclusters by one polymer chain 6	6
Figure 7. The schematic representation of the electrosteric stabilization of transition metal nanoclusters..... 8	8
Figure 8. The methods most commonly used in the characterization of metal nanoparticles 11	11
Figure 9. The classification of catalysts..... 13	13
Figure 10. Generic potential energy diagram showing the effect of a catalyst in a hypothetical exothermic chemical reaction $X + Y$ to give Z . The presence of the catalyst opens a different reaction pathway (shown in red) with a lower activation energy. The final result and the overall thermodynamics are the same. 15	15
Figure 11. The change in percentage of surface iron atoms depending on the size of iron(0) nanoclusters 17	17

Figure 12. The relation between the total number of atoms in full shell clusters and the percentage of surface atoms.	18
Figure 13. Hydrogen mass density versus hydrogen volume density of many compounds considered to be a chemical hydrogen storage material [57].	21
Figure 14. Parr-5101 Low pressure reactor system for measurement of volume of hydrogen generated from the catalytic hydrolysis of sodium borohydride or ammonia borane.....	30
Figure 15. The experimental setup used in performing the catalytic hydrolysis of ammonia borane and measuring the hydrogen generation rate.....	36
Figure 16. A schematic representation of the experimental setup used for the preparation of PVP stabilized transition metal(0) nanoclusters via our own developed method.....	41
Figure 17. UV-Visible spectra of nickel(II) chloride and PVP stabilized nickel(0) nanoclusters taken from the methanol solutions.	42
Figure 18. (a) TEM image and (b) associated histogram for PVP stabilized nickel(0) nanoclusters formed from the reduction of nickel(II) chloride in the presence of PVP by sodium borohydride after one hour reflux in methanol.	43
Figure 19. X-Ray photoelectron (a) survey (b) high resolution spectra of PVP stabilized nickel(0) nanoclusters formed from the reduction of nickel(II) chloride (8.4 mM) in the presence of PVP (42 mM) by sodium borohydride (300 mM) after one hour reflux in methanol.....	45
Figure 20. X-ray diffraction pattern of PVP stabilized nickel(0) nanoclusters.....	46
Figure 21. (a) TEM image and (b) associated histogram for PVP stabilized cobalt(0) nanoclusters sample isolated from the reduction of cobalt(II) chloride (8.4 mM) in the presence of PVP (42 mM) by sodium borohydride (150 mM) after one hour reflux in methanol.	48
Figure 22. X-Ray photoelectron (a) survey, (b) high resolution spectra of PVP stabilized cobalt(0) nanoclusters sample isolated from the reduction of cobalt(II) chloride hexahydrate (8.4 mM) in the presence of PVP (42 mM) by sodium borohydride (150 mM) after one hour reflux in methanol.....	50
Figure 23. UV-Vis spectra of cobalt(II) chloride and PVP stabilized cobalt(0) nanoclusters taken from the methanol solutions.	51

Figure 24. X-ray diffraction pattern of PVP stabilized cobalt(0) nanoclusters.....	52
Figure 25. UV-Vis spectra of ruthenium(III) chloride and PVP stabilized ruthenium(0) nanoclusters taken from the methanol solutions.....	53
Figure 26. (a) TEM image and (b) associated histogram for PVP stabilized ruthenium(0) nanoclusters sample isolated from the reduction of ruthenium(III) chloride (3.6 mM) in the presence of PVP (18 mM) by sodium borohydride (300 mM) after one hour reflux in methanol.....	54
Figure 27. X-Ray photoelectron (a) survey, (b) high resolution spectra of PVP stabilized ruthenium(0) nanoclusters sample isolated from the reduction of ruthenium(III) chloride hydrate (3.6 mM) in the presence of PVP (18 mM) by sodium borohydride (150 mM) after one hour reflux in methanol.....	56
Figure 28. X-ray diffraction pattern of PVP stabilized ruthenium(0) nanoclusters..	57
Figure 29. FT-IR spectra of PVP stabilized metal(0) nanoclusters taken from KBr pellets in the CO stretching range: (a) neat PVP, (b) PVP/metal =0.5, (c) PVP/metal = 0.1.	58
Figure 30. The volume of hydrogen versus time plot for the hydrolysis of sodium borohydride catalyzed by nickel(0) nanoclusters having different PVP to nickel ratio at 25 ± 0.5 °C.	60
Figure 31. The rate of hydrogen generation from the hydrolysis of NaBH ₄ in the...	61
Figure 32. The volume of hydrogen versus time plot depending on the nickel concentration for the catalytic hydrolysis of sodium borohydride (150 mM) at 25.0 ± 0.5 °C. The inset shows the plot of hydrogen generation rate versus the concentration of nickel (both in logarithmic scale) for the hydrolysis of sodium borohydride.	62
Figure 33. The volume of hydrogen versus time plots for the hydrolysis of sodium borohydride at different NaBH ₄ concentrations at constant catalyst concentration (1.4 mM Ni) and 25.0 ± 0.5 °C. The inset shows the plot of hydrogen generation rate versus the NaBH ₄ concentration (both in logarithmic scale) for the hydrolysis of sodium borohydride.	63
Figure 34. Volume of hydrogen generation versus time for the hydrolysis of sodium borohydride (150 mM) catalyzed by PVP stabilized nickel(0) nanoclusters (1.4 mM Ni) in the temperature range of 25-45 °C. The inset shows the Arrhenius plot (ln k versus the reciprocal absolute temperature $1/T$ (K ⁻¹)).	64

Figure 35. Eyring plot ($\ln(k/T)$) versus the reciprocal absolute temperature $1/T$ (K^{-1}) for the hydrolysis of sodium borohydride (150 mM) catalyzed by PVP stabilized nickel(0) nanoclusters (1.4 mM Ni) in the temperature range 25-45 °C..... 66

Figure 36. The volume of hydrogen versus time plots depending on the nickel concentrations for the hydrolysis of ammonia borane (100 mM) at 25 ± 0.5 °C The inset shows the plot of hydrogen generation rate versus the concentration of cobalt (both in logarithmic scale). 67

Figure 37. The volume of hydrogen versus time plots depending on the substrate concentrations at constant catalyst concentration for the hydrolysis of ammonia borane catalyzed by PVP stabilized nickel(0) nanoclusters. The inset shows the plot of hydrogen generation rate versus the concentration of the substrate (both in logarithmic scale)..... 68

Figure 38. The volume of hydrogen versus time plots at different temperatures for the hydrolysis of ammonia borane (100 mM) catalyzed by PVP stabilized nickel(0) nanoclusters (2.0 mM Ni) in the temperature range 20-40 °C. The inset shows Arrhenius plot ($\ln k$ versus the reciprocal absolute temperature $1/T$ (K^{-1})). 69

Figure 39. Eyring plot ($\ln(k/T)$) versus the reciprocal absolute temperature $1/T$ (K^{-1}) for the hydrolysis of ammonia borane (100 mM) catalyzed by PVP stabilized nickel(0) nanoclusters (2.0 mM Ni) in the temperature range 20-40 °C..... 70

Figure 40. The volume of hydrogen versus time plots depending on the cobalt concentrations for the hydrolysis of sodium borohydride (150 mM) at 25 ± 0.5 °C The inset shows the plot of hydrogen generation rate versus the concentration of cobalt (both in logarithmic scale)..... 71

Figure 41. The volume of hydrogen versus time plots depending on the substrate concentrations at constant catalyst concentration for the hydrolysis of sodium borohydride. The inset shows the plot of hydrogen generation rate versus the concentration of the substrate (both in logarithmic scale) 72

Figure 42. The volume of hydrogen versus time plots at different temperatures for the hydrolysis of sodium borohydride (150 mM) catalyzed by PVP stabilized cobalt(0) nanoclusters (1.5 mM Co) in the temperature range 20-40 °C. The inset shows Arrhenius plot ($\ln k$ versus the reciprocal absolute temperature $1/T$ (K^{-1})). .. 74

Figure 43. Eyring plot ($\ln(k/T)$) versus the reciprocal absolute temperature $1/T$ (K^{-1}) for the hydrolysis of sodium borohydride (150 mM) catalyzed by PVP stabilized cobalt(0) nanoclusters (1.5 mM Co) in the temperature range 20-40 °C.....	75
Figure 44. The volume of hydrogen versus time plots depending on the cobalt concentrations for the hydrolysis of ammonia borane (100 mM) at 25 ± 0.5 °C The inset shows the plot of hydrogen generation rate versus the concentration of cobalt (both in logarithmic scale).	76
Figure 45. The volume of hydrogen versus time plots depending on the substrate concentrations at constant catalyst concentration (2.0 mM Co) for the hydrolysis of sodium borohydride. The inset shows the plot of hydrogen generation rate versus the concentration of the substrate (both in logarithmic scale)	77
Figure 46. The volume of hydrogen versus time plots at different temperatures for the hydrolysis of ammonia borane (100 mM) catalyzed by PVP stabilized cobalt(0) nanoclusters (2.0 mM Co) in the temperature range 20-40 °C. The inset shows Arrhenius plot ($\ln k$ versus the reciprocal absolute temperature $1/T$ (K^{-1})).	79
Figure 47. Eyring plot ($\ln(k/T)$) versus the reciprocal absolute temperature $1/T$ (K^{-1}) for the hydrolysis of ammonia borane (100 mM) catalyzed by PVP stabilized cobalt(0) nanoclusters (1.5 mM Co) in the temperature range 20-40 °C.....	79
Figure 48. Plot of the volume of hydrogen (mL) versus time (s) for the hydrolysis of 50 mL of 150 mM sodium borohydride catalyzed by PVP stabilized cobalt(0) nanoclusters (2 mM Co) in 1.0, 2.0, 3.0, 4.0, 5.0, and 10.0% wt NaOH solutions at 25.0 ± 0.5 °C. The inset shows the plot of hydrogen generation rate change depending on the % wt of NaOH.	81
Figure 49. Plot of the volume of hydrogen versus time for the hydrolysis of sodium borohydride (150 mM) in 2% wt NaOH solution catalyzed by PVP stabilized cobalt(0) nanoclusters with different cobalt(0) concentrations at 25.0 ± 0.5 °C. The inset shows the plot of hydrogen generation rate versus catalyst concentration (both in logarithmic scale) for the PVP stabilized cobalt(0) nanoclusters catalyzed hydrolysis of $NaBH_4$ in 2% wt NaOH solution at 25.0 ± 0.5 °C.	82
Figure 50. Plot of the volume of hydrogen versus time for the hydrolysis of sodium borohydride in 2% wt NaOH solution catalyzed by PVP stabilized cobalt(0) nanoclusters with different $NaBH_4$ concentrations at 25.0 ± 0.5 °C. The inset shows	

the plot of hydrogen generation rate versus NaBH_4 concentration (both in logarithmic scale) for the PVP stabilized cobalt(0) nanoclusters catalyzed hydrolysis of NaBH_4 in 2% wt NaOH solution at 25.0 ± 0.5 °C.....	83
Figure 51. Plot of the volume of hydrogen (mL) generated versus time (s) for the hydrolysis of 50 mL of 150 mM sodium borohydride in 2% wt NaOH solution at different temperatures (15, 20, 25, 30, and 35°C) catalyzed by PVP-stablized cobalt(0) nanoclusters ($[\text{Co}] = 2.0$ mM). The inset shows the Arrhenius plot for the PVP stabilized cobalt(0) nanoclusters catalyzed hydrolysis of sodium borohydride in 2 wt % NaOH solution.	84
Figure 52. Plot of the volume of hydrogen (mL) versus time (s) for the hydrolysis of NaBH_4 (284 mg, 150mM in 50 mL) catalyzed by PVP stabilized ruthenium(0) nanoclusters with different ruthenium concentrations in the range of 0.25-0.65 mM at 25.0 ± 0.5 °C. The inset shows the rate of hydrogen generation versus ruthenium concentration both in logarithmic scale.	87
Figure 53. Plot of the volume of hydrogen (mL) versus time (s) for the hydrolysis of NaBH_4 catalyzed by PVP stabilized ruthenium(0) nanoclusters ($[\text{Ru}] = 0.35$ mM) solution (50 mL) in different substrate concentrations in the range of 150-900 mM NaBH_4 at 25.0 ± 0.5 °C.....	89
Figure 54. Plot of the volume of hydrogen (mL) versus time (s) for the hydrolysis of NaBH_4 (284 mg, 150mM in 50 mL) catalyzed by PVP stabilized ruthenium(0) nanoclusters ($[\text{Ru}] = 0.35$ mM) at different temperatures in the range of 15-35 °C. 90	
Figure 55. Eyring plot ($\ln(k/T)$) versus the reciprocal absolute temperature $1/T$ (K^{-1}) for the hydrolysis of sodium borohydride (150 mM) catalyzed by PVP stabilized ruthenium(0) nanoclusters (0.35 mM Ru) in the temperature range of 15-35 °C	91
Figure 56. Plot of the volume of hydrogen (mL) versus time (s) for the hydrolysis of sodium borohydride ($[\text{NaBH}_4] = 150$ mM) catalyzed by PVP stabilized ruthenium(0) nanoclusters ($[\text{Ru}] = 0.75$ mM) in different wt% NaOH solutions at 25.0 ± 0.5 °C. .	93
Figure 57. Plot of the volume of hydrogen (mL) versus time (s) for the hydrolysis of sodium borohydride ($[\text{NaBH}_4] = 150$ mM) in 5 wt % NaOH solution catalyzed by PVP stabilized ruthenium(0) nanoclusters with different ruthenium(0) concentrations at 25.0 ± 0.5 °C.	94

Figure 58. Plot of the volume of hydrogen (mL) generated versus time (s) for the hydrolysis of sodium borohydride (150 mM) catalyzed by PVP stabilized ruthenium(0) nanoclusters in 5 wt% NaOH solution at different temperatures ([Ru] = 0.75 mM).....	95
Figure 59. The Eyring plot for the hydrolysis of sodium borohydride catalyzed by PVP stabilized ruthenium(0) nanoclusters in 5 wt% NaOH solution.	96
Figure 60. Plot of the volume of hydrogen (mL) versus time (s) for the hydrolysis of ammonia borane (63.0 mg, 100 mM in 20 mL) catalyzed by PVP stabilized ruthenium(0) nanoclusters with different ruthenium concentrations at 25.0 ± 0.5 °C. The inset shows the rate of hydrogen generation versus ruthenium concentration both in logarithmic scale.	98
Figure 61. The volume of hydrogen versus time plots depending on the substrate concentrations at constant catalyst concentration for the hydrolysis of ammonia borane catalyzed by PVP stabilized ruthenium(0) nanoclusters. The inset shows the plot of hydrogen generation rate versus the concentration of the substrate (both in logarithmic scale).....	99
Figure 62. Plot of the volume of hydrogen (mL) versus time (s) for the hydrolysis of H_3NBH_3 (63.0 mg, 100 mM in 50 mL) catalyzed by PVP stabilized ruthenium(0) nanoclusters ([Ru] = 0.35 mM) at different temperatures in the range of 15-35 °C.	100
Figure 63. Eyring plot ($\ln(k/T)$) versus the reciprocal absolute temperature $1/T$ (K^{-1}) for the hydrolysis of ammonia borane (100 mM) catalyzed by PVP stabilized ruthenium(0) nanoclusters (0.35 mM Ru) in the temperature range of 15-35 °C	101
Figure 64. UV-Visible spectra of (a) nickel(II) chloride and PSSA-co-MA stabilized nickel(0) nanoclusters, (b) cobalt(II) chloride and PSSA-co-MA stabilized cobalt(0) nanoclusters taken from the aqueous solutions.....	103
Figure 65. TEM, HRTEM images and corresponding particle size distributions of PSSA-co-MA stabilized nickel(0) nanoclusters (a,c,e), cobalt(0) nanoclusters (b,d,f)	105
Figure 66. XRD patterns of PSSA-co-MA stabilized (a) nickel(0) nanoclusters (b) cobalt(0) nanoclusters	107

Figure 67. The volume of hydrogen versus time plots depending on the different [PSSA-co-MA]/[Metal] ratios for (a) nickel nanoclusters (b) cobalt nanoclusters. The insets show the plots of hydrogen generation rate versus the concentration of metal (both in logarithmic scale) for the hydrolysis of AB (100 mM) at 25 ± 0.5 °C.	109
Figure 68. The volume of hydrogen versus time plots depending on the metal concentrations for PSSA-co-MA stabilized (a) nickel(0) nanoclusters (b) cobalt(0) nanoclusters at 25 ± 0.5 °C. The inset of each figures show the plot of hydrogen generation rate versus the concentration of metal (both in logarithmic scale).	111
Figure 69. The volume of hydrogen versus time plots depending on AB concentrations for PSSA-co-MA stabilized (a) nickel(0) nanoclusters (b) cobalt(0) nanoclusters at 25.0 ± 0.5 °C. The inset of each figures show the plot of hydrogen generation rate versus the concentration of metal (both in logarithmic scale).	112
Figure 70. Volume of hydrogen versus time plots at different temperatures for the hydrolysis of AB (100 mM) catalyzed by PSSA-co-MA stabilized (a) Ni nanoclusters (2.0 mM) (b) Co nanoclusters (2.0 mM) in the temperature range 15-35 °C. The insets of each figure show Arrhenius plot ($\ln k$ versus the reciprocal absolute temperature $1/T$ (K^{-1})).	114
Figure 71. Eyring plot ($\ln(k/T)$ versus the reciprocal absolute temperature $1/T$ (K^{-1})) for the hydrolysis of ammonia borane (100 mM) catalyzed by PSSA-co-MA stabilized (a) nickel(0) nanoclusters (2.0 mM Ni) (b) cobalt(0) nanoclusters (2.0 mM Co) in the temperature range 15-35 °C	115
Figure 72. UV-Visible spectra of ruthenium(III) chloride and PSSA-co-MA stabilized ruthenium(0) nanoclusters taken from the aqueous solutions.	117
Figure 73. (a) TEM images and (b) associated histograms for PSSA-co-MA stabilized ruthenium(0) formed in-situ from the reduction of ruthenium(III) chloride (0.7 mM).	119
Figure 74. XRD pattern of PSSA-co-MA stabilized ruthenium(0) nanoclusters....	120
Figure 75. The volume of hydrogen versus time plots depending on the different [PSSA-co-MA]/[Metal] ratios for ruthenium(0) nanoclusters. The inset shows the plot of hydrogen generation rate versus the concentration of Ru (both in logarithmic scale) for the hydrolysis of AB (100 mM) at 25 ± 0.5 °C.....	121

Figure 76. The volume of hydrogen versus time plots depending on the metal concentrations for PSSA-co-MA stabilized ruthenium(0) nanoclusters The inset of figure shows the plot of hydrogen generation rate versus the concentration of ruthenium (both in logarithmic scale).	122
Figure 77. The volume of hydrogen versus time plots depending on the substrate concentrations at constant catalyst concentration for the hydrolysis of AB catalyzed by PSSA-co-MA stabilized ruthenium(0) nanoclusters (0.7 mM Ru) The inset of figure shows the plot of hydrogen generation rate versus the concentration of the substrate (both in logarithmic scale).	123
Figure 78. The volume of hydrogen versus time plots at different temperatures for the hydrolysis of AB (100 mM) catalyzed by PSSA-co-MA stabilized ruthenium(0) nanoclusters (0.7 mM) in the temperature range 15-35 °C. The inset of figure shows Arrhenius plot ($\ln k$ versus the reciprocal absolute temperature $1/T$ (K^{-1})).	124
Figure 79. Eyring plot ($\ln(k/T)$ versus the reciprocal absolute temperature $1/T$ (K^{-1}) for the hydrolysis of ammonia borane (100 mM) catalyzed by PSSA-co-MA stabilized ruthenium(0) nanoclusters (0.7 mM Ru)	125
Figure 80. The volume of hydrogen versus time plots for the hydrolysis of ammonia borane (200 mM) catalyzed by PSSA-co-MA stabilized nickel(0) nanoclusters (2.0 mM Ni) with and without addition of 200 equiv. Hg(0) at 25.0 ± 0.5 °C.	126
Figure 81. The volume of hydrogen versus time plots for the hydrolysis of ammonia borane (200 mM) catalyzed by PSSA-co-MA stabilized cobalt(0) nanoclusters (2.0 mM Co) with and without addition of 150 equiv. Hg(0) at 25.0 ± 0.5 °C.....	127
Figure 82. The volume of hydrogen versus time plots for the hydrolysis of ammonia borane (300 mM) catalyzed by PSSA-co-MA stabilized ruthenium(0) nanoclusters (0.7 mM Ru) with and without addition of 150 equiv. Hg(0) at 25.0 ± 0.5 °C.	127

LIST OF TABLES

TABLES

Table 1. IUPAC names and chemical structures of the polymer used for the stabilization of nickel(0), cobalt(0) and ruthenium(0) nanoclusters in this dissertation.....	27
Table 2. The catalyst systems employed in the hydrolysis of sodium borohydride in the basic medium and obtained activation energies in different reaction conditions.	97
Table 3. Activities in terms of TOF values ($\text{mol H}_2 \cdot (\text{mol catalyst})^{-1} \cdot \text{min}^{-1}$) of the non-noble metal catalysts or their alloys have been tested in hydrogen generation from the hydrolysis of AB at 25 °C. (The TOF values were estimated from the data given in respective references).....	116
Table 4. Summary of the kinetic data of hydrogen generation from the hydrolysis of sodium borohydride and ammonia borane catalyzed by PVP stabilized nickel(0), cobalt(0) and ruthenium(0) nanoclusters.....	129
Table 5. Summary of the kinetic data of hydrogen generation from the hydrolysis of ammonia borane catalyzed by in-situ generated PSSA-co-MA stabilized nickel(0), cobalt(0) and ruthenium(0) nanoclusters.....	132

LIST OF ABBREVIATIONS

NPs	: Nanoparticles
NCs	: Nanoclusters
PVP	: Poly(N-vinyl-2-pyrrolidone)
PSSA-co-MA	: Poly(4-styrene sulfonicacid-co-maleic acid)
AB	: Ammonia Borane
E_a^{apparent}	: Apparent activation Energy
HOMO	: Highest Occupied Molecular Orbital
LUMO	: Lowest Unoccupied Molecular Orbital
TOF	: Turnover Frequency
TON	: Total Turnover Number
ν	: Rate of Reaction
ΔG	: Change in Gibbs Free Energy
ΔH^\ddagger	: Enthalpy of Activation
ΔS^\ddagger	: Entropy of Activation
J	: Coupling constant
k_{app}	: Apparent rate constant
ppm	: Parts per Million
MTL	: Mass Transfer Limitation

CHAPTER 1

INTRODUCTION

1.1. Colloidal Transition Metal Nanoclusters

Transition metal nanoclusters are isolable particles in size about 1–10 nm (10–100 Å) [1]. They have generated intense interest over the past decade due to their unique properties, derived in part from the fact that these particles and their properties lie somewhere between those of bulk and single-particle species [2]. A particle should have the following criteria to be defined as a nanocluster [3]; a) the size of the particle is to be smaller than 10 nm with a narrow size distribution, $\sigma \leq 15\%$; b) its synthesis should be reproducible; c) it has to be compositionally well-defined, isolable, and redissolvable.

The main reason to make metal nanoclusters scientifically so interesting is their unique properties which do not follow the classical physical laws as all bulk materials do [4]. This phenomenon can be simply as seen in Figure 1 depending on the fact that the number of surface atoms becomes larger as the particle size decreases. Additionally, the surface atoms in metal nanoclusters do not necessarily order themselves in the same way that those in the bulk do [2]. Furthermore, owing to the quantum size effect, confinement of electrons to small regions of space in one, two, or three dimensions, the electrons in nanoclusters are confined to spaces that can be as small as a few atom-widths across [5]. In this regard, they have found many applications including quantum dots [6], quantum computers [7], quantum devices [8], chemical sensors [9], light-emitting diodes [10], ferrofluids for biological

applications [11], optics [12] and a new type of highly active and selective catalysts [13].

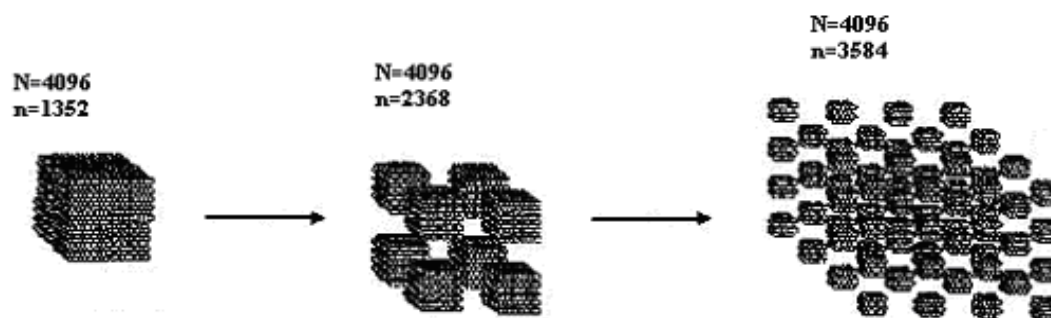


Figure 1. The effect of particle size on the ratio of the number of surface atoms to the total number of atoms. N = the total number atoms; n = the number of surface atoms.

When a metal particle with bulk properties is reduced to the nanometer size scale, the density of states in the valence and the conduction band decreases to such an extent that the quasi-continuous density of states is replaced by a discrete energy level structure and the electronic properties change dramatically as shown in Figure 2. Such a dramatic change in the electronic properties of a metal in nanometer size results in many different physical and chemical properties which can be exemplified by gold case. If bulk gold is reduced to ca. 50 nm in solution, the yellow color spontaneously disappears and turns to blue, further reduction results in purple and finally red colors [4]. Additionally, the bulk gold is catalytically inactive but there are many studies on gold nanoparticle catalyzed reactions [14].

However, transition metal nanoclusters are only kinetically stable and thermodynamically unstable in solution to agglomerate into bulk metal. Therefore, special precautions have to be taken to avoid their aggregation or precipitation during the preparation of such nanoclusters in solution [1,15]. Consequently, considerable effort has been focused on the stabilization of transition metal nanoclusters in solution which is crucial if practical applications of metal nanoclusters are to be realized. Therefore, general and critical aspects on the stabilization of transition metal nanoclusters should be mentioned before beginning a description of synthetic methods for the preparation of them.

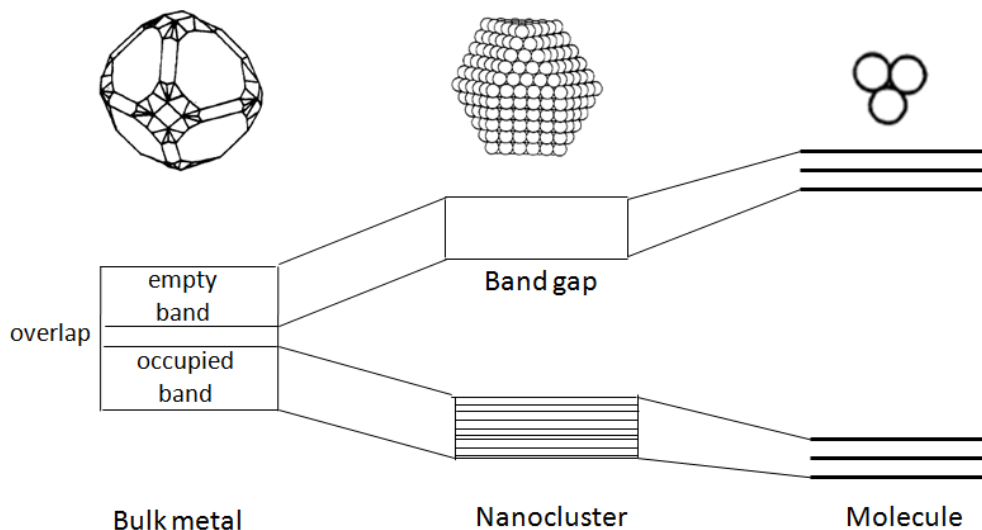


Figure 2. Formation of discrete electronic energy levels on the way from bulk to molecule [16].

1.1.1. Stabilization of Transition Metal Nanoclusters

At short interparticle distances, two particles would be attracted to each other by Van der Waals forces and in the absence of repulsive forces two counteract this attraction an unprotected sol would coagulate [17]. In the literature of colloidal stability [18] and in Derjaguin-Landau-Verway-Overbeek (DLVO) theory [19], colloidal stabilization is well established to involve both: (i) *electrostatic stabilization* and (ii) *steric stabilization*;

(i) ***Electrostatic stabilization***; the adsorption of negatively or positively charged ions to the coordinatively unsaturated surface of the nanoparticles results in a coulombic repulsion between the particles. The coulombic repulsion opposes Van Der Waals attractions and the net result is shown schematically in Figure 3. The coulombic repulsion between the particles decays approximately exponentially with the particle distance. The weak minimum in potential energy defines a stable situation. Thus, if the electric potential resulting from the double layers is high enough, electrostatic repulsion prevents aggregation [20]

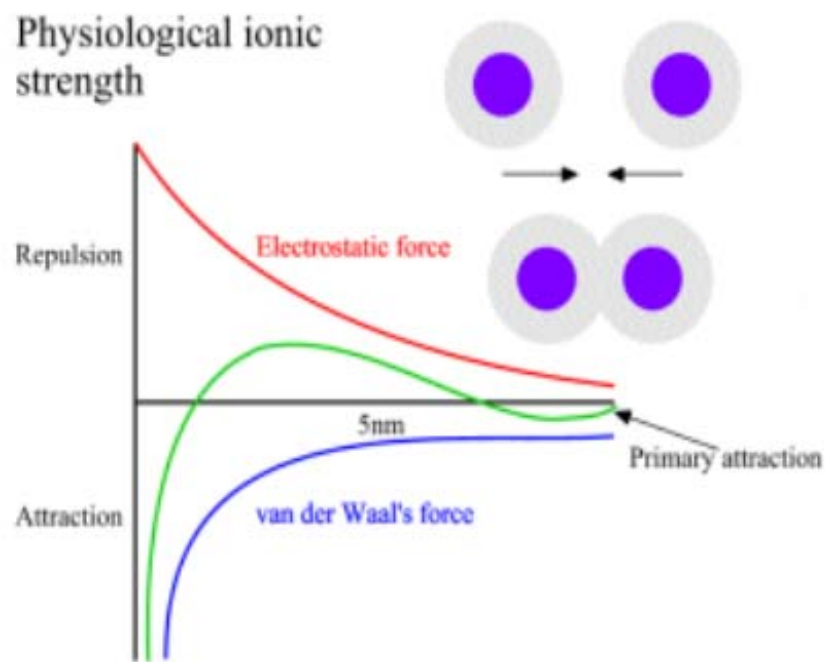


Figure 3. Schematic representation of the electrostatic stabilization of transition metal nanoclusters.

(ii) **Steric stabilization:** it is achieved by the absorption of molecules such as polymers, surfactants or long chain ligands at the surface of the nanoclusters, thus providing a protective layer [21]. These large adsorbates provide a steric barrier which prevents close contact of metal nanoclusters to each other as demonstrated in Figure 4.

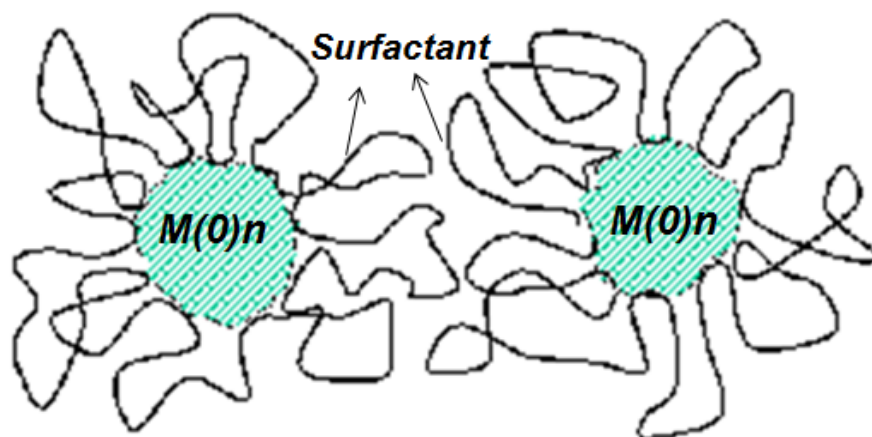


Figure 4. The schematic representation of the steric stabilization of transition metal nanoclusters.

Steric Stabilization by polymers: polymers are widely used, and it is obvious that the protectant, in order to function effectively, must not only coordinate to the particle surface, but must also be adequately solvated by the dispersing fluid such polymers are termed amphiphilic. The structure of polymer stabilized metal nanoclusters can be illustrated in Figure 5, where the polymers were thought to adsorb physically on the surface of metal nanoclusters [22]. Detailed characterization studies of the adsorbed polymer have demonstrated that the polymers can coordinate to the metal forming rather strong chemical bonds. The polymer molecule can coordinate to the metal particle at multiple sites.

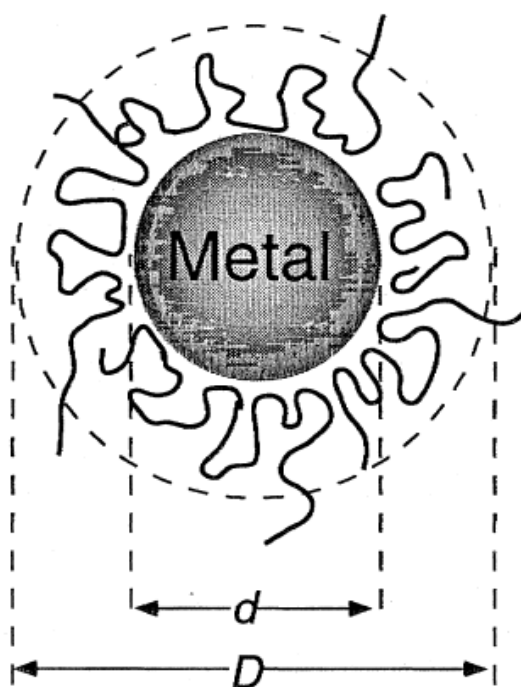


Figure 5. Structure model of polymer-stabilized metal nanoclusters [23].

Two models are suggested for the stabilization of the metal nanocluster by a polymer as shown in Figure 6; (a) the stabilization of each nanoclusters by one polymer chain (the widely accepted one, Figure 6a) (b) the stabilization of many nanoclusters by one polymer chain (Figure 6b). As clearly seen for the both models, there still exists a large catalytically active exposed surface which is crucial for heterogeneous catalytic applications.

The choice of polymer as a stabilizer is determined by consideration of the solubility of the metal colloid precursor, the solvent of choice, and the ability of the polymer to stabilize the reduced metal particles in the colloidal state [4]. For this reason, it is important to investigate a broad variety of protective polymers for their ability to stabilize metal nanoclusters. The use of polymeric matrix as stabilizer improves some properties of the nanoclusters such as the solubility, thermal stability and catalytic activity [22,24].

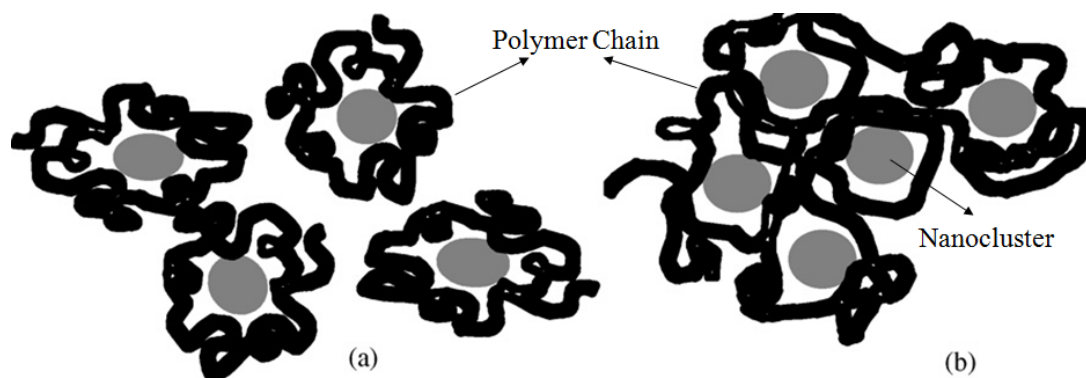


Figure 6. Two models suggested for the stabilization of the metal nanocluster by a polymer; (a) the stabilization of each nanocluster by one polymer chain (the widely accepted one); (b) the stabilization of many nanoclusters by one polymer chain

Steric stabilization by polymers has several distinct advantages over electrostatic stabilization [25]:

- *Relative insensitivity to the presence of electrolytes;* for instance, for 1:1 electrolytes ($I = z_+ z_- c$), a charge-stabilized dispersion will not be stable and coagulate when the concentration of electrolytes exceeds the 10⁻¹ M limit. The dimensions of polymer chains display no such dramatic sensitivity and sterically stabilized dispersions are relatively insensitive to the presence of electrolyte.
- *Equal efficacy in both aqueous and nonaqueous dispersion media;* charge stabilization is less effective in nonaqueous dispersion media than it is in aqueous media. This is primarily due to the low relative dielectric constant (<10) of most

nonaqueous media. In contrast, steric stabilization is effective in both nonaqueous media and aqueous media.

- *Equal efficacy at both high and low solids content*; in charge stabilization in nonaqueous media, the thickness of the double layers can be so large, (due to the low dielectric constant of the dispersion medium), that the mere preparation of high solids dispersions forces the particles too close together which then leads to coagulation. In aqueous dispersion media, the preparation of charge-stabilized particles at high solids dispersions is often difficult because of the gel formation induced by the interactions between the double layers surrounding each particle.
- *Reversibility of flocculation*; the coagulation of charge-stabilized particles (induced by the addition of electrolyte) is usually irreversible by subsequent dilution. In contrast, flocculation of sterically stabilized dispersions (induced by the addition of a nonsolvent for the stabilizing moieties) can usually be reversed spontaneously by mere dilution of the nonsolvent concentration to a suitably low value. This difference is due to the fact that sterically stabilized dispersions may be thermodynamically stable while charge stabilized dispersions are only thermodynamically metastable. As a consequence, for charge stabilized dispersions, the coagulated state represents a lower energy state and the coagulation can be reversed only after input of work into the system.
- Another crucial consequence of the thermodynamic stability of sterically stabilized dispersions is that they can + which is very important for catalytic applications.

Another source of colloidal stabilization, *electrosteric stabilization*, is the combination of electrostatic and steric stabilization like as in the use of long-chain alkyl ammonium cations and surfactants [26]. This kind of stabilization is generally provided by means of ionic surfactants. These compounds bear a polar head group able to generate an electrical double layer and a lyophobic side chain able to provide steric repulsion (Figure 7). The electrosteric stabilization can be also obtained from polyoxoanions such as the couple ammonium (Bu_4N^+)/polyoxoanion ($\text{P}_2\text{W}_{15}\text{Nb}_3\text{O}_{62}^{9-}$).

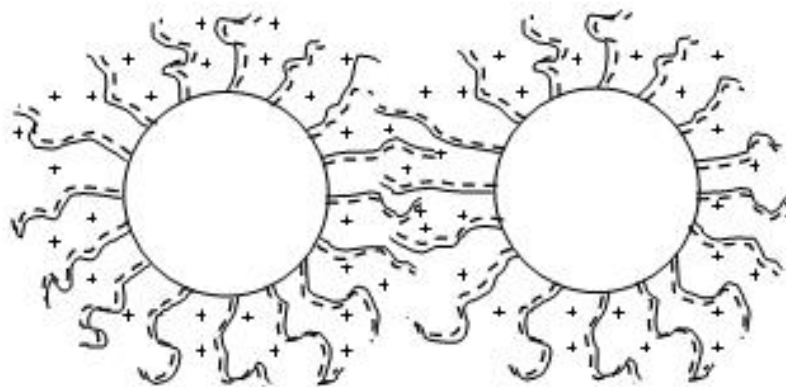


Figure 7. The schematic representation of the electrosteric stabilization of transition metal nanoclusters.

1.1.2. Preparation of Transition Metal Nanoclusters

Transition metal nanoclusters can be obtained via so called ‘*top down methods or physical route*’ e.g., by the mechanical grinding of bulk metals and subsequent stabilization of the resulting nanosized particles by the addition of colloidal protecting agents [27]. However, the top-down approach yields poor dispersions where the particle size distribution is very broad typically larger (>10 nm) and not reproducibly prepared giving irreproducible catalytic activity [28]. The most widely used approach is the so called ‘*bottom-up methods or chemical route*’. In the bottom up methods, the nanoclusters are prepared via wet chemical techniques, through which the nucleation and growth of metallic atoms take place. The bottom-up approach provides more convenient ways to control the size of the particles than top down methods and it includes following synthetic methods: (i) chemical reduction of transition metal complexes [29] including electrochemical pathways, (ii) thermolysis [30] including photolytic and sonochemical pathways [31], (iii) Ligand reduction and ligand displacement from organometallics [32].

(i) ***Chemical reduction of transition metal complexes:*** the reduction of transition metal salts in solution is the most widely accomplished method for the generation of colloidal metal nanoparticles. All chemical based synthetic routes to

nanosized metal particles start with the reduction of positively charged metal atoms, either as simple ions or as centers of complexes in solution [4]. Solvents can vary from water to very nonpolar media depending on the nature of the metal salt or the complex used. In aqueous systems, the reducing agent must be added or generated in situ, but in non-aqueous systems the solvent and reducing agent can be one and the same [16]. The kind of reducing agent is determined on the nature of metal compound. A wide range of reducing agents have been used to obtain colloidal materials, gas such as hydrogen or carbon monoxide, hydrides or salts such as sodium borohydride or sodium citrate, or even oxidizable solvents such as alcohols [33].

(ii) **Thermolysis:** this technique is based on the thermal decomposition of many organometallic compounds of transition metals to their respective metals under relatively mild conditions, these compounds provide a rich source of nanoparticle precursors. The method is widely applicable. The thermolysis of carbonyl-containing complexes of rhodium, iridium, ruthenium, osmium, palladium, and platinum in polymer solutions has been used to prepare polymer-stabilized colloidal metals with particle sizes in the range 1-10 nm, possibly by decomposition of polymer-bound organometallic intermediates [34].

(iii) **Ligand reduction and ligand displacement from organometallics:** reduction of metal can be carried out prior to colloid preparation, giving a zerovalent metal complex as the immediate colloid precursor. The synthesis of metal carbonyls and their subsequent thermolysis in nanoparticles synthesis is an example of this approach. The zero-valent palladium and platinum complexes with dibenzylideneacetone $\text{Pd}(\text{dba})_2$ and $\text{M}_2(\text{dba})_3$ ($\text{M} = \text{Pd}, \text{Pt}$) have been known since 1970 to react under mild conditions with either hydrogen or carbon monoxide with the formation of metal [35].

Among the preparation methods mentioned above, the chemical reduction of transition metal salts is the most convenient route to prepare the transition metal nanoclusters in the laboratory conditions as it provides reproducible syntheses of the nanoclusters in size of 1-10 nm with a well defined surface composition and size control [3,16].

1.1.3. Characterization of Transition Metal(0) Nanoclusters

The characterization of metallic nanoclusters is a complex task since many aspects have to be considered as the structures of metal nanocluster depend on many parameters such as: composition, preparation method, heat treatments, environmental variables, supports and so on. The properties of colloidal metal nanoclusters that are of interest include size, structure and composition. In order to entirely understand the physico-chemical behaviour of metal nanoclusters and their properties, many complementary techniques have to be used to figure out the many parameters involved [36]. The most widely used and essential technique for the characterization of nanoparticles is transmission electron microscopy (TEM) and high resolution transmission electron microscopy (HRTEM) which provide direct visual information of the size, dispersity, structure and morphology of nanoparticles. In this technique, a high voltage electron beam passes through a very thin sample, and the sample areas that do not allow the passage of electrons form an image to be presented. Thanks to the advancements in electronics, computers and cameras, the image of heavy atoms in nanoparticle sizes and shapes are easily imaged with modern high voltage instruments having resolution up to 0.08-0.05 nm. Other commonly used methods for the characterization of metal nanoparticles can be summarized as follows: (i) *UV-Visible spectroscopy*; the reduction of metal precursors and the formation of the metal nanoclusters in the presence of a stabilizer can be followed nicely [37]. Such observations done by UV-Vis spectroscopy depend on the disappearing of an absorption of the metal precursor and growing of a new absorption feature for the nanoclusters [38]. (ii) *X-ray photoelectron spectroscopy (XPS)*; is a semi-quantitative technique used for the determination of the surface chemical properties of the materials. The oxidation state of the metal atom on the surface of metal nanoclusters can be determined via XPS which is very important issue in heterogeneous catalysis [39]. (iii) *X-ray diffraction*; probes the average crystallographic structure in samples and allow, through an accurate analysis of diffraction line shape, the extraction of relevant information relating to crystallite size, crystallographic defects as well as compositional and chemical inhomogenities [40]. To a less extent the following methods are used for the characterization of metal nanoparticles: scanning electron

microscopy (SEM), infrared spectroscopy (IR), elemental analysis (ICP-OES), energy dispersive spectroscopy (EDS), nuclear magnetic resonance spectroscopy (NMR), extended X-ray absorption fine structure (EXAFS), scanning tunneling microscopy (STM), atomic force microscopy (AFM). An overall picture of the methods most commonly used in the characterization of metal nanoparticles are given in Figure 8 [41].

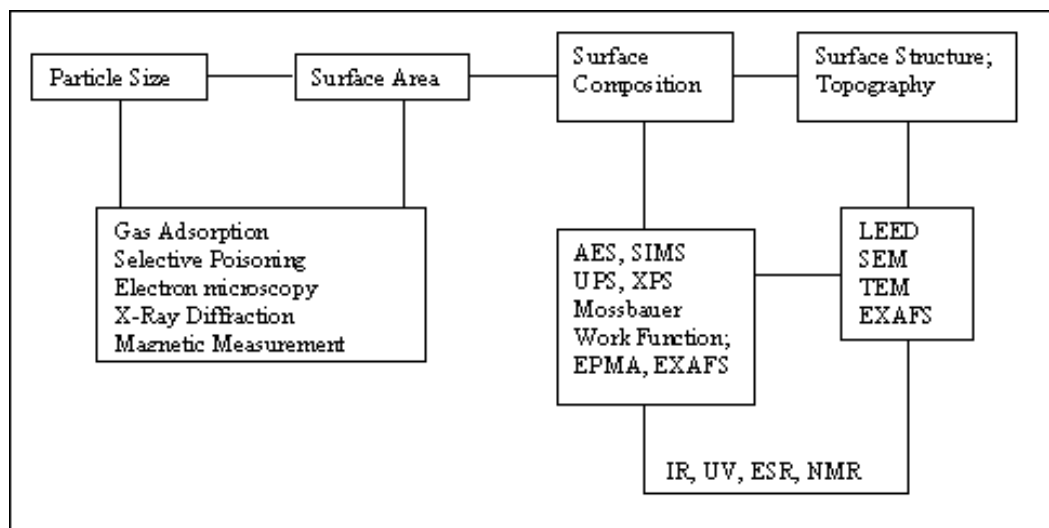


Figure 8. The methods most commonly used in the characterization of metal nanoparticles

1.1.4. Applications of Transition Metal Nanoclusters

Transition metal nanoclusters are of considerable current interest, both fundamentally and for their possible applications in catalysis, in nanobased chemical sensor, as light emitting diodes, in ‘quantum computers’ or other molecular electronic devices. There are also additional possible applications of nanoclusters: as ferrofluids for cell separations or in optical, electronic, or magnetic devices constructed via a building block ‘bottoms-up’ approach. However, our main interest has been focused on the synthesis, characterization of transition metal(0) nanoclusters and their applications in catalysis [37]. For this reason, the following

chapter of this dissertation will give brief information about the general principles of catalysis and the use of transition metal nanoclusters as catalyst.

CHAPTER 2

CATALYSIS

2.1. General Principles of Catalysis

A *catalyst* is a substance that makes a reaction go faster, without being stoichiometrically consumed in the process. The phenomenon occurring when a catalyst acts is termed *catalysis*. Because the catalyst is not consumed in the process, each catalyst molecule can take part in many repeated cycles, so we need only a small amount of catalyst relative to substrate. There are many types of catalyst ranging from the proton, through the lewis acids, organometallic complexes, organic or inorganic polymers, enzymes and so on. However, to simplify things, the catalysis can be divided into three main categories; (i) *heterogeneous catalysis*, (ii) *homogeneous catalysis*, and (iii) *biocatalysis* as shown in Figure 9.

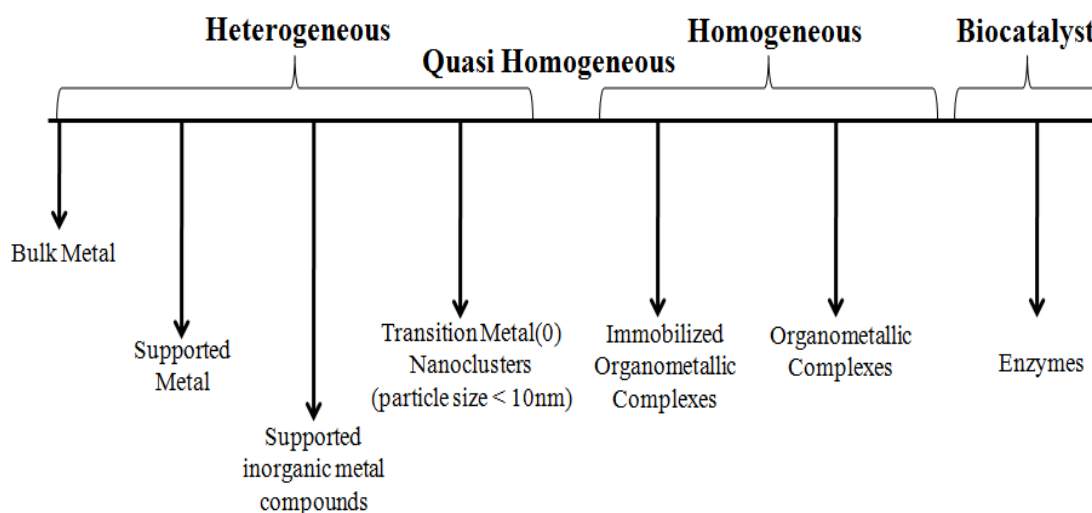


Figure 9. The classification of catalysts [42].

The classification of homogeneous and heterogeneous catalysis depends on existence of catalyst in the same phase as the substrate or not. In homogeneous catalysis, the catalyst is in the same phase as the reactants and products. Many homogeneous catalysts are transition metal atom which is stabilized by a ligand. The ligands are usually organic molecules that attach to the metal atom. The properties of such a homogeneous catalyst can be altered by changing the type of ligand.

In heterogeneous catalysts are those that act in different phase than substrates. In heterogeneous catalysis, the reactants diffuse to the catalyst surface (generally metal surface) and adsorb onto it, via the formation of chemical bonds. After reaction, the products desorb from the surface and diffuse away. For solid heterogeneous catalysts, the surface area of the catalyst is critical since it determines the availability of catalytic sites. Heterogeneous catalysis is of paramount importance in many areas of the chemical and energy industries. Most catalytic processes are heterogeneous in nature, typically involving a solid catalyst and gas- or liquid-phase reactants. Today, the majority of the industrial processes involve heterogeneous catalysis [43], because of their advantages such as easy separation of reaction products, reusability, stability, low-cost and low-toxicity [44]. Heterogeneous catalysis has attracted Nobel prizes for Fritz Haber and Carl Bosch in 1918, Irving Langmuir in 1932, and Gerhard Ertl in 2007 and other e.g. Ziegler-Natta etc. However, heterogeneous catalysts often tend to require high temperatures and pressures and they have low selectivity compared to homogeneous catalysts.

The biocatalysis is rather special case, somewhere between homogeneous and heterogeneous catalysis. The biocatalyst is generally an enzyme- a complex protein that catalyzes the reactions in living cells [45]. They are not only the highly efficient catalyst that they can catalyze the 1000 catalytic cycles in one second but also very selective catalysts.

Catalysts increase the rate of reaction by providing an alternative mechanism involving a different transition state and lower activation energy that is called as transition-state theory. In the transition-state theory, the entropy of activation in a catalyzed reaction will usually be less than in corresponding uncatalyzed reaction because the transition state is immobilized on the catalyst surface with consequent loss of translational freedom. There must therefore be a corresponding decrease in

the enthalpy of activation to compensate for this, or to overcompensate for efficient catalysis. Thus, according to the theory the activation energy for a catalyzed reaction ought to be less than for the same uncatalyzed reaction (Figure 10). Consequently, more molecular collisions have the energy needed to reach the transition state. Hence, catalysts can enable reactions that would otherwise be blocked or slowed by a kinetic barrier. However, the apparent activation energy (E_a^{apparent}) term is generally used for the activation energy of a catalytic reaction go on many steps because there are many ways to product side in this type of reactions and so there are many rate constants (k_{app}) affect by temperature. The E_a^{apparent} is the combination of these rate constants. Catalysts do not change the extent of a reaction: they have no effect on the chemical equilibrium of a reaction because the rate of both the forward and the reverse reaction are both affected. If a catalyst does change the equilibrium, then it must be consumed as the reaction proceeds, and thus it is also a reactant. The activity of a catalyst can also be described by the turnover number (or TON) and the catalytic efficiency by the turnover frequency (TOF).

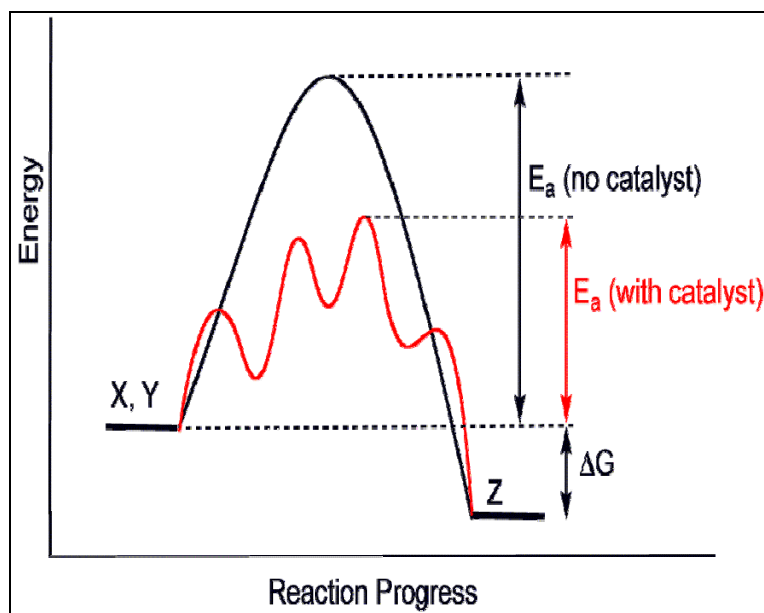


Figure 10. Generic potential energy diagram showing the effect of a catalyst in a hypothetical exothermic chemical reaction $X + Y$ to give Z . The presence of the catalyst opens a different reaction pathway (shown in red) with a lower activation energy. The final result and the overall thermodynamics are the same.

2.2. Key Definitions in Catalysis

The catalytic lifetime of a catalyst is usually expressed as *total turnover number (TTON)* which equals to the number of moles of product per mole of catalyst Eq. (1); this number indicates the number of total catalytic cycles before deactivation of the active catalyst in a given process.

$$\text{TTON} = \frac{\text{mole of product}}{\text{mole of catalyst}} \quad (1)$$

The *turnover frequency, N*, is often used to express the efficiency of a catalyst. For the conversion of A to B catalyzed by Q and with a rate v , Eq.(2);



the turnover frequency is given by the Eq. (3), ($|Q|$ is mole of the catalyst)

$$N = \frac{v}{|Q|} \quad (3)$$

Selectivity; is another important parameter that should be considered in the evaluation of the performance of any catalyst. A selective catalyst yields a high proportion of the desired product with minimum amount of the side products. High selectivity plays a key role in industry to reduce waste, to reduce the work-up equipment of a plant, and to ensure a more effective use of the feedstocks.

2.3. Enhancement of Catalytic Activity by Decreasing the Particle Size in Heterogeneous Catalysis

As mentioned earlier part of the dissertation, from macroscale to nanoscale there exists a considerable change in the intrinsic properties of materials. One of the best example for these changes is the increasing activity of the heterogeneous catalyst by the reduction of particle size as the activity of heterogeneous catalysts is directly related to surface area [46]. Of particular interest, metal nanoclusters exhibit

unusual surface morphologies and possess more reactive surfaces, hereby open a new perspective in the surface chemistry. For these reasons, they opened a great potential in catalysis because of their large surface area. The resultant huge surface areas of them dictate that many of the atoms lie on the surface, thus allowing a good ‘atom economy’ in surface-gas, surface-liquid, or even surface-solid reactions [47].

Transition metal nanoclusters have a high percentage of surface atoms and they do not necessarily order themselves in the same way that those in bulk do. As an illustrative example Klabunde and co-workers calculated the percentage of surface iron atoms on spherical iron(0) nanoclusters depending on their size (Figure 11).

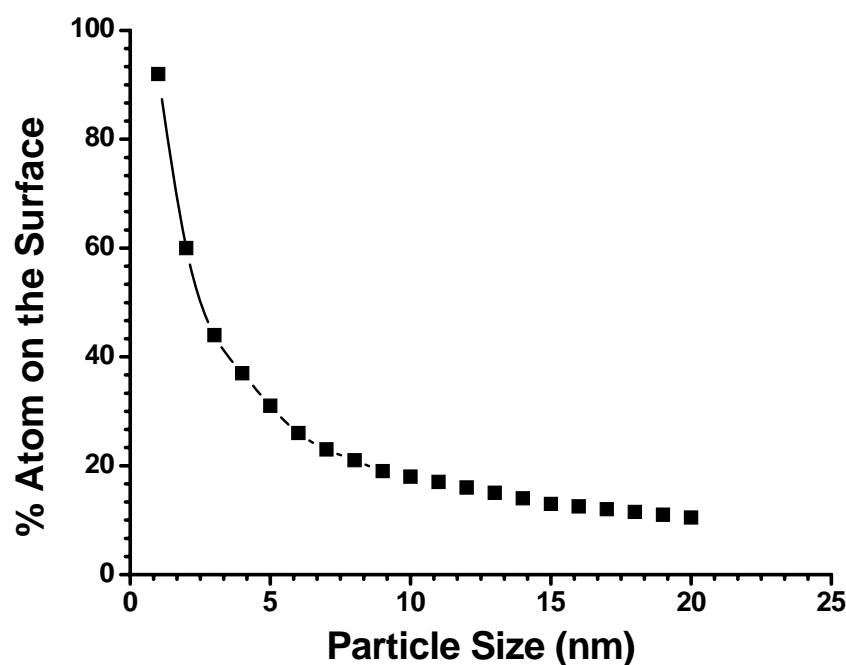


Figure 11. The change in percentage of surface iron atoms depending on the size of iron(0) nanoclusters [48].

The increasing proportion of surface atoms with decreasing particle size, compared with bulk metals, makes metal nanoclusters more active catalysts than their bulk counterparts, as surface atoms are the active centers for catalytic elementary processes. Among the surface atoms, those sitting on the edges and

corners are more active than those in planes. Metal clusters which have a complete, regular outer geometry are designated full-shell, or ‘magic number’, clusters. Many nanocluster distributions center around one of these full-shell geometries. Each metal atom has the maximum number of nearest neighbors, which imparts some degree of extra stability to full-shell clusters. Note that as the number of atoms increases, the percentage of surface atoms decreases as illustrated in Figure 12.






Full-Shell "Magic Number" Clusters					
Number of shells	1	2	3	4	5
Number of atoms in cluster	M ₁₃	M ₅₅	M ₁₄₇	M ₃₀₉	M ₅₆₁
Percentage surface atoms	92%	76%	63%	52%	45%

Figure 12. The relation between the total number of atoms in full shell clusters and the percentage of surface atoms [49].

Among the chemical properties of transition metal nanoclusters discussed above, catalysis is of great interest because of their high surface to volume ratio and a unique combination of reactivity, stability, and selectivity.

CHAPTER 3

HYDROGEN ECONOMY

3.1. Hydrogen as an Energy Carrier

Currently more than 80 % of the world energy supply comes from fossil fuels, resulting in strong ecological and environmental impacts [50]. Besides the exhaustion of reserves and resources, air pollution and modification of the atmospheric composition, with their impacts on climate and on human health, are now of primary importance. Greenhouse gas emissions, especially CO₂ produced by the combustion of fossil fuels, are in the centre of the environmental concerns. Moreover, fuel supply security is a serious concern, particularly for the transportation sector. A variety of efficient end-use technologies and alternative energy sources such as solar, wind, hydropower energy have been proposed to help address future energy-related environmental and/or supply security challenges in fuel use. However, besides their relatively high cost, energy production from renewable sources has the problem of discontinuity; for example, solar or wind energy is not always available. The obvious solution to this predicament is the energy storage. In this context, hydrogen appears to be the best energy carrier as it has an abundant and secure source, clean, renewable, and widely available from diverse sources [51]. Hydrogen is the simplest and lightest of all chemical elements and the most spread in the universe. It is not a primary source of energy as it occurs only in nature in combination with other elements, primarily with oxygen in water and with carbon, nitrogen and oxygen in living materials and fossil fuels. However when split from these other elements to form molecular hydrogen, it becomes an environmentally

attractive fuel. It can be burned or combined with oxygen in a fuel cell without generating CO₂, producing only water. Hydrogen can be made from widely available primary energy sources including natural gas, coal, biomass, wastes, solar, wind, hydro, geothermal or nuclear power, enabling a more diverse primary supply for fuels. Hydrogen can be used in fuel cells and internal combustion engines with high conversion efficiency and essentially zero tailpipe emissions of green house gases and air pollutants. If hydrogen is made from renewables, nuclear energy, or fossil sources with capture and sequestration of carbon, it would be possible to produce and use fuels on a global scale with nearly zero full fuel cycle emissions of green house gases and greatly reduced emissions of air pollutants. Technologies for hydrogen production, storage and distribution exist, but need to be adapted for use in an energy system. Building a new hydrogen energy infrastructure would be expensive and involves logistical problems in matching supply and demand during a transition. Hydrogen technologies such as fuel cells, and zero-emission hydrogen production systems are making rapid progress, but technical and cost issues remain before they can become economically competitive with today's vehicle and fuel technologies.

3.2. Hydrogen Storage: A Big Challenge in Hydrogen Economy

Storage of hydrogen is clearly one of the key challenges to the transition of the world into hydrogen economy because high-pressure and cryogenic hydrogen storage systems are impractical for mobile applications due to safety concerns and volumetric constraints [52]. In this regard, various kinds of solid materials for hydrogen storage such as metal hydrides [53], metal organic frameworks [54], nanostructures [55] and chemical compounds [56] have been investigated. Among the solid state hydrogen storage materials, chemical hydrogen storage materials, due to their high hydrogen contents, are one of the best promising hydrogen sources for fuel cells applications at ambient conditions (Figure 13) [57].

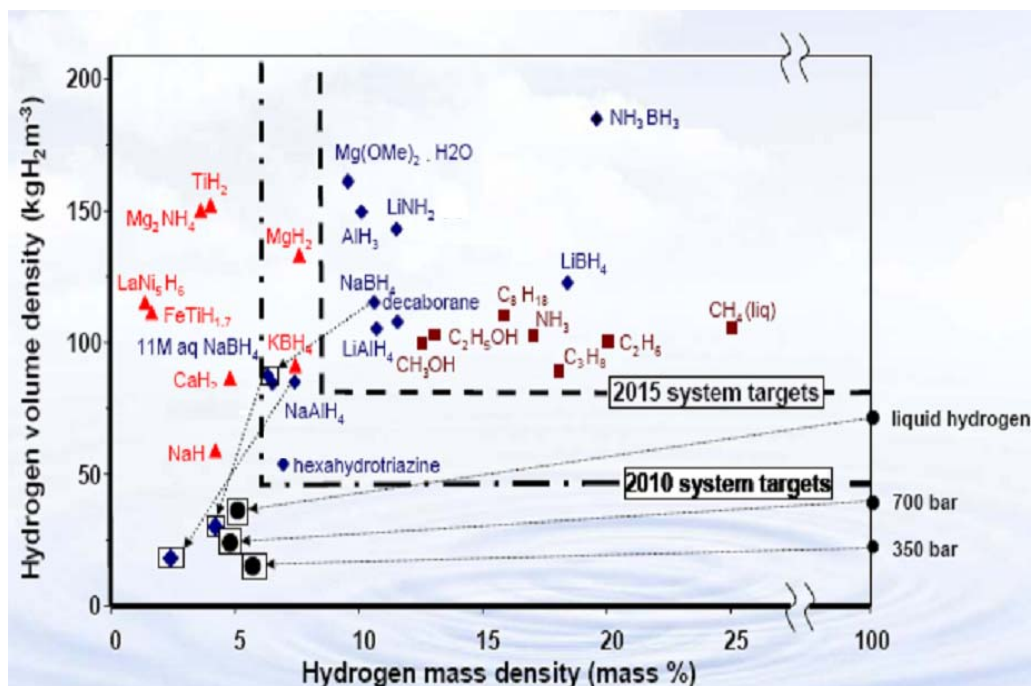


Figure 13. Hydrogen mass density versus hydrogen volume density of many compounds considered to be a chemical hydrogen storage material [57].

Recently, much attention has been paid to hydrogen generation from the hydrolysis of sodium borohydride (NaBH_4) that can theoretically release very high hydrogen content of 10.3 wt % [58] at room temperature, respectively. NaBH_4 is stable in alkaline solution; however, hydrolysis in the presence of a suitable catalyst generates hydrogen gas in the amount twice its hydrogen content and also water-soluble sodium metaborate, NaBO_2 , at moderate temperature [59] Eq. (4). By this way hydrogen can be generated safely for the fuel cells.



Catalytic hydrogen gas generation from NaBH_4 solutions has many advantages: NaBH_4 solutions are nonflammable, the reaction products are environmentally benign, rate of H_2 generation is easily controlled, the reaction product NaBO_2 can be recycled, H_2 can be generated even at low temperatures. Such a hydrolysis of NaBH_4 can be accelerated by catalysts [60], by acid [61], or under elevated temperature [62].

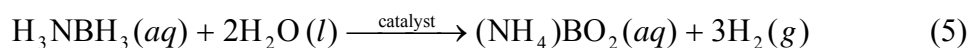
This reaction occurs to some extent even without a catalyst if the solution $\text{pH} < 9$. However to increase the shelf life of NaBH_4 solutions (and to prevent H_2 gas from being slowly produced upon standing), NaBH_4 solutions are typically maintained as a strongly alkaline solution by adding NaOH . The key feature of using a catalyzed reaction to produce H_2 is that H_2 generation in alkaline ($\text{pH} > 14$) NaBH_4 solutions occurs only when these solutions contact selected heterogeneous catalysts. Without a catalyst, strongly alkaline NaBH_4 solutions do not produce appreciable H_2 . This reaction is extremely efficient on a weight basis, since out of the 4 moles of H_2 that is produced, half comes from NaBH_4 , and the other half from H_2O . The reaction is exothermic, so no energy input is needed to generate H_2 .

The only other product of reaction, sodium metaborate (in solutions with $\text{pH} > 11$ the predominant solution product is sodium tetrahydroxyborate $\text{NaB}(\text{OH})_4$), is water soluble and environmentally innocuous. Since the hydrolysis of NaBH_4 is completely inorganic reaction and does not contain sulfur, it produces virtually no fuel poisons such as sulfur compounds, carbon monoxide, soot, or aromatics. Therefore this reaction is considerably safer, more efficient, and more easily controllable than producing H_2 by other chemical methods [59]. The heat generated by the reaction 75 kJ/mole H_2 formed is considerably less than typical > 125 kJ/mole H_2 , produced by reacting other chemical hydrides with water [63]. This promises a safer and more controllable reaction.

More recently, ammonia–borane (AB, H_3NBH_3) complex, which is formed through a dative bond in which the lone pair of the NH_3 interacts with empty p_z orbital of boron in BH_3 , is identified as one of the leading candidates as a solid state hydrogen reservoir owing to its high hydrogen content (19.6 wt%), high stability under ordinary fuel cell reaction conditions and nontoxicity [64]. AB is isoelectronic to ethane; however, the physical properties are very different. AB is synthesized by facile methods for laboratory-scale preparation. The combination of ammonium salts with borohydrides (salt metathesis) gives AB in a high yield [65]. AB is a tetragonal white crystal at room temperature with a melting point of > 110 °C, having a staggered conformation with a B–N bond distance of 1.564(6) Å, B–H bond distance of 0.96(3)–1.18(3)Å, and N–H bond distance of 0.96(3)–1.14(2)Å [66]. The solid state structure exhibits short BH/HN intermolecular contacts; the hydridic

hydrogen atoms on boron are 2.02 Å away from the protic hydrogen atoms on nitrogen of an adjacent molecule, a distance less than the Van der Waals distance of 2.4 Å, implying an interaction constituting a dihydrogen bond [67]. The stability conferred by the dihydrogen bonding (ca. 90.4 kJ mol⁻¹) contributes to the existence of AB as a solid under standard conditions.

Hydrogen stored in the AB complex can be released through either pyrolysis or solvolysis route. Experimental results have revealed that hydrogen release of only 6.5 wt % of the initial mass was obtained upon thermal decomposition of AB at 385 K and the release of more hydrogen from AB requires much higher temperatures (> 500 °C) [68]. In contrast, the rapid hydrogen generation rate can be obtained via catalytic hydrolysis of AB [69]. The hydrolysis of AB in the presence of a suitable catalyst provides 3 moles of hydrogen per mole of AB at room temperature Eq. (5).



In this dissertation, water soluble polymer stabilized transition metal(0) (metal : Ni, Co and Ru) nanoclusters were developed as catalyst in hydrogen generation from the hydrolysis of NaBH₄ and AB. The kinetics of hydrogen generation from both catalytic hydrolysis reactions were studied depending on catalyst concentration, substrate concentration and temperature as well as the activation parameters (Arrhenius activation energy (E_a), activation enthalpy (ΔH[‡]) and activation entropy (ΔS[‡]) of both catalytic hydrolysis calculated from the kinetic data.

3.3. The Motivation of the Dissertation

As mentioned in the previous sections, the stabilization of transition metal(0) nanoclusters in solution is of great importance to obtain stable nanocluster with controllable size to their potential applications in many fields, including catalysis. In my MS thesis [70], we reported the ‘Synthesis and characterization of hydrogenphosphate stabilized nickel(0) nanoclusters as catalyst for the hydrolysis of sodium borohydride’. However, hydrogenphosphate stabilized nickel(0) nanoclusters showed low catalytic lifetime as determined by measuring the total turnover number

(TTON = 1450) for the hydrolysis of sodium borohydride which can be attributed to the weak electrostatic stabilization of nanoclusters. The electrostatic interactions become weaker at high pH which is a requirement for the hydrolysis of sodium borohydride for application of safe hydrogen generation in fuel cells [71]. Therefore, a stronger stabilizer such as polymer is needed to prevent agglomeration of nickel(0) nanoclusters in aqueous solution at high pH medium, acting as catalyst in the hydrolysis of sodium borohydride. The use of polymeric matrix as stabilizer improves some properties of the nanoclusters such as the solubility, thermal stability and catalytic activity [72]. A variety of preparative methods is available for obtaining polymer-stabilized metal nanoclusters [73]. The most widely used synthetic method involves the reduction of the metal ions in solution to its colloidal metal in zerovalent state within the polymer medium, followed by coalescence of the polymer onto the nanoclusters [74]. Polymers possessing a hydrophobic backbone and hydrophilic side groups, such as vinyl addition homopolymers, are frequently employed as a stabilizer for the metal nanoclusters in polar solvents. By considering the advantages of polymer stabilization, we developed a facile method for the preparation of PVP stabilized metal(0) (Ni, Co and Ru) nanoclusters from the reduction of metal chlorides by sodium borohydride in methanol solution at reflux conditions [75]. Compared to the hydrogenphosphate-stabilized nickel(0) nanoclusters [70], PVP stabilized nickel(0) nanoclusters were much more stable, and catalytically more active providing 8700 total turnovers in the hydrolysis of NaBH₄ over 27 hours at ambient temperatures. PVP stabilized cobalt(0) and ruthenium(0) nanoclusters were also showed very high activity and stability in hydrogen generation from the hydrolysis of NaBH₄. After obtaining such good results with PVP stabilized nickel(0), cobalt(0) and ruthenium(0) nanoclusters in the hydrolysis of NaBH₄, their catalytic applications were extended to hydrolysis of AB which is recently considered as the best candidate for chemical hydrogen storage.

In the second part of the dissertation, we aimed to prepare polymer stabilized transition metal(0) nanoclusters in the catalytic reaction medium by considering the difficulties in the separation processes of a catalyst that generally results in a significant loss of catalyst. In this regard, for the first time, poly(4-styrene sulfonic acid-co-maleic acid), PSSA-co-MA, stabilized nickel(0), cobalt(0) and ruthenium(0)

nanoclusters were in situ generated during the hydrolysis of AB. The PSSA-co-MA stabilized nickel(0), cobalt(0) and ruthenium(0) nanoclusters showed much better activity than PVP stabilized ones and most of the catalyst system tested in the hydrolysis of AB.

As a summary, in this dissertation, we present our detailed study on the synthesis and characterization of water soluble polymer stabilized nickel(0), cobalt(0) and ruthenium(0) nanoclusters as catalyst in hydrogen generation from the hydrolysis of NaBH_4 and AB.

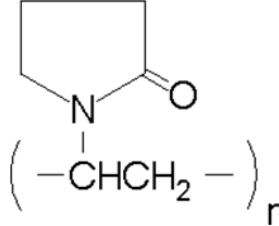
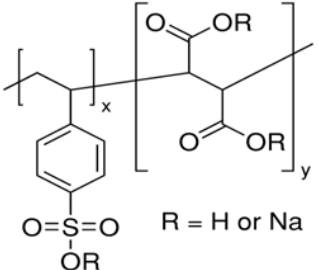
CHAPTER 4

EXPERIMENTAL

4.1. Materials

Nickel(II) chloride hexahydrate (> 98%), cobalt(II) chloride hexahydrate (> 97%), ruthenium(III) chloride hydrate ($\text{RuCl}_3 \cdot x\text{H}_2\text{O}$), sodium borohydride (NaBH_4 , 98%), borane-ammonia complex (H_3NBH_3 , AB, >97%), poly(N-vinyl-2-pyrrolidone) (PVP-40, average molecular weight 40.000), poly(styrene sulfonic acid-co-maleic acid) sodium salt, poly(2-ethyl-2-oxazoline), poly(ethylene glycol), poly(diallyldimethyl ammonium chloride), poly(acrylic acid), sodium hydroxide, D_2O and $\text{BF}_3(\text{C}_2\text{H}_5)_2\text{O}$ were purchased from Aldrich®, methanol (acetone free) were purchased from Riedel-De Haen AG Hannover, and mercury was purchased from Merck, and used as received. Deionized water was distilled by water purification system (Milli-Q system). All glassware and Teflon coated magnetic stir bars were cleaned with acetone, followed by copious rinsing with distilled water before drying in an oven at 150 °C.

Table 1. IUPAC names, chemical structures, average molecular weights and the abbreviations of the polymer used for the stabilization of nickel(0), cobalt(0) and ruthenium(0) nanoclusters in this dissertation.

IUPAC Name	Chemical Structure	Average Mw (g.mol ⁻¹)	Abbreviation
Poly(N-vinyl-2-pyrrolidone)		40000	PVP
Poly(4-styrene sulfonic acid-co-maleic acid)		20000	PSSA-co-MA

4.2. Preparation and Characterization of PVP stabilized Transition Metal(0) (Metal: Ni, Co and Ru) Nanoclusters

4.2.1. Preparation of PVP stabilized Nickel(0), Cobalt(0) and Ruthenium(0) Nanoclusters

PVP stabilized nickel(0), cobalt(0) and ruthenium(0) nanoclusters were prepared by using our own developed method which is the modified version of alcohol reduction method [76]. In a typical procedure for the synthesis of PVP stabilized nickel(0) or cobalt(0) nanoclusters, in 250 mL three-necked round bottom flask, 200.0 mg (0.9 mmol) of NiCl₂.6H₂O or CoCl₂.6H₂O and 499.0 mg (4.5 mmol monomer unit) of PVP-40 were dissolved in 50 mL of methanol (mol PVP/ mol nickel or cobalt = 5). The mixture of metal precursor (NiCl₂.6H₂O) or (CoCl₂.6H₂O) and polymer (PVP-40) in methanol was refluxed for one hour. Then, 10 mL of 300 mM solution of sodium borohydride (3.0 mmol = 116.0 mg NaBH₄) was added into metal-polymer mixture immediately after the reflux. The abrupt color change from

pale green for nickel and purple for cobalt to dark brown indicates that the formation of PVP stabilized nickel(0) or cobalt(0) nanoclusters was completed. Methanol was removed from the solution by evaporation in a rotavap (Heidolph Laborata-4000) and washed with ethanol several times. PVP stabilized nickel(0) or cobalt(0) nanoclusters in solid form were collected from the residue after evaporation in the round bottom flask.

The same procedure described above for the synthesis of PVP stabilized nickel(0) or cobalt(0) nanoclusters was also followed for the synthesis of PVP stabilized ruthenium(0) nanoclusters, but the amount of the reagents used were as following: 84.0 mg (0.4 mmol) of $\text{RuCl}_3 \cdot x\text{H}_2\text{O}$ and 222.0 mg (2 mmol monomer unit) of PVP-40 were dissolved in 50 mL of methanol (mol PVP/ mol Ru = 5).

4.2.2. Characterization of PVP stabilized Nickel(0), Cobalt(0) and Ruthenium(0) Nanoclusters

TEM analysis: The samples used for the TEM experiments were harvested from the preparation of PVP stabilized metal(0) nanoclusters solution as described above: 5 mL aliquot of PVP stabilized metal(0) nanoclusters solution in methanol was transferred into a clean screw-capped glass vial with a disposable polyethylene pipette. The colloidal solution was deposited on the silicon oxide coated copper TEM grid by immersing the grid into the solution for 5 seconds and then evaporating the volatiles from the grid under inert gas atmosphere. This sample on the grid was then sealed under N_2 and sent to Dr. JoAn Hudson at Clemson University for TEM analysis with a Hitachi H7600T TEM instrument operating at 120 kV. Samples were examined at magnification between 100 and 600k.

X-Ray photoelectron spectroscopy (XPS): X-ray photoelectron spectra of PVP stabilized transition metal(0) nanoclusters were taken at the Middle East Technical University Central Laboratory using SPECS spectrometer equipped with a hemispherical analyzer and using monochromatic Mg- $K\alpha$ radiation (1250.0 eV, the X-ray tube working at 15 kV and 350 W) and pass energy of 48 eV. To better access the metal core in the sample by scraping off the polymer matrix from the surface, the sample surface was bombardment by argon ion by passing 3000 eV energy for 3

minutes for two times. Peak fittings were done according to Gaussian function by using Origin 8.0 program.

UV-Visible Spectroscopy: The reduction of corresponding precursor metal salts and the formation of metal(0) nanoclusters in the presence of PVP were followed by UV-Visible spectroscopy. UV-Vis electronic absorption spectra of precursor metal salts and PVP stabilized metal(0) nanoclusters were recorded in methanol solution on Varian-Carry100 double beam instrument.

X-ray Diffraction: XRD patterns were obtained on a Bruker AXS D8-Advanced diffractometer with Cu K α radiation ($\lambda = 1.5418 \text{ \AA}$) at Brown University, RI, USA.

FT-IR Spectroscopy: The FT-IR spectra of the PVP stabilized metal(0) nanoclusters having different PVP to metal ratio (5, 0.5, 0.1) and neat PVP were taken from KBr pellet on a Nicolet 510 FTIR Spectrophotometer using Omnic software.

NMR Spectroscopy: ^{11}B -NMR spectra were recorded on a Bruker Avance DPX 400 with an operating frequency of 128.15 MHz for ^{11}B .

4.2.3. Method for Testing the Catalytic Activity of PVP stabilized Nickel(0), Cobalt(0) and Ruthenium(0) Nanoclusters in The Hydrolysis of Sodium Borohydride and Ammonia Borane

The catalytic activity of PVP stabilized nickel(0), cobalt(0) and ruthenium(0) nanoclusters in the hydrolysis of NaBH_4 and AB was determined by measuring the rate of hydrogen generation. To determine the rate of hydrogen generation, the catalytic hydrolysis of NaBH_4 or AB were performed in Parr-5101 low-pressure reactor equipped with circulating water-bath for constant temperature control, and mechanical stirrer (Figure 14). The Parr-5101 low-pressure reactor was connected with a digital transmitter to a computer using RS-232 module. The progress of an individual hydrolysis reaction was followed by monitoring the increase in the pressure of hydrogen gas with the program Calgrafix. The temperature was also controlled via thermocouple within the reactor with the Calgrafix program. The pressure vs time data was processed using Microsoft Office Excel 2003 and Origin 8.0, and then converted into the values in the proper unit,

volume of hydrogen (mL). Before starting the catalytic activity test experiments, the reactor (300 mL) was thermostated at 25.0 ± 0.5 °C. In a typical experiment, 284.0 mg (7.5 mmol) NaBH_4 or 63.0 mg (2.0 mmol) H_3NBH_3 were dissolved in 40 mL and 20 mL water, respectively. The solution was transferred with a glass pipette into the reactor. Then, aliquots of aqueous solution of prepared PVP stabilized nickel(0), cobalt(0) or ruthenium(0) nanoclusters was transferred into the reactor using a 10 mL gastight syringe. The stirring rate of the mechanical mixer of reactor was set to 600 rpm.

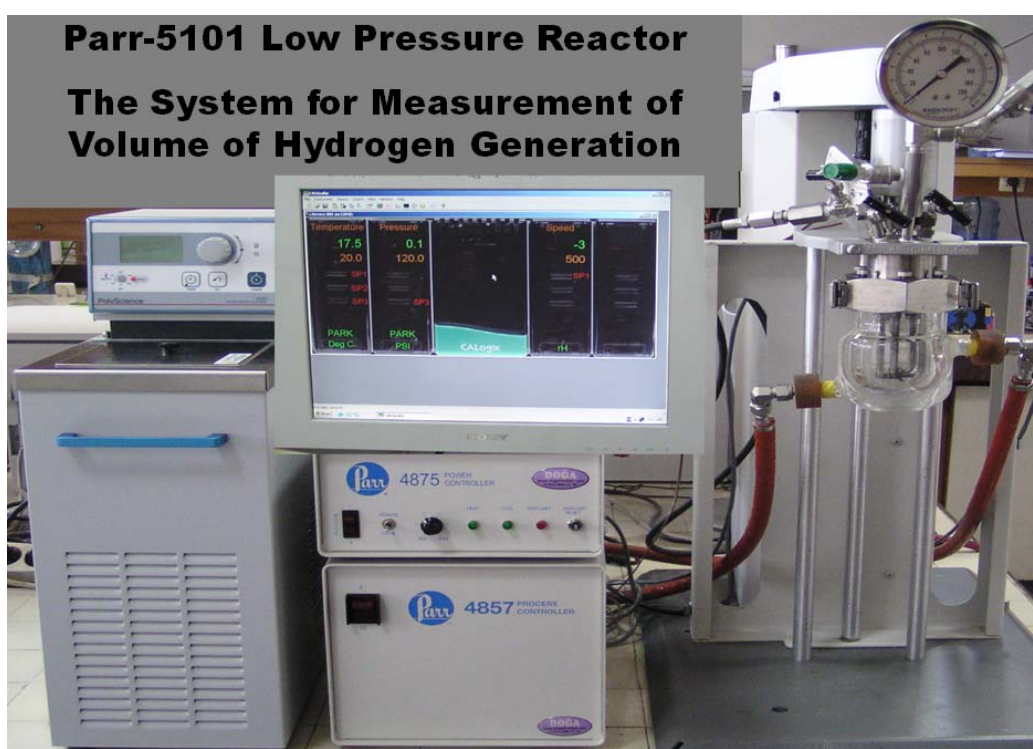


Figure 14. Parr-5101 Low pressure reactor system for measurement of volume of hydrogen generated from the catalytic hydrolysis of sodium borohydride or ammonia borane

4.2.4. Self Hydrolysis of Sodium Borohydride and Ammonia borane

In a 100 mL beaker, 284.0 mg NaBH_4 or 63.0 mg H_3NBH_3 were dissolved in 50 mL water, respectively. Then, the solution was transferred with a 50 mL pipette

into the reactor thermostated at 25.0 ± 0.5 °C. The experiment was started by closing the reactor and turning on the stirring at 600 rpm simultaneously, and the volume of hydrogen generated was measured exactly in the same way as described in the section 4.2.3.

4.2.5. Kinetic Study of Catalytic Hydrolysis Of Sodium Borohydride or Ammonia borane Catalyzed by PVP stabilized Nickel(0), Cobalt(0) and Ruthenium(0) Nanoclusters

In order to establish the rate law for catalytic hydrolysis of NaBH_4 and H_3NBH_3 in aqueous solution using PVP stabilized nickel(0), cobalt(0) and ruthenium(0) nanoclusters as catalyst, three different sets of experiments were performed for each of these two substrates in the same ways described in the section 4.2.3. The detailed kinetics of catalytic hydrolysis of NaBH_4 was also studied in basic medium for PVP stabilized nickel(0), cobalt(0) and ruthenium(0) nanoclusters. However, PVP stabilized nickel(0) nanoclusters were totally deactivated in the hydrolysis of NaBH_4 in basic medium. For this reason, the results of the kinetic studies on hydrogen generation from the hydrolysis of NaBH_4 in basic medium were given for PVP stabilized cobalt(0) and ruthenium(0) nanoclusters.

4.2.5.1. Effect of PVP Concentration On The Catalytic Activity Of Nickel(0), Cobalt(0) and Ruthenium(0) Nanoclusters

In order to study the effect of PVP concentration on the catalytic activity of nickel(0), cobalt(0) and ruthenium(0) nanoclusters in the hydrolysis of NaBH_4 (150 mM) or AB, catalytic activity tests were performed starting with metal(0) nanoclusters synthesized having different PVP/Metal ratio (5, 10, 20, 30, 40) at 25.0 ± 0.5 °C. In all the experiments the total volume of solution was kept constant at 50 mL. All the experiments were performed in the same way as described in the section 4.3.3. The good stability and the highest activity of PVP stabilized metal(0) nanoclusters in the hydrolysis of NaBH_4 was obtained at PVP to metal molar ratio of 5. Thus, the PVP to metal ratio of 5, was selected for the further kinetic experiments.

4.2.5.2. Kinetics of Hydrolysis of Sodium Borohydride Catalyzed by PVP stabilized Nickel(0), Cobalt(0) and Ruthenium(0) Nanoclusters

In the first set of experiments, the concentration of the NaBH₄ was kept constant at 150 mM and the catalyst concentration was varied in the range of (1.00, 1.20, 1.40, 1.60, 1.80, 2.00 mM) for nickel, (0.50, 1.00, 1.50, 2.00 and 2.50 mM) for cobalt and (0.25, 0.35, 0.45, 0.55, 0.65 mM) for ruthenium. In the second set of experiments, the catalyst concentrations were held constant at 1.40 mM for nickel, 1.50 mM for cobalt, and 0.45 mM for ruthenium and NaBH₄ concentration was varied in the range of 150-900 mM. Finally, the catalytic hydrolysis of NaBH₄ was performed in the presence of the PVP stabilized nickel(0), cobalt(0) and ruthenium(0) nanoclusters at constant NaBH₄ (150 mM) and catalyst concentration (1.40 mM for Ni, 1.50 mM for Co and 0.25 mM for Ru) at various temperatures in the range of 15-40 °C in order to obtain the activation energy (E_a), enthalpy (ΔH^\ddagger), and entropy (ΔS^\ddagger).

Catalytic Life time experiment: A lifetime experiment was started with a 50 mL solution of PVP stabilized nickel(0), cobalt(0) or ruthenium(0) nanoclusters (1.0 mM for Ni, 1.0 mM for Co, and 0.25 mM for Ru) and 1 M NaBH₄ at 25.0 ± 0.5 °C. A new batch of 1.9 g NaBH₄ was added into the reaction solution after all of the conversion of sodium borohydride present in the solution completed by checking the stoichiometric volume of hydrogen. Hydrolysis of NaBH₄ was continued until hydrogen gas evolution was slowed down to the level of self hydrolysis. The volume of hydrogen versus time data were corrected by subtracting the self hydrolysis data of NaBH₄ in order to obtain the volume of hydrogen generated only from the catalytic reaction.

4.2.5.3. Kinetics of Hydrolysis of Ammonia Borane Catalyzed by PVP stabilized Nickel(0), Cobalt(0) and Ruthenium(0) Nanoclusters

In the first set of experiments, the hydrolysis reaction was performed starting with different initial concentration of the PVP stabilized nickel(0), cobalt(0) and ruthenium(0) nanoclusters in the range of (1.0, 1.5, 2.0, 2.5, 3.0 mM) for nickel, (1.0, 1.5, 2.0, 2.5, 3.0 mM) for cobalt and (0.1, 0.2, 0.3, 0.4, 0.5 mM) for ruthenium by

keeping the initial AB concentration constant at 100 mM. The second set of experiments were performed by keeping the initial concentration of PVP stabilized nickel(0), cobalt(0) and ruthenium(0) nanoclusters constant at 2 mM for nickel, 2 mM for cobalt and 0.3 mM for ruthenium varying the AB concentration in the range of 50-500 mM. Finally, the catalytic hydrolysis of AB was performed in the presence of PVP stabilized nickel(0), cobalt(0) and ruthenium(0) nanoclusters at constant substrate (100 mM) and catalyst concentration (2 mM for Ni, 2 mM Co and 0.1 for Ru) at various temperatures in the range of 15-40 °C in order to obtain the activation energy (E_a), enthalpy (ΔH^\ddagger), and entropy (ΔS^\ddagger). In addition to the volumetric measurement of the hydrogen evolution, in each experiment the conversion of ammonia borane to ammonium metaborate was also checked by comparing the intensities of signals of AB and metaborate anion at $\delta = -23.9$ and 9 ppm, respectively, in the ^{11}B -NMR spectra of the solution.

Catalytic Life time experiment: Lifetime experiment was started with a 20 mL solution containing PVP stabilized nickel(0), cobalt(0) or ruthenium(0) nanoclusters (1 mM for Ni, 1 mM for Co and 0.1 mM for Ru) and 1 M H_3NBH_3 at 25.0 ± 0.5 °C. A new batch of 310.0 mg H_3NBH_3 was added into the reaction solution after all conversion of ammonia borane present in the solution was completed.

4.3. PSSA-co-MA stabilized Nickel(0), Cobalt(0) or Ruthenium(0) Nanoclusters

4.3.1. In Situ Generation of PSSA-co-MA Stabilized Nickel(0), Cobalt(0) or Ruthenium(0) Nanoclusters and Concomitant Hydrogen Generation from the Hydrolysis of Ammonia Borane

Both the in situ generation of PSSA-co-MA stabilized nickel(0), cobalt(0) or ruthenium(0) nanoclusters and the catalytic hydrolysis of AB were performed in the same medium. In a typical procedure for in situ generation of PSSA-co-MA stabilized ruthenium(0) nanoclusters and concomitant hydrolysis of AB, a jacketed reaction flask (50 mL) containing a Teflon-coated stir bar was placed on a magnetic stirrer (IKA[®] RCT Basic) and thermostated to 25.0 ± 0.5 °C by circulating water

through its jacket from a constant temperature bath (Polyscience). Then, a graduated cylinder glass tube filled with water was connected to the reaction flask to measure the volume of the hydrogen gas to be evolved from the reaction (Figure 15). Next, desired amount of AB and PSSA-co-MA were dissolved in 15 mL water and transferred with a glass-pipette into the reaction flask. Then, 5 mL aliquot of 2.8 mM ruthenium(III) chloride was transferred into the reaction flask using a 10 mL gastight syringe and the solutions were stirred at 1200 rpm. The initial concentrations of AB, ruthenium were 100 mM AB and 0.7 mM Ru. Molar ratio of AB to metal precursors greater than 100 was used to ensure complete reduction of Ru^{3+} to its zero oxidation state and to observe the catalytic hydrolysis of AB at the same time. A fast color change from corresponding color of metal precursor solutions to dark brown was observed which indicates the formation of ruthenium(0) nanoclusters. However, in the case of PSSA-co-MA stabilized nickel(0) or cobalt(0) nanoclusters, the use of sodium borohydride was found to be necessary for the reduction of nickel(II) chloride or cobalt(II) chloride to their metallic state because no reduction and hydrogen generation were observed by performing the catalytic hydrolysis reaction only in the presence of AB under the same conditions. For this reason, a minimum amount of NaBH_4 (5.0 mg) were added into the reaction solution at the beginning to initiate the reduction of nickel(II) chloride or cobalt(II) chloride. The extended procedure for in situ preparation of PSSA-co-MA stabilized nickel(0) or cobalt(0) nanoclusters can be given as following: a mixture of sodium borohydride (NaBH_4 , 5.0 mg), AB (62.0 mg) and optimum amount of PSSA-co-MA was dissolved in 15 mL water in a jacketed reaction flask (40 mL) containing a Teflon-coated stir bar placed on a magnetic stirrer and thermostated to 25.0 ± 0.5 °C by circulating water through its jacket from a constant temperature bath (PolyScience). Then, a graduated cylinder filled with water was connected to the reaction flask to measure the volume of the hydrogen gas to be evolved from the reaction. Next, 5 mL aliquots of 2.0 mM nickel(II) chloride or 2.0 mM cobalt(II) chloride were transferred into the reaction flask using a 10 mL gastight syringe and the solutions were stirred at 1200 rpm. The initial concentrations of AB, NaBH_4 , nickel or cobalt were 100 mM AB, 6 mM NaBH_4 , 0.5 mM Ni or 0.5 mM Co. A fast color change from the original color of the metal precursor solutions (green for nickel(II) chloride and pale purple for cobalt(II)

chloride) to dark brown was observed indicating the formation of nickel(0) or cobalt(0) nanoclusters. When the nanoclusters formation was completed (within less than 1 minute) the catalytic hydrolysis was started and followed by monitoring the volume of hydrogen gas evolved. The volume of hydrogen gas evolved was measured by recording the displacement of water level with certain time intervals at constant pressure. The reaction was stopped when no more hydrogen evolution was observed. The control tests using acid/base indicator showed no detectable amount of ammonia evolution in our experiments due to the short reaction times and mild reaction conditions.

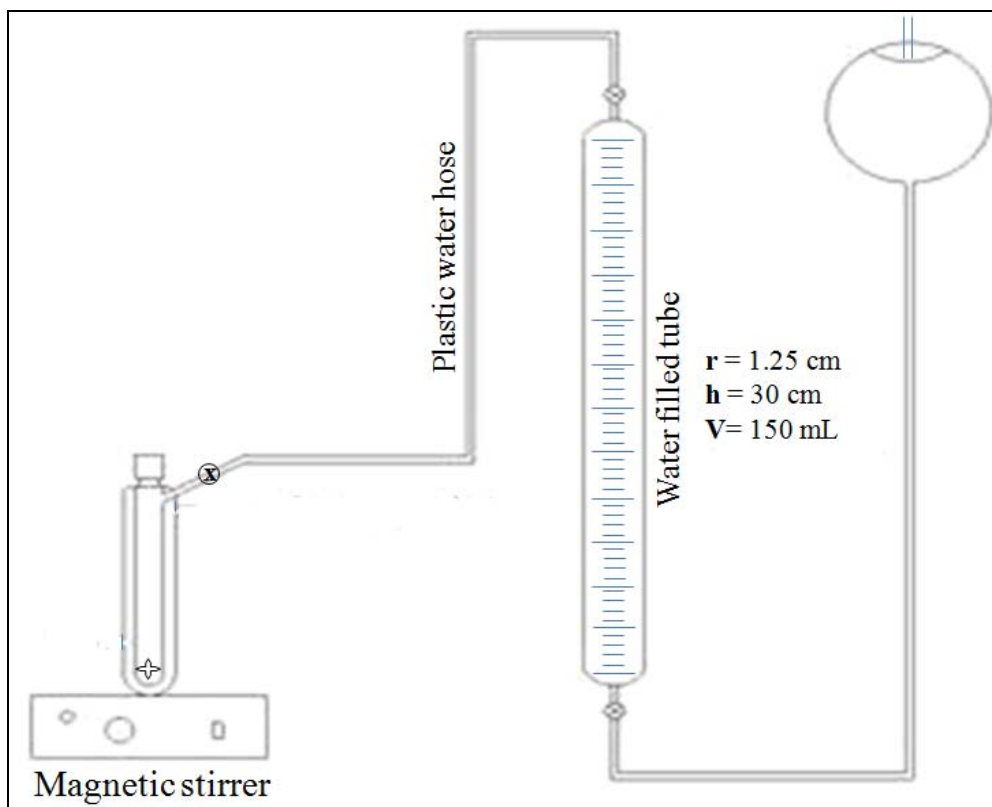


Figure 15. The experimental setup used in performing the catalytic hydrolysis of ammonia borane and measuring the hydrogen generation rate.

4.3.2. Characterization of In Situ Generated PSSA-co-MA Stabilized Nickel(0), Cobalt(0) or Ruthenium(0) Nanoclusters

The TEM images were obtained using a JEM-2010 (JEOL) TEM instrument operating at 200 kV. The samples used for the TEM experiments were harvested from the polymer stabilized metal(0) nanoclusters solution as described in the section 4.4.1. The nanoclusters solution was centrifuged at 8000 rpm for 8 minutes. The separated nanoclusters were washed with ethanol to remove the excess polymer and other residuals. Then, the nanoclusters sample was redispersed in 5 mL water. One drop of the colloidal solutions were deposited on the silicon oxide coated copper grid and evaporated in a vacuum under inert atmosphere at 50 °C. Samples were examined at magnifications between 100 and 600k. Particle size of the nanoclusters is calculated directly from the TEM image by counting non-touching particles. Size

distributions are quoted as the mean diameter \pm the Standard deviation. UV-Vis electronic absorption spectra of precursor metal salts and PSSA-co-MA stabilized metal nanoclusters were recorded in aqueous solution on Varian-Carry100 double beam instrument. XRD patterns were obtained on a Bruker AXS D8-Advanced diffractometer with Cu K α radiation ($\lambda = 1.5418 \text{ \AA}$). FT-IR spectra were recorded with a Bruker Bruker Vertex 70 spectrophotometer by an Attenuated Total Reflectance (ATR) module. For controlling conversion of AB at the end of the hydrolysis reaction, the resulting solutions were filtered and the filtrates were collected for ^{11}B -NMR analysis to check the conversion of AB to ammonium metaborate corresponds to signals at $\delta = -23.9$ and 9.3 ppm, respectively. ^{11}B -NMR spectra were recorded on a Bruker Avance DPX 400 with an operating frequency of 128.15 MHz for ^{11}B .

4.3.3. Kinetic Study of PSSA-co-MA Stabilized Nickel(0), Cobalt(0) and Ruthenium(0) Nanoclusters in Catalytic Hydrolysis of Ammonia Borane

4.3.3.1. Effect of PSSA-co-MA Concentration on the Catalytic Activity of Nickel(0), Cobalt(0) and Ruthenium(0) Nanoclusters

In order to study the effect of PSSA-co-MA concentration on the catalytic activity of nickel(0), cobalt(0) and ruthenium(0) nanoclusters in the hydrolysis of AB (100 mM), catalytic activity tests were performed at 25.0 ± 0.5 °C starting with various concentrations of PSSA-co-MA (0.5, 1, 1.5, 2, 2.5 and 5 mM corresponding to [PSSA-co-MA]/[Metal] ratio of 1, 2, 3, 4, 5, 10 for the in-situ generation of nickel or cobalt nanoclusters. In the case of ruthenium, 0.5, 1, 1.5, 2, 2.5, 5, 10, 15 mM PSSA-co-MA which are corresponds to [PSSA-co-MA]/[Ru] ratios of 1, 2, 3, 4, 5, 10, 20, 30 were used. In all experiments, the total volume of solution was kept constant at 20 mL. All the experiments were performed in the same way as described in the section 4.3.1.

4.3.3.2. Determination of Rate law and Activation Parameters for Hydrolysis of Ammonia Borane Catalyzed by PSSA-co-MA Stabilized Nickel(0), Cobalt(0) or Ruthenium(0) Nanoclusters

In order to establish the rate law for catalytic hydrolysis of AB catalyzed by in-situ-prepared PSSA-co-MA stabilized nickel(0), cobalt(0) or ruthenium(0) nanoclusters, three different sets of experiments were performed for each of these catalysts in the same way as described in the section 4.3.1.

In the first set of experiments, the concentration of AB was kept constant (100 mM) and nickel or cobalt concentration was varied in the range of 1.0 - 3.0 mM and ruthenium concentration 0.5-1.0 mM. In the second set of experiments, the catalysts concentrations were held constant at 2.0 mM Ni or 2.0 mM Co or 0.7 mM Ru while AB concentration was varied in the range of 50 - 300 mM. Finally, the catalytic hydrolysis of AB was performed in the presence of the PSSA-co-MA stabilized nickel(0) or cobalt(0) or ruthenium(0) nanoclusters at constant AB (100 mM) and catalyst concentration (2.0 mM Ni or 2.0 mM Co or 0.5 mM for Ru) at various temperatures in the range of 15-35 °C in order to obtain the activation energy (E_a), enthalpy (ΔH^\ddagger), and entropy (ΔS^\ddagger).

4.3.3.3. Determination of the Catalytic Lifetime of PSSA-co-MA Stabilized Nickel(0), Cobalt(0) or Ruthenium(0) Nanoclusters in the Hydrolysis of Ammonia Borane

The catalytic lifetime of PSSA-co-MA stabilized nickel(0), cobalt(0) or ruthenium(0) nanoclusters in the hydrolysis of AB were determined by measuring the total turnover number (TTON). Such a lifetime experiment was started with a 20 mL solution containing 0.5 mM Ni or 0.5 mM Co or 0.1 mM Ru and 500 mM AB at 25.0 ± 0.5 °C. After all conversion of added AB completed by checking stoichiometric H₂ gas evolution (3.0 mol H₂/mol H₃NBH₃), a new batch of 310.0 mg AB added and the reaction was kept on in this way until no hydrogen gas was evolved. The test reaction to check whether ammonia generation takes place during the TTON experiments or not was performed before addition of new batch of AB by using acid/base titration.

4.3.3.4. Quantification of the Liberated NH₃ Gas

The gas generated from the catalytic reaction was passed through 25 mL standardized solution of 0.001 M HCl at room temperature. After gas generation was ceased, the resulted solution was titrated with standard solution of 0.01 M NaOH by using phenolphthalein acid-base indicator. The quantity of the liberated ammonia gas was calculated from the difference between two HCl solutions before and after the reaction.

4.3.3.5. Mercury Poisoning as Heterogeneity Test for In situ Prepared PSSA-co-MA Stabilized Nickel(0), Cobalt(0) or Ruthenium(0) Nanoclusters

To determine whether the in-situ prepared PSSA-co-MA stabilized nickel(0), cobalt(0) or ruthenium(0) nanoclusters are acting as homogeneous or heterogeneous catalyst in the hydrolysis of AB, mercury poisoning experiments were carried out by adding mercury during the catalytic hydrolysis of AB and measuring the catalytic activity before and after addition. In a typical mercury poisoning experiment, firstly, PSSA-co-MA stabilized nickel(0), cobalt(0) or ruthenium(0) nanoclusters were prepared in-situ in the hydrolysis of AB, and then addition of mercury ($[\text{Hg}]/[\text{Ni}] = 200$, $[\text{Hg}]/[\text{Co}] = 150$, $[\text{Hg}]/[\text{Ru}] = 150$) into the nanoclusters solution including 0.5 mM Ni or 0.5 mM Co or 0.7 mM Ru in 20 mL of 100 mM AB solution at 25.0 ± 0.5 °C. The catalytic activity was measured by monitoring the rate of hydrogen generation before and after the addition of mercury.

CHAPTER 5

RESULTS AND DISCUSSIONS

5.1. Preparation and Characterization of PVP stabilized Transition Metal(0) (Metal: Ni, Co and Ru) Nanoclusters

PVP stabilized nickel(0), cobalt(0) and ruthenium(0) nanoclusters were prepared by using our own developed method which is a modified version of the alcohol reduction method [76]. In a typical alcohol reduction method, an alcohol (methanol, ethanol or propanol) is used as a mild reducing agent. It should be noted that the alcohol has a double function as a reducing agent and solvent in the method. The reduction of the metal precursor is usually performed at reflux temperatures. At reflux conditions, alcohols having α -hydrogen atoms are oxidized to the corresponding carbonyl compound (e.g., methanol to formaldehyde) and concomitant reduction of metal ion to its zerovalent state takes place [77]. Thus, the metal precursor is reduced in the presence of stabilizer (e.g., polymer) and stable metal(0) nanoclusters are formed. However, in the case of nickel(II) chloride, no reduction was observed after 4 hours reflux in methanol. Obviously, methanol is not a strong reducing agent for the nickel(II) precursors. Therefore, a stronger reducing agent, sodium borohydride, was added into the solution after reflux to reduce nickel(II) ions to zerovalent nickel. Upon addition of NaBH_4 , the color of the solution was immediately changed from pale green of the nickel(II) ion to dark brown of the nickel(0) nanoclusters. Prior to the reduction by sodium borohydride, a reflux of one hour was found to be necessary to obtain the nickel(0) nanoclusters. Most probably, this preheating of the solution leads to the initial complex formation of nickel(II) ion with the PVP stabilizer [78], which can subsequently be reduced to zerovalent metal

more easily. Our method is more suitable for the preparation of size controlled metal nanoclusters with a narrow particle size distribution because the injection of reducing agent into the hot coordinating solution results in the burst nucleation (the saturation of the solution with metal(0) atoms) and slow growth of the particles which are the desired process for the preparation of uniform nanoclusters [79]. However, in the case of alcohol reduction method, due to the slow nucleation step, many different nuclei are formed and the growth of the particles occurs nonuniformly. Our facile method is also applicable for the preparation PVP stabilized cobalt(0) and ruthenium(0) nanoclusters. The PVP stabilized water-soluble nickel(0), cobalt(0) and ruthenium(0) nanoclusters formed in this way were stable in solution. For example, no bulk metal formation was observed in solution standing for two weeks at room temperature under argon atmosphere. The PVP stabilized nickel(0), cobalt(0) and ruthenium(0) nanoclusters can be isolated as solid materials from solution by removing the volatiles in vacuum. The isolated nanoclusters were also stable in argon atmosphere for months. Furthermore, they were redispersible in water and yet catalytically active when redispersed in aqueous solution, for example, in the hydrolysis of NaBH_4 and AB (see later).

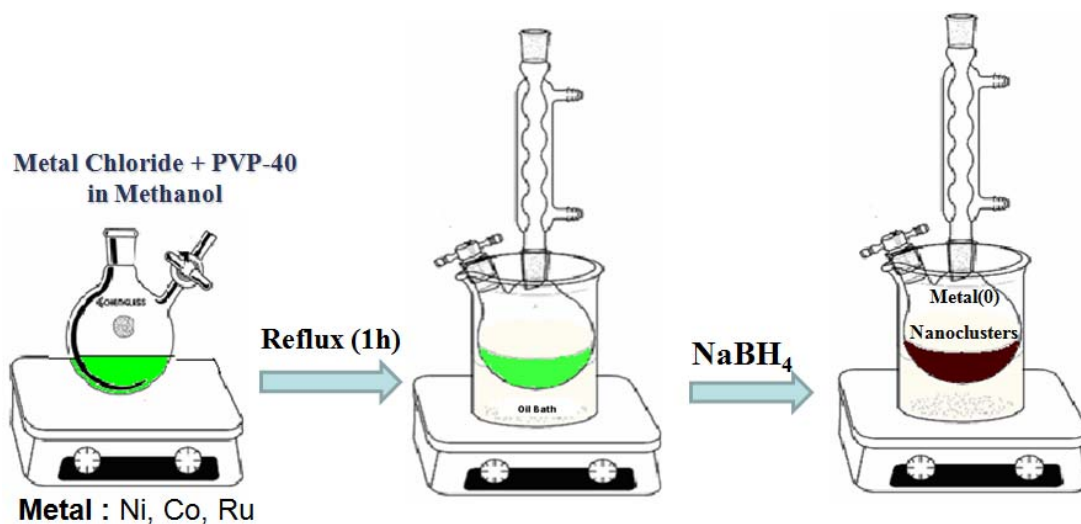


Figure 16. A schematic representation of the experimental setup used for the preparation of PVP stabilized transition metal(0) nanoclusters via our own developed method.

5.1.1. Characterization of PVP stabilized Nickel(0) Nanoclusters

The reduction of nickel(II) chloride and the formation of PVP stabilized nickel(0) nanoclusters were followed by UV-Vis spectroscopy. Figure 17 shows the UV-Visible electronic absorption spectra of a solution containing nickel(II) chloride and PVP in methanol before and after addition of NaBH₄. The d-d transition absorptions of nickel(II) chloride in methanol solution observed at 750 and 420 nm disappear after addition of NaBH₄ and a broad absorption continuum grows which is assigned to the characteristic surface plasmon resonance of the nickel(0) nanoclusters [38]. This observation indicates the reduction of nickel(II) to the metallic nickel and formation of particles in nanosize upon addition of NaBH₄.

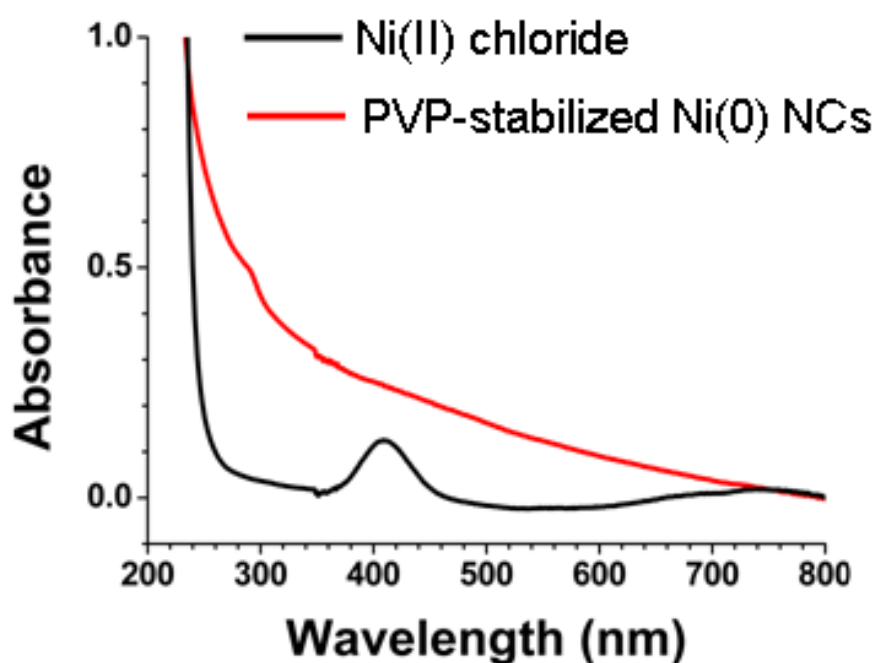


Figure 17. UV-Visible spectra of nickel(II) chloride and PVP stabilized nickel(0) nanoclusters taken from the methanol solutions.

Figure 18 shows the TEM image and the corresponding histogram of nickel(0) nanoclusters prepared from the reduction of nickel(II) chloride (8.4 mM) by NaBH₄ in the presence of PVP-40 (42 mM) after refluxing for one hour in methanol. The particle size histogram in Figure 18b was constructed by counting 200 non-touching particles in the TEM image. The particle size of the PVP stabilized

nickel(0) nanoclusters ranges from 2.0 to 6.0 nm with a mean value of 3.6 nm and a standard deviation of 1.6 nm (3.6 ± 1.6 nm). As clearly seen from the TEM image that PVP stabilized nickel(0) nanoclusters are well dispersed in methanol solution and there are no agglomerated particles.

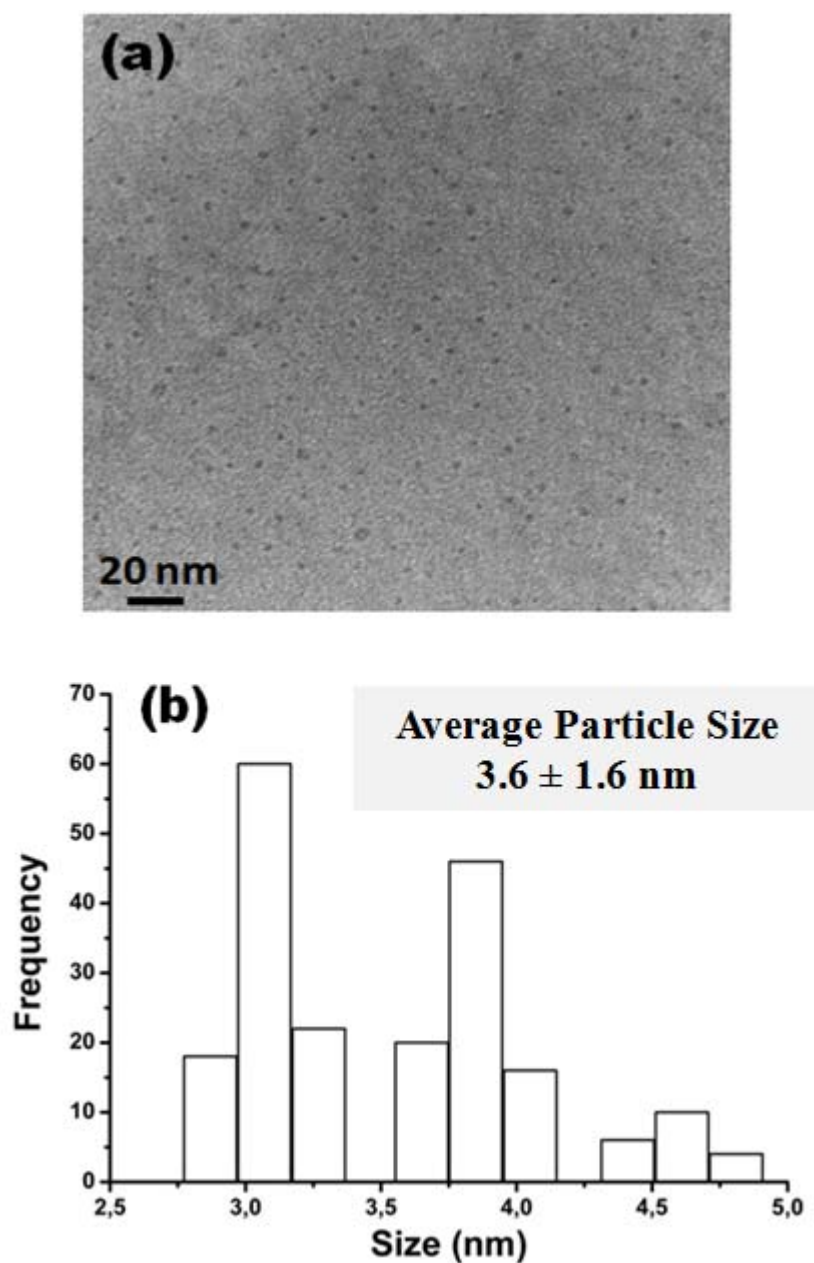


Figure 18. (a) TEM image and (b) associated histogram for PVP stabilized nickel(0) nanoclusters formed from the reduction of nickel(II) chloride in the presence of PVP by sodium borohydride after one hour reflux in methanol.

Figure 19a shows the XPS survey spectrum of PVP stabilized nickel(0) nanoclusters obtained from the reduction of nickel(II) chloride by NaBH_4 in the presence of PVP after refluxing for one hour in methanol solution indicating the presence of nickel with the other elements of the PVP (C, O, N). The XPS spectrum also shows two peaks for Si which most probably mixed to nanoclusters samples from mortar or glasswares during the sample preparation for XPS analysis. The high resolution XPS spectrum in Figure 19b exhibits essentially two bands at 852.5 and 869.9 eV which can be assigned to Ni(0) $2p_{3/2}$ and Ni(0) $2p_{1/2}$, respectively, by comparing with the values of bulk nickel (852.3 and 869.7 eV, respectively) [80]. The intensity of this spectral component significantly increases under argon ion bombardment (3000 eV for 3 minutes), indicating the metallic character of the Ni core in both samples. The ‘Hopping’ mechanism between Ni particles is responsible for the absence of relative energy shifts in these XPS spectra. Therefore, assays of the PVP stabilized nickel nanoclusters consist primarily of nickel in metallic state. The XPS spectrum shows two additional, slightly higher energy bands at 853.8 and 872.8 eV, though with relatively weak intensities. These bands can be attributed to Ni(II) $2p_{3/2}$ and Ni(II) $2p_{1/2}$, respectively. By taking the spectral data for NiO as reference, it is possible to assume that a small amount of NiO can also exist in both samples, presumably in the form of a very thin oxide coating around Ni cores. Ni(II) species might have been formed by oxidation during the XPS sample preparation, since the PVP stabilized nickel(0) nanoclusters are sensitive to aerobic atmosphere. Since the oxidation product may exist in different form depending on the ligand (hydroxide, oxo group or nitrogen donor), additional weak bands can be attributed to the different Ni(II) species.

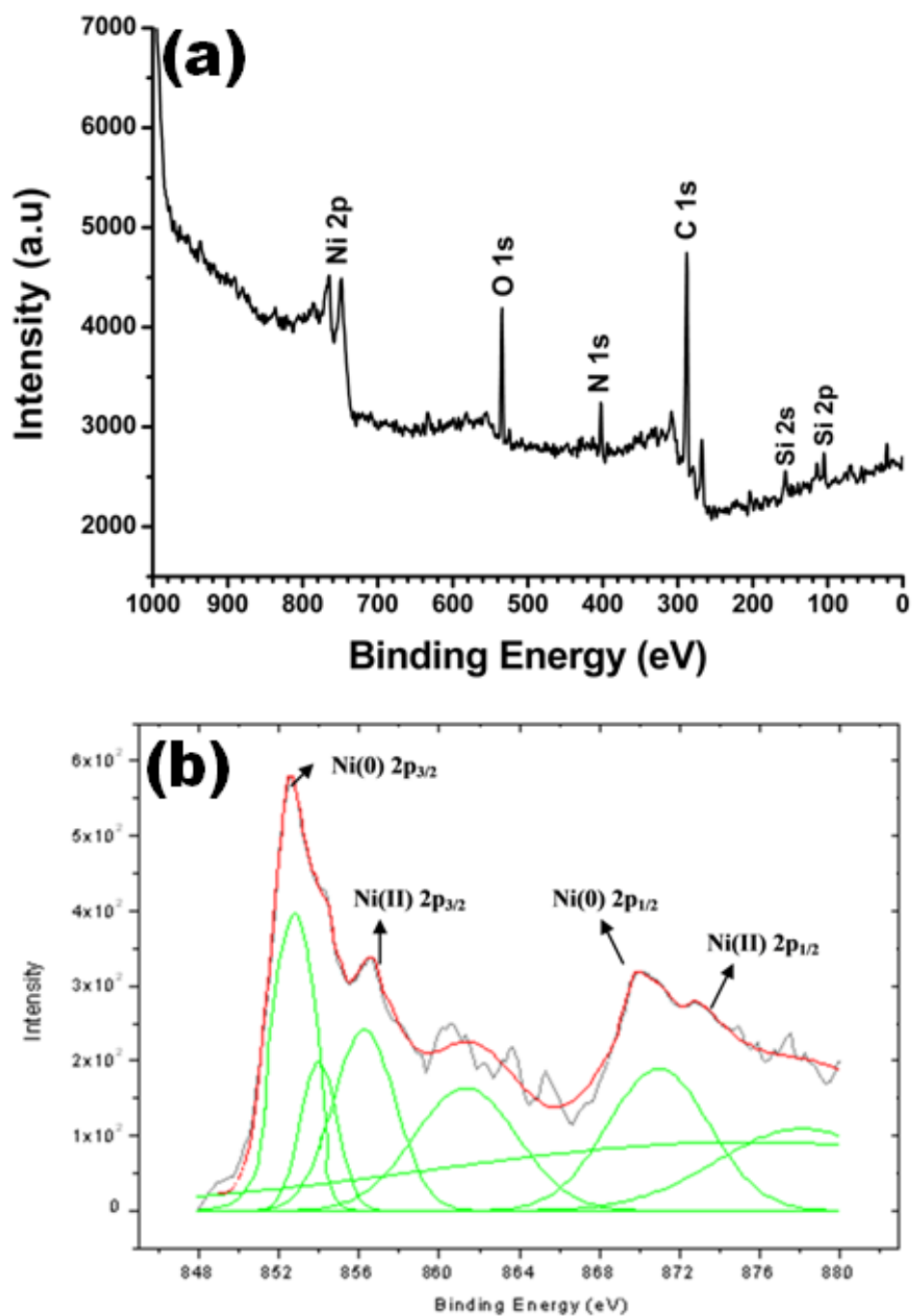


Figure 19. X-Ray photoelectron (a) survey (b) high resolution spectra of PVP stabilized nickel(0) nanoclusters formed from the reduction of nickel(II) chloride (8.4 mM) in the presence of PVP (42 mM) by sodium borohydride (300 mM) after one hour reflux in methanol.

The crystallinity of PVP stabilized nickel(0) nanoclusters were examined by powder X-ray diffraction. Figure 20 shows the the XRD pattern of isolated PVP stabilized nickel(0) nanoclusters after washing with ethanol and drying under inert atmosphere. There was no clear reflectance peak observed for PVP stabilized nickel(0) nanoclusters, which implies that the PVP stabilized nickel(0) nanoclusters were existed in mostly amorphous phase. However, the shoulders observed at $\approx 2\theta = 45^\circ$ and 60° indicates that powder sample of PVP stabilized nickel(0) nanoclusters contains small amount of nickel crystallized in face centered cubic structure. Considering the very broad peak observed at $\approx 2\theta = 35^\circ$ which is characteristic for polymers, we can conclude that the surface of the nickel(0) nanoclusters is mostly covered by PVP molecule in solid state.

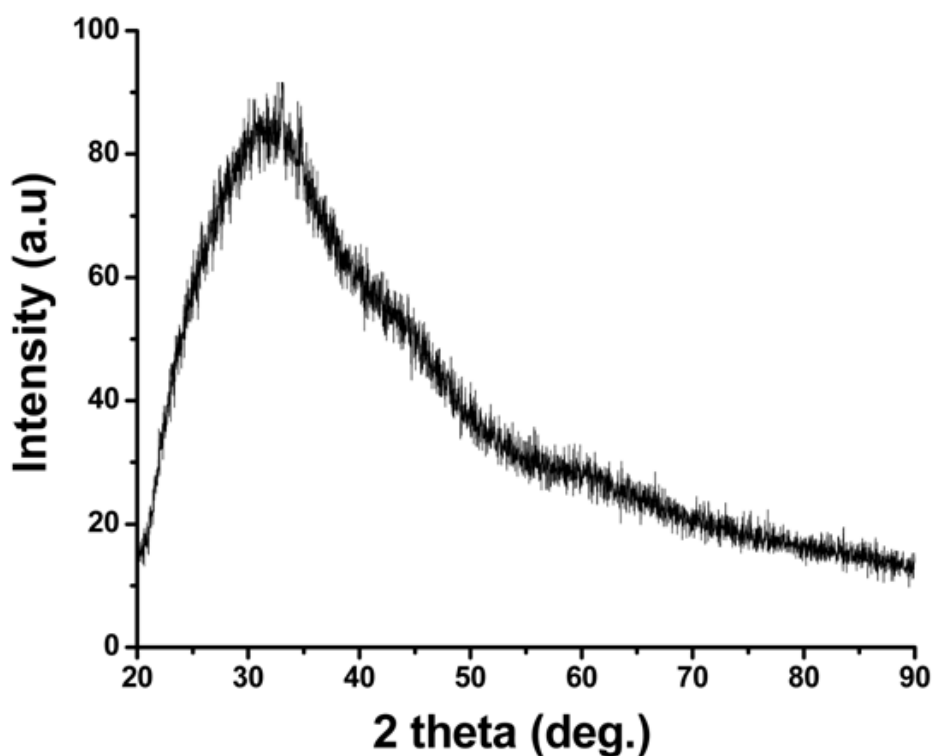


Figure 20. X-ray diffraction pattern of PVP stabilized nickel(0) nanoclusters

5.1.2. Characterization of PVP stabilized Cobalt(0) Nanoclusters

The as-prepared PVP stabilized cobalt(0) nanoclusters were stable in solution and no bulk metal formation was observed in solution standing for one week at room temperature in inert gas atmosphere. The PVP stabilized cobalt(0) nanoclusters can be isolated as dark-brown solid from the reaction mixture by removing the volatiles in vacuum. The isolated nanoclusters were stable in inert gas atmosphere for months. Furthermore, they were redispersible in water and yet catalytically active when redispersed in aqueous solution, for example, in the hydrolysis of NaBH_4 and AB (see later).

The morphology and particle size of the PVP stabilized cobalt(0) nanoclusters were studied by using TEM (Figure 21). The cobalt nanoclusters having particle size of 7.2 ± 2.1 nm were obtained as shown in the histogram (Figure 21b). As clearly seen from the TEM image that, PVP stabilized cobalt(0) nanoclusters are spherical in shape and highly dispersible in methanol solution.

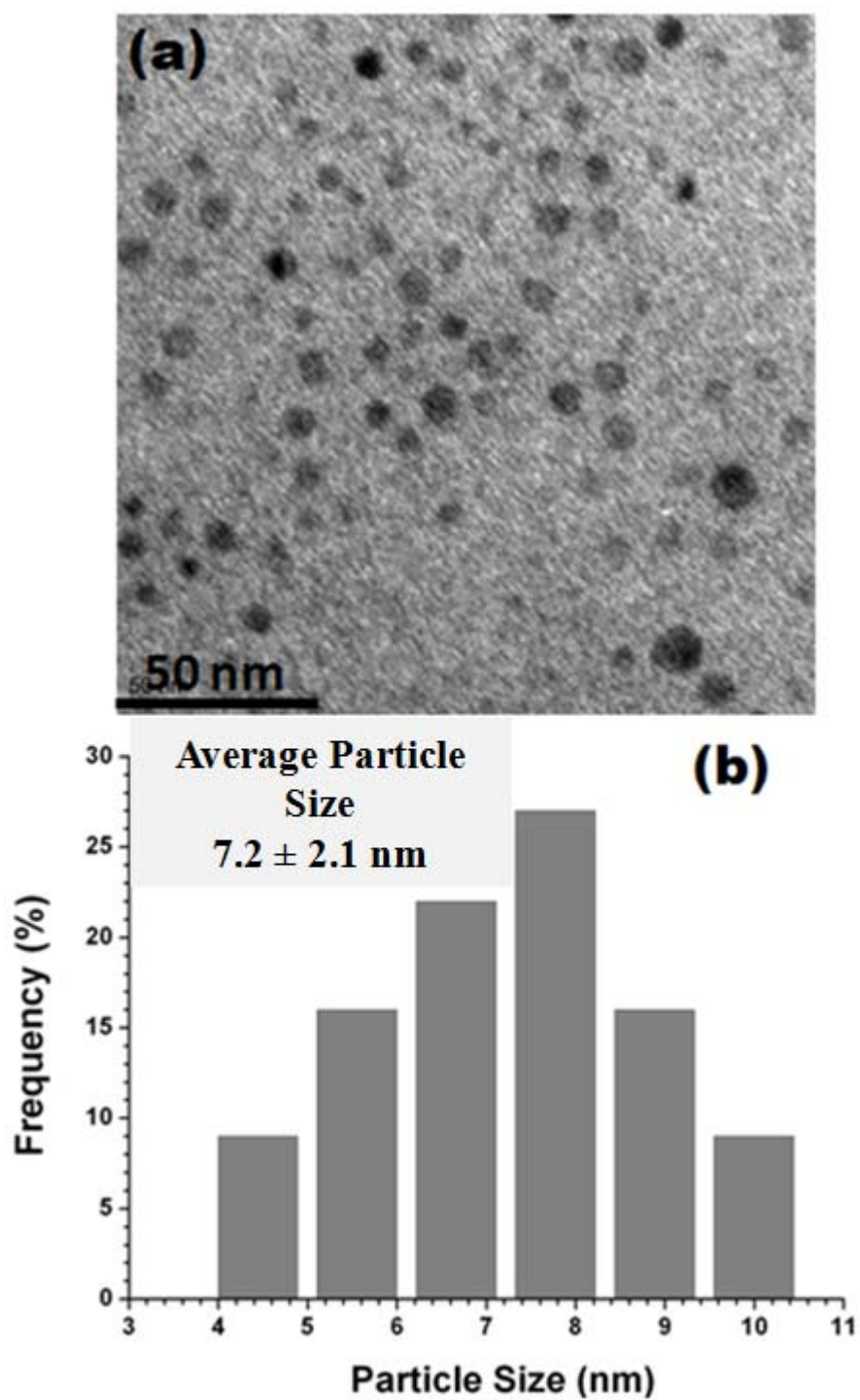


Figure 21. (a) TEM image and (b) associated histogram for PVP stabilized cobalt(0) nanoclusters sample isolated from the reduction of cobalt(II) chloride (8.4 mM) in the presence of PVP (42 mM) by sodium borohydride (150 mM) after one hour reflux in methanol.

Figure 22a shows the XPS survey spectrum of PVP stabilized cobalt(0) nanoclusters obtained from the reduction of cobalt(II) chloride by sodium borohydride in the presence of PVP after refluxing for one hour in methanol solution indicating the presence of cobalt with the other elements of the PVP (C, O, N). The high resolution XPS spectrum in Figure 22b exhibits two prominent bands at 778.6 and 794.2 eV, readily assigned to Co(0) 2p_{3/2} and Co(0) 2p_{1/2}, respectively, by comparing with the values of bulk cobalt [81]. However, there are two additional bands observed at 783.8 and 799.2 eV which can be attributed to a higher oxidation states of cobalt, presumably formed by oxidation during the XPS sample preparation, since the cobalt(0) nanoclusters are sensitive to aerobic atmosphere. Since the oxidation product may exist in different form depending on the ligand (hydroxide, oxo group or nitrogen donor), additional weak bands can be attributed to the different cobalt(II) species [82]. One particular aspect comes into the mind that is formation of Co_xB species during the catalysis. However, Co_xB species are generally formed in the hydrolysis of sodium borohydride under the unaeorobic reaction conditions and low reaction temperatures (5-10 °C) [83]. Under aerobic reaction conditions, the Co_xB species reduced the metallic cobalt where boron oxidizes to B₂O₃. We performed all the reaction in air so in our nanoclusters cobalt is mainly its metallic state which is also supported by the XPS spectrum.

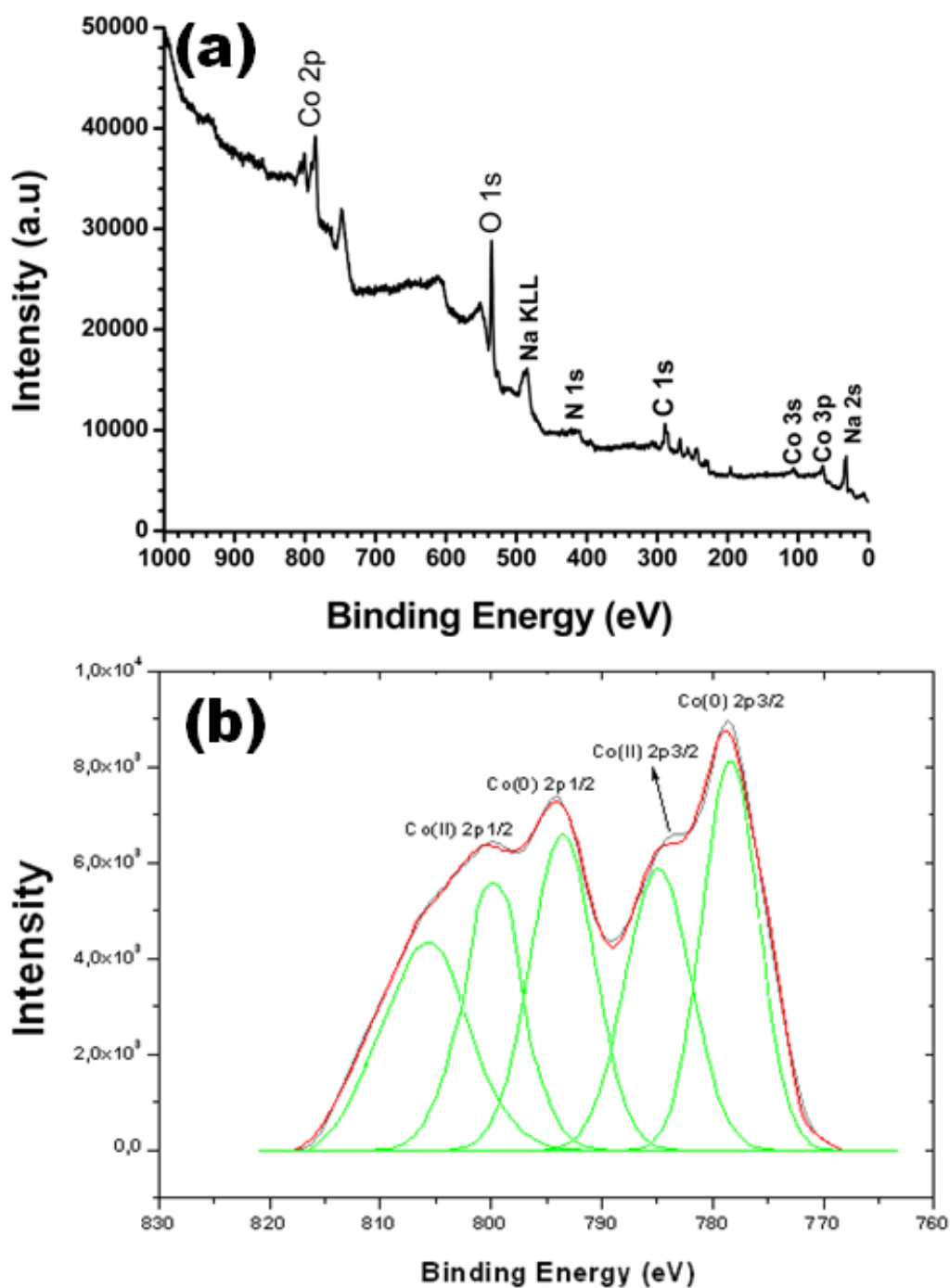


Figure 22. X-Ray photoelectron (a) survey, (b) high resolution spectra of PVP stabilized cobalt(0) nanoclusters sample isolated from the reduction of cobalt(II) chloride hexahydrate (8.4 mM) in the presence of PVP (42 mM) by sodium borohydride (150 mM) after one hour reflux in methanol.

The reduction of cobalt(II) chloride and the formation of cobalt(0) nanoclusters in the presence of PVP were also followed by UV-Vis spectroscopy. Figure 23 shows the UV-Vis electronic absorption spectra of a solution containing cobalt(II) chloride and PVP in methanol before and after addition of sodium borohydride. The broad absorption band at 510 nm observed for cobalt(II) chloride in methanol solution disappears after addition of NaBH₄, while a broad absorption feature grows in at 295 nm which is assigned to the characteristic surface plasmon resonance of the cobalt(0) nanoclusters [84]. This observation indicates the reduction of cobalt(II) to the metallic cobalt and formation of particles in nanosize upon addition of NaBH₄.

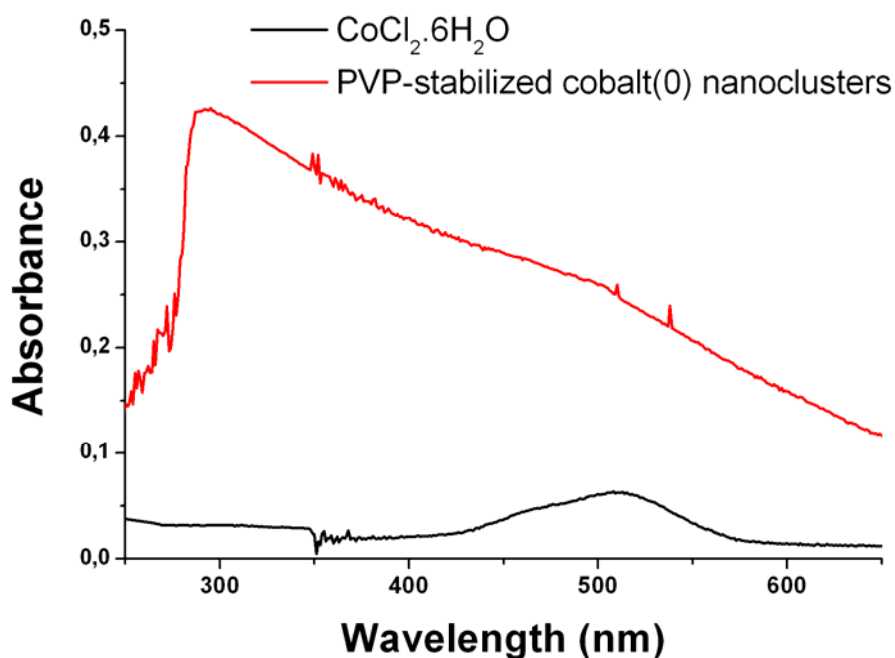


Figure 23. UV-Vis spectra of cobalt(II) chloride and PVP stabilized cobalt(0) nanoclusters taken from the methanol solutions.

Figure 24 shows the XRD pattern of the PVP stabilized cobalt(0) nanoclusters after washing with ethanol and drying in argon atmosphere. It is clear that no obvious diffraction pattern was found in the sample, which implies that the PVP stabilized cobalt(0) nanoclusters were existed in an amorphous phase.

Compared with its crystalline counterpart, the amorphous catalyst is considered to possess much more structure distortion and hold much more catalytic active sites. Thus it can be considered that the high catalytic activity of the present cobalt particles may be attributed to its amorphous state [85].

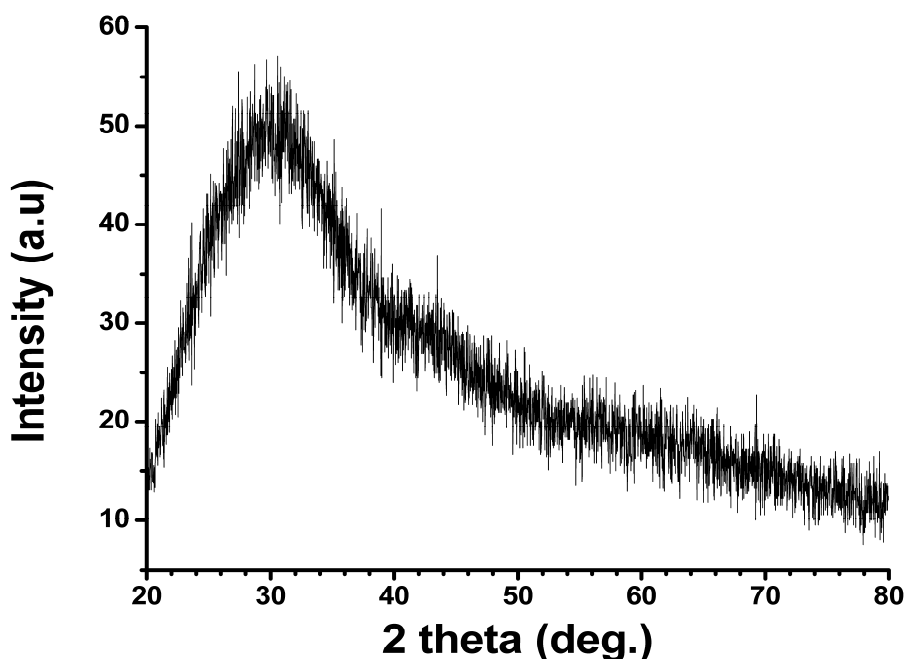


Figure 24. X-ray diffraction pattern of PVP stabilized cobalt(0) nanoclusters

5.1.3. Characterization of PVP stabilized Ruthenium(0) Nanoclusters

Figure 25 shows the UV-Vis electronic absorption spectra of solutions containing ruthenium(III) chloride in the presence of PVP stabilizer in methanol solution before and after reduction by NaBH_4 . The UV-Vis spectrum of ruthenium(III) chloride exhibits two absorption bands at 406 and 540 nm, attributable to the ligand to metal charge transfer and d-d transition, respectively (Figure 25). After reduction these bands of ruthenium(III) ions disappear and one observes a typical Mie exponential decay profile for the PVP stabilized ruthenium(0) nanoclusters, in consistence with earlier studies [86, 87].

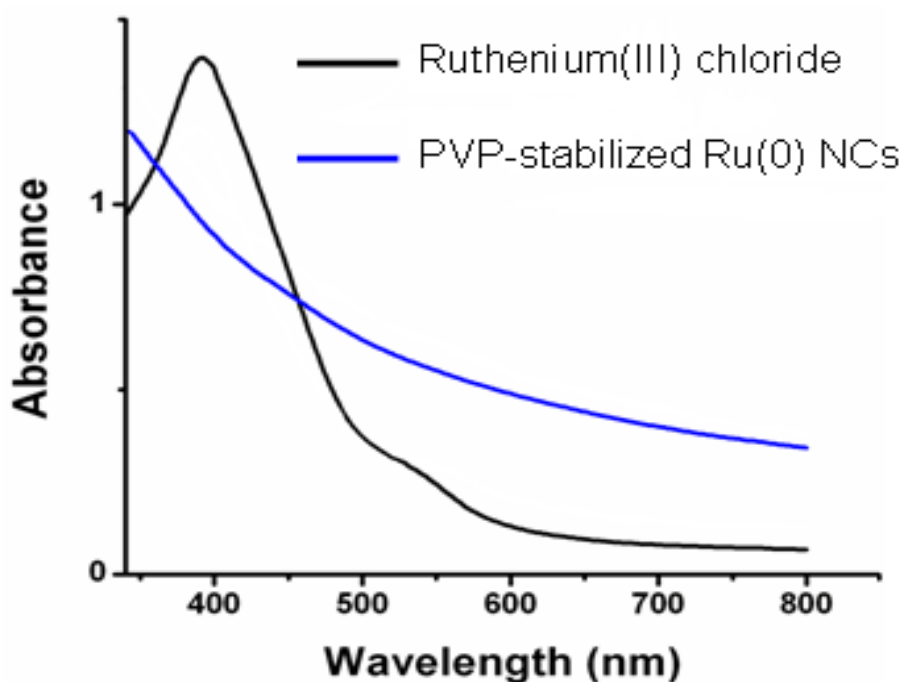


Figure 25. UV-Vis spectra of ruthenium(III) chloride and PVP stabilized ruthenium(0) nanoclusters taken from the methanol solutions.

Ruthenium(0) nanoclusters formed from the reduction of the respective precursor complex by NaBH_4 in the presence of PVP were stable in solution. No bulk metal formation was observed in solution standing for weeks at room temperature in inert gas atmosphere. The PVP stabilized ruthenium(0) nanoclusters can be isolated from the reaction solution as dark-brown solid by removing the volatiles in vacuum. The nanoclusters isolated can be redispersed in aqueous solution. When redispersed the nanoclusters are yet catalytically active in the hydrolysis of NaBH_4 or AB (see later).

The particle size distribution and morphology of the PVP stabilized ruthenium(0) nanoclusters were studied by using TEM images in Figure 26. The average particle size of PVP stabilized ruthenium(0) nanoclusters were calculated as 5.1 ± 1.2 nm by counting 100 non-touching particles in the corresponding TEM images. They show narrow particle size distribution and there is no agglomerated particles indicating the good dispersion of PVP stabilized ruthenium(0) nanoclusters in methanol solution.

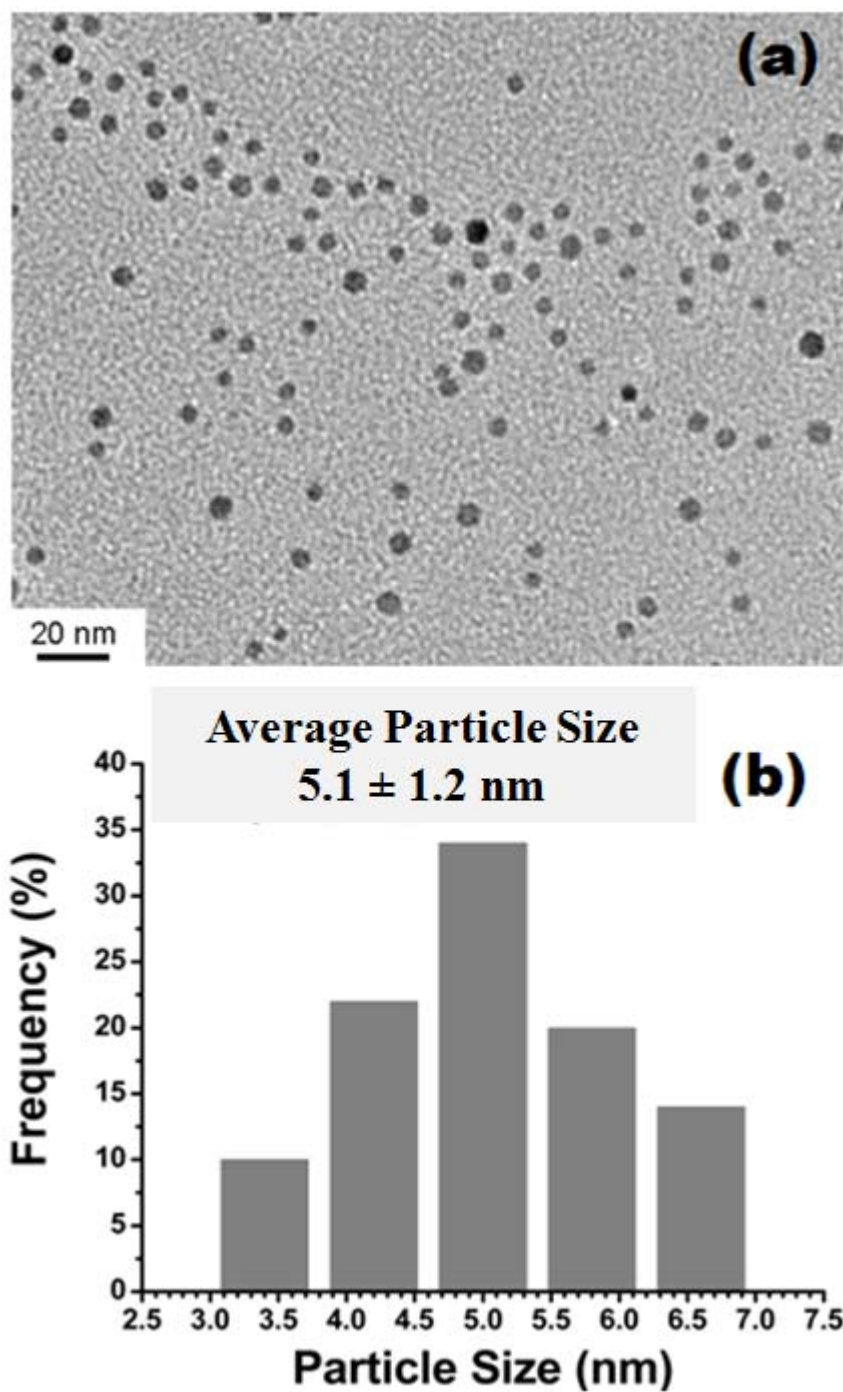


Figure 26. (a) TEM image and (b) associated histogram for PVP stabilized ruthenium(0) nanoclusters sample isolated from the reduction of ruthenium(III) chloride (3.6 mM) in the presence of PVP (18 mM) by sodium borohydride (300 mM) after one hour reflux in methanol.

Figure 27a shows the XPS survey spectra of PVP stabilized ruthenium(0) nanoclusters sample isolated from the reduction of ruthenium(III) chloride (3.6 mM) in the presence of PVP (18 mM) by NaBH₄ (150 mM) after one hour reflux in methanol indicating the presence of ruthenium with the other elements of PVP (C, O, N). Figure 27b shows the high resolution XPS spectrum of PVP stabilized ruthenium(0) nanoclusters exhibits two well resolved signal at 281.2 and 285.8 eV for Ru 3d_{5/2} and Ru 3p_{3/2}, respectively. These signals are readily assigned to the Ru(0). The binding energies of PVP stabilized ruthenium(0) nanoclusters were shifted toward higher values by 1.1 and 1.3 eV for Ru 3d_{5/2} and Ru 3p_{3/2}, respectively, which might be attributed to both the quantum size effect [4] and peculiar electronic properties of the polymer matrix [88]. However, additional peaks are observable at 282.4 and 287 eV, which can be assigned to higher oxidation states of ruthenium such as Ru(IV) in RuO₂. The formation of Ru oxides in the XPS sampling procedure is a known phenomenon [89]. The energy differences of 4.1 eV between the Ru 3d_{5/2} and Ru 3p_{3/2} signal are consistent with theoretical value calculated for the metallic ruthenium [90].

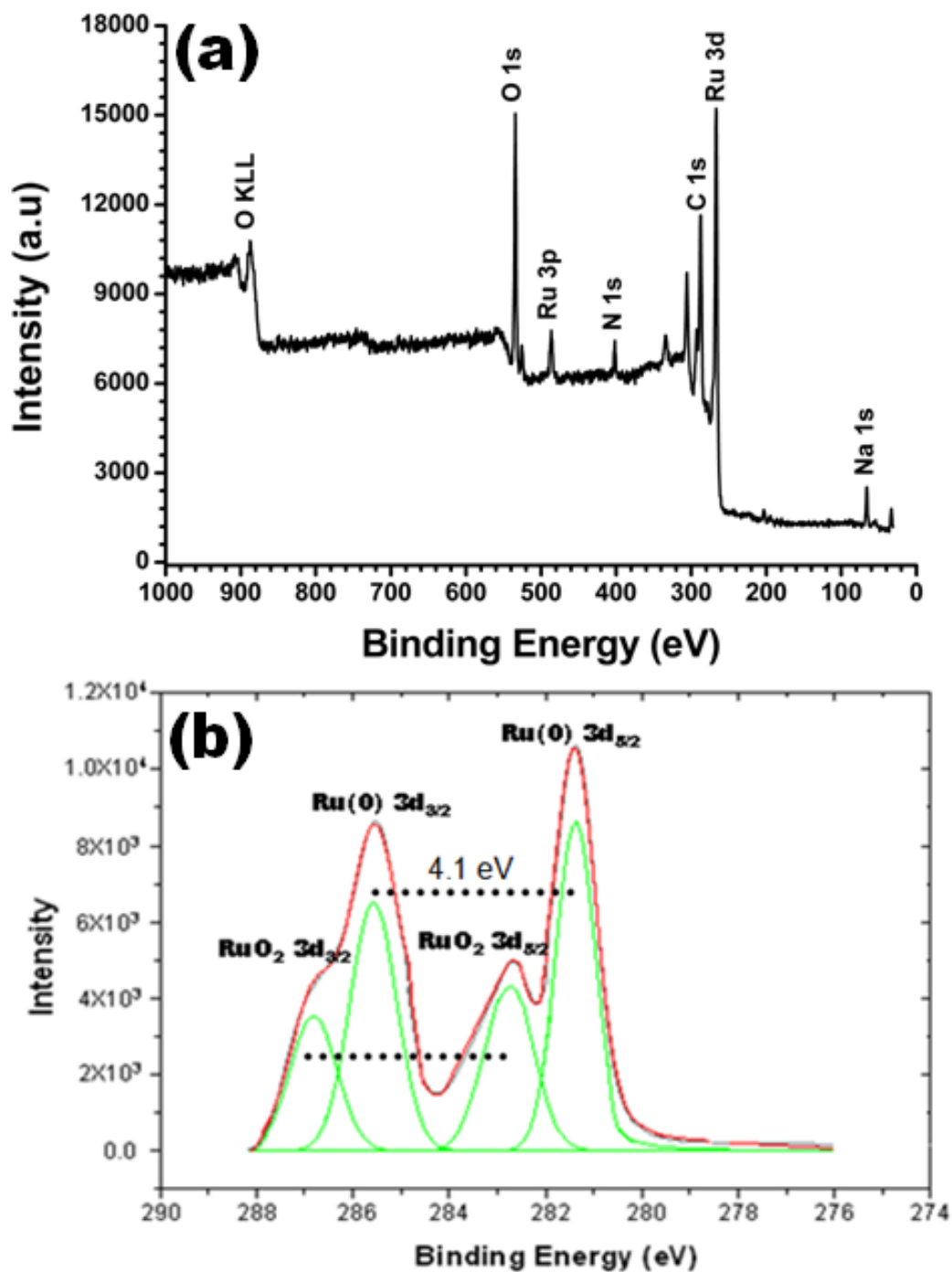


Figure 27. X-Ray photoelectron (a) survey, (b) high resolution spectra of PVP stabilized ruthenium(0) nanoclusters sample isolated from the reduction of ruthenium(III) chloride hydrate (3.6 mM) in the presence of PVP (18 mM) by sodium borohydride (150 mM) after one hour reflux in methanol.

The powder X-ray diffraction pattern of a representative sample of PVP stabilized ruthenium(0) nanoclusters is shown in Figure 28. A broad peak around $2\theta=44^\circ$ correlate with (101) plane of face centered cubic structure of metallic ruthenium [91]. The broadening observed for 101 plane is characteristic for the particles in nanometer scale [89]. However, the reflectances for other planes ((100) plane at $2\theta=38.5^\circ$ and (002) plane at $2\theta=42.8^\circ$ metallic ruthenium were not observable in the XRD pattern most probably due to the interaction of the PVP molecule with nanocluster surface atoms by these planes.

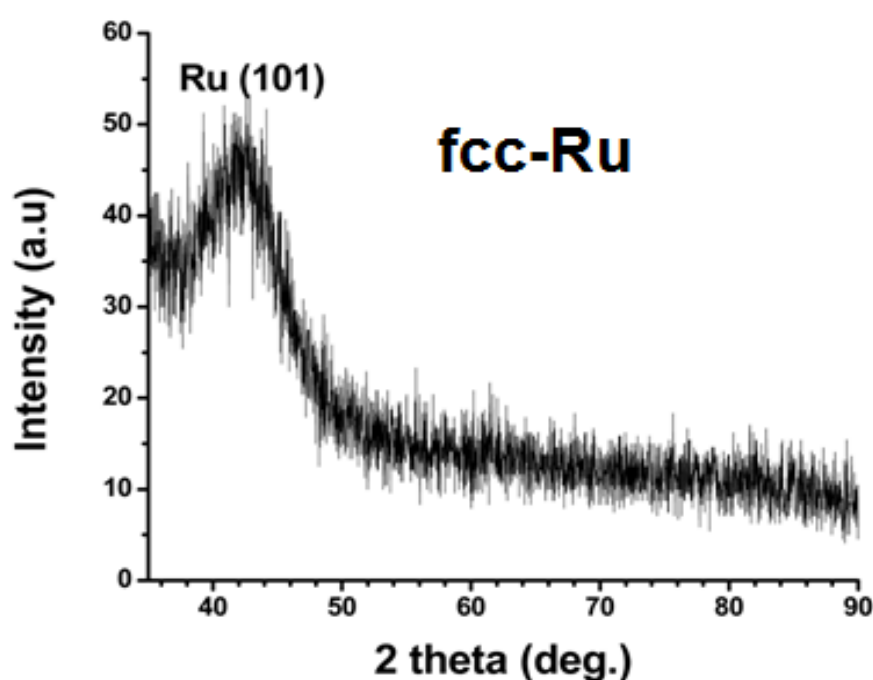


Figure 28. X-ray diffraction pattern of PVP stabilized ruthenium(0) nanoclusters

5.1.4. Integrity of PVP on the Stabilization of Transition Metal(0) Nanoclusters

Comparative FT-IR spectra of both the PVP stabilized metal(0) nanoclusters having different PVP to metal ratio and the neat PVP polymer give insight to the bonding mode of PVP on the nanoclusters surface. The FT-IR spectra of neat PVP

and PVP stabilized metal(0) nanoclusters samples show no essential difference with the exception of carbonyl band. Figure 29 demonstrates the spectral change in the CO stretching range of 2000-1500 cm^{-1} with the PVP/Metal ratio. In low PVP/Metal ratio, one observes an additional band for the CO stretching at lower wavenumber (1600 cm^{-1}) than the main band at 1663 cm^{-1} of the neat PVP polymer. This additional lower frequency band is assigned to the carbonyl group coordinated to the nickel atoms on the nanoclusters surface [92]. The appearance of a relatively weak band with large coordination shift ($\Delta\nu_{\text{C=O}} = 63 \text{ cm}^{-1}$) indicates that a small portion of the carbonyl groups on the PVP chain are bound to the nanoclusters surface. As the PVP/Metal ratio increases the fraction of the bound carbonyl decreases, so that the additional band at lower frequency due to the bound carbonyl groups is losing intensity. In the spectrum of sample with PVP/Metal ratio of 5, the band is not discernible as the fraction of the bound carbonyl groups is negligibly small.

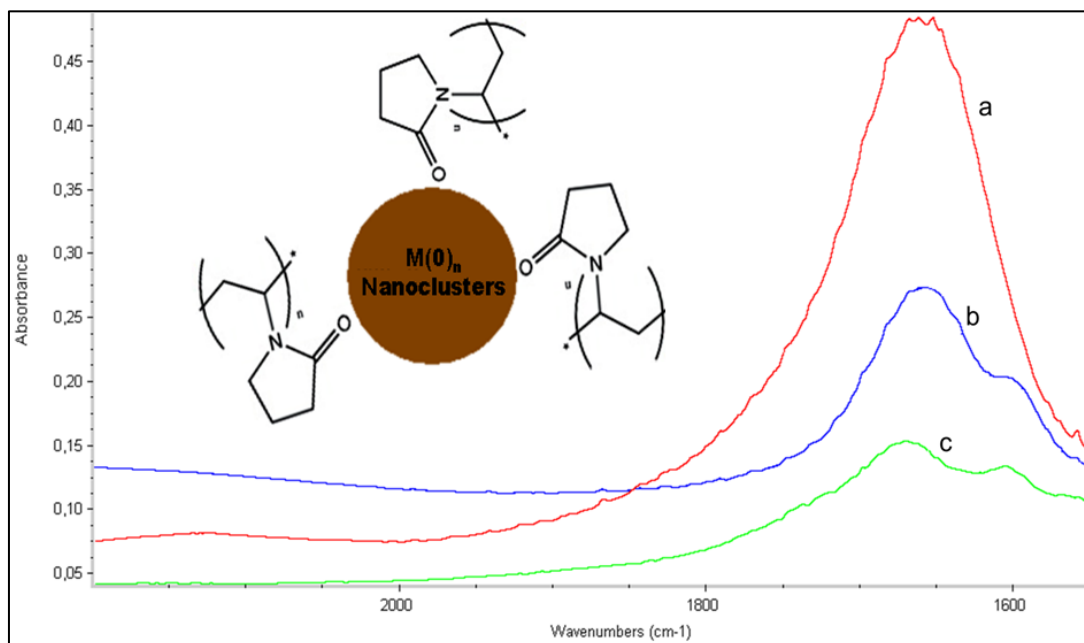


Figure 29. FT-IR spectra of PVP stabilized metal(0) nanoclusters taken from KBr pellets in the CO stretching range: (a) neat PVP, (b) PVP/metal = 0.5, (c) PVP/metal = 0.1.

5.2. Catalytic Activity of PVP Stabilized Nickel(0), Cobalt(0) and Ruthenium(0) Nanoclusters in Hydrogen Generation from the Hydrolysis of Sodium Borohydride and Ammonia Borane

5.2.1. Catalytic Activity of PVP stabilized Nickel(0) Nanoclusters in The Hydrolysis of Sodium Borohydride and Ammonia borane

5.2.1.1. Kinetics of the Hydrolysis of Sodium Borohydride Catalyzed by PVP stabilized Nickel(0) Nanoclusters

In order to study the effect of PVP concentration on the catalytic activity of nickel(0) nanoclusters in the hydrolysis of NaBH₄ (150 mM) or AB, catalytic activity tests were performed at 25.0 ± 0.5 °C starting with five sets of nickel(0) nanoclusters having different PVP/Ni ratio (5, 10, 20, 30, 40). Figure 30 shows the plots of the hydrogen generation from the hydrolysis of NaBH₄ in the presence of nickel(0) nanoclusters having different PVP/Ni ratio. The rate of hydrogen generation was calculated from the slope of the linear portion of curves which decrease with the increasing PVP/Ni ratio.

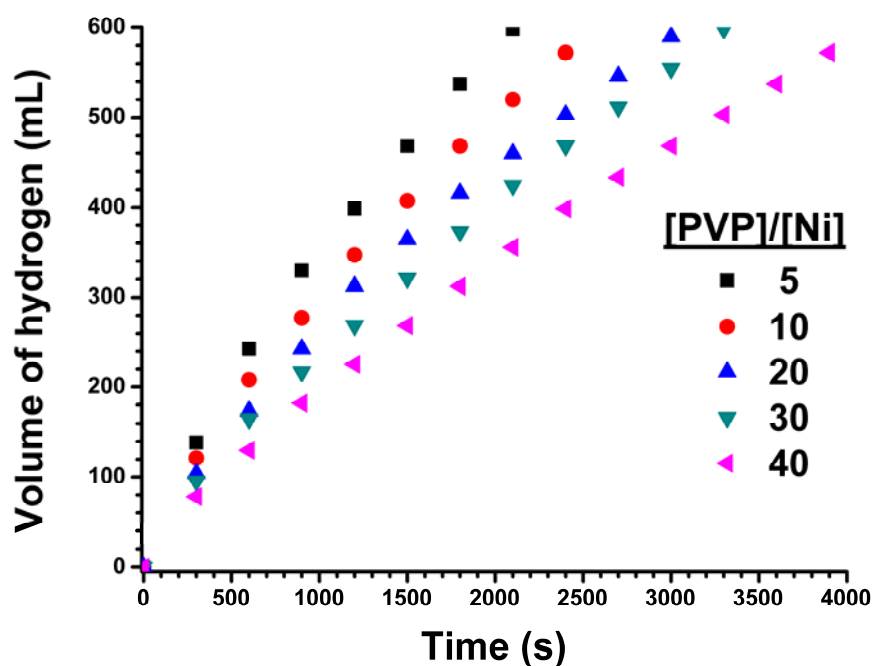


Figure 30. The volume of hydrogen versus time plot for the hydrolysis of sodium borohydride catalyzed by nickel(0) nanoclusters having different PVP to nickel ratio at 25.0 ± 0.5 °C.

The PVP molecule adsorbed on the nanoclusters surface via carbonyl groups provides steric stabilization against coagulation of the particles. At high PVP concentrations, almost whole surface atom of the metal nanoclusters are covered; thus, the catalytically active sites are blocked leading to the deactivation of catalyst. At low PVP concentrations, the nanoclusters are not stable enough to be employed as catalyst. Hence, one has to make a compromise between stability and catalytic activity. In this case, the optimum PVP/Ni ratio was found to be 5 (the PVP concentration of 7 mM monomer), for obtaining nickel(0) nanoclusters which are stable and show the highest catalytic activity in the hydrolysis of sodium borohydride (Figure 31). Thus, the PVP to nickel ratio of 5 was selected for the further experiments.

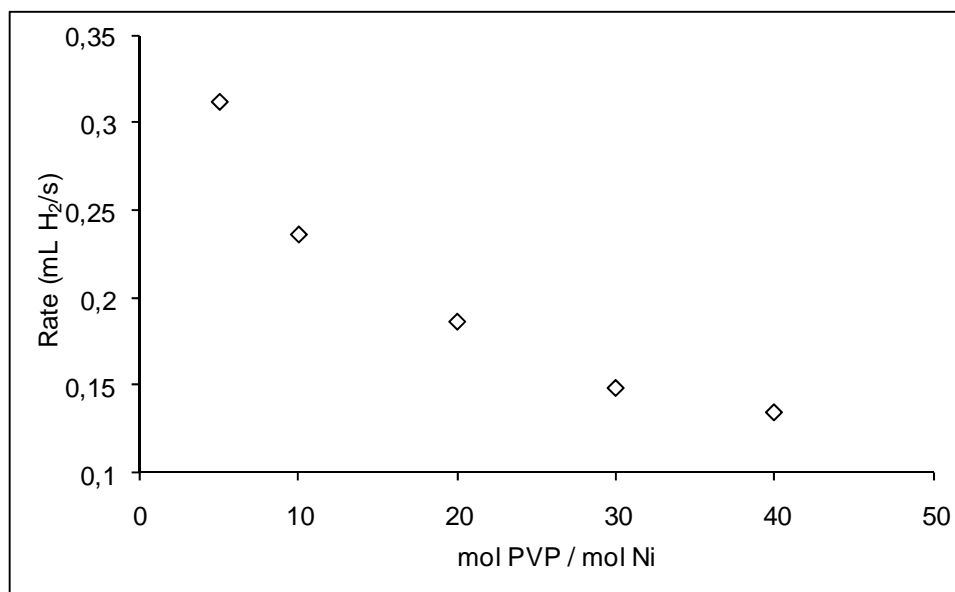


Figure 31. The rate of hydrogen generation from the hydrolysis of NaBH₄ in the presence of nickel(0) nanoclusters at different PVP/Ni ratios.

The PVP stabilized nickel(0) nanoclusters are found to be active catalyst for the hydrolysis of NaBH₄ even at low concentrations and room temperature. Figure 32 shows the plots of the volume of hydrogen generated versus time during the catalytic hydrolysis of 150 mM NaBH₄ solution in the presence of nickel(0) nanoclusters at different Ni concentrations at 25.0 ± 0.5 °C. The hydrogen generation rate was determined from the linear portion of the plot for each nickel concentration. The inset in Figure 32 shows the plot of hydrogen generation rate versus nickel concentration, both in logarithmic scale. The slope of the line in the inset of Figure 32 is $1.2 \approx 1.0$ indicating that the hydrolysis of NaBH₄ is first order with respect to the nickel concentration.

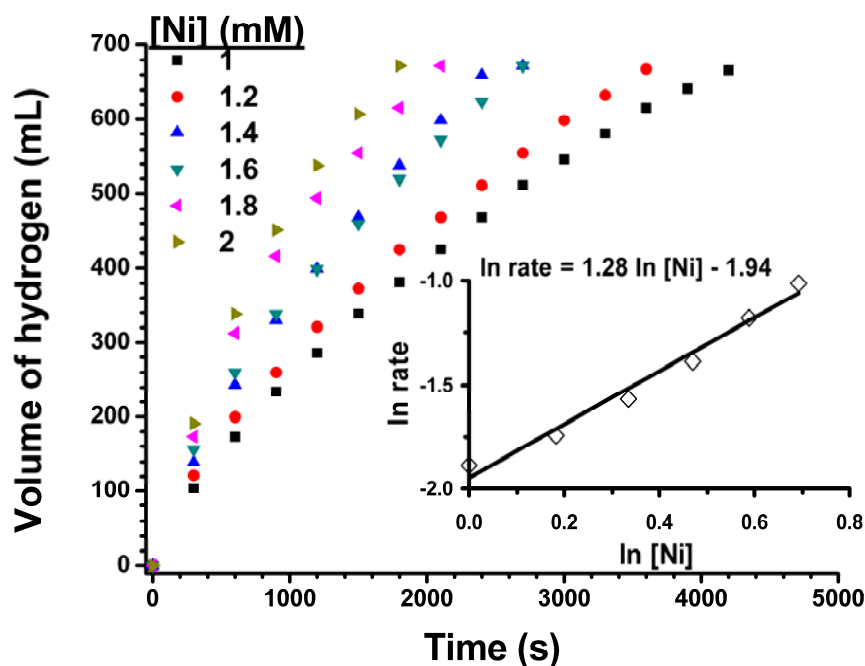


Figure 32. The volume of hydrogen versus time plot depending on the nickel concentration for the catalytic hydrolysis of sodium borohydride (150 mM) at 25.0 ± 0.5 °C. The inset shows the plot of hydrogen generation rate versus the concentration of nickel (both in logarithmic scale) for the hydrolysis of sodium borohydride.

The effect of substrate concentration on the hydrogenation rate from the catalytic hydrolysis of NaBH_4 was also studied by performing a series of experiments starting with varying initial concentration of NaBH_4 while keeping the catalyst concentration constant at 1.4 mM Ni at 25 ± 0.5 °C (Figure 33). The slope of the line inset ($0.03 \approx 0.0$) in the inset of Figure 33 indicated that the hydrogen generation rate was practically independent of the NaBH_4 concentration. Hence, the hydrolysis of sodium borohydride catalyzed by PVP stabilized nickel(0) nanoclusters is zero order with respect to the NaBH_4 concentration. Consequently, the rate law for the hydrolysis of NaBH_4 catalyzed by PVP stabilized nickel(0) nanoclusters can be given as, Eq. (6);

$$\frac{-4d[\text{NaBH}_4]}{dt} = \frac{d[\text{H}_2]}{dt} = k[\text{Ni}] \quad (6)$$

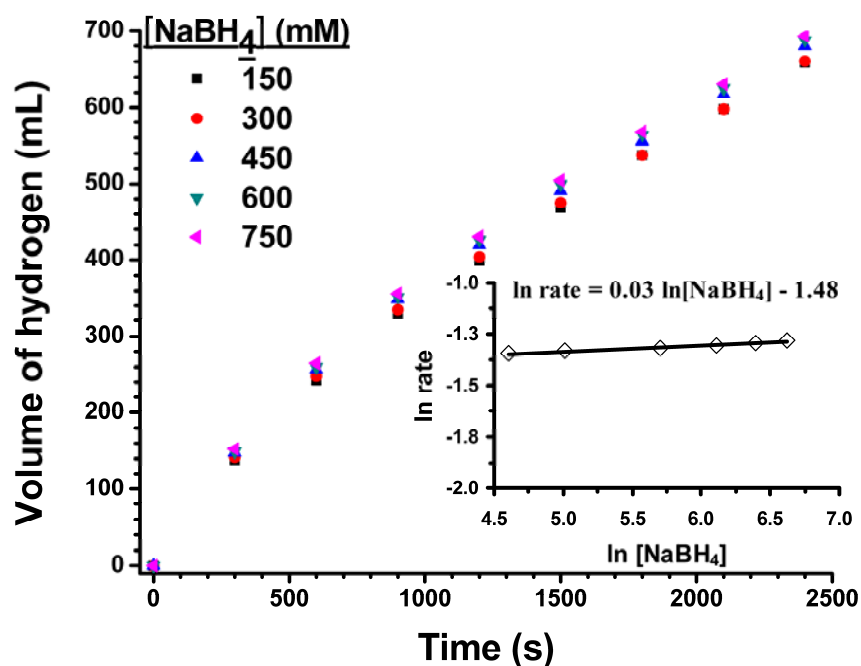


Figure 33. The volume of hydrogen versus time plots for the hydrolysis of sodium borohydride at different NaBH₄ concentrations at constant catalyst concentration (1.4 mM Ni) and 25.0 ± 0.5 °C. The inset shows the plot of hydrogen generation rate versus the NaBH₄ concentration (both in logarithmic scale) for the hydrolysis of sodium borohydride.

Both PVP stabilized nickel(0) nanoclusters catalyzed and self hydrolysis of sodium borohydride were carried out at various temperature in the range of 25-45 °C starting with an initial substrate concentration of 150 mM NaBH₄ and catalyst concentration of 1.4 mM Ni. The values of rate constant k_{app} (Table A1 in the Appendix A) for the sole catalyzed hydrolysis were calculated from the hydrogen volume versus time data obtained by subtracting the self hydrolysis hydrogen generation values from those of nickel(0) nanoclusters catalyzed hydrolysis of NaBH₄ and were used to create the Arrhenius, Eq. (7), [93], and Eyring, Eq. (8), [94] plots as shown in the inset of Figure 34 and in Figure 35, respectively.

$$\ln(k) = \frac{-E_a}{RT} + \ln(A) \quad (7)$$

$$\ln \frac{k}{T} = \frac{-\Delta H^*}{RT} + \ln \frac{k_B}{h} + \frac{\Delta S^*}{R} \quad (8)$$

The Arrhenius activation energy for the hydrolysis of NaBH₄ catalyzed by PVP stabilized nickel(0) nanoclusters was calculated as $E_a^{\text{apparent}} = 46 \pm 2$ kJ/mol. However, this type of activation energy is formed by the combination of the rate constants (k_{app}) of many reaction steps for the catalytic hydrolysis of NaBH₄ and so should be called as E_a^{apparent} . This activation energy is lower than the value found for the same hydrolysis catalyzed by hydrogenphosphate-stabilized nickel(0) nanoclusters (54 kJ/mol) [37] and much more less than other bulk metal catalysts: 75 kJ/mol for cobalt, 71 kJ/mol for nickel, and 63 kJ/mol for Raney nickel [95].

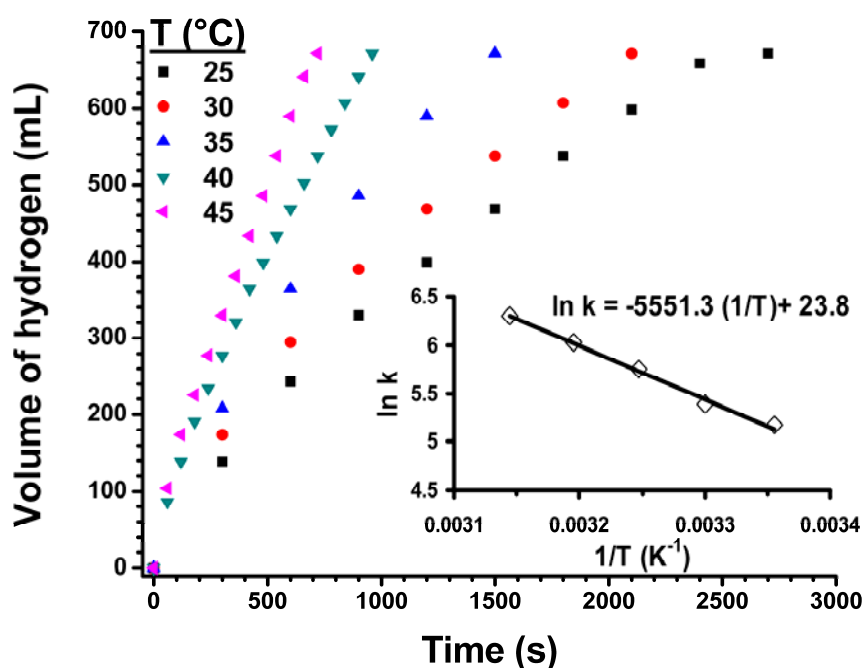
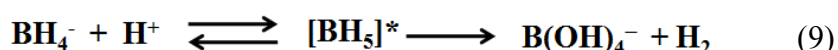


Figure 34. Volume of hydrogen generation versus time for the hydrolysis of sodium borohydride (150 mM) catalyzed by PVP stabilized nickel(0) nanoclusters (1.4 mM Ni) in the temperature range of 25-45 °C. The inset shows the Arrhenius plot ($\ln k$ versus the reciprocal absolute temperature $1/T$ (K⁻¹)).

The Eyring plot given in Figure 35 gives the activation enthalpy, $\Delta H^\ddagger = 45 \pm 2$ kJ/mol; and the activation entropy, $\Delta S^\ddagger = -94 \pm 3$ J/K·mol, for the hydrolysis of NaBH₄ catalyzed by PVP stabilized nickel(0) nanoclusters. The small positive value of activation enthalpy and the large negative value of activation entropy are indicative of an associative mechanism for the hydrolysis of NaBH₄ catalyzed by PVP stabilized nickel(0) nanoclusters in line with the mechanism suggested for the hydrolysis of sodium borohydride given in the literature [96]. According to a suggested mechanism for metal catalysed hydrolysis of NaBH₄ in alkaline media, the attack on BH₄⁻ anion by the protic solvent (H₂O) on the metal catalyst surface is thought to afford a pentacoordinate [BH₅]* intermediate. This short-lived intermediate may eventually evolve in two different directions, either relaxing back to Borohydride (with H/D scrambling if the hydrolysis is carried in a deuterated solvent) or decomposing irreversibly to molecular hydrogen and B(OH)₄⁻ possibly via a BH₃ intermediate as shown in Eq. (9);



A catalyst lifetime experiment was performed starting with a 50 mL solution of PVP stabilized nickel(0) nanoclusters containing 1.4 mM Ni and 1 M NaBH₄ (1.9 g) at 25.0 ± 0.5 °C. It was found that the PVP stabilized nickel(0) nanoclusters provide 8700 turnovers in hydrogen generation from the hydrolysis of NaBH₄ over 27 hours before deactivation. However, that the hydrogen generation slows down as the reaction proceeds may be because of increasing viscosity of the solution as the continuously added NaBH₄ is converted to sodium metaborate. Therefore, this value should be considered as a lower limit. A much higher TTON value might be obtained when the increase in viscosity could be avoided. Note that the turnover frequency starts with an initial value of TOF = 10.2 mol H₂·(mol Ni)⁻¹·min⁻¹ or 174 mmol H₂·(g Ni)⁻¹·min⁻¹. Both TTON and TOF values refer to the sole catalytic hydrogen generation after subtraction of self hydrolysis.

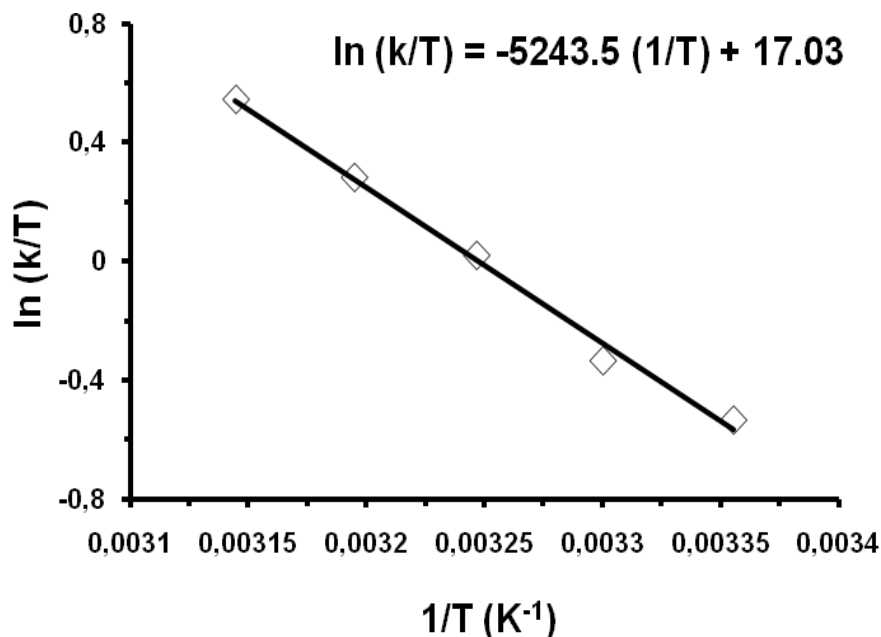


Figure 35. Eyring plot ($\ln(k/T)$) versus the reciprocal absolute temperature $1/T$ (K^{-1}) for the hydrolysis of sodium borohydride (150 mM) catalyzed by PVP stabilized nickel(0) nanoclusters (1.4 mM Ni) in the temperature range 25-45 °C

5.2.1.2. Kinetics of the Hydrolysis of Ammonia Borane Catalyzed by PVP Stabilized Nickel(0) Nanoclusters

Figure 36 shows the plots of the volume of hydrogen generated versus time during the catalytic hydrolysis of 100 mM H_3NBH_3 solution in the presence PVP stabilized nickel(0) nanoclusters catalyst at different metal concentration (1, 1.5, 2, 2.5, 3 mM) at 25 ± 0.5 °C. The hydrogen generation rate was determined from the linear portion of the plot for each metal concentration. The plot of hydrogen generation rate versus metal concentration, both in logarithmic scale (the inset in Figure 36) gives a straight line with a slope of $0.95 \approx 1$, indicating that the hydrolysis reaction is first order with respect to the catalyst concentration.

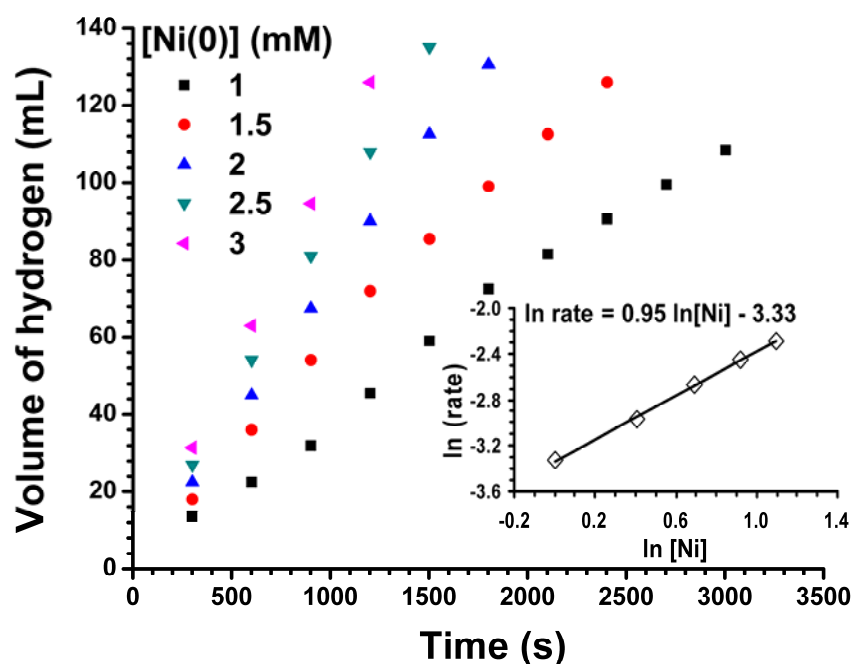


Figure 36. The volume of hydrogen versus time plots depending on the nickel concentrations for the hydrolysis of ammonia borane (100 mM) at 25 ± 0.5 °C. The inset shows the plot of hydrogen generation rate versus the concentration of cobalt (both in logarithmic scale).

The effect of ammonia borane concentration on the hydrogen generation rate from the hydrolysis of AB catalyzed by PVP stabilized nickel(0) nanoclusters was also studied by performing a series of experiments starting with various initial concentration of H_3NBH_3 while keeping the catalyst concentration constant at 2.0 mM Ni. Figure 37 shows the plots of the volume of hydrogen generated versus time during the catalytic hydrolysis of AB at various substrate concentrations. The hydrogen generation rate was determined from the linear portion of the plot for each AB concentration and used for constructing the plot of hydrogen generation rate versus ammonia borane concentration, both in logarithmic scale (the inset in Figure 37). The slope of the line given in the inset of Figure 37, $0.91 \approx 1$ indicates that the hydrolysis reaction is first order with respect to the AB concentration.

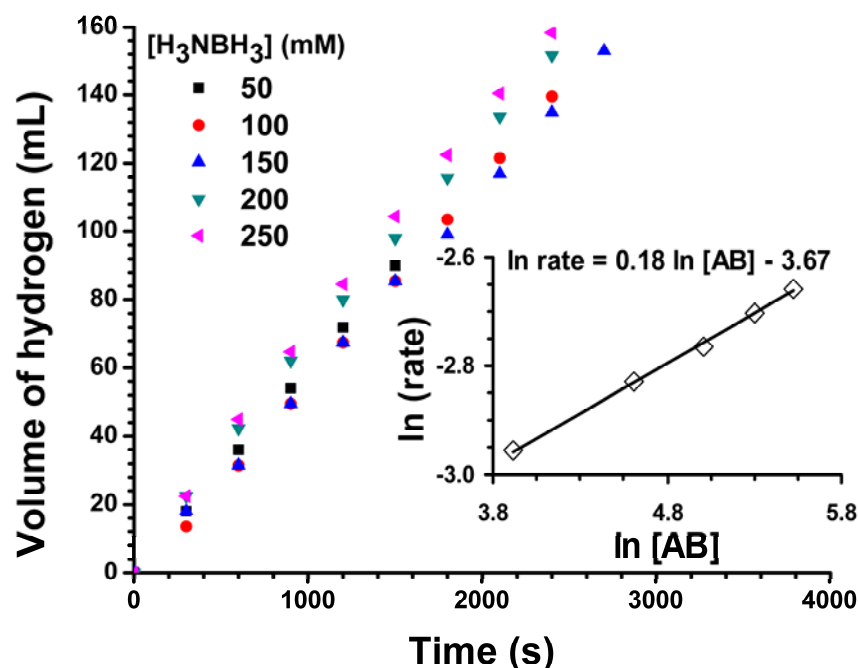


Figure 37. The volume of hydrogen versus time plots depending on the substrate concentrations at constant catalyst concentration for the hydrolysis of ammonia borane catalyzed by PVP stabilized nickel(0) nanoclusters. The inset shows the plot of hydrogen generation rate versus the concentration of the substrate (both in logarithmic scale)

Consequently, the rate law for the hydrolysis of AB catalyzed by PVP stabilized nickel(0) nanoclusters can be given as Eq.(10);

$$\frac{-3d[H_3NBH_3]}{dt} = \frac{d[H_2]}{dt} = k[Ni] \quad (10)$$

PVP stabilized nickel(0) nanoclusters catalyzed hydrolysis of AB was carried out at various temperature in the range of 20-40 °C starting with the initial substrate concentration of 100 mM H_3NBH_3 and an initial catalyst concentration of 2 mM Ni. The values of rate constants (k_{app}) (Table A2 in the Appendix A) for PVP stabilized nickel(0) nanoclusters catalyzed hydrolysis of AB were calculated from the slope of the linear part of each plot in Figure 38 and used to calculate the apparent activation energy (Arrhenius plot is shown in the Inset of Figure 38): Apparent activation

energy $E_a^{\text{apparent}} = 58 \pm 2 \text{ kJ}\cdot\text{mol}^{-1}$, The value of activation energy is lower than the value reported for the hydrolysis of AB using Ni/ γ -Al₂O₃ (62 kJ/mol) [69], and Ru/C (76 kJ/mol) [69].

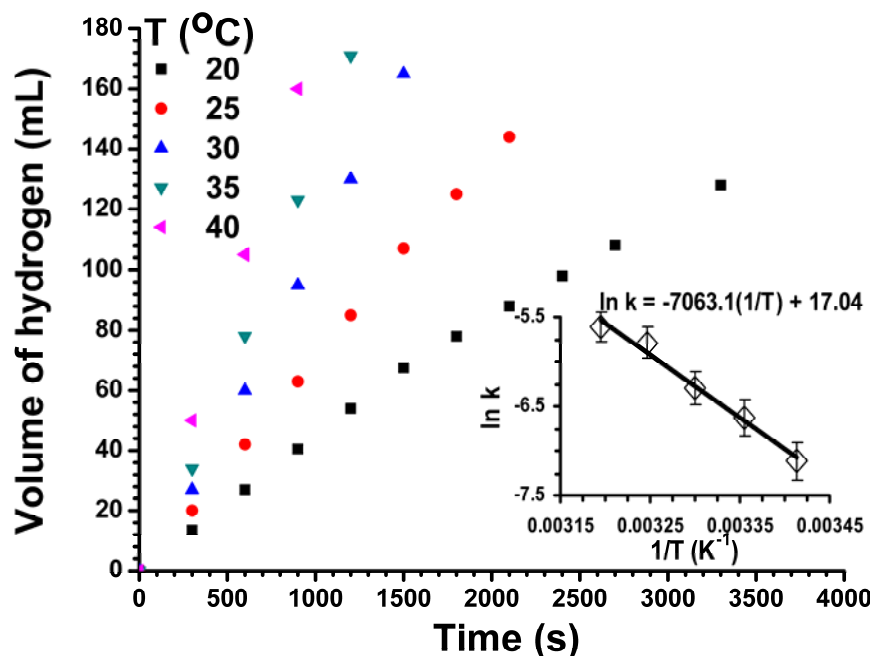


Figure 38. The volume of hydrogen versus time plots at different temperatures for the hydrolysis of ammonia borane (100 mM) catalyzed by PVP stabilized nickel(0) nanoclusters (2.0 mM Ni) in the temperature range 20-40 °C. The inset shows Arrhenius plot (ln k versus the reciprocal absolute temperature $1/T$ (K⁻¹)).

The Eyring plot given in Figure 39 gives the activation enthalpy, $\Delta H^\ddagger = 56 \pm 3 \text{ kJ/mol}$; and the activation entropy, $\Delta S^\ddagger = -111 \pm 5 \text{ J/K}\cdot\text{mol}$, for the hydrolysis of AB catalyzed by PVP stabilized nickel(0) nanoclusters. The high positive value of activation enthalpy and the high negative value of activation entropy of hydrolysis of AB catalysed by PVP stabilized nickel(0) nanoclusters indicate an associative mechanism. A propose mechanism can be suggested for the metal catalyzed hydrolysis of AB under the light of these kinetic results where the adsorption of the H₃NBH₃ molecule on the surface of metal catalyst via nitrogen or boron atom is occurred at the first step of the mechanism. Then, the native bond between the

nitrogen and boron atom is weakened on the surface of metal catalyst which is followed by the attack of water molecule to weakened bond. This step should be the rate determining step because the weakening of the native bond between the N-B need high energy. Next, the reaction of BH_3 molecule with water takes place resulting in the formation of hydrogen gas and borate species in the second step.

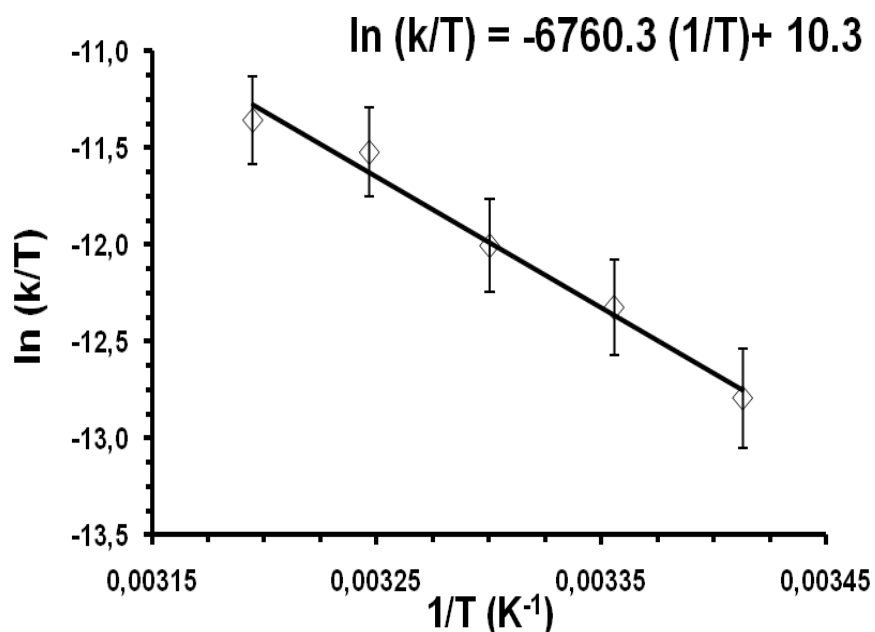


Figure 39. Arrhenius plot ($\ln(k/T)$ versus the reciprocal absolute temperature $1/T$ (K^{-1}) for the hydrolysis of ammonia borane (100 mM) catalyzed by PVP stabilized nickel(0) nanoclusters (2.0 mM Ni) in the temperature range 20-40 °C

A catalyst lifetime experiment was performed starting with a 20 mL solution of PVP stabilized nickel(0) nanoclusters containing 1.5 mM Ni and 1.0 M H_3NBH_3 at 25.0 ± 0.5 °C. PVP stabilized nickel(0) nanoclusters provided 17450 turnovers over 24 h. The deactivation of the catalyst in 24 h can be explained by the increasing viscosity and pH due to the formation of $[\text{NH}_4][\text{BO}_2]$ which was identified by the ^{11}B -NMR spectral shift at $\delta = 11.8$ ppm of the crystalline product at the bottom of the reactor.

5.2.2. Catalytic Activity of The PVP stabilized Cobalt(0) Nanoclusters in The Hydrolysis of Sodium Borohydride or Ammonia borane

5.2.2.1. Kinetics of the Hydrolysis of Sodium Borohydride Catalyzed by PVP Stabilized Cobalt(0) Nanoclusters in Aqueous Medium

Figure 40 shows the plots of the volume of hydrogen generated versus time during the catalytic hydrolysis of 150 mM NaBH₄ solution in the presence PVP stabilized cobalt(0) nanoclusters catalyst in various metal concentration (0.5, 1, 1.5, 2, 2.5 mM) at 25 ± 0.5 °C. The hydrogen generation rate was determined from the linear portion of the plot for each metal concentration. The inset shows the plot of hydrogen generation rate versus cobalt concentration, both in logarithmic scale, which indicates that the hydrolysis of NaBH₄ is first order with respect to the cobalt concentration.

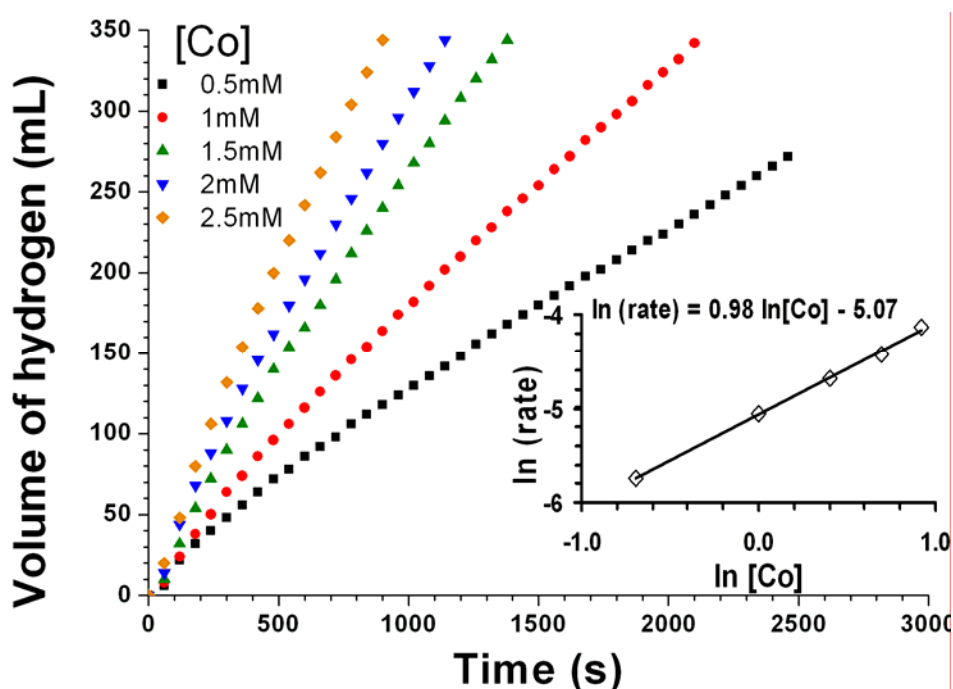


Figure 40. The volume of hydrogen versus time plots depending on the cobalt concentrations for the hydrolysis of sodium borohydride (150 mM) at 25.0 ± 0.5 °C. The inset shows the plot of hydrogen generation rate versus the concentration of cobalt (both in logarithmic scale).

The effect of NaBH_4 concentration on the hydrogen generation rate from the hydrolysis of NaBH_4 was also studied by performing a series of experiments starting with varying initial concentration of NaBH_4 while keeping the catalyst concentrations constant at 1.5 mM Co. Figure 41 shows the plots of the volume of hydrogen generated versus time during the catalytic hydrolysis of sodium borohydride at different NaBH_4 concentration. The hydrogen generation rate was determined from the linear portion of the plot for each NaBH_4 concentration and was used for the construction of the plot of hydrogen generation rate versus NaBH_4 concentration, both in logarithmic scale (the inset in Figure 41). One obtains a straight line with a slope of $0.83 \approx 1$. This indicates that the hydrolysis reaction is also first order with respect to the NaBH_4 concentration.

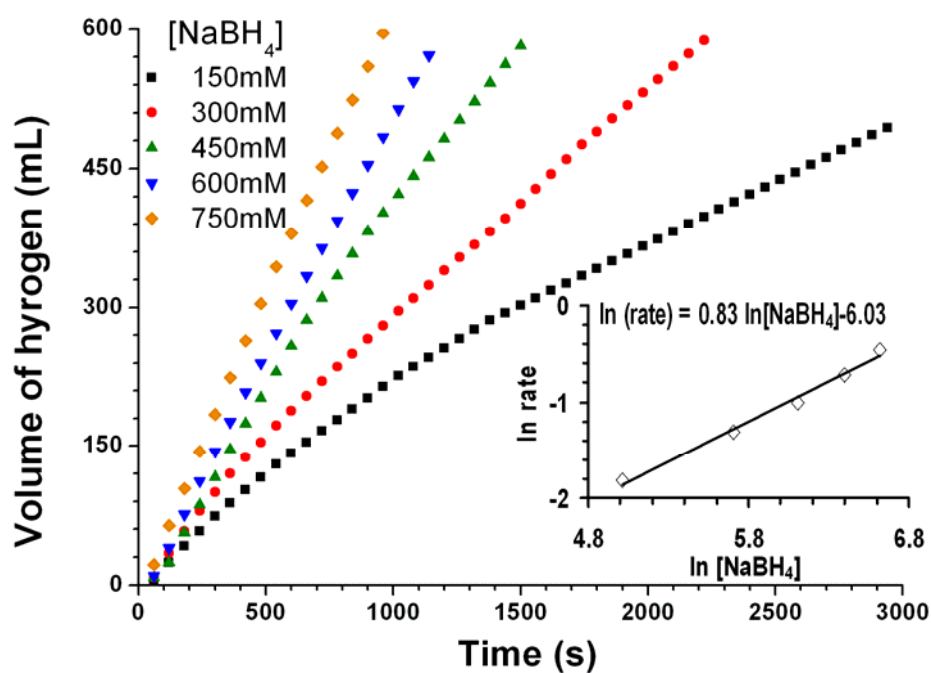


Figure 41. The volume of hydrogen versus time plots depending on the substrate concentrations at constant catalyst concentration for the hydrolysis of sodium borohydride. The inset shows the plot of hydrogen generation rate versus the concentration of the substrate (both in logarithmic scale)

Consequently, the rate law for the catalytic hydrolysis of NaBH₄ catalyzed by PVP stabilized cobalt(0) nanoclusters can be given as, Eq. (11)

$$\frac{-4d[NaBH_4]}{dt} = \frac{d[H_2]}{dt} = k[Co][NaBH_4] \quad (11)$$

Both the self hydrolysis and the PVP stabilized cobalt(0) nanoclusters catalyzed hydrolysis of NaBH₄ were carried out at various temperature in the range of 20-40 °C starting with the initial NaBH₄ concentration of 150 mM NaBH₄ and an initial catalyst concentration of 1.5 mM Co in the latter case. Figure 42 shows the plots of volume of hydrogen generated versus time for the hydrolysis of NaBH₄ at five different temperatures. Note that the values used for the plots were obtained by subtracting the hydrogen volume for the self hydrolysis from those of corresponding metal nanoclusters catalyzed hydrolysis of NaBH₄ at each temperature. The values of rate constant (k_{app}) (Table A3 in the Appendix A) for the sole catalytic hydrolysis were obtained from the slope of the linear part of each plot in Figure 43 and used to calculate the apparent activation energy (Arrhenius plot is shown in the Inset of Figure 42): Apparent activation energy $E_a^{apparent} = 63 \pm 2 \text{ kJ.mol}^{-1}$.

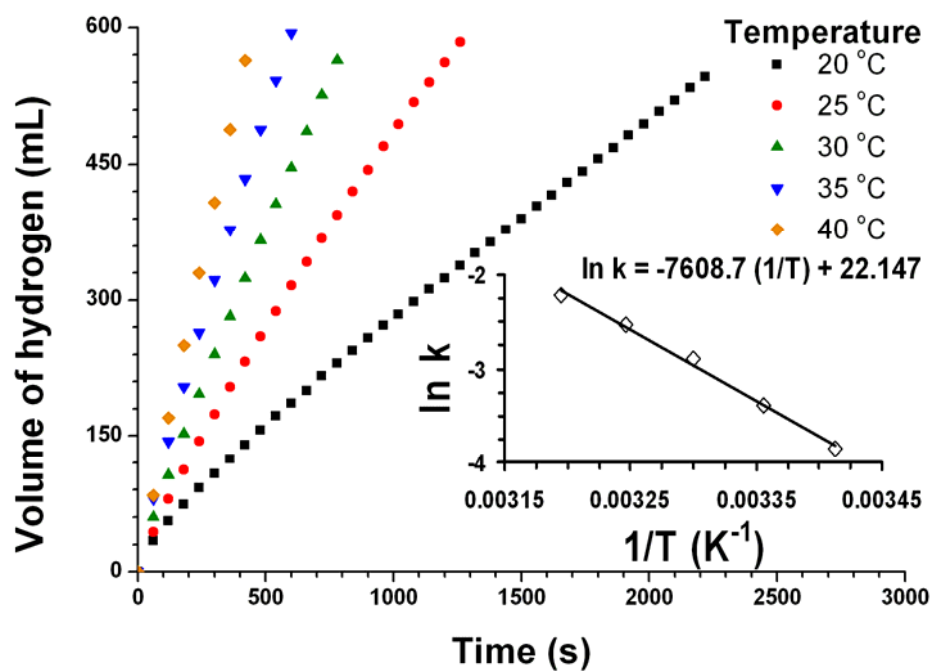


Figure 42. The volume of hydrogen versus time plots at different temperatures for the hydrolysis of sodium borohydride (150 mM) catalyzed by PVP stabilized cobalt(0) nanoclusters (1.5 mM Co) in the temperature range 20-40 °C. The inset shows Arrhenius plot ($\ln k$ versus the reciprocal absolute temperature $1/T$ (K^{-1})).

The Eyring plot given in Figure 43 gives the activation enthalpy, $\Delta H^\ddagger = 61 \pm 2$ kJ/mol; and the activation entropy, $\Delta S^\ddagger = -49 \pm 3$ J/K·mol, for the hydrolysis of NaBH_4 catalyzed by PVP stabilized cobalt(0) nanoclusters. The large positive value of activation enthalpy and the small negative value of activation entropy are indicative of a dissociative mechanism for the hydrolysis of NaBH_4 catalyzed by PVP stabilized cobalt(0) nanoclusters in line with the rate law which is first order with respect to the NaBH_4 concentration.

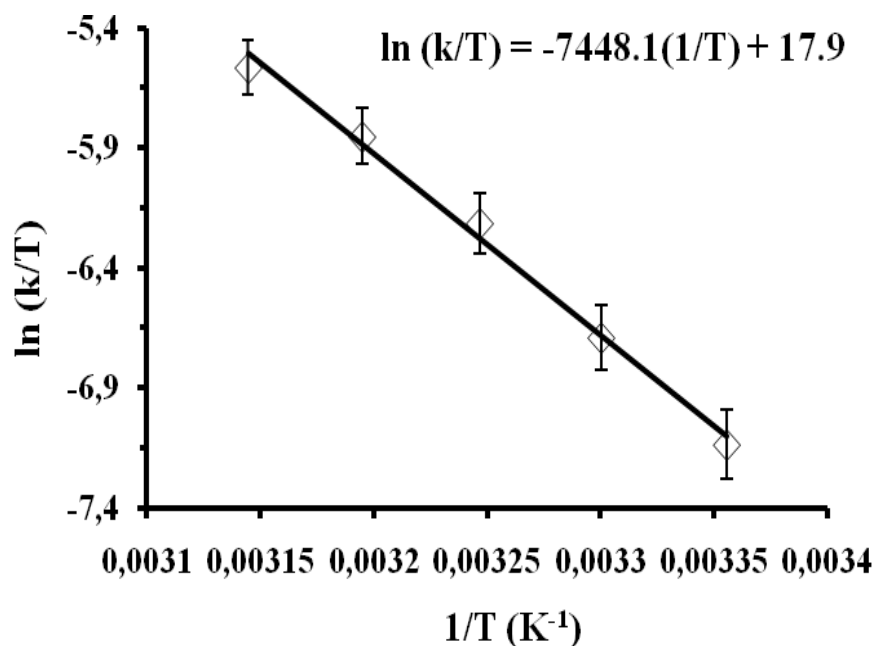


Figure 43. Eyring plot ($\ln(k/T)$) versus the reciprocal absolute temperature $1/T$ (K^{-1}) for the hydrolysis of sodium borohydride (150 mM) catalyzed by PVP stabilized cobalt(0) nanoclusters (1.5 mM Co) in the temperature range 20-40 °C

A catalyst lifetime experiment was performed starting with a 50 mL solution of PVP stabilized cobalt nanoclusters containing 1.5 mM Co and 1 M NaBH_4 (1.9 g) at 25.0 ± 0.1 °C. PVP stabilized cobalt(0) nanoclusters provided 5100 turnovers over 19 h in the hydrolysis of NaBH_4 . However, the hydrogen generation slows down as the reaction proceeds, may be, because of increasing viscosity of the solution as the continuously added NaBH_4 is converted to sodium metaborate. Therefore, this TTON value should be considered as a lower limit. A much higher TTON value might be obtained when the increase in viscosity could be avoided.

5.2.2.2. Kinetics of the Hydrolysis of Ammonia Borane Catalyzed by PVP Stabilized Cobalt(0) Nanoclusters

Figure 44 shows the plots of the volume of hydrogen generated versus time during the catalytic hydrolysis of 100 mM H_3NBH_3 solution in the presence PVP stabilized cobalt(0) nanoclusters catalyst at different metal concentrations (1, 1.5, 2, 2.5, 3 mM) at 25 ± 0.5 °C. The hydrogen generation rate was determined from the linear portion of the plot for each metal concentration. The plot of hydrogen generation rate versus metal concentration, both in logarithmic scale (the inset in Figure 44) gives a straight line with a slope of $1.15 \approx 1$, indicating that the hydrolysis reaction is first order with respect to the catalyst concentration. The control tests using a trap containing copper(II) sulfate showed no ammonia evolution in detectable amount in the experiments.

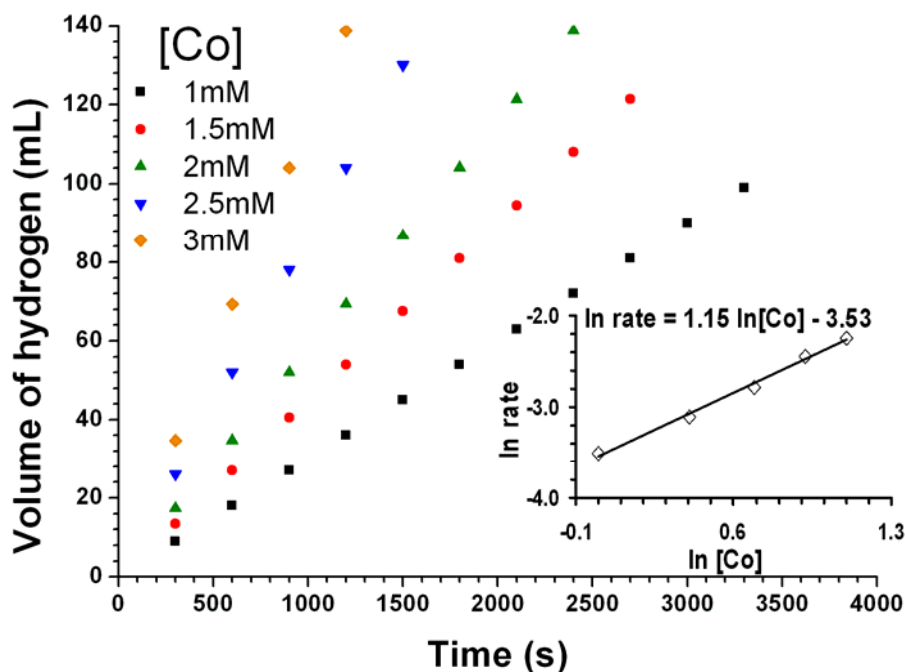


Figure 44. The volume of hydrogen versus time plots depending on the cobalt concentrations for the hydrolysis of ammonia borane (100 mM) at 25.0 ± 0.5 °C. The inset shows the plot of hydrogen generation rate versus the concentration of cobalt (both in logarithmic scale).

The effect of ammonia borane concentration on the hydrogen generation rate was also studied by performing a series of experiments starting with various initial concentration of H_3NBH_3 while keeping the catalyst concentration constant at 2.0 mM Co. Figure 45 shows the plots of the volume of hydrogen generated versus time during the catalytic hydrolysis of AB at various substrate concentrations. The hydrogen generation rate was determined from the linear portion of the plot for each AB concentration and used for constructing the plot of hydrogen generation rate versus AB concentration, both in logarithmic scale (the inset in Figure 45). The slope of the line given in the inset of Figure 45, $0.91 \approx 1$, indicates that the hydrolysis reaction is first order with respect to the AB concentration.

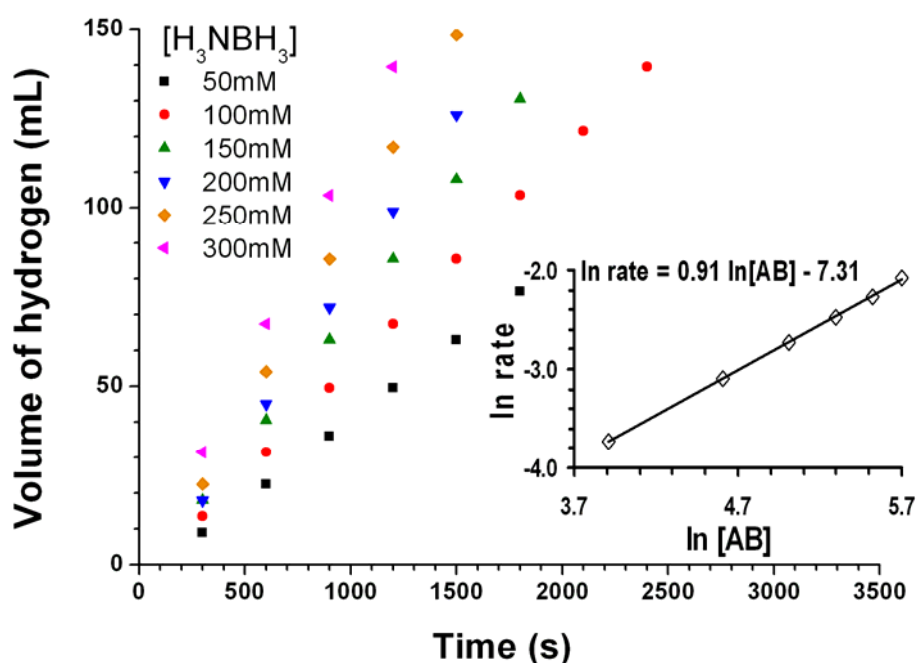


Figure 45. The volume of hydrogen versus time plots depending on the substrate concentrations at constant catalyst concentration (2.0 mM Co) for the hydrolysis of sodium borohydride. The inset shows the plot of hydrogen generation rate versus the concentration of the substrate (both in logarithmic scale)

Consequently, the rate law for the hydrolysis of AB catalyzed by PVP stabilized cobalt(0) nanoclusters can be given as Eq.(12);

$$\frac{-3d[H_3NBH_3]}{dt} = \frac{d[H_2]}{dt} = k[Co][H_3NBH_3] \quad (12)$$

PVP stabilized cobalt(0) nanoclusters catalyzed hydrolysis of AB was carried out at various temperature in the range of 20-40 °C starting with the initial substrate concentration of 100 mM H₃NBH₃ and an initial catalyst concentration of 2.0 mM Co. The values of rate constant (k_{app}) (Table A4 in the Appendix A) for PVP stabilized cobalt(0) nanoclusters catalyzed hydrolysis of AB were calculated from the slope of the linear part of each plot in Figure 46 and used to calculate the apparent activation energy (Arrhenius plot is shown in the Inset of Figure 46): Apparent activation energy $E_a^{apparent} = 46 \pm 2 \text{ kJ.mol}^{-1}$. The value of activation energy is lower than the value reported for the hydrolysis of AB using Co/ γ -Al₂O₃ (62 kJ/mol) [97], and Ru/C (76 kJ/mol) [98].

The Eyring plot given in Figure 47 gives the activation enthalpy, $\Delta H^\ddagger = 43 \pm 3 \text{ kJ/mol}$; and the activation entropy, $\Delta S^\ddagger = -126 \pm 5 \text{ J/K}\cdot\text{mol}$, for the hydrolysis of AB catalyzed by PVP stabilized cobalt(0) nanoclusters.

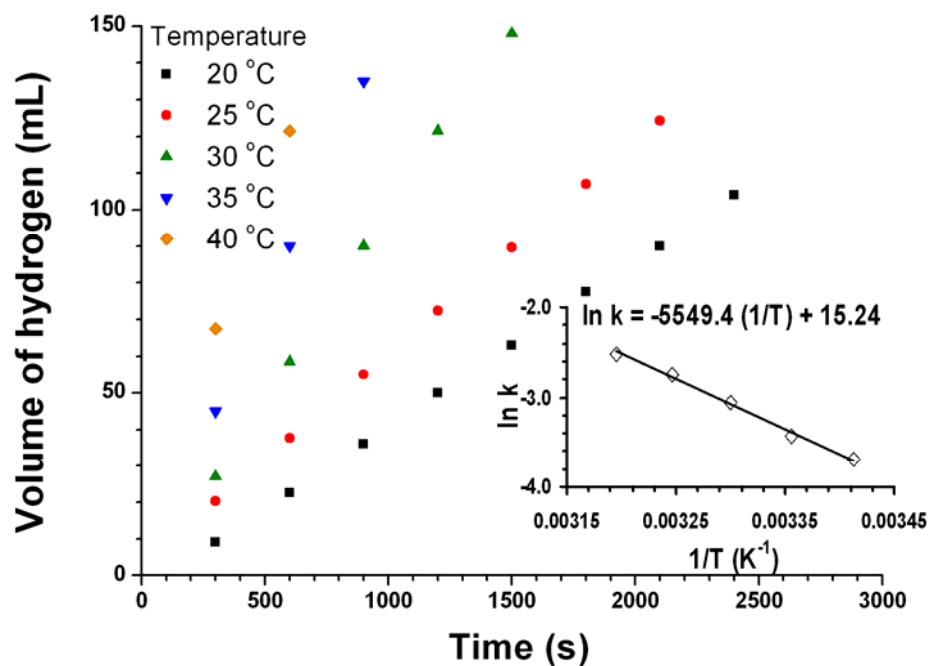


Figure 46. The volume of hydrogen versus time plots at different temperatures for the hydrolysis of ammonia borane (100 mM) catalyzed by PVP stabilized cobalt(0) nanoclusters (2.0 mM Co) in the temperature range 20-40 °C. The inset shows Arrhenius plot ($\ln k$ versus the reciprocal absolute temperature $1/T$ (K^{-1})).

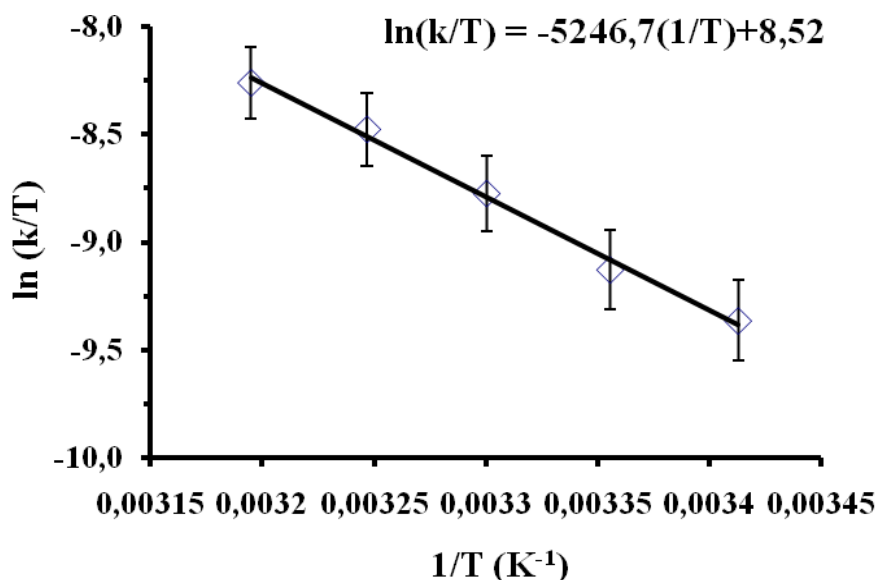


Figure 47. Eyring plot ($\ln(k/T)$ versus the reciprocal absolute temperature $1/T$ (K^{-1})) for the hydrolysis of ammonia borane (100 mM) catalyzed by PVP stabilized cobalt(0) nanoclusters (1.5 mM Co) in the temperature range 20-40 °C

A catalyst lifetime experiment was performed starting with a 20 mL solution of PVP stabilized cobalt(0) nanoclusters containing 1.5 mM Co and 1 M H_3NBH_3 at 25.0 ± 0.5 °C. PVP stabilized cobalt(0) nanoclusters provided 12640 turnovers over 15 h. The ^{11}B -NMR spectral shift at $\delta = 11.8$ ppm of the crystalline product at the bottom of the reactor indicates the formation of $[\text{NH}_4][\text{BO}_2]$ during the TTO experiment. The deactivation of the catalyst in 15 h can be explained by the increasing viscosity and pH due to the formation of $[\text{NH}_4][\text{BO}_2]$.

5.2.2.3. Catalytic Activity of PVP stabilized Cobalt(0) Nanoclusters in the Hydrolysis of Sodium Borohydride in the Basic Medium

According to the established mechanism [99], in acidic medium the hydrolysis of sodium borohydride is initiated by the attack of hydronium ion on the borohydride anion. In alkaline solution, the reduction of proton concentration causes a decrease in the rate of hydrolysis. Since most of the prior studies on the catalytic hydrolysis of NaBH_4 have been carried out in alkaline medium, for comparison we also performed the hydrolysis of NaBH_4 in the basic medium by using PVP stabilized cobalt(0) nanoclusters as catalyst. In order to understand the effect of NaOH concentration on the catalytic activity of PVP stabilized cobalt(0) nanoclusters, the catalytic hydrolysis of NaBH_4 was performed in six different NaOH solutions (1.0, 2.0, 3.0, 4.0, 5.0 and 10% wt NaOH). Figure 48 shows the volume of hydrogen generated versus time during the hydrolysis of 150 mM NaBH_4 in various NaOH solutions catalyzed by PVP stabilized cobalt(0) nanoclusters (2.0 mM Co) at 25.0 ± 0.5 °C. As clearly seen from the inset of Figure 48, the rate of hydrogen generation first increases until the 2 % wt NaOH surprisingly and, then, decreases with the increasing concentration of NaOH expectedly. This observation dictates the use of 2% wt NaOH for the kinetic studies of catalytic hydrolysis of NaBH_4 using PVP stabilized cobalt(0) nanoclusters catalyst.

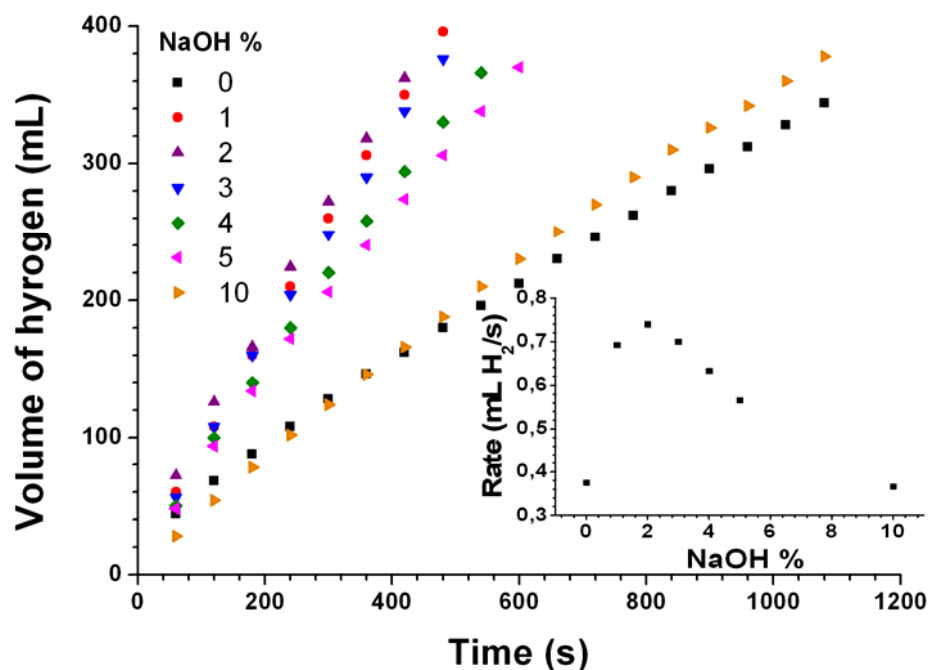


Figure 48. Plot of the volume of hydrogen (mL) versus time (s) for the hydrolysis of 50 mL of 150 mM sodium borohydride catalyzed by PVP stabilized cobalt(0) nanoclusters (2 mM Co) in 1.0, 2.0, 3.0, 4.0, 5.0, and 10.0% wt NaOH solutions at 25.0 ± 0.5 °C. The inset shows the plot of hydrogen generation rate change depending on the % wt of NaOH.

Figure 49 shows the volume of hydrogen generated versus time in the catalytic hydrolysis of NaBH_4 (150 mM) in the presence of PVP stabilized cobalt(0) nanoclusters with different cobalt concentration (1.0-3.0 mM Co) in 2 % wt NaOH solution at 25.0 ± 0.5 °C. Although the hydrolysis reactions were performed in alkaline solution, the hydrogen generation starts immediately after addition of the catalyst. The presence of sodium hydroxide does not cause an induction period in the formation of the nanoclusters catalyst. Plotting the hydrogen generation rate versus cobalt concentration, both on logarithmic scales, gives a straight line (the inset in Figure 49), the slope of which is found to be 0.94. This result indicates that the hydrolysis of NaBH_4 using PVP stabilized cobalt(0) nanoclusters as catalyst in 2% wt NaOH solution is first-order with respect to the catalyst concentration.

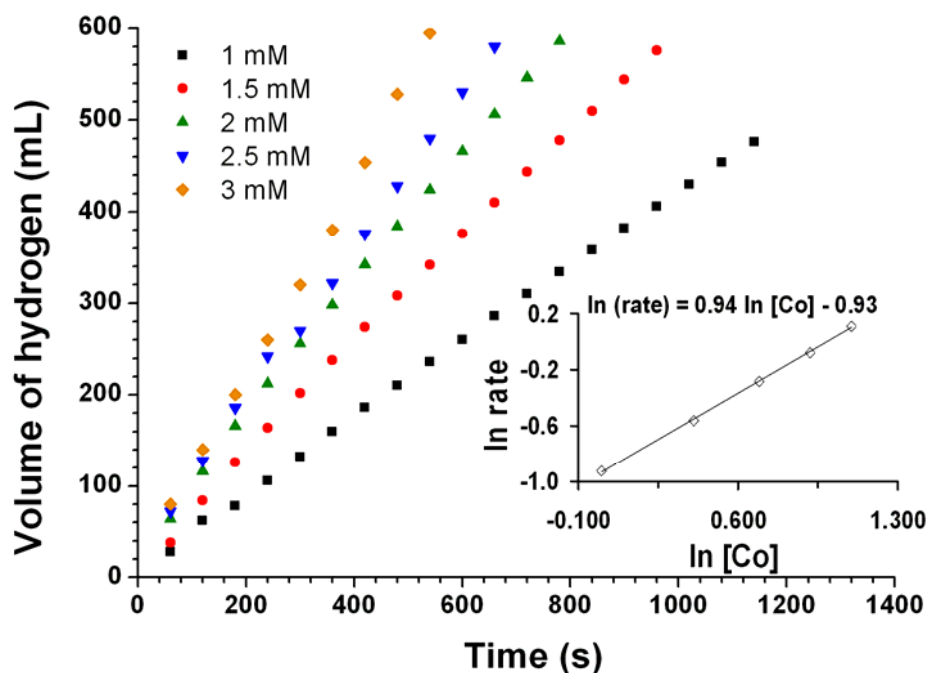


Figure 49. Plot of the volume of hydrogen versus time for the hydrolysis of sodium borohydride (150 mM) in 2% wt NaOH solution catalyzed by PVP stabilized cobalt(0) nanoclusters with different cobalt(0) concentrations at 25.0 ± 0.5 °C. The inset shows the plot of hydrogen generation rate versus catalyst concentration (both in logarithmic scale) for the PVP stabilized cobalt(0) nanoclusters catalyzed hydrolysis of NaBH_4 in 2% wt NaOH solution at 25.0 ± 0.5 °C.

The effect of substrate concentration on the hydrogen generation rate was also studied by performing a series of experiments starting with various initial concentration of NaBH_4 while the catalyst concentration is kept constant at 2.0 mM Co in 2% wt NaOH solution at 25.0 ± 0.5 °C (Figure 50). The slope of plot (the inset of Figure 50) shows that the catalytic hydrolysis is zeroth order with respect to NaBH_4 concentration.

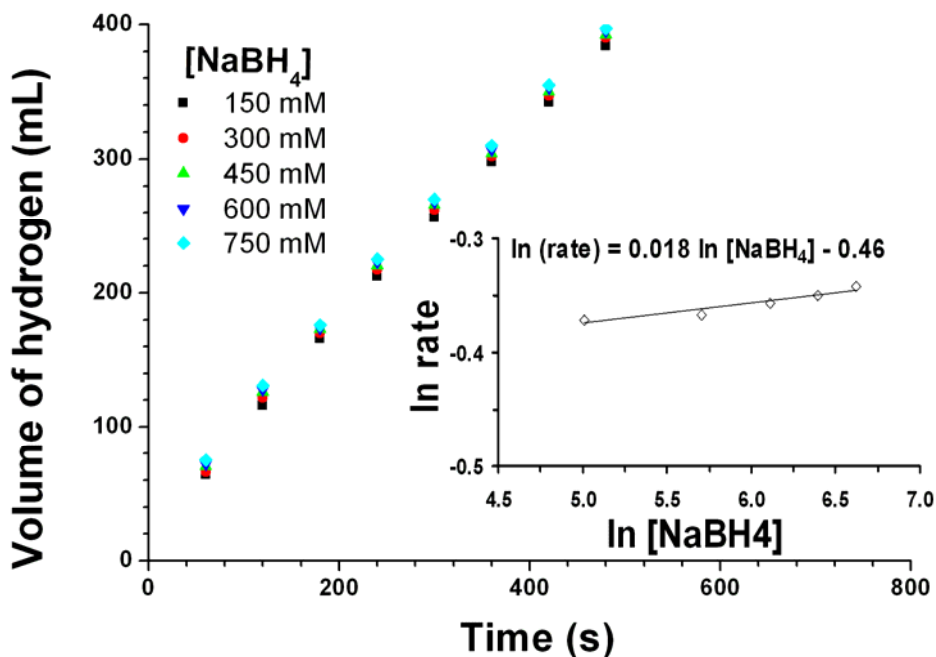


Figure 50. Plot of the volume of hydrogen versus time for the hydrolysis of sodium borohydride in 2% wt NaOH solution catalyzed by PVP stabilized cobalt(0) nanoclusters with different NaBH₄ concentrations at 25.0 ± 0.5 °C. The inset shows the plot of hydrogen generation rate versus NaBH₄ concentration (both in logarithmic scale) for the PVP stabilized cobalt(0) nanoclusters catalyzed hydrolysis of NaBH₄ in 2% wt NaOH solution at 25.0 ± 0.5 °C.

Consequently, the rate law for the catalytic hydrolysis of NaBH₄ catalyzed by PVP stabilized cobalt(0) nanoclusters in 2% wt NaOH solution can be given as, Eq. (13)

$$\frac{-4d[NaBH_4]}{dt} = \frac{d[H_2]}{dt} = k[Co] \quad (13)$$

The hydrolysis of sodium borohydride was carried out at various temperatures in the range of 20-40 °C starting with the initial substrate concentration of 150 mM NaBH₄ and an initial catalyst concentration of 2.0 mM Co in 2% wt NaOH solution (Figure 51). The values of rate constant (k_{app}) (Table A5 in the

Appendix A) determined from the linear portions of the volume of hydrogen versus time plots at six different temperatures were used to draw Arrhenius plot (the inset of Figure 51) and calculate the activation parameters: apparent activation energy, $E_a^{\text{apparent}} = 37 \pm 2 \text{ kJ/mol}$; activation enthalpy, $\Delta H^\ddagger = 36 \pm 2 \text{ kJ/mol}$; and activation entropy, $\Delta S^\ddagger = -134 \pm 3 \text{ J/K} \cdot \text{mol}$ for the PVP stabilized cobalt(0) nanoclusters catalyzed hydrolysis of 150 mM NaBH_4 in 2% wt NaOH solution. The value of activation energy is lower than the value reported for the hydrolysis of NaBH_4 in basic solution using bulk cobalt (75 kJ/mol), nickel (71 kJ/mol), and Raney nickel (63 kJ/mol) [95], bulk ruthenium (47 kJ/mol) [100], and Co-B catalyst (45 kJ/mol) [101]. It is noteworthy that the activation energy and enthalpy for the hydrolysis of NaBH_4 in basic solution are both lower than the values found for the same reaction catalyzed by PVP stabilized cobalt(0) nanoclusters in the absence of NaOH.

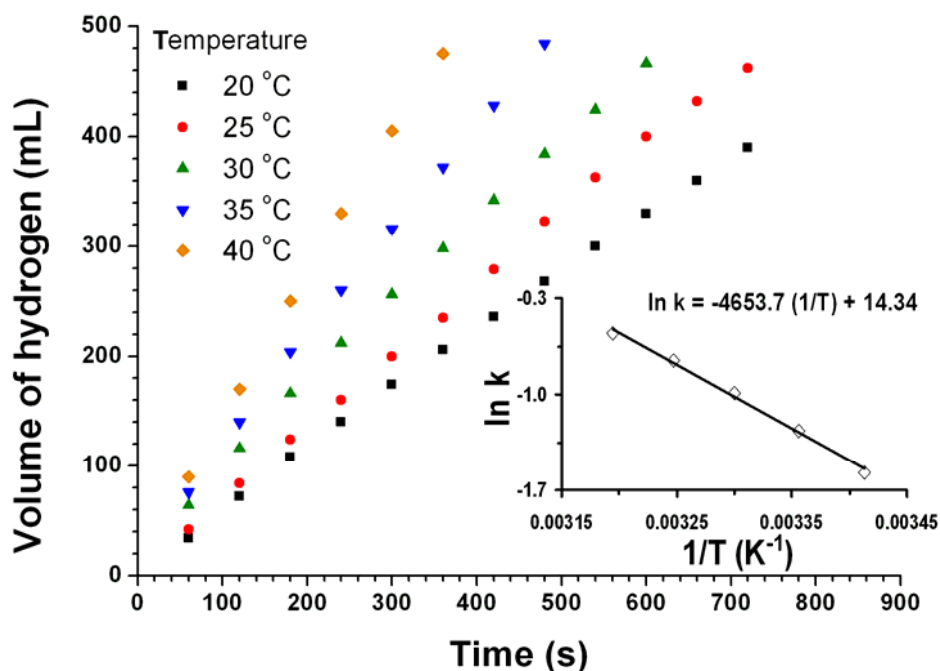


Figure 51. Plot of the volume of hydrogen (mL) generated versus time (s) for the hydrolysis of 50 mL of 150 mM sodium borohydride in 2% wt NaOH solution at different temperatures (15, 20, 25, 30, and 35°C) catalyzed by PVP-stabilized cobalt(0) nanoclusters ($[\text{Co}] = 2.0 \text{ mM}$). The inset shows the Arrhenius plot for the PVP stabilized cobalt(0) nanoclusters catalyzed hydrolysis of sodium borohydride in 2 wt % NaOH solution.

Our kinetic studies on the hydrolysis of sodium borohydride catalyzed by PVP stabilized cobalt(0) nanoclusters reveals that NaOH stabilized and non-stabilized aqueous solutions of sodium borohydride shows zero and first order dependency with respect to the NaBH_4 concentration, respectively. This is one particular aspect of the catalytic hydrolysis of NaBH_4 that show difference involving change in the hydrolysis rate with changing NaBH_4 and NaOH concentration for different metal catalysts. For example, Amendola et al. [59] and Jeong et al. [102] have shown that the reaction rate decreases with increasing NaBH_4 concentration. The work of Kaufman et al.[95] and our previous study [37], however, shows that the reaction is zero-order, indicating that a change in concentration of NaBH_4 should not change the rate of hydrolysis reaction. In terms of the NaOH concentration, general thought in increasing the NaOH concentration would decrease the hydrolysis rate, especially in the light that the solution is base stabilized to prevent hydrolysis. It is generally concluded that increasing $[\text{NaBH}_4]$ increases solution viscosity and, therefore, decreases reaction rate, a deviation from the zero-order kinetics described by Kaufman [95]. Therefore, the effect of increasing NaOH on the reaction rate of hydrolysis of NaBH_4 is still not well-established. However, a mechanistic study proposed by Halbrook and Twist [103] can give more insights to understand the effect of NaOH concentration on the hydrolysis of NaBH_4 . In this mechanism, reaction begins with the attachment of the BH_4^- ion to a catalytic site which is called as anodic step. However, the rate of the reaction is determined by cathodic step where an electron is combined with a water molecule and available site to form the MH complex and hydroxyl ion. This step is called non-catalyzed intermediate reaction. In this step, the increase in NaOH pushes forward to increasing $[\text{MH}]$ and thereby reduces rate of the overall reaction when a hydrogen adsorbing catalyst is used such as Ru. In contrast, non-noble metals such as Co for our case, hydrogen adsorption is weak, and so the rate of overall reaction increases by increasing concentration of NaOH up to the point of saturation. In the light of these mechanistic explanations, the increase in the initial concentration of NaBH_4 increases the pH of the unstabilized borohydride solution which is resulted in the increase in rate of hydrolysis reaction. However, in the case of NaOH stabilized borohydride solution which has high pH value, the increase in the initial concentration of NaBH_4 has no

effect on the pH of the solution, and so there is no change in the rate of hydrolysis reaction. Therefore, hydrolysis of unstabilized borohydride solution catalyzed by polymer-stabilized cobalt nanoclusters shows first-order dependency, but the hydrolysis of NaOH stabilized borohydride solution show zeroth order dependency with respect to the NaBH_4 concentration.

5.2.3. Catalytic Activity of The PVP stabilized Ruthenium(0) Nanoclusters in The Hydrolysis of Sodium Borohydride and Ammonia borane

5.2.3.1. Kinetics of the Hydrolysis of Sodium Borohydride Catalyzed by PVP Stabilized Ruthenium(0) Nanoclusters in Aqueous Medium

Figure 52 shows the plots of hydrogen volume generated versus time during the catalytic hydrolysis of NaBH₄ solution in the presence of PVP stabilized ruthenium(0) nanoclusters at different ruthenium concentrations at 25.0 ± 0.5 °C. A fast hydrogen evolution starts immediately without induction period, indicating a rapid dispersion of the catalyst in reaction medium.

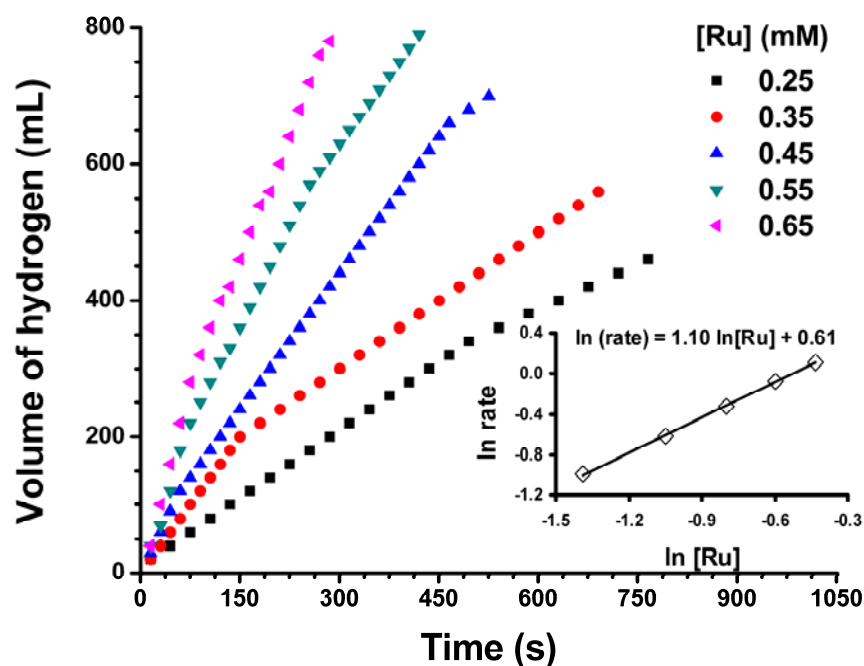


Figure 52. Plot of the volume of hydrogen (mL) versus time (s) for the hydrolysis of NaBH₄ (284.0 mg, 150 mM in 50 mL) catalyzed by PVP stabilized ruthenium(0) nanoclusters with different ruthenium concentrations in the range of 0.25-0.65 mM at 25.0 ± 0.5 °C. The inset shows the rate of hydrogen generation versus ruthenium concentration both in logarithmic scale.

The rate of hydrogen generation from the hydrolysis of NaBH₄ in the presence of PVP stabilized ruthenium(0) nanoclusters is in the range of 40-140 mL

of $\text{H}_2 \cdot \text{min}^{-1}$ at the catalyst concentrations in the range of 0.25-0.65 mM Ru corresponding to TOF value up to $193 \text{ mol H}_2 \cdot (\text{mol Ru} \cdot \text{min})^{-1}$ at room temperature. Plotting the hydrogen generation rate, determined from the linear portion of the plots in Figure 52, versus ruthenium concentration, both in logarithmic scales (the inset of Figure 52), gives a straight line with a slope of $1.10 \approx 1.0$, indicating that the hydrolysis of NaBH_4 is first-order with respect to the catalyst concentration.

The effect of substrate concentration on the hydrogen generation rate was also studied by performing a series of experiments starting with varying initial concentration of NaBH_4 while the ruthenium concentration is kept constant at 0.35 mM. Figure 53 shows the plot of hydrogen volume generated versus time for various initial concentration of NaBH_4 in the range of 150-900 mM NaBH_4 . Plotting the hydrogen generation rate determined from the linear portion of the plots in Figure 53 versus ruthenium concentration, both in logarithmic scales (the inset in Figure 53) shows that the catalytic hydrolysis of NaBH_4 proceeds zeroth order with respect to substrate concentration.

Consequently, the rate law for the hydrolysis of NaBH_4 catalyzed by PVP stabilized ruthenium(0) nanoclusters can be given as, Eq. (14)

$$\frac{-4d[\text{NaBH}_4]}{dt} = \frac{d[\text{H}_2]}{dt} = k[\text{Ru}] \quad (14)$$

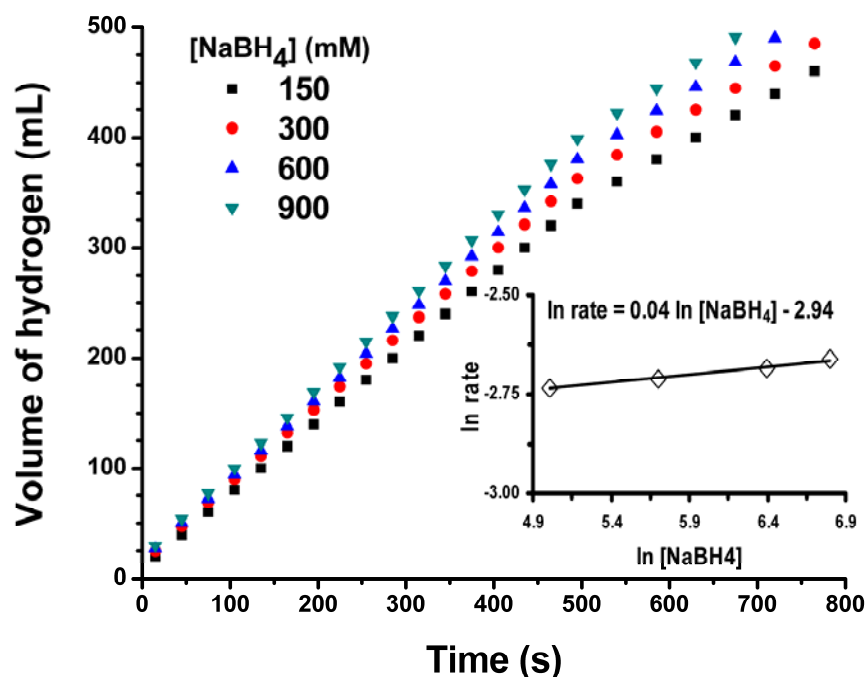


Figure 53. Plot of the volume of hydrogen (mL) versus time (s) for the hydrolysis of NaBH_4 catalyzed by PVP stabilized ruthenium(0) nanoclusters ($[\text{Ru}] = 0.35 \text{ mM}$) solution (50 mL) in different substrate concentrations in the range of 150-900 mM NaBH_4 at $25.0 \pm 0.5 \text{ }^\circ\text{C}$.

The hydrolysis of NaBH_4 in the presence of PVP stabilized ruthenium(0) nanoclusters was carried out at various temperatures (20, 25, 30, 35, 40 and 45 $^\circ\text{C}$) starting with a 150 mM initial substrate concentration and an initial ruthenium concentration of 0.35 mM. The values of rate constant (k_{app}) (Table A6 in Appendix A) determined from the linear portions of the hydrogen volume versus time plots at six different temperatures (Figure 54) are used to construct the Arrhenius and Eyring plots as shown in the inset of Figure 54 and Figure 55, respectively. The apparent activation energy was found to be $E_a^{\text{apparent}} = 56 \pm 2 \text{ kJ}\cdot\text{mol}^{-1}$. This activation energy is higher than the value found for the same hydrolysis reaction catalyzed by acetate-stabilized ruthenium(0) nanoclusters (41 kJ/mol) [104] and PVP stabilized nickel(0) nanoclusters (46 $\text{kJ}\cdot\text{mol}^{-1}$) but it is lower than found for the hydrolysis of NaBH_4 catalyzed by bulk ruthenium (57 $\text{kJ}\cdot\text{mol}^{-1}$)[105], PVP stabilized cobalt(0)

nanoclusters ($63 \text{ kJ}\cdot\text{mol}^{-1}$) and other bulk metal catalysts: 75 kJ/mol for cobalt, 71 kJ/mol for nickel, and 63 kJ/mol for Raney nickel [106].

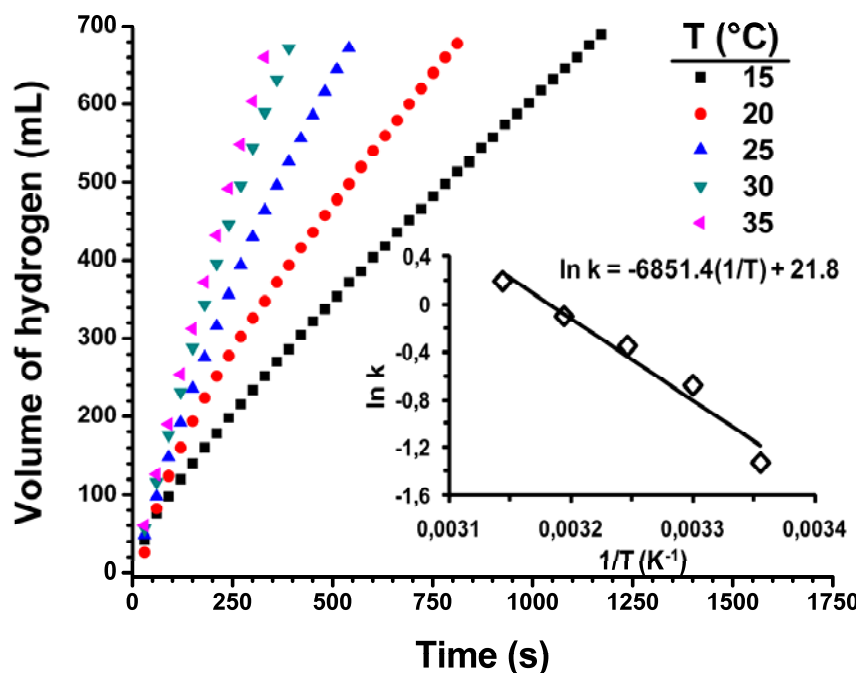


Figure 54. Plot of the volume of hydrogen (mL) versus time (s) for the hydrolysis of NaBH_4 (284.0 mg, 150 mM in 50 mL) catalyzed by PVP stabilized ruthenium(0) nanoclusters ($[\text{Ru}] = 0.35 \text{ mM}$) at different temperatures in the range of 15-35 °C.

The Eyring plot given in Figure 55 gives the activation enthalpy, $\Delta H^\ddagger = 54 \pm 2 \text{ kJ}\cdot\text{mol}^{-1}$; and the activation entropy, $\Delta S^\ddagger = -72 \pm 3 \text{ J}\cdot(\text{K}\cdot\text{mol})^{-1}$ for the hydrolysis of NaBH_4 catalyzed by PVP stabilized ruthenium(0) nanoclusters.

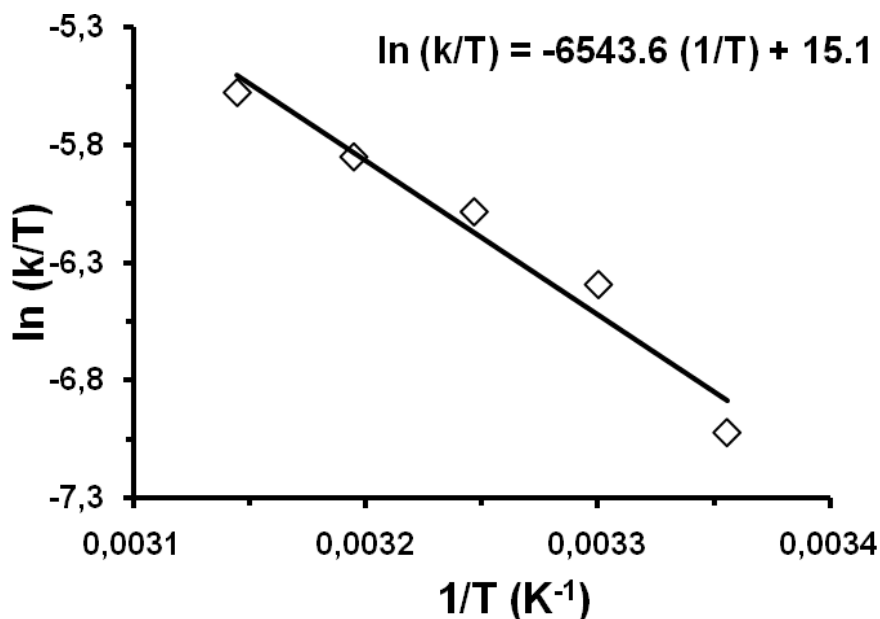


Figure 55. Eyring plot ($\ln(k/T)$) versus the reciprocal absolute temperature $1/T \text{ (K}^{-1}\text{)}$ for the hydrolysis of sodium borohydride (150 mM) catalyzed by PVP stabilized ruthenium(0) nanoclusters (0.35 mM Ru) in the temperature range of 15-35 °C

A catalyst lifetime experiment for PVP stabilized ruthenium(0) nanoclusters in the hydrolysis of NaBH_4 was started with 0.25 mM Ru at $25.0 \pm 0.5 \text{ }^\circ\text{C}$. The PVP stabilized ruthenium(0) nanoclusters were found to provide 38800 turnovers in the hydrolysis of NaBH_4 over 39 h before deactivation. This is one of the highest TTON value in the catalytic hydrolysis of NaBH_4 as considered to the one of the previous highest value for acetate stabilized ruthenium(0) nanoclusters was $\text{TTON} = 5170$ [104], note the improvement by a factor of 7. Thus, it is proved one more time that the use of polymer stabilizer increases the catalytic lifetime of transition metal(0) nanoclusters by preserving their activity.

5.2.3.2. Kinetics of the Hydrolysis of Sodium Borohydride Catalyzed by PVP Stabilized Ruthenium(0) Nanoclusters in Basic Medium

As we mentioned in the previous sections, in the acidic medium the hydrolysis of NaBH_4 is initiated by the attack of hydronium ion on the borohydride

anion according to the established mechanism [107,108]. In the basic solution, the reduction of proton concentration causes a decrease in the rate of hydrolysis. Since most of the prior studies on the catalytic hydrolysis of NaBH_4 have been carried out in alkaline medium (mostly in 5 wt % NaOH solution) [109], we also performed the hydrolysis of NaBH_4 in the basic medium by using PVP stabilized ruthenium(0) nanoclusters as catalyst to make comparison. In order to understand the effect of NaOH concentration on the catalytic activity of PVP stabilized ruthenium(0) nanoclusters, the catalytic hydrolysis of NaBH_4 was performed in four different solutions that contain 2.0, 3.0, 4.0, and 5.0 wt % NaOH. Figure 56 shows the volume of hydrogen generated versus time for the hydrolysis of NaBH_4 catalyzed by PVP stabilized ruthenium(0) nanoclusters in the solutions including different wt % NaOH at 25.0 ± 0.5 °C. In contrast to PVP stabilized cobalt(0) nanoclusters (see section 5.2.2.3) , the rate of hydrogen generation decreases with the increasing concentration of sodium hydroxide, expectedly. The dramatic change in the rate of hydrogen generation was observed from 2 wt% to 3 wt% NaOH indicating that 2 wt % NaOH is not enough to stabilize aqueous NaBH_4 solution. As seen from the Figure 56, the rate changed slightly after 3 wt% NaOH. For this reason, we selected 5 wt% NaOH solution for the hydrolysis of NaBH_4 catalyzed by PVP stabilized ruthenium(0) nanoclusters in alkaline solution for further kinetic experiments.

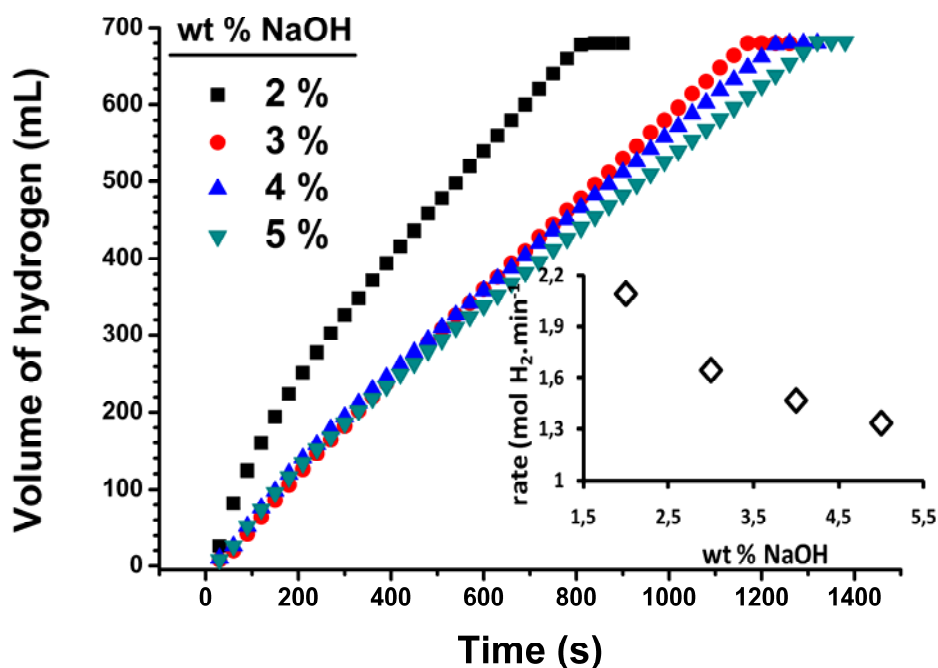


Figure 56. Plot of the volume of hydrogen (mL) versus time (s) for the hydrolysis of sodium borohydride ($[\text{NaBH}_4] = 150 \text{ mM}$) catalyzed by PVP stabilized ruthenium(0) nanoclusters ($[\text{Ru}] = 0.75 \text{ mM}$) in different wt% NaOH solutions at $25.0 \pm 0.5 \text{ }^\circ\text{C}$.

Figure 57 shows the volume of hydrogen generated versus time for the hydrolysis of NaBH_4 (150mM) in the presence of PVP stabilized ruthenium(0) nanoclusters with different ruthenium concentrations in the range of 0.25-1.25 mM in 5.0 wt% NaOH solution at $25.0 \pm 0.5 \text{ }^\circ\text{C}$. The inset of the Figure 57 shows the hydrogen generation rate versus ruthenium concentration, both in logarithmic scales, gives a straight line, the slope of which is found to be 0.98. This result indicates that the hydrolysis of NaBH_4 in the presence of PVP stabilized ruthenium(0) nanoclusters is first order with respect to the catalyst concentration in 5.0 wt% NaOH solution.

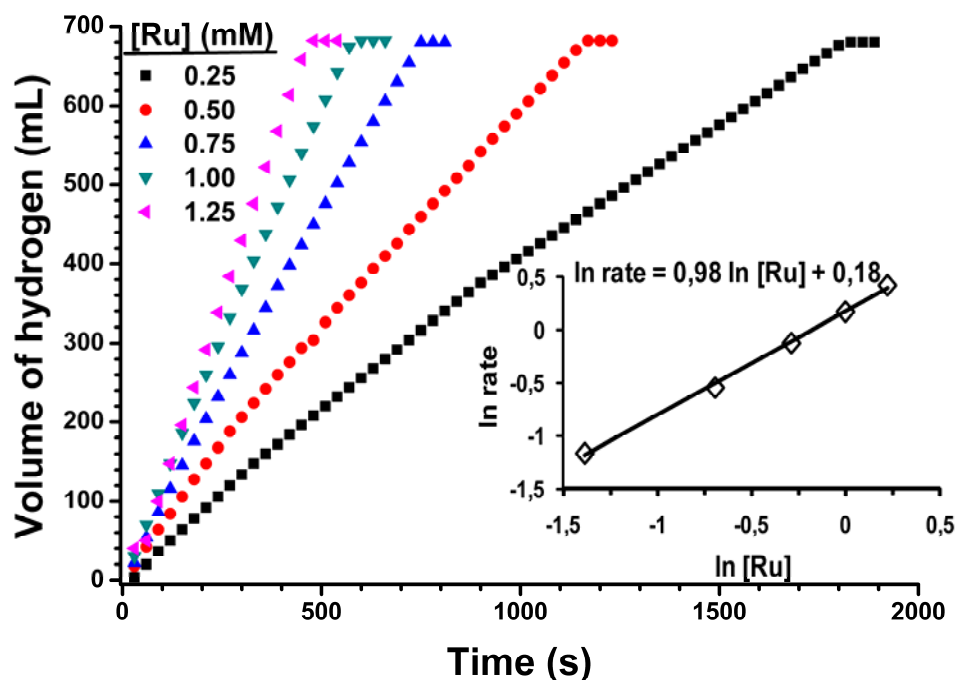


Figure 57. Plot of the volume of hydrogen (mL) versus time (s) for the hydrolysis of sodium borohydride ($[\text{NaBH}_4] = 150 \text{ mM}$) in 5 wt % NaOH solution catalyzed by PVP stabilized ruthenium(0) nanoclusters with different ruthenium(0) concentrations at $25.0 \pm 0.5 \text{ }^\circ\text{C}$.

The effect of substrate concentration on the hydrogen generation rate was also studied by performing a series of experiments starting with various initial concentration of NaBH_4 while the catalyst concentration is kept constant at 0.75 mM Ru in 5 wt % NaOH solution at $25.0 \pm 0.5 \text{ }^\circ\text{C}$. The results indicate that the catalytic hydrolysis is zeroth order with respect to substrate concentration in the presence of 5 wt % NaOH.

The hydrolysis of NaBH_4 was carried out at various temperature in the range of 20-45 °C starting with the initial substrate concentration of 150 mM NaBH_4 and an initial catalyst concentration of 0.75 mM Ru in 5 wt % NaOH solution (Figure 58). The values of rate constant (k_{app}) (Table A7 in the Appendix A) determined from the linear portions of the H_2 volume versus time plots at six different temperatures are used to calculate the activation parameters: apparent activation energy, $E_a^{\text{apparent}} = 33 \pm 2 \text{ kJ}\cdot\text{mol}^{-1}$ (the inset of Figure 58); activation enthalpy, $\Delta H^\ddagger = 30 \pm 2 \text{ kJ/mol}$; and activation entropy, $\Delta S^\ddagger = -118 \pm 3 \text{ J}\cdot(\text{K}\cdot\text{mol})^{-1}$ (Figure 59) that were found for the PVP stabilized ruthenium(0) nanoclusters catalyzed hydrolysis of NaBH_4 (150 mM) in 5 wt% NaOH solution.

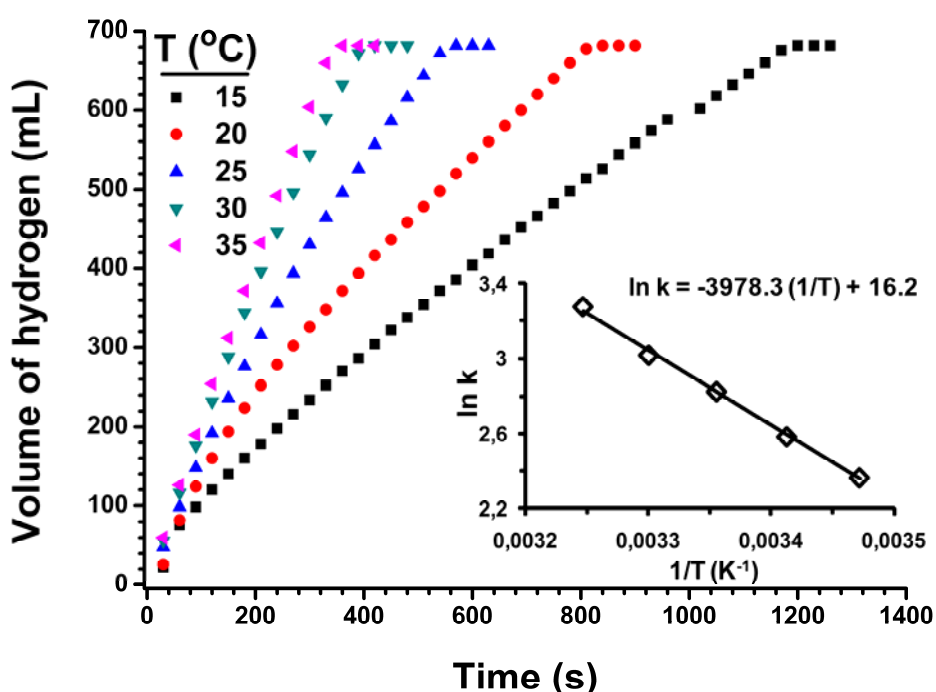


Figure 58. Plot of the volume of hydrogen (mL) generated versus time (s) for the hydrolysis of sodium borohydride (150 mM) catalyzed by PVP stabilized ruthenium(0) nanoclusters in 5 wt% NaOH solution at different temperatures ($[\text{Ru}] = 0.75 \text{ mM}$)

The value of activation energy is lower than the value of $47 \text{ kJ}\cdot\text{mol}^{-1}$ found for bulk ruthenium at 5.6 M NaBH_4 concentration [110]. Table 1 shows the activation energies determined for the hydrolysis of NaBH_4 in basic medium catalyzed by other catalysts for comparison. The observed small value of activation enthalpy and the large negative value of activation entropy reveal that the zeolite framework stabilized ruthenium(0) nanoclusters catalyzed hydrolysis of NaBH_4 followed associative mechanism in basic medium.

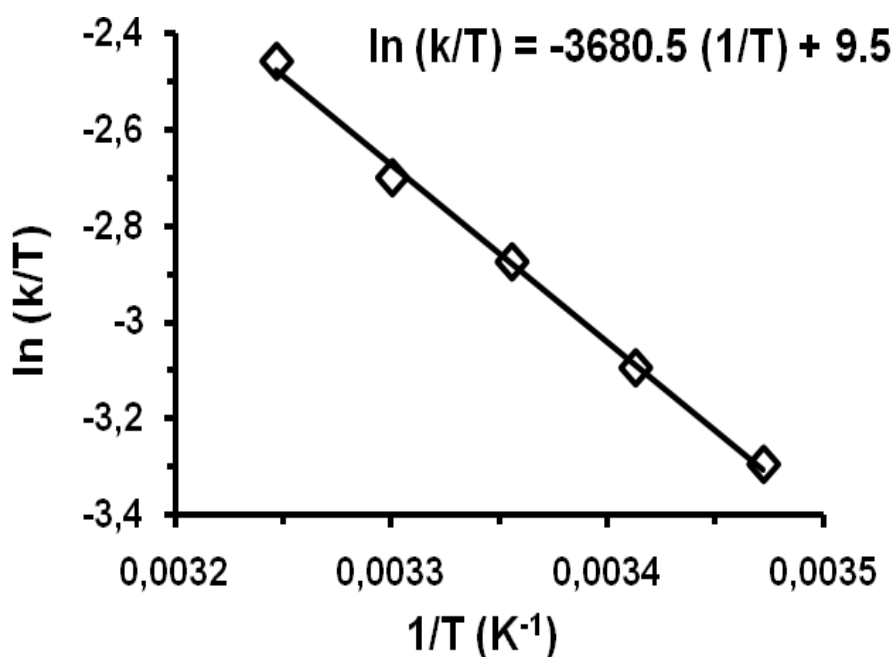


Figure 59. The Eyring plot for the hydrolysis of sodium borohydride catalyzed by PVP stabilized ruthenium(0) nanoclusters in 5 wt% NaOH solution.

Table 2. The catalyst systems employed in the hydrolysis of sodium borohydride in the basic medium and obtained activation energies in different reaction conditions.

Entry	Catalyst	Ea (kJ/mol)	NaBH ₄	NaOH	Reference
1	Acetate stabilized Ru(0) NCs	43	0.15 M	10 %	[104]
2	Ru-IRA 400	47	20 %	10 %	[110]
3	Ni-Co-B	62	0.16 g	15 %	[111]
4	Co-B / Ni foam	33	20 %	10 %	[112]
5	Ni _x B	38	1.5%	10 %	[113]
6	Co-B	45	2 %	5 %	[114]
7	Co/ γ -Al ₂ O ₃	33	5 %	5 %	[115]
8	Co-B/ C	58	0.2 M	20 mmol	[116]
9	Ru promoted sulphated Zr	76	0.6 M	1.3 M	[117]
10	Pt/LiCoO ₂	70	10 %	5 %	[118]
11	Ru/LiCoO ₂	68	10 %	5 %	[118]
12	Co-Mn-B nanocomposites	55	5 %	5 %	[119]
13	Ru/C	67	1 M	4 %	[120]
14	PtPd@CNT	19	0.15 M	1 %	[121]
15	Co-W-B/Ni	29	20 %	5 %	[122]
16	PVP stabilized Co(0) NCs	37	0.15 M	5 %	[123]
17	PVP stabilized Ru(0) NCs	33	0.15 M	5 %	[this study]

5.2.3.3. Kinetics of the Hydrolysis of Ammonia Borane Catalyzed by PVP Stabilized Ruthenium(0) Nanoclusters

Figure 60 shows the plots of hydrogen volume generated versus time during the hydrolysis of AB solution catalyzed by PVP stabilized ruthenium(0) nanoclusters at different ruthenium concentrations at 25.0 ± 0.5 °C. The rate of hydrogen generation determined from the linear portion of the plots in Figure 60 from the hydrolysis of AB in the presence of PVP stabilized ruthenium(0) nanoclusters is in the range of 20-100 mL of $\text{H}_2 \cdot \text{min}^{-1}$ for the catalyst concentrations in the range of 0.10-0.50 mM Ru corresponding to TOF value up to $446 \text{ mol H}_2 \cdot (\text{mol Ru} \cdot \text{min})^{-1}$ at room temperature. A straight line with a slope of $1.10 \approx 1.0$ was obtained when plotting the hydrogen generation rate versus ruthenium concentration, both in logarithmic scales (the inset of Figure 60) indicating that the hydrolysis of AB is first-order with respect to the ruthenium concentration.

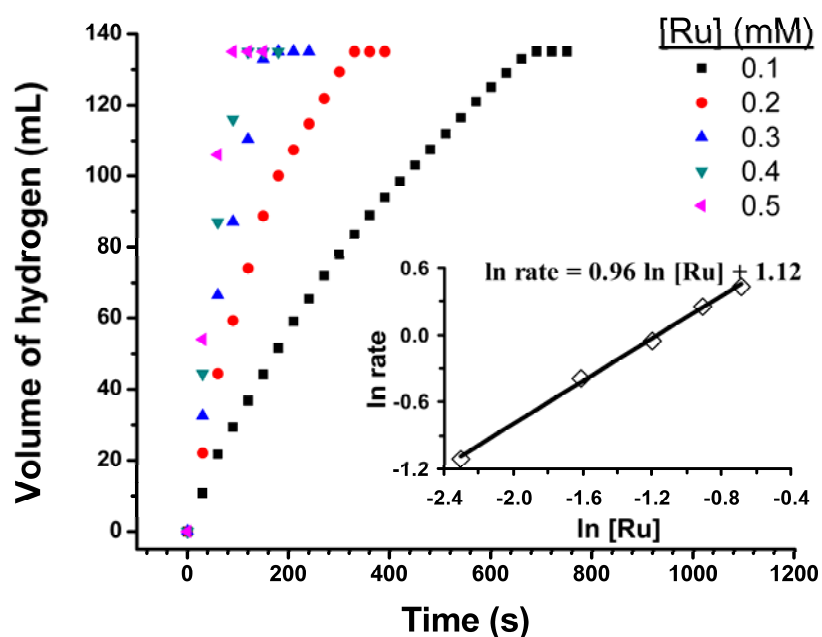


Figure 60. Plot of the volume of hydrogen (mL) versus time (s) for the hydrolysis of ammonia borane (63.0 mg, 100 mM in 20 mL) catalyzed by PVP stabilized ruthenium(0) nanoclusters with different ruthenium concentrations at 25.0 ± 0.5 °C. The inset shows the rate of hydrogen generation versus ruthenium concentration both in logarithmic scale.

The effect of substrate concentration on the hydrogen generation rate was also studied by performing a series of experiments starting with varying initial concentration of AB while the ruthenium concentration is kept constant at 0.30 mM. Figure 61 shows the plot of hydrogen volume generated versus time for various initial concentration of AB in the range of 100-500 mM H_3NBH_3 . The slope of the plot in the inset of Figure 61 which is the hydrogen generation rate versus ruthenium concentration, both in logarithmic scales shows that the catalytic hydrolysis of AB proceeds zeroth order with respect to substrate concentration.

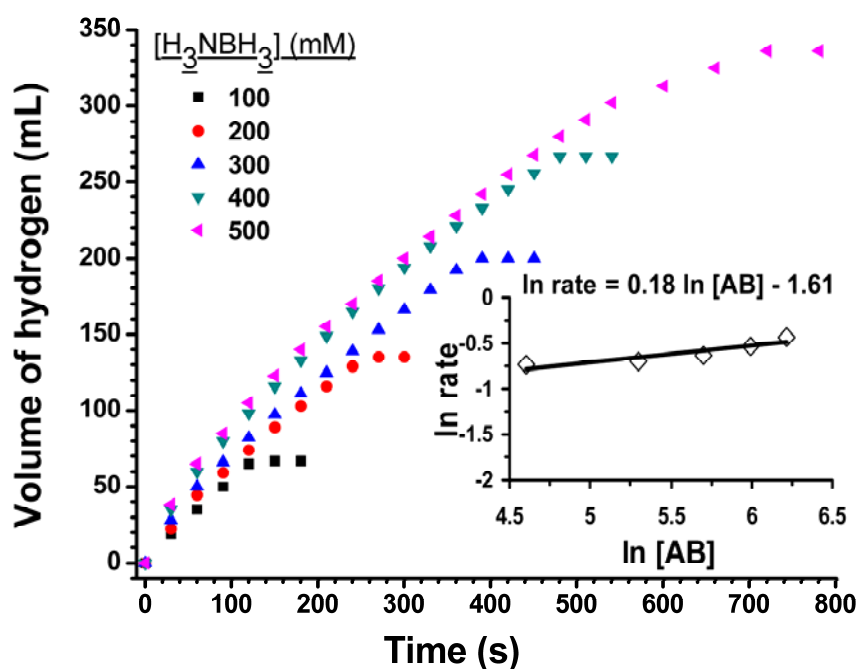


Figure 61. The volume of hydrogen versus time plots depending on the substrate concentrations at constant catalyst concentration for the hydrolysis of ammonia borane catalyzed by PVP stabilized ruthenium(0) nanoclusters. The inset shows the plot of hydrogen generation rate versus the concentration of the substrate (both in logarithmic scale)

Consequently, the rate law for the hydrolysis of AB catalyzed by PVP stabilized ruthenium(0) nanoclusters can be given as, Eq. (15);

$$\frac{-3d[H_3NBH_3]}{dt} = \frac{d[H_2]}{dt} = k[Ru] \quad (15)$$

The hydrolysis of AB was carried out at various temperatures in the range of 15-35 °C starting with a 100 mM initial H_3NBH_3 concentration and an initial ruthenium concentration of 0.30 mM. The values of rate constant (k_{app}) (Table A8 in the Appendix A) determined from the linear portions of the hydrogen volume versus time plots at five different temperatures (Figure 62) are used to construct the Arrhenius and Eyring plots as shown in the inset of Figure 62 and Figure 63, respectively. The apparent activation energy was found to be $E_a^{apparent} = 38 \pm 2$ $\text{kJ}\cdot\text{mol}^{-1}$.

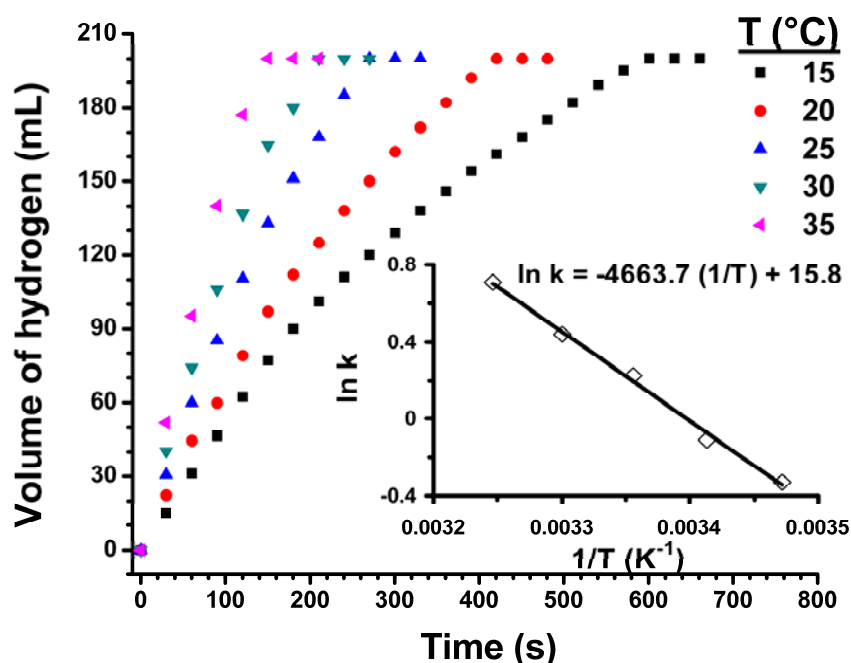


Figure 62. Plot of the volume of hydrogen (mL) versus time (s) for the hydrolysis of H_3NBH_3 (63.0 mg, 100 mM in 50 mL) catalyzed by PVP stabilized ruthenium(0) nanoclusters ($[Ru] = 0.35$ mM) at different temperatures in the range of 15-35 °C.

The Eyring plot given in Figure 63 gives the activation enthalpy, $\Delta H^\ddagger = 54 \pm 2$ $\text{kJ}\cdot\text{mol}^{-1}$; and the activation entropy, $\Delta S^\ddagger = -72 \pm 3$ $\text{J}\cdot(\text{K}\cdot\text{mol})^{-1}$ for the hydrolysis of AB catalyzed by PVP stabilized ruthenium(0) nanoclusters.

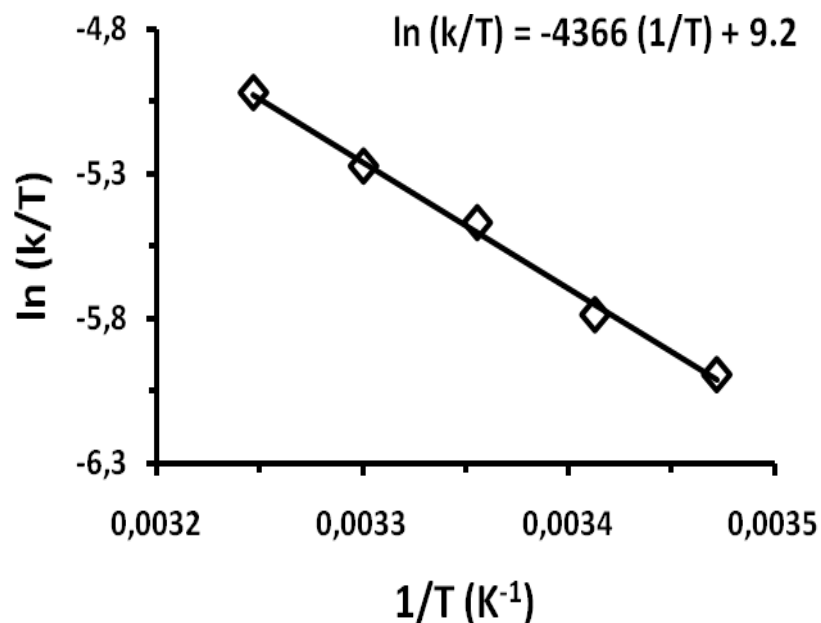


Figure 63. Eyring plot ($\ln(k/T)$) versus the reciprocal absolute temperature $1/T \text{ (K}^{-1}\text{)}$ for the hydrolysis of ammonia borane (100 mM) catalyzed by PVP stabilized ruthenium(0) nanoclusters (0.35 mM Ru) in the temperature range of 15-35 °C

A catalyst lifetime experiment for PVP stabilized ruthenium(0) nanoclusters in the hydrolysis of AB was started with 0.10 mM Ru at $25.0 \pm 0.5 \text{ }^\circ\text{C}$. PVP stabilized ruthenium(0) nanoclusters provided 44320 turnovers in the hydrolysis of AB over 52 h before deactivation. This is one of the highest TTON value in the catalytic hydrolysis of AB compared to other catalyst systems tested in the hydrolysis of AB.

5.3. PSSA-co-MA Stabilized Nickel(0), Cobalt(0) and Ruthenium(0) Nanoclusters

5.3.1. In Situ Generation and Characterization of PSSA-co-MA Stabilized Nickel(0) or Cobalt(0) Nanoclusters

The PSSA-co-MA stabilized nickel(0) or cobalt(0) nanoclusters were generated in situ from the reduction of nickel(II) chloride or cobalt(II) chloride by minimum amount of sodium borohydride shortly before their employment as catalysts in the hydrolysis of AB at room temperature. The use of sodium borohydride was found to be necessary for the reduction of metal ions to their metallic state because no reduction and hydrogen generation were observed by performing the catalytic hydrolysis reaction only in the presence of AB under the same conditions. In the present system, the use of NaBH₄ as a reducing agent results in generation of additional hydrogen gas from its hydrolysis. However, the maximum amount of hydrogen generated from the hydrolysis of sodium borohydride is 11 mL, which is subtracted from the total volume of hydrogen generated from the system to find the volume of sole hydrogen generation from the catalytic hydrolysis of AB. In all the experiments, the molar ratio of the total hydrogen generated from the sole hydrolysis of AB to the initial AB in the presence of both PSSA-co-MA stabilized nickel(0) or cobalt(0) nanoclusters was 2.8 - 2.9, very close the theoretical value of 3.0 [69]. These results indicate that the sole hydrolysis of AB is almost completed in the presence of PSSA-co-MA stabilized nickel(0) or cobalt(0) nanocluster catalysts.

Nickel(0) or cobalt(0) nanoclusters formed from the reduction of the respective precursor complex by sodium borohydride during the catalytic hydrolysis of ammonia borane in the presence of polymeric stabilizer are very stable in aqueous solution. No bulk metal formation was observed in solution standing for weeks at room temperature in inert gas atmosphere. The PSSA-co-MA stabilized nickel(0) or cobalt(0) nanoclusters can be isolated from the reaction solution as dark-brown solid by centrifugation. The isolated nanoclusters can be redispersed in water and still preserve their catalytic activity in the hydrolysis of AB after redispersion.

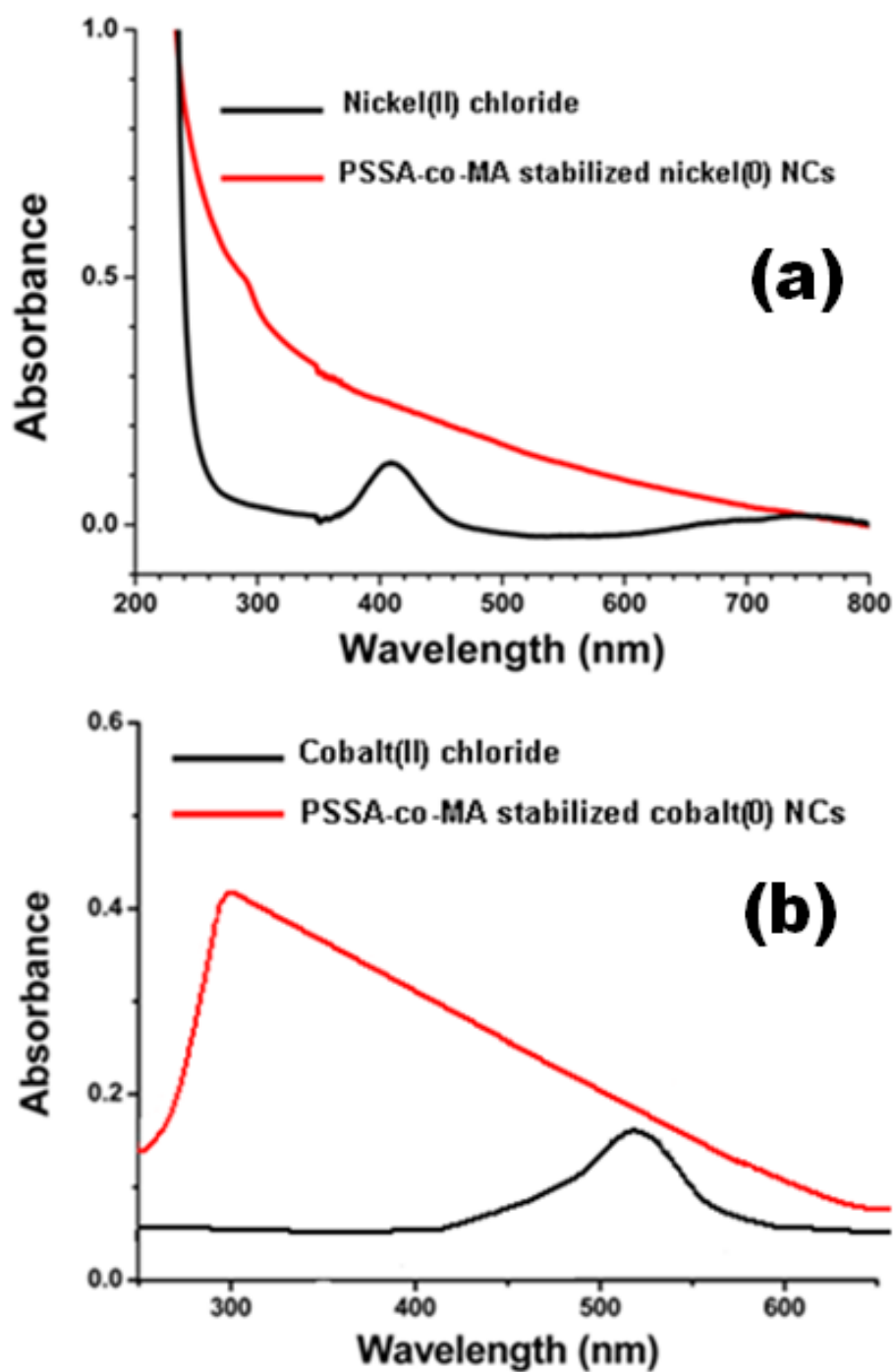


Figure 64. UV-Visible spectra of (a) nickel(II) chloride and PSSA-co-MA stabilized nickel(0) nanoclusters, (b) cobalt(II) chloride and PSSA-co-MA stabilized cobalt(0) nanoclusters taken from the aqueous solutions.

Figure 64 shows the UV-visible electronic absorption spectra of the aqueous solutions of nickel(II) chloride or cobalt(II) chloride in the presence of PSSA-co-MA stabilizer before and after reduction by NaBH₄. The UV-visible spectrum of nickel(II) chloride exhibits absorption bands at 410 nm and 780 nm, attributable to the d-d transitions (Figure 64a). After reduction, these bands disappeared and one observed a typical Mie exponential decay profile for the PSSA-co-MA stabilized nickel(0) nanoclusters [38, 124]. In the case of cobalt (Figure 64b), the d-d absorption band at 520 nm of cobalt(II) chloride disappeared leaving an absorption continuum characteristic for the cobalt(0) nanoclusters [38, 125]. The weak absorption around 300 nm in both spectra was attributed to $n \rightarrow \pi^*$ excitation of C=O groups in PSSA-co-MA molecules, by comparing with the spectrum of PSSA-co-MA. These observations indicate the reduction of nickel(II) or cobalt(II) to their metallic states and subsequently the formation of nanoclusters in the presence of PSSA-co-MA upon addition of sodium borohydride. The existence of PSSA-co-MA in the nanoclusters sample was also proved by comparing the FTIR spectra of poly(4-styrenesulfonic acid-co-maleic acid) sodium salt and PSSA-co-MA stabilized metal(0) nanoclusters.

The morphologies and particle size distribution of the as-synthesized PSSA-co-MA stabilized nickel(0) and cobalt(0) nanoclusters were examined by TEM, HRTEM (Figure 65). The TEM image of the PSSA-co-MA stabilized nickel(0) nanoclusters (Figure 65a) reveals that very small nanoclusters were embedded in polymer matrix. The HRTEM image of PSSA-co-MA stabilized nickel(0) nanoclusters given in Figure 65c indicated that the nanoclusters having an average particle size of 2.1 ± 0.6 nm were dispersed in and stabilized by polymer matrix. In the case of the PSSA-co-MA stabilized cobalt(0) nanoclusters, they were not embedded in the polymer matrix, they were stabilized by polymer and well dispersed in aqueous solution but show a broader size distribution compared to nickel nanoclusters, with an average size of 5.3 ± 1.6 nm (Figure 65b and Figure 65d).

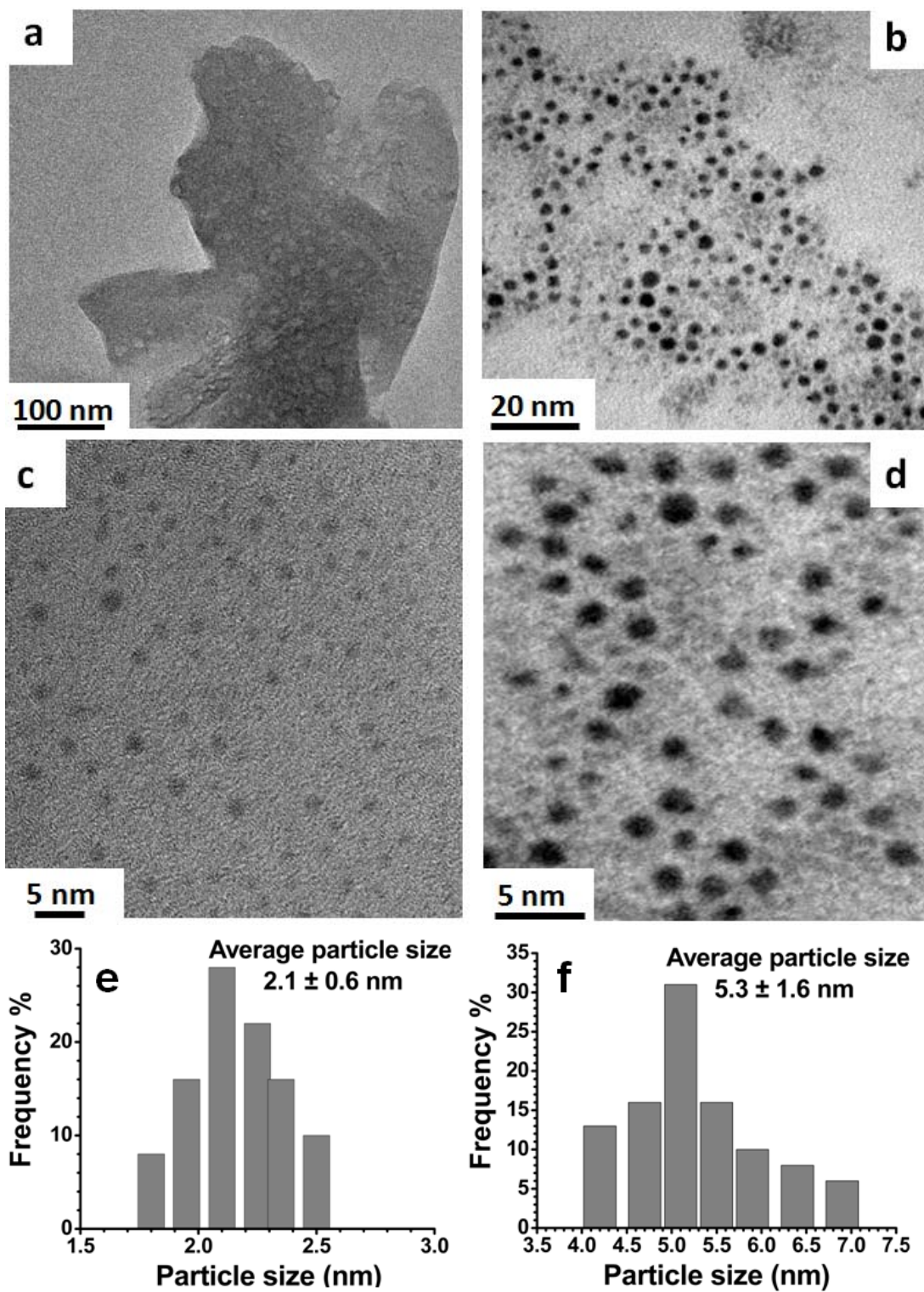


Figure 65. TEM, HRTEM images and corresponding particle size distributions of PSSA-co-MA stabilized nickel(0) nanoclusters (a,c,e), cobalt(0) nanoclusters (b,d,f)

The crystallinity of the in-situ generated PSSA-co-MA stabilized nickel(0) or cobalt(0) nanoclusters were examined by powder X-ray diffraction. Figure 66 shows the the XRD pattern of the PSSA-co-MA stabilized nickel(0) and cobalt(0) nanoclusters after washing with ethanol and drying under inert atmosphere. It is clear that no obvious diffraction pattern was found for cobalt(0) nanoclusters (Figure 66b), which implies that the in situ generated cobalt(0) nanoclusters were existed in amorphous phase. However, in the case of nickel(0) nanoclusters, the broad diffraction observed at $2\theta = 44.5^\circ$ belongs to 111 plane of fcc-Ni indicating the fcc structure of nickel(0) nanoclusters (Figure 66a). The higher activity of the PSSA-co-MA stabilized cobalt(0) nanoclusters compared to nickel(0) nanoclusters might stem from the amorphous nature of cobalt in the nanoclusters as reported by Xu et al [56b,85].

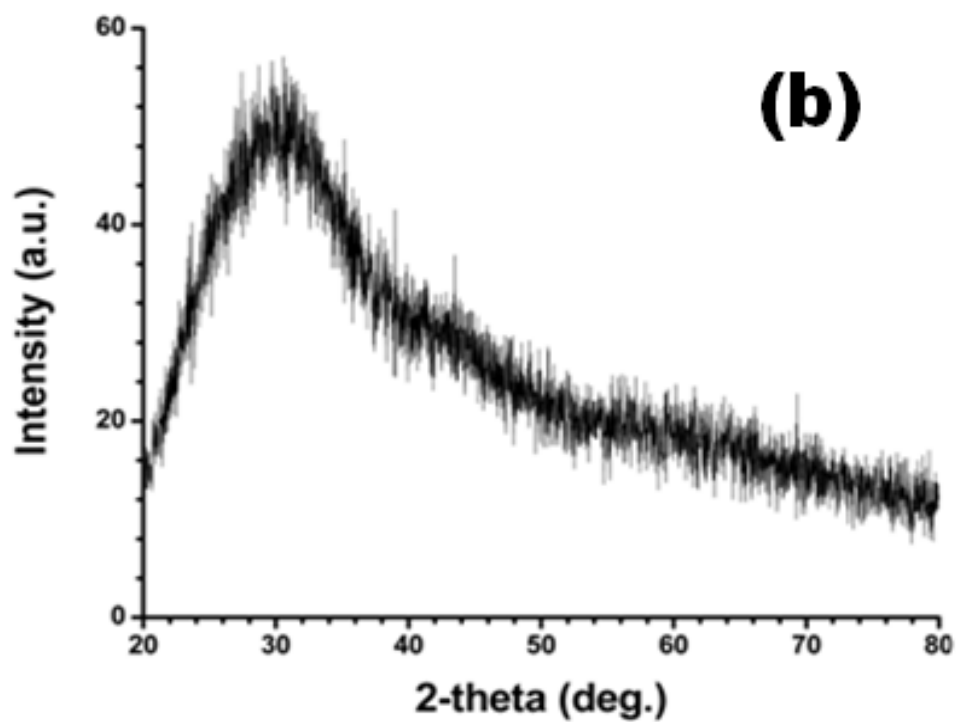
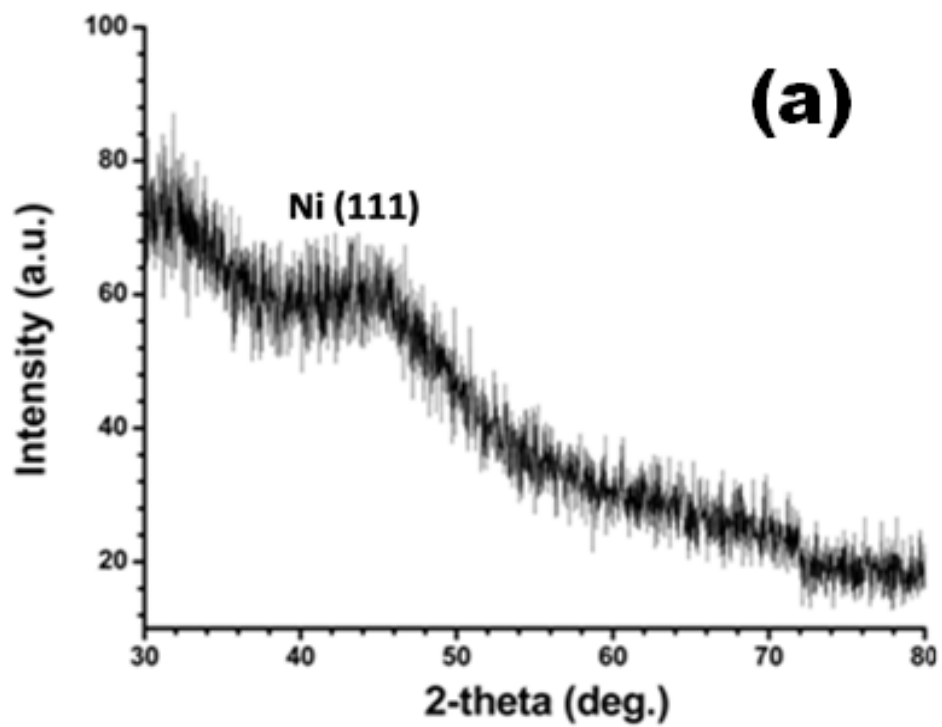


Figure 66. XRD patterns of PSSA-co-MA stabilized (a) nickel(0) nanoclusters (b) cobalt(0) nanoclusters

5.3.2. Kinetics of Hydrolysis of Ammonia Borane Catalyzed By PSSA-co-MA stabilized Nickel(0) or Cobalt(0) Nanoclusters

Figure 67 shows the plots of volume of hydrogen generated versus time during the hydrolysis of AB catalyzed by in-situ generated PSSA-co-MA stabilized nickel(0) or cobalt(0) nanoclusters at different PSSA-co-MA concentrations. The insets in Figure 67 show the plots of the hydrogen generation rate versus the PSSA-co-MA/[Metal] ratio for the hydrolysis of AB catalyzed by PSSA-co-MA stabilized nickel(0) or cobalt(0) nanoclusters starting with various concentrations of PSSA-co-MA at 25.0 ± 0.5 °C. For both nanoclusters, the hydrogen generation rate decreases with the increasing concentration of polymeric stabilizer as expected [126]. By considering both the stability and catalytic activity of the nanoclusters in the hydrolysis of ammonia borane, it was concluded to perform the further kinetic experiments with the [PSSA-co-MA]/[Metal] ratio of 1 for both nanoclusters.

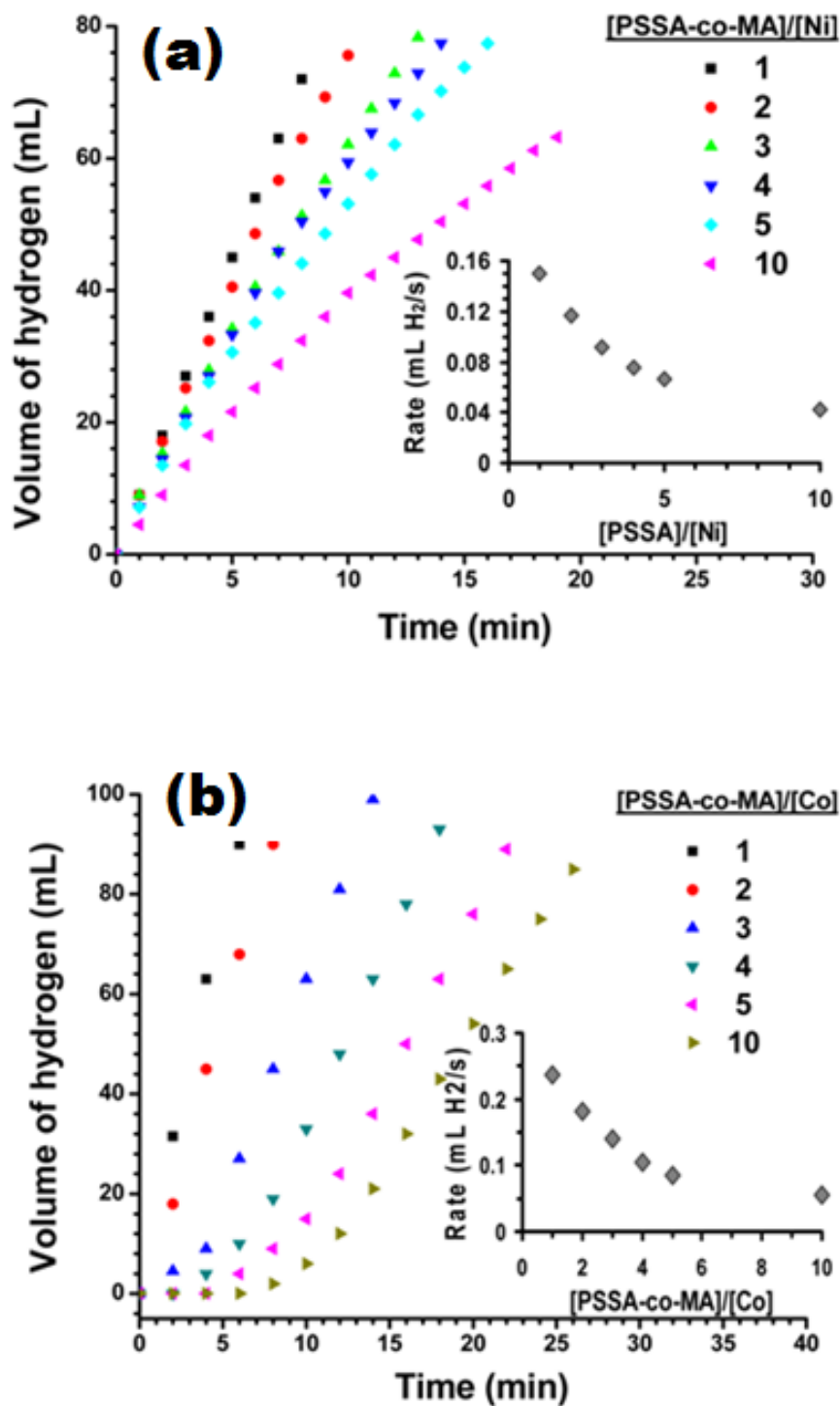


Figure 67. The volume of hydrogen versus time plots depending on the different [PSSA-co-MA]/[Metal] ratios for **(a)** nickel nanoclusters **(b)** cobalt nanoclusters. The insets show the plots of hydrogen generation rate versus the concentration of metal (both in logarithmic scale) for the hydrolysis of AB (100 mM) at 25 ± 0.5 °C.

The PSSA-co-MA stabilized nickel(0) or cobalt(0) nanoclusters are found to be highly active catalysts in the hydrolysis of AB even at low catalyst concentration and room temperature. Figure 68 shows the plots of the volume of hydrogen generated versus time during the catalytic hydrolysis of 100 mM AB solution in the presence of nickel(0) nanoclusters (Figure 68a) or cobalt(0) nanoclusters (Figure 68b) at different catalyst concentrations at 25.0 ± 0.5 °C. The hydrogen generation rate was determined from the linear portion of the plot for each experiment. The insets in Figure 68 show the plots of hydrogen generation rate versus initial concentration of nickel or cobalt, both in logarithmic scale. The slopes of $1.09 \approx 1.00$ in the inset of Figure 68a and $0.96 \approx 1.00$ in the inset of Figure 68b indicate that hydrolysis of AB catalyzed by PSSA-co-MA stabilized nickel(0) or cobalt(0) nanoclusters is first order with respect to the catalyst concentration.

The effect of substrate concentration on hydrogen generation rate was also studied by performing a series of experiments starting with varying initial concentration of AB while keeping the catalyst concentration constant at 2.0 mM Ni or 2.0 mM Co at 25.0 ± 0.5 °C (Figure 69). It is clearly seen from Figure 69a and 69b that the hydrogen generation from the catalytic hydrolysis of AB is practically independent of AB concentration for both catalysts.

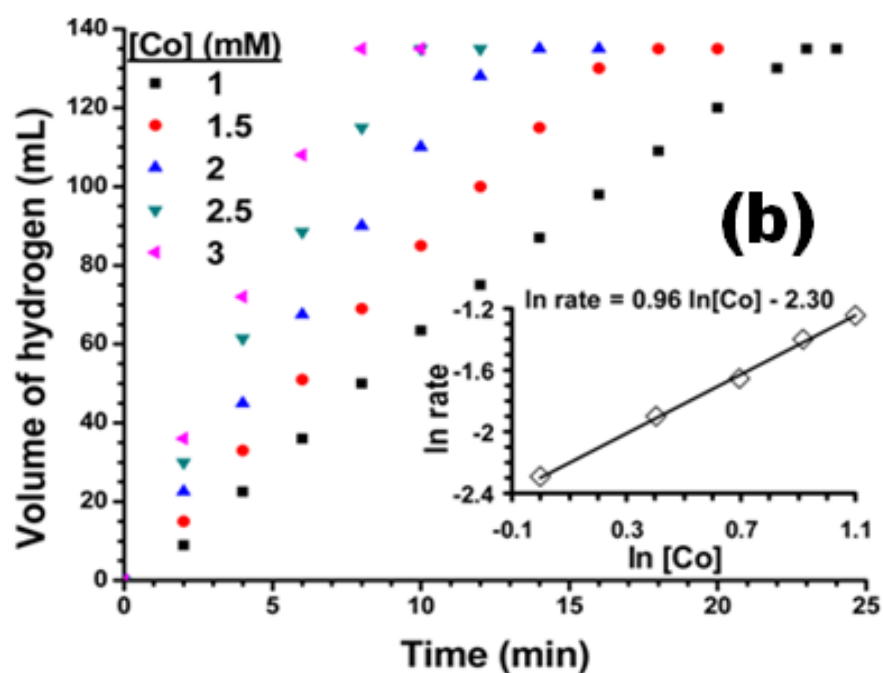
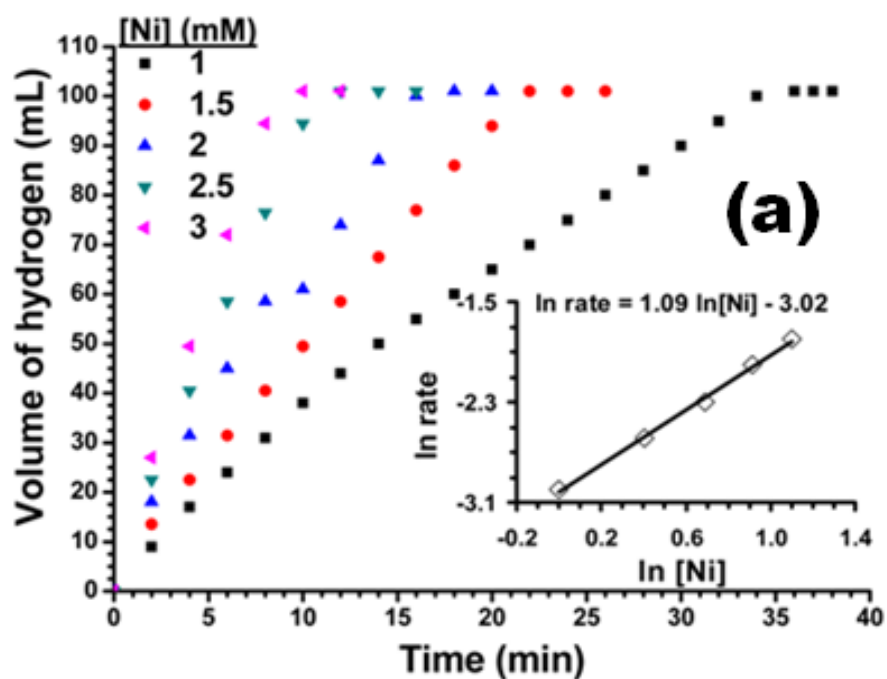


Figure 68. The volume of hydrogen versus time plots depending on the metal concentrations for PSSA-co-MA stabilized (a) nickel(0) nanoclusters (b) cobalt(0) nanoclusters at 25.0 ± 0.5 °C. The inset of each figures show the plot of hydrogen generation rate versus the concentration of metal (both in logarithmic scale).

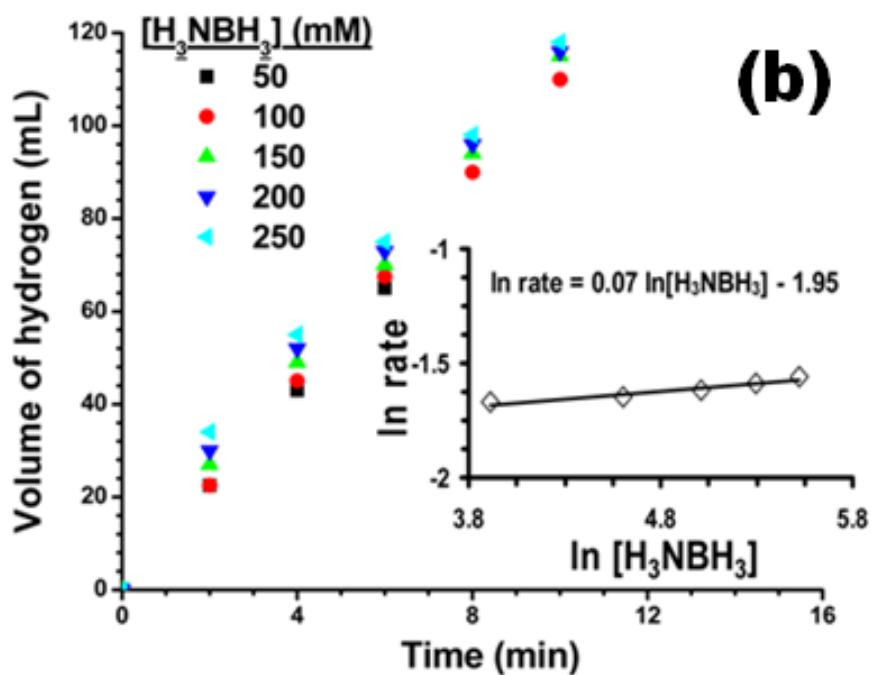
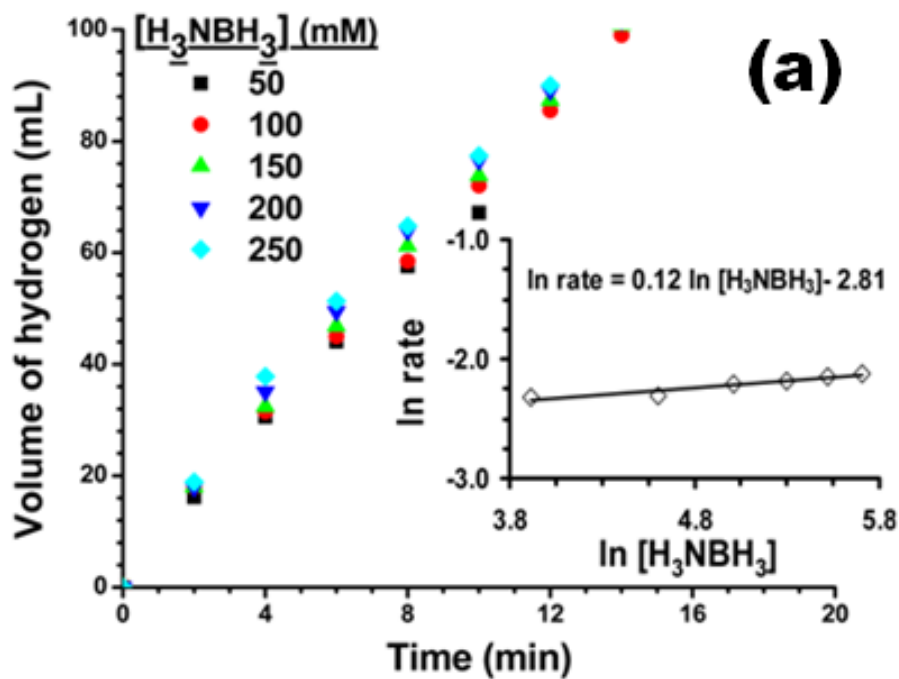


Figure 69. The volume of hydrogen versus time plots depending on AB concentrations for PSSA-co-MA stabilized (a) nickel(0) nanoclusters (b) cobalt(0) nanoclusters at 25.0 ± 0.5 °C. The inset of each figures show the plot of hydrogen generation rate versus the concentration of metal (both in logarithmic scale).

Consequently, the rate law for the catalytic hydrolysis of AB catalyzed by PSSA-co-MA stabilized nickel(0) or cobalt(0) nanoclusters can be given as in Eq.(16);

$$\frac{-3d[NH_3BH_3]}{dt} = \frac{d[H_2]}{dt} = k[Catalyst] \quad (16)$$

The PSSA-co-MA stabilized nickel(0) or cobalt(0) nanoclusters catalyzed hydrolysis of AB was carried out at various temperatures (15-35 °C) starting with an initial substrate concentration of 100 mM AB for Ni or Co catalyst and an initial catalyst concentration of 2.0 mM Ni or 2.0 mM Co. The values of rate constant (k_{app}) at different temperatures (Table A9 and A10 in the Appendix A) for the PSSA-co-MA stabilized nickel(0) or cobalt(0) nanoclusters catalyzed hydrolysis of AB were calculated from the slope of the linear part of each plot in Figure 70a and 70b, respectively. They were also used to calculate the activation energies (Arrhenius plots are shown in the Insets of Figure 70a and 70b): apparent activation energies $E_a^{apparent} = 32 \pm 2 \text{ kJ.mol}^{-1}$ for Ni and $E_a^{apparent} = 34 \pm 1 \text{ kJ.mol}^{-1}$ for Co.

Catalyst lifetime experiments were performed starting with a 20 mL solution of as- prepared PSSA-co-MA stabilized nickel(0) or cobalt(0) nanoclusters containing 1.0 mM Ni or 1.0 mM Co, and 0.5 M AB at $25.0 \pm 0.5 \text{ }^\circ\text{C}$. The PSSA-co-MA stabilized nickel(0) nanoclusters provide 22450 turnovers over 48 h in the hydrolysis of AB at $25.0 \pm 0.5 \text{ }^\circ\text{C}$ before deactivation while the PSSA-co-MA stabilized cobalt(0) nanoclusters provide 17650 turnovers over 36 h for the same reaction under the same conditions. The ammonia generation during the TTO experiments for both catalysts in the hydrolysis of AB was checked at certain time intervals by using acid/base titration test, but no detectable amount of ammonia was observed. The detection limit for our titration method is ~0.12 % by weight and so the amount of ammonia generated should be lower than our detection limit [127]. The more sensitive analytical method such as gas chromatography (GC) should be used for the determination of such a lower ammonia concentration.

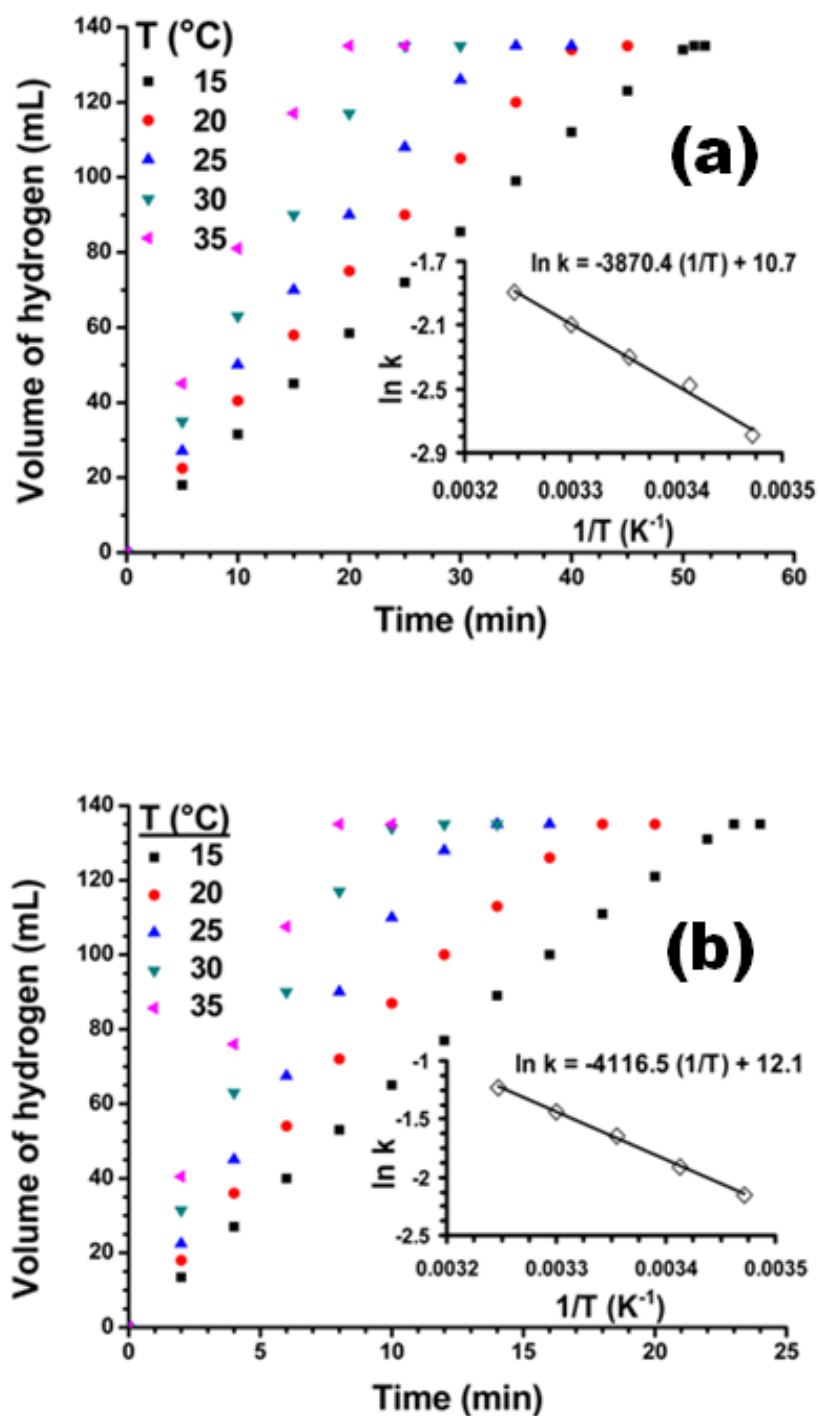


Figure 70. Volume of hydrogen versus time plots at different temperatures for the hydrolysis of AB (100 mM) catalyzed by PSSA-co-MA stabilized (a) Ni nanoclusters (2.0 mM) (b) Co nanoclusters (2.0 mM) in the temperature range 15-35 °C. The insets of each figure show Arrhenius plot ($\ln k$ versus the reciprocal absolute temperature $1/T$ (K^{-1})).

The Eyring plot given in Figure 71 gives the activation enthalpies, $\Delta H^\ddagger = 29 \pm 2$ kJ/mol for Ni; $\Delta H^\ddagger = 31 \pm 2$ kJ/mol for Co and the activation entropies, $\Delta S^\ddagger = -165 \pm 4$ J/K·mol for Ni; $\Delta S^\ddagger = -152 \pm 4$ J/K·mol for Co for the hydrolysis of ammonia borane catalyzed by PSSA-co-MA stabilized nickel(0) or cobalt(0) nanoclusters.

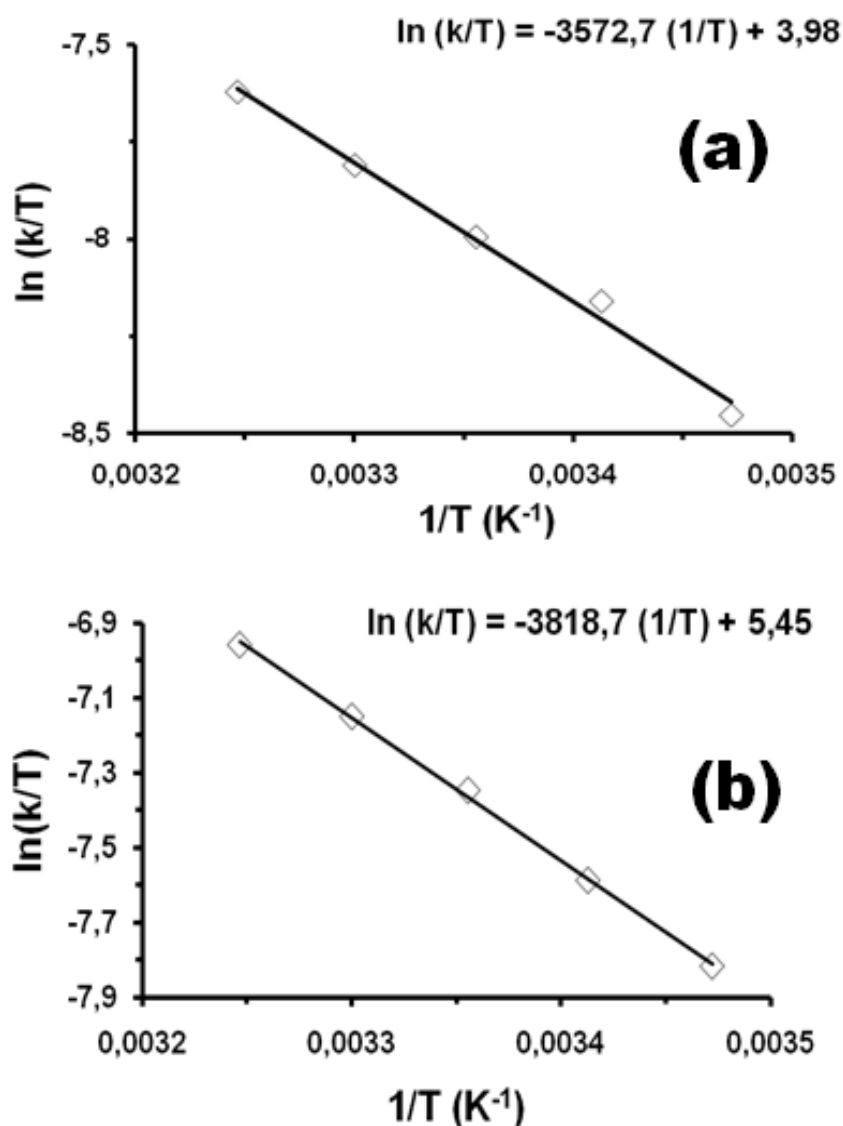


Figure 71. Eyring plot ($\ln(k/T)$) versus the reciprocal absolute temperature $1/T$ (K^{-1}) for the hydrolysis of ammonia borane (100 mM) catalyzed by PSSA-co-MA stabilized (a) nickel(0) nanoclusters (2.0 mM Ni) (b) cobalt(0) nanoclusters (2.0 mM Co) in the temperature range 15-35 °C

Table 3 shows the activities in terms of TOF values ($\text{mol H}_2 \cdot \text{catalyst}^{-1} \cdot \text{min}^{-1}$) of the various non-noble metal catalyst systems or their alloys which have been tested in the hydrolysis of AB at 25.0 ± 0.5 °C. It can be clearly seen from the table that PSSA-co-MA stabilized nickel(0) nanoclusters are the best one with a TOF value of 10.1 min^{-1} among the nickel catalysts and PSSA-co-MA stabilized cobalt(0) nanoclusters has the second highest activity with a TOF value of 25.7 min^{-1} among the cobalt catalysts.

Table 3. Activities in terms of TOF values ($\text{mol H}_2 \cdot (\text{mol catalyst})^{-1} \cdot \text{min}^{-1}$) of the non-noble metal catalysts or their alloys have been tested in hydrogen generation from the hydrolysis of AB at 25 °C. (The TOF values were estimated from the data given in respective references).

Catalyst	TOF ($\text{mol H}_2 \cdot (\text{mol catalyst})^{-1} \cdot \text{min}^{-1}$)
In-situ Co(0) nanoparticles	39.8 [128a]
<i>PSSA-co-MA stabilized Co(0) nanoclusters</i>	<i>25.7 [This study]</i>
In-situ $\text{Fe}_{1-x}\text{Ni}_x$ nanoparticles	10.9 [128b]
<i>PSSA-co-MA stabilized Ni(0) nanoclusters</i>	<i>10.1 [This study]</i>
Bimetallic Au-Ni	9.8 [128c]
3.2 nm Ni/C	8.8 [128d]
In-situ Starch-Stabilized Ni nanoparticles	6.6 [128e]
PVP stabilized Ni nanoparticles	4.5 [128f]
Hollow-Ni nanoparticles	4.3 [128g]
In-situ Fe(0) nanoparticles	3.4 [128h]
Intrazeolite Cobalt(0) NCs	2.4 [128i]
Ni/ $\gamma\text{-Al}_2\text{O}_3$	1.7 [128j]
Co/ $\gamma\text{-Al}_2\text{O}_3$	1.5 [128j]
NiCl_2	0.40 [128k]
Cu@Cu ₂ O	0.22 [128m]

5.3.3. In situ Generation and Characterization of PSSA-co-MA Stabilized Ruthenium(0) Nanoclusters

The PSSA-co-MA stabilized ruthenium(0) nanoclusters were formed in-situ during the hydrolysis of ammonia borane. The color change and the UV-vis electronic absorption spectra show that the reduction of the precursor complexes is fast and without an observable induction period the hydrolysis of ammonia borane starts immediately releasing hydrogen gas. Figure 72 shows the UV-Vis electronic absorption spectra of solutions containing ruthenium(III) chloride in the presence of PSSA-co-MA stabilizer in aqueous solution before and after reduction by ammonia borane. The UV-visible spectrum of ruthenium(III) chloride exhibits two absorption bands at 330 and 406 nm, attributable to the ligand to metal charge transfer and d-d transition, respectively (Figure 72). After reduction these bands of ruthenium(III) ions disappear and one observes a typical Mie exponential decay profile for the PSSA-co-MA stabilized ruthenium(0) nanoclusters, in consistence with earlier studies [86,87].

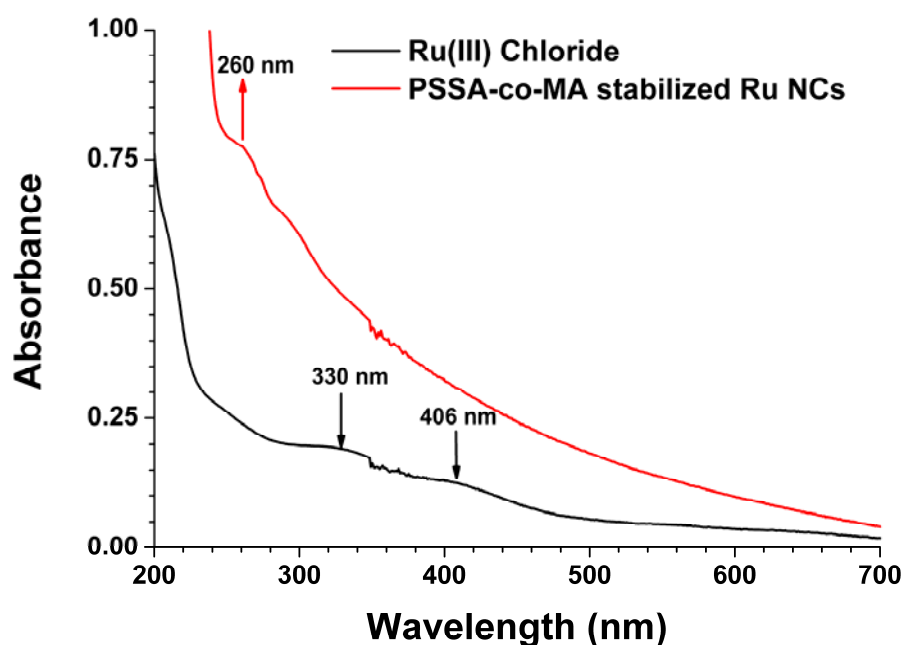


Figure 72. UV-Visible spectra of ruthenium(III) chloride and PSSA-co-MA stabilized ruthenium(0) nanoclusters taken from the aqueous solutions.

Ruthenium(0) nanoclusters formed from the reduction of the respective precursor complex by ammonia borane in the presence of PSSA-co-MA are stable in aqueous solution. No bulk metal formation was observed in solution standing for weeks at room temperature in inert gas atmosphere. The PSSA-co-MA stabilized ruthenium(0) nanoclusters can be isolated from the reaction solution as dark-brown solid by removing the volatiles in vacuum. The nanoclusters isolated can be redispersed in aqueous solution. When redispersed the nanoclusters are yet catalytically active in the hydrolysis of ammonia borane (see later).

The morphology and particle size of the PSSA-co-MA stabilized ruthenium(0) nanoclusters catalysts were studied by using TEM image given in Figure 73. The average particle size of in-situ prepared PSSA-co-MA stabilized ruthenium(0) nanoclusters was calculated from the corresponding TEM image as 1.9 ± 0.6 nm.

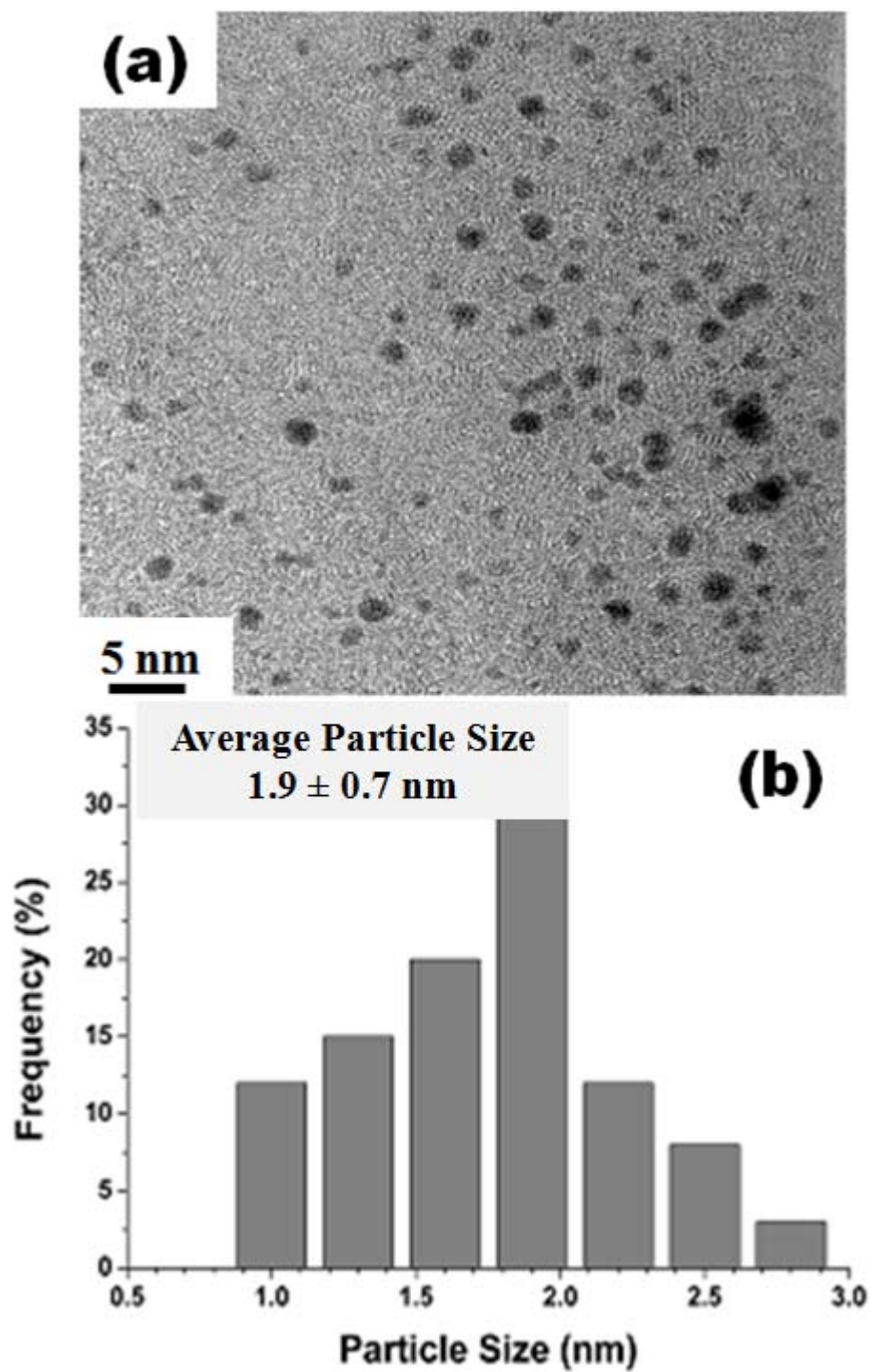


Figure 73. (a) TEM image and (b) associated histogram for PSSA-co-MA stabilized ruthenium(0) formed in-situ from the reduction of ruthenium(III) chloride (0.7 mM).

The powder X-ray diffraction pattern of a representative sample of PSSA-co-MA stabilized ruthenium(0) nanoclusters is shown in Figure 74. A broad peak around $2\theta=44^\circ$ correlate with (101) plane of face centered cubic structure of metallic ruthenium [129]. The broadening observed for 101 plane is characteristic for the particles in nanometer scale [89]. However, the reflectances for other planes (100) plane at $2\theta=38.5^\circ$ and (002) plane at $2\theta=42.8^\circ$ metallic ruthenium were not observable in the XRD pattern most probably due to the interaction of the PSSA-co-MA molecule with nanocluster surface atoms by these planes. The another broad reflectance observed at $\approx 2\theta=32^\circ$ is also indicative of the presence of polymer on surface of nanoclusters.

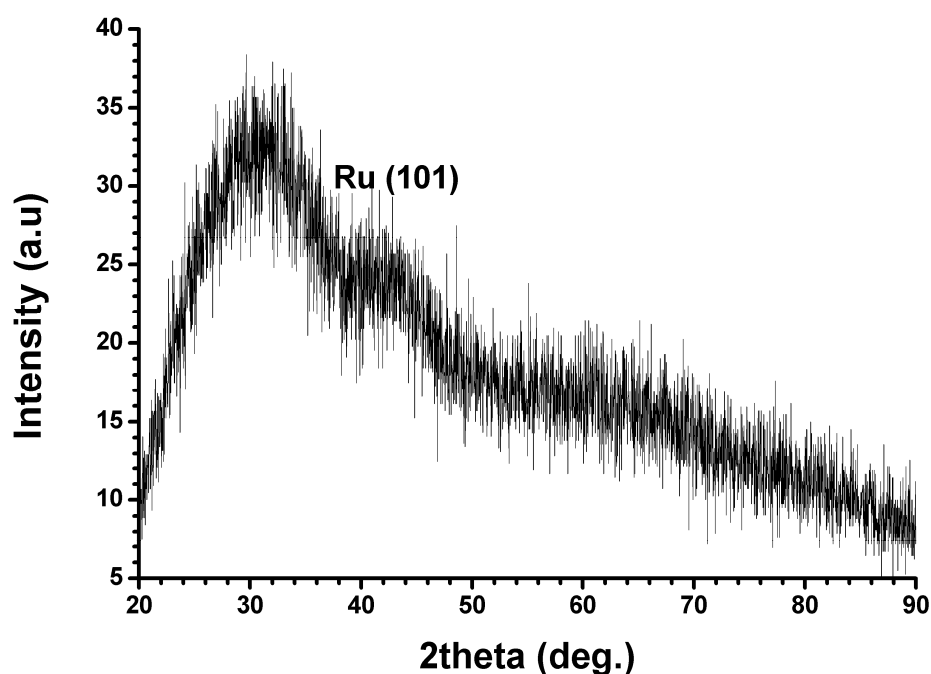


Figure 74. XRD pattern of PSSA-co-MA stabilized ruthenium(0) nanoclusters

5.3.4. Kinetics of Hydrolysis of Ammonia Borane Catalyzed By PSSA-co-MA Stabilized Ruthenium(0) Nanoclusters

Figure 75 shows the plot of volume of hydrogen generated versus time during these hydrolysis of ammonia borane catalyzed by PSSA-co-MA stabilized

ruthenium(0) nanoclusters. The inset in Figure 75 shows the plot of the hydrogen generation rate versus the $[PSSA-co-MA]/[Ru]$ ratio for the hydrolysis of AB catalyzed by PSSA-co-MA stabilized ruthenium(0) nanoclusters starting with various concentration of PSSA-co-MA at 25.0 ± 0.5 °C. The hydrogen generation rate decreases with the increasing concentration of polymeric stabilizer as expected [126]. By considering both the stability and catalytic activity of the nanoclusters in the hydrolysis of ammonia borane, it was concluded to start the further kinetic experiments with the $[PSSA-co-MA]/[Metal]$ ratio of 1 for ruthenium(0) nanoclusters catalyst.

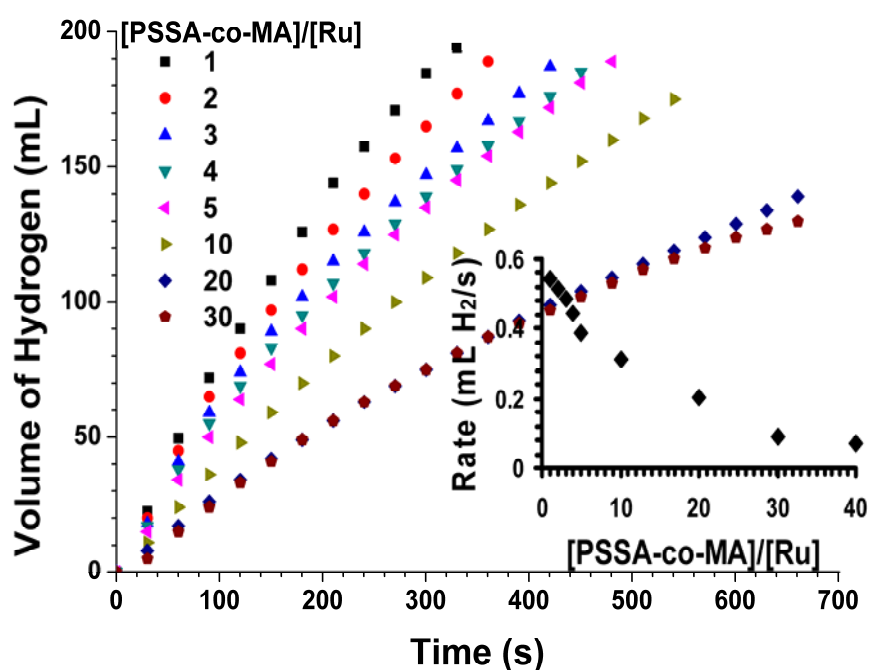


Figure 75. The volume of hydrogen versus time plots depending on the different $[PSSA-co-MA]/[Metal]$ ratios for ruthenium(0) nanoclusters. The inset shows the plot of hydrogen generation rate versus the concentration of Ru (both in logarithmic scale) for the hydrolysis of AB (100 mM) at 25 ± 0.5 °C.

Figure 76 shows the plot of the volume of hydrogen generated versus time during the catalytic hydrolysis of 100 mM AB solution in the presence of ruthenium(0) nanoclusters at different catalyst concentrations at 25.0 ± 0.5 °C. The

hydrogen generation rate was determined from the linear portion of the plot for each experiment. The inset in Figure 76 shows the plot of hydrogen generation rate versus initial concentration of ruthenium, both in logarithmic scale. The slope of $1.05 \approx 1.00$ in the inset of Figure 76 indicates that hydrolysis of ammonia borane catalyzed by PSSA-co-MA stabilized ruthenium(0) nanoclusters is first order with respect to the Ru concentration.

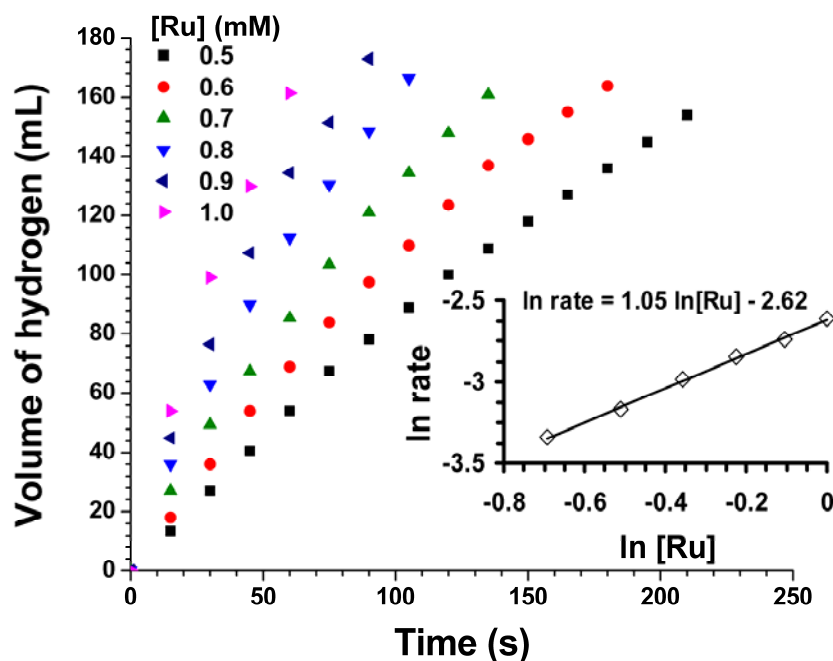


Figure 76. The volume of hydrogen versus time plots depending on the metal concentrations for PSSA-co-MA stabilized ruthenium(0) nanoclusters. The inset of figure shows the plot of hydrogen generation rate versus the concentration of ruthenium (both in logarithmic scale).

The effect of substrate concentration on the hydrogen generation rate was also studied by performing a series of experiments starting with varying initial concentration of AB while keeping the catalyst concentration constant at 0.7 mM Ru. Figure 77 shows the volume of hydrogen generated versus time plots depending on the substrate concentrations at constant catalyst concentration. The inset of Figure 77 shows the plot of hydrogen generation rate versus the concentration of the substrate,

both in logarithmic scale, for the hydrolysis of AB in the presence of PSSA-co-MA stabilized ruthenium(0) nanoclusters. The hydrogen generation from the catalytic hydrolysis of ammonia borane was found to be practically independent of AB concentration.

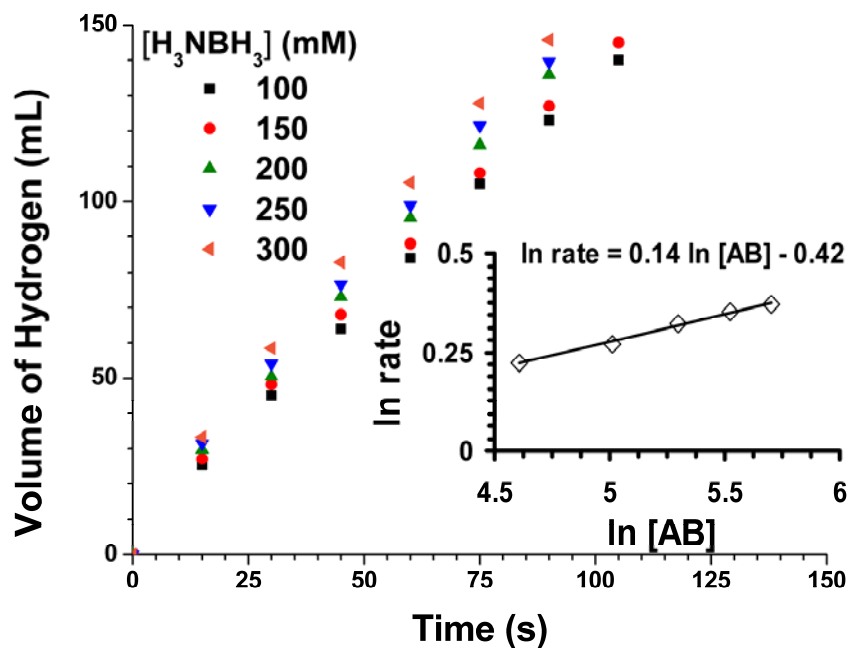


Figure 77. The volume of hydrogen versus time plots depending on the substrate concentrations at constant catalyst concentration for the hydrolysis of AB catalyzed by PSSA-co-MA stabilized ruthenium(0) nanoclusters (0.7 mM Ru). The inset of figure shows the plot of hydrogen generation rate versus the concentration of the substrate (both in logarithmic scale).

Consequently, the rate law for the catalytic hydrolysis of AB catalyzed by PSSA-co-MA stabilized ruthenium(0) nanoclusters can be given as in Eq.(18).

$$\frac{-3d[NH_3BH_3]}{dt} = \frac{d[H_2]}{dt} = k[Ru] \quad (17)$$

The PSSA-co-MA stabilized ruthenium(0) nanoclusters catalyzed hydrolysis of ammonia borane was carried out at various temperatures in the range of 15-35 °C starting with the initial substrate concentration of 150 mM AB and an initial catalyst concentration of 0.7 mM Ru. The values of rate constant (k_{app}) at different temperatures (Table A11 in the Appendix A) for PSSA-co-MA stabilized ruthenium(0) nanoclusters catalyzed hydrolysis of AB were calculated from the slope of the linear part of each plot in Figure 78. They were also used to calculate the activation parameters (Arrhenius plots are shown in the inset of Figure 78): apparent activation energy, $E_a^{apparent} = 54 \pm 1 \text{ kJ.mol}^{-1}$, activation enthalpy, $\Delta H^\ddagger = 52 \pm 2 \text{ kJ.mol}^{-1}$, activation entropy $\Delta S^\ddagger = -92 \pm 2 \text{ J.(K.mol)}^{-1}$ (Figure 79). The activation energies obtained for the hydrolysis of ammonia borane catalyzed ruthenium(0) is smaller than the values reported in literature for the same reaction using different catalysts.

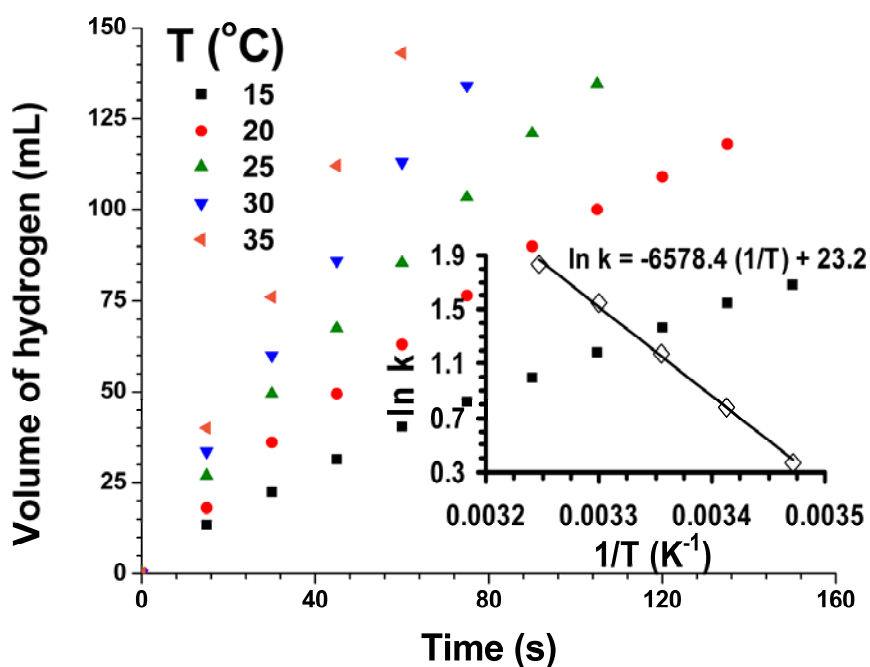


Figure 78. The volume of hydrogen versus time plots at different temperatures for the hydrolysis of AB (100 mM) catalyzed by PSSA-co-MA stabilized ruthenium(0) nanoclusters (0.7 mM) in the temperature range 15-35 °C. The inset of figure shows Arrhenius plot ($\ln k$ versus the reciprocal absolute temperature $1/T \text{ (K}^{-1}\text{)}$).

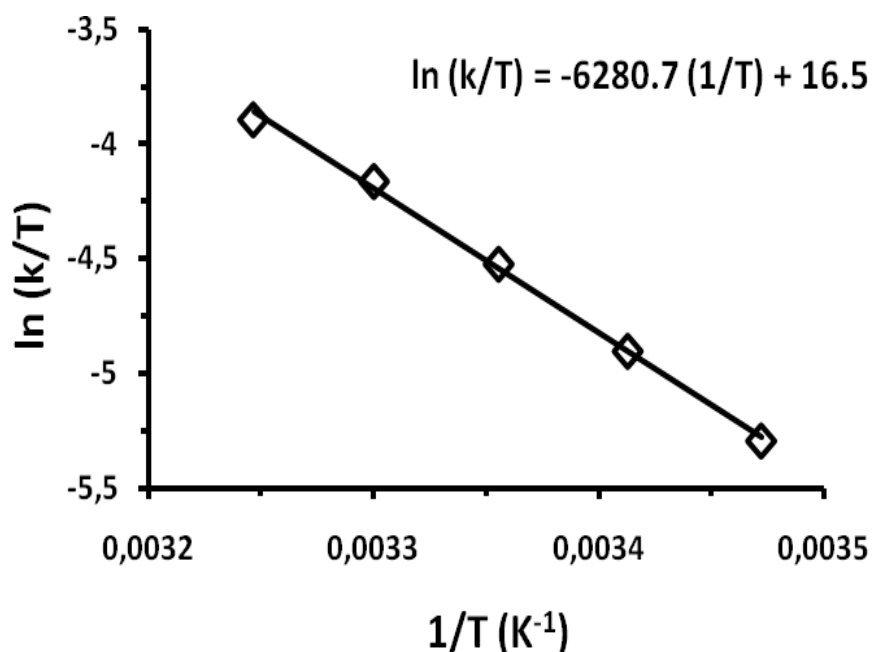


Figure 79. Eyring plot ($\ln(k/T)$) versus the reciprocal absolute temperature $1/T (K^{-1})$ for the hydrolysis of ammonia borane (100 mM) catalyzed by PSSA-co-MA stabilized ruthenium(0) nanoclusters (0.7 mM Ru)

A catalyst lifetime experiment for PSSA-co-MA stabilized ruthenium nanoclusters in the hydrolysis of AB was performed starting with a 20 mL solution of in-situ prepared PSSA-co-MA stabilized ruthenium(0) nanoclusters containing 0.1 mM Ru and 0.5 M AB at 25.0 ± 0.5 °C. The PSSA-co-MA stabilized ruthenium(0) nanoclusters provided 51720 turnovers over 58 h in the hydrolysis of ammonia borane at 25.0 ± 0.5 °C before deactivation which is the one of the best value ever reported for the hydrolysis of AB. The ammonia generation during the TTO experiments for both catalyst in the hydrolysis of AB was checked at certain time intervals by using acid/base titration test, but no detectable amount of ammonia was observed. The hydrogen generation slows down as the reaction proceeds and ultimately stops, may be, because of increasing viscosity of the solution or deactivation effect of increasing metaborate concentration. Therefore, these TTO values should be considered as a lower limit. Much higher TTO values might be obtained when the increase in viscosity could be avoided.

5.3.5. Mercury Poisoning as Heterogeneity Test for In situ Prepared PSSA-co-MA Stabilized Nickel(0), Cobalt(0) or Ruthenium(0) Nanoclusters

The poisoning experiment is usually performed by adding Hg(0) to the solution during the catalytic reaction. The suppression of catalysis by Hg(0) is considered as a compelling evidence for the heterogeneity of the catalysis; if Hg(0) does not suppress catalysis, that is (negative) evidence for a homogeneous catalysis [3]. In the case of PSSA-co-MA stabilized nickel(0), cobalt(0) or ruthenium(0) nanoclusters catalyzed hydrolysis of ammonia borane, the addition of 200 for Ni, 150 for Co and 150 for Ru equivalent mercury into the reaction solution after about 40% of conversion in a typical hydrolysis experiment at 25.0 ± 0.5 °C ultimately stops the hydrogen evolution as shown in Figure 80, Figure 81 and Figure 82, respectively. The cease of the catalytic hydrolysis of ammonia borane completely upon mercury addition is the evidence that PSSA-co-MA stabilized nickel(0), cobalt(0) and ruthenium(0) nanoclusters are the heterogeneous catalysts in the hydrolysis of ammonia borane.

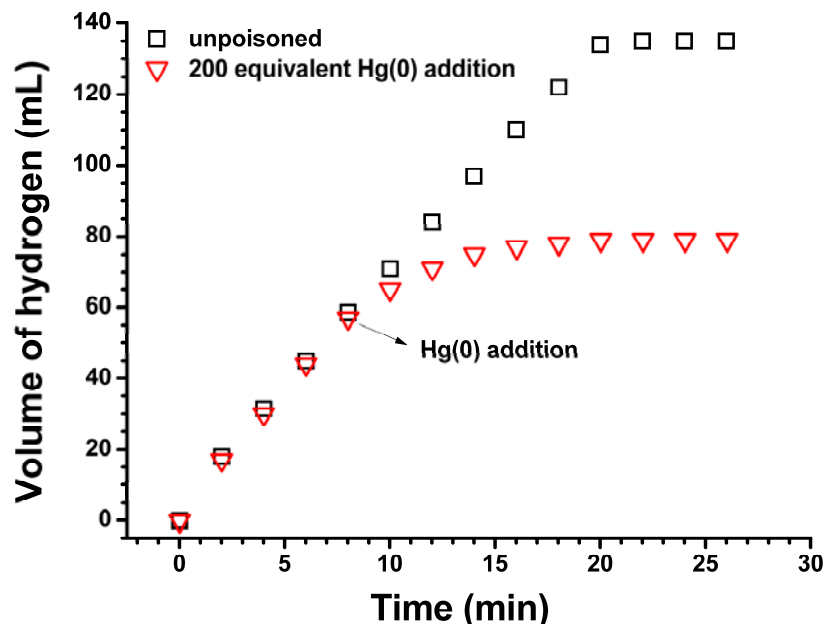


Figure 80. The volume of hydrogen versus time plots for the hydrolysis of ammonia borane (200 mM) catalyzed by PSSA-co-MA stabilized nickel(0) nanoclusters (2.0 mM Ni) with and without addition of 200 equiv. Hg(0) at 25.0 ± 0.5 °C.

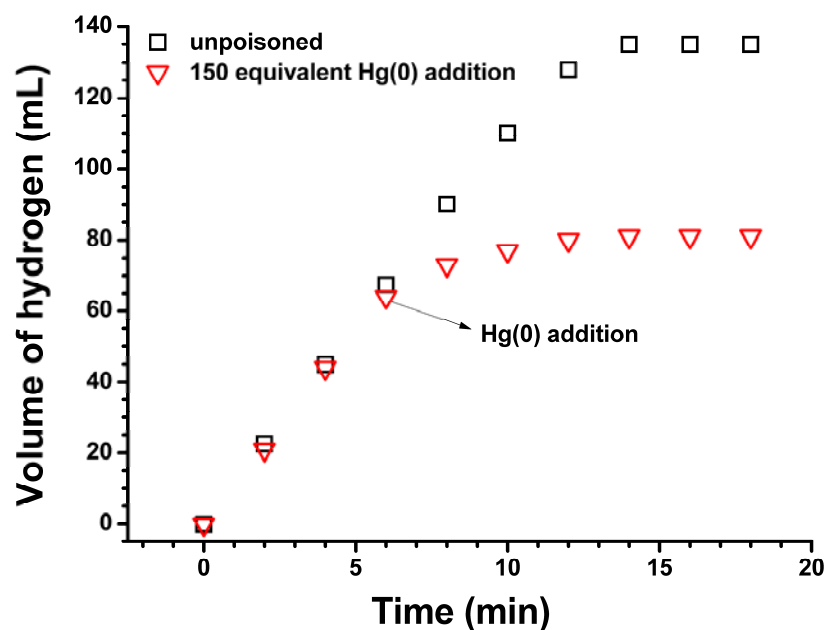


Figure 81. The volume of hydrogen versus time plots for the hydrolysis of ammonia borane (200 mM) catalyzed by PSSA-co-MA stabilized cobalt(0) nanoclusters (2.0 mM Co) with and without addition of 150 equiv. Hg(0) at 25.0 ± 0.5 °C.

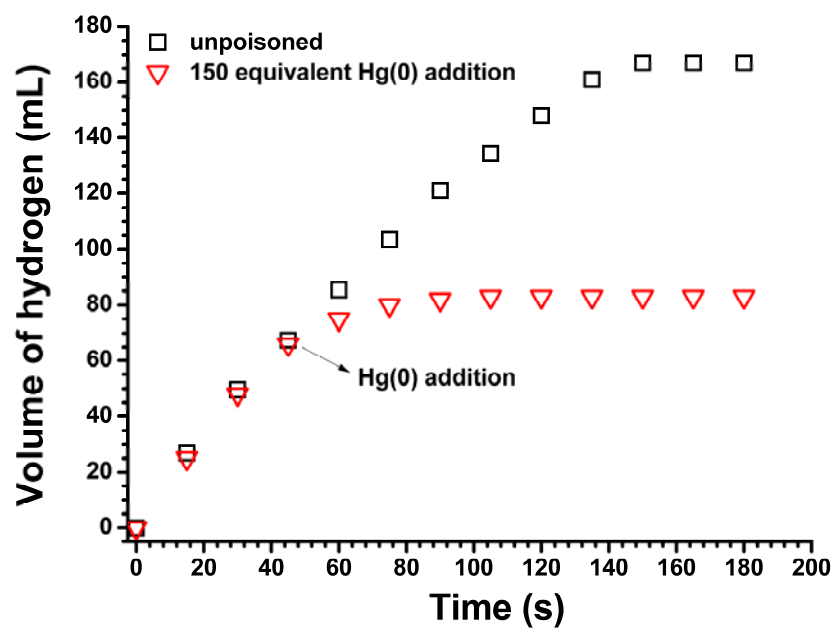


Figure 82. The volume of hydrogen versus time plots for the hydrolysis of ammonia borane (300 mM) catalyzed by PSSA-co-MA stabilized ruthenium(0) nanoclusters (0.7 mM Ru) with and without addition of 150 equiv. Hg(0) at 25.0 ± 0.5 °C.

CHAPTER 6

CONCLUSIONS

In summary, my dissertation on the preparation and characterization of water soluble polymer stabilized nickel(0), cobalt(0) and ruthenium(0) nanoclusters as catalyst in hydrogen generation from the hydrolysis of sodium borohydride and ammonia borane has led to the following conclusions and insights;

Part-I: PVP stabilized transition metal(0) nanoclusters

- PVP stabilized nickel(0), cobalt(0) and ruthenium(0) nanoclusters with an average particle size of 3.6, 7.2 and 5.1 nm, respectively, can be generated easily from the reduction of commercially available precursor materials with NaBH₄ in methanol by using our own developed method.
- TEM analyses of the PVP stabilized nickel(0), cobalt(0) and ruthenium(0) nanoclusters indicated that all of the nanoclusters are in spherical shape with narrow particle size distributions.
- XRD patterns of PVP stabilized nickel(0), cobalt(0) and ruthenium(0) nanoclusters showed that nickel(0) and cobalt(0) nanoclusters are existed in amorphous phase while ruthenium(0) nanoclusters are existed in fcc crystal structure.

- The attachment of PVP on the surface of the metal(0) nanoclusters through the C=O groups was concluded from the observation of change in C=O stretching frequency of PVP in the FT-IR spectra.
- PVP stabilized nickel(0), cobalt(0) and ruthenium(0) nanoclusters were highly active catalysts in hydrogen generation from the hydrolysis of NaBH₄ and AB at ambient conditions.
- Kinetics of hydrogen generation from the hydrolysis of NaBH₄ and AB catalyzed by PVP stabilized nickel(0), cobalt(0) and ruthenium(0) nanoclusters can be summarized in the Table 4;

Table 4. Summary of the kinetic data of hydrogen generation from the hydrolysis of sodium borohydride and ammonia borane catalyzed by PVP stabilized nickel(0), cobalt(0) and ruthenium(0) nanoclusters.

Catalyst	Hydrolysis of Sodium Borohydride			Hydrolysis of Ammonia Borane		
	Rate Law	Apparent Activation Energy (E_a apparent) (kJ.mol ⁻¹)	Lifetime (TTON)	Rate Law	Apparent Activation Energy (E_a apparent) (kJ.mol ⁻¹)	Lifetime (TTON)
<i>PVP-stabilized Ni(0) NCs</i>	k.[Ni]	46 ± 2	8700 over 27 h	k.[Ni]	58 ± 2	17450 over 24 h
<i>PVP-stabilized Co(0) NCs</i>	k.[Co][NaBH ₄]	63 ± 2 37 ± 2 (in basic medium)	5900 over 19 h	k.[Co][H ₃ NBH ₃]	46 ± 2	12640 over 19 h
<i>PVP-stabilized Ru(0) NCs</i>	k.[Ru]	56 ± 2 33 ± 2 (in basic medium)	28800 over 36 h	k.[Ru]	38 ± 2	44320 over 52 h

- The rate of hydrogen generation from the catalytic hydrolysis of NaBH₄ was faster than that of AB under the same catalyst concentrations and reaction conditions in the presence of PVP stabilized nickel(0), cobalt(0) and

ruthenium(0) nanoclusters. This is most probably due to the acid-catalyzed self hydrolysis and taking a part of H₂O in hydrogen generation from the hydrolysis of NaBH₄ '5.2.2.1'. However, hydrogen generation from the AB has a big advantage over the hydrolysis of NaBH₄ for on-board applications that aqueous solution of NaBH₄ must be stabilized by using NaOH to prevent the acid-catalyzed self-hydrolysis.

- The both hydrolysis reactions showed first order dependency with respect to the substrate concentration in the presence of PVP stabilized cobalt(0) nanoclusters but that of for PVP stabilized nickel(0) or ruthenium(0) nanoclusters is zeroth order which could be explained by using the effect of pH on the catalytic activity of cobalt(0) nanoclusters as described in the section '5.2.2.3'.
- The rate of hydrogen generation from hydrolysis of AB showed less temperature dependency than hydrolysis of NaBH₄ in the case of cobalt(0) nanoclusters taking into consideration of activation energies: $E_a^{\text{apparent}} = 46 \pm 2$ kJ.mol⁻¹ for hydrolysis of AB, $E_a^{\text{apparent}} = 63 \pm 2$ kJ.mol⁻¹ for hydrolysis NaBH₄ while the opposite is observed for PVP stabilized nickel(0) and ruthenium(0) nanoclusters considering the activation energies (E_a : 46 and 58 kJ.mol⁻¹ for nickel; $E_a^{\text{apparent}} = 33$ and 38 kJ.mol⁻¹ for ruthenium, respectively).
- Although the PVP stabilized ruthenium(0) nanoclusters provided the highest activity in terms of TOF values among the all metal catalysts in both hydrolysis reactions, they also have higher activation than others. This complexity can be explained by considering different reaction mechanisms for the catalytic hydrolysis reactions in the presence of different metal catalyst. For different catalytic systems, the reaction proceeds on different pathways and we cannot talk about only one rate constant (k). There are many rate constants for different reaction steps. Under these circumstances, we should consider the apparent rate constant (k_{app}) which includes all the rate constant of different reaction steps. Therefore, the activation energy

calculated by using k_{app} is called as apparent activation energy ($E_a^{apparent}$). In our reaction condition, the calculated rate constants and activation energies are the k_{app} and $E_a^{apparent}$, respectively. For this reason, the catalyst with the highest activity can also have the high activation energy.

- PVP stabilized metal(0) nanoclusters had the longer catalytic lifetime in the hydrolysis of AB providing 17450 TTON for nickel, 12650 TTON for cobalt and 44320 TTON for ruthenium than the hydrolysis of NaBH_4 providing 8700, 5100 and 38800 TTON for nickel, cobalt and ruthenium, respectively.
- It can be concluded by considering all of the kinetic data that hydrogen generation from hydrolysis of NaBH_4 or AB catalyzed by PVP stabilized metal(0) nanoclusters follow different reaction mechanisms.

Part-II : PSSA-co-MA stabilized transition metal(0) nanoclusters

- Water-soluble PSSA-co-MA stabilized ruthenium(0), nickel(0) and cobalt(0) nanoclusters with an average particle size of 1.9, 2.1 and 5.3 nm respectively, can be generated in-situ using commercially available precursor materials during the hydrolysis of AB.
- TEM analyses of the PSSA-co-MA stabilized ruthenium(0), nickel(0) and cobalt(0) indicated that all of the nanoclusters are actually embedded in polymer matrix with a narrow particle size distribution and spherical in shape.
- XRD patterns of PSSA-co-MA stabilized ruthenium(0), nickel(0) and cobalt(0) showed that nickel(0) and ruthenium(0) nanoclusters are existed in fcc crystal structure but cobalt(0) nanoclusters are existed in amorphous phase. The higher catalytic activity of the cobalt(0) nanoclusters compared to nickel(0) nanoclusters can be attributed to the its amorphous phase.

- PSSA-co-MA stabilized ruthenium(0), nickel(0) and cobalt(0) nanoclusters were found to be highly active catalysts in hydrogen generation from the hydrolysis of AB at ambient conditions.
- Kinetics of hydrogen generation from the hydrolysis of AB catalyzed by PSSA-co-MA stabilized nickel(0), cobalt(0) and ruthenium(0) nanoclusters can be summarized in the Table 5;

Table 5. Summary of the kinetic data of hydrogen generation from the hydrolysis of ammonia borane catalyzed by in-situ generated PSSA-co-MA stabilized nickel(0), cobalt(0) and ruthenium(0) nanoclusters.

Catalyst	Rate Law	Apparent Activation Energy (E_a^{apparent}) (kJ.mol⁻¹)	Lifetime (TTON)
<i>PSSA-co-MA stabilized Ru(0) NCs</i>	k.[Ru]	54 ± 2	51720 over 48 h
<i>PSSA-co-MA stabilized Ni(0) NCs</i>	k.[Ni]	32 ± 2	22450 over 38 h
<i>PSSA-co-MA stabilized Co(0) NCs</i>	k.[Co]	34 ± 2	17650 over 27 h

- PSSA-co-MA stabilized ruthenium(0) nanoclusters provide the second highest activity with a TOF value of 42.7 mol H₂.(mol Ru.min)⁻¹ among the all catalyst systems tested in the hydrolysis of ammonia borane.
- Compared to PSSA-co-MA stabilized ruthenium(0) nanoclusters, the PSSA-co-MA stabilized nickel(0) and cobalt(0) nanoclusters showed lower activity with the TOF values of 10.1 min⁻¹ for nickel and 25.7 mol min⁻¹ for cobalt, expectedly. However, compared to the other non-noble metal catalysts tested

in the hydrolysis of AB, the PSSA-co-MA stabilized nickel(0) nanoclusters is the best among the all nickel catalysts and the cobalt(0) is the second best catalyst among the all non-noble metal catalysts.

- Although the PSSA-co-MA stabilized ruthenium(0) nanoclusters provided the highest activity in terms of TOF values among the all metal catalysts in the hydrolysis of AB, they also have the highest activation energy. This intricacy can be also explained by the apparent rate constants and activation energy as we mentioned in the Chapter-2 and the Part-I of conclusion part.
- All of the nanoclusters showed first order dependency with respect to the catalyst concentration and zeroth order dependency with respect to the substrate concentration in the hydrolysis of AB. Compared to PVP stabilized nickel(0) and ruthenium(0) nanoclusters, the zeroth order dependency is not surprising for nickel and ruthenium. However, PVP stabilized cobalt(0) nanoclusters showed first order dependency with respect to the substrate concentration but PSSA-co-MA stabilized cobalt(0) nanoclusters showed zeroth order. The change in the dependency on substrate concentration for same metal in the same catalytic reaction can be explained by considering the acidity of PSSA-co-MA that eliminates the pH effect on the activity of cobalt(0) nanoclusters as explained with detailed mechanism in the section 5.2.2.3.
- PSSA-co-MA stabilized nickel(0), cobalt(0) and ruthenium(0) nanoclusters were found to be long-lived catalysts in the hydrolysis of AB providing 22450, 17650 and 51720 turnovers, respectively.

As a final remark, easy preparation, high stability, and the high catalytic performance of the PVP or PSSA-co-MA stabilized nickel(0), cobalt(0) and ruthenium(0) nanoclusters make them promising candidate to be employed as catalyst in developing highly efficient portable hydrogen generation systems using sodium borohydride or ammonia borane as solid hydrogen storage material.

REFERENCES

- [1] Aiken III J.D., Lin, Y., Finke R.G., *J. Mol. Catal. A*, **1996**, 114, 29.
- [2] Pool, R., *Science*, **1990**, 248, 1186.
- [3] Feldheim, D.R., Foss Jr, C. A. (Eds.), *Metal Nanoparticles: Synthesis, Characterization, and Applications*, Marcel Dekker, NewYork, **2002**.
- [4] Schmid, G. (Ed), *Clusters and Colloids: From Theory to Applications*, Wiley-VCH Publishers, Weinheim, **1994**.
- [5] (a) Schmid, G., Bäuml, M., Geerkens, M., Heim, I., Osemann, C., Sawitowski, T., *Chem. Soc. Rev.*, **1999**, 128, 79. (b) Schmid, G., *Chem. Rev.*, **1992**, 92, 1709.
- [6] Simon, U., Schön, G., Schmid, G., *Angew Chem. Int. Ed. Eng.*, **1990**, 248, 1186.
- [7] Glanz, J., *Science*, **1995**, 269, 1363.
- [8] Antonietti, M.; Göltner, C.; *Angew Chem. Int. Ed. Eng.*, **1997**, 36, 910.
- [9] Elghanian, R.; Storhoff, J.J.; Mucic, R.C.; Setinger, R.L.; Mirkin, C.A.; *Science*, **1997**, 277, 1078.
- [10] Colvin, V.L., Schlamp, M.C., Alivisatos, A.P., *Nature*, **1994**, 370, 354.
- [11] Sonti, S.V., Bose, A., *J. Colloid Int. Sci.*, **1995**, 170, 575.
- [12] Vossmeier, T., Delenno, E., Heath, J.R., *Angew. Chem., Int. Ed. Eng.*, **1997**, 36, 1080.

- [13] (a) Schmid, G., Maihack, V., Lantermann, F., Pechel, S., *J. Chem. Soc. Dalton Trans.*, **1996**, 199, 589 (b) Lin, Y., Finke, R.G., *J. Am. Chem. Soc.*, **1994**, 116, 8335. (c) Bönnehan, H.; Braun, G.A., *Angew Chem. Int. Ed. Eng.*, **1996**, 35, 1992. (d) Lewis, L.N.; Lewis, N., *J. Am. Chem. Soc.*, **1986**, 108, 7228. (e) Wilcoxon, J.P.; Martinho, T.; Klavetter, E.; Sylwester, A.P., *Nanophase Mater.* **1994**, 771. (f) Na, Y.; Park, S.; Bong, S.H.; *J. Am. Chem. Soc.*, **2004**, 126, 250. (g) Pelzer, K.; Vidoni, O.; Phillot, K.; Chaudret, B.; Collière, V., *Adv. Func. Mater.*, **2003**, 12, 118. (h) Hostetler, M.; Wingate, J.; Zong, C.; Evans, N.; Murray, R., *Langmuir*, **1998**, 14, 17-30 (i) Pelzer, K.; Phillot, K.; Chaudret, B., *Z. Anorg. Allg. Chem.*, **2003**, 629, 1217.
- [14] Campbell, T.C. *Science*, **2004**, 306, 234-235 and references therein.
- [15] Roucoux A.; Schulz J.; Patin H., *Chem Rev.*, **2002**, 102, 3757.
- [16] Corain, B., Schmid, G., Toshima N., Eds., *Metal Nanoclusters in Catalysis and Materials Science*, Elsevier, Amsterdam, Netherlands, **2008**.
- [17] Ninham, B.W., *Adv. Coll. Int. Sci.*, **1999**, 83, 85.
- [18] (a) Hirtzel, C.S., Rajagopalan, R., *Colloidal Phenomena: Advanced Topics*, Noyes Publications, New Jersey, **1985**. (b) Hunter, R.J., *Foundations of Colloid Science*, Oxford University Press, New York, Vol 1, p. 316-492, **1987**.
- [19] Verwey, E.J.W., Overbeek, J.T.G., *Theory of the Stability of Lyophobic Colloids*, Dover Publications, Mineola, New York, **1999**.
- [20] Klabunde K.J. (Ed), *Nanoscale Materials in Chemistry*, Wiley-Interscience Publishers, Newyork, **2001**.
- [21] Ott, L.S., Hornstein, B.J., Finke, R.G., *Langmuir*, **2006**, 22, 9357.

- [22] Hirai, H., Toshima N., *In Catalysis by Metal Complexes: Tailored Metal Catalyst*, Iwasawa Y (Ed.), Reidel Publishing Company, Dordrecht, **1986**.
- [23] Toshima, N., *Macromol. Symp.*, **2000**, 156, 45.
- [24] Schmid, G., *Nanoparticles: From Theory To Application*, Wiley-VCH, Weinheim, **2004**.
- [25] (a) Sato T., Ruch, R. (Eds.) *Stabilization of colloidal dispersion by polymer adsorption*, Marcel Dekker Inc., New York, **1980**. (b) Napper D.H., (Ed.) *Polymeric Stabilization of Colloidal Dispersions*, Academic Press, London, **1983**.
- [26] Zahmakiran, M., Özkar, S., *Inorg. Chem.*, **2009**, 48, 8955.
- [27] Gaffet, E., Tachikart, M., El Kedim, O., Rahouadj, R. *Mater. Charact.*, **1996**, 36, 185.
- [28] Willner, I., Mandler, D., *J. Am. Chem. Soc.*, **1989**, 111, 1330
- [29] (a) Fu, X., Wang, Y., Wu, N., Gui, L., *Langmuir*, **2002**, 18, 4619. (b) Narayanan, R., El-Sayed M.A., *J. Phys. Chem. B*, **2004**, 108, 5726. (c) Crooks, R.M., Zhao, M., Sun, L., Chechik, V., Yeung, L.K. *Acc. Chem. Res.*, **2001**, 34, 181. (d) Bönneman, H., Richards, R.M., *Eur. J. Inorg. Chem.*, **2001**, 10, 2445.
- [30] (a) Tano, T., Esumi, K., Meguro, K., *J. Colloid Interface Sci.*, **1989**, 133, 530. (b) Esumi, K., Tano, T., Torigoe, K., Meguro, K. *Chem. Mater.*, **1990**, 2, 564. (c) Esumi, K., Tano, T., Torigoe, K., Meguro, K. *J. Colloid Interface Sci.*, **1992**, 149, 295. (d) Toshima, N., Wang, Y., *Chem. Lett.*, **1993**, 22, 1611.
- [31] (a) Tano, T., Esumi, K., Meguro K., *J. Colloid Interface Sci.*, **1989**, 133, 530. (b) Esumi, K., Tano, T., Meguro, K., *Langmuir*, **1989**, 5, 268. (c) Dhas, N.A.,

- Suslick, K.S., *J. Am. Chem. Soc.*, **2005**, 127, 2368. (d) Suslick, K.A., Choe, S.-B., Cichowias, A.A., Grinstaff, M.W., *Nature*, **1991**, 353, 414.
- [32] Duteil, A., Queau, R., Chaudret, B., Mazel, R., Roucau, C., Bradley, J.S., *Chem. Mater.*, **1993**, 5, 341.
- [33] Finke R.G.; Özkar S., *Coordination Chem. Rev.*, **2004**, 248, 135.
- [34] (a) Smith T.W., *US Patent 4252671*, **1981**. (b) Smith T.W., *US Patent 4252672*, **1981**. (c) Smith T.W., *US Patent 4252673*, **1981**. (d) Smith T.W., *US Patent 4252674*, **1981**. (e) Smith T.W., *US Patent 4252675*, **1981**.
- [35] Takahashi Y., Ito T., Sakai S., Ishii Y., *Chem. Commun.*, **1970**, 1065.
- [36] (a) Cheysaac, P.; Kofman, R.; Merli, P.G.; Migliori, A.; Stella, A. *Mater. Res. Soc. Symp. Proc.* **1994**, 332, 109. (b) Cheysaac, P.; Kofman, R.; Mattei, G.; Merli, P. G.; Migliori, A.; Stella, A. *Superlattices Microstruct.* , **1995**, 17, 47.
- [37] (a) Metin, Ö.; Özkar, S. *Int. J. Hydrogen Energy*, **2007**, 32, 1707. (b) Metin, Ö.; Özkar, S. *J. Mol. Catal. A: Chem.*, **2008**, 295, 39. (c) Metin, Ö.; Özkar, S. *Energy&Fuels*, **2009**, 23, 3517. (d) Erdogan, H.; Metin, Ö.; Özkar, S. *Phys. Chem. Chem. Phys.*, **2009**, 11, 10519. (e) Metin, Ö.; Sahin, S.; Özkar, S. *Int. J. Hydrogen Energy*, **2009**, 34, 6304.
- [38] Creighton, J.A.; Eadon, D.G., *J. Chem. Soc. Faraday Trans.*, **1991**, 87, 3881.
- [39] Niemantsverdriet, J.W., *Spectroscopy in Catalysis: An Introduction*, Wiley-VCH, Weinheim, Germany, **2000**.
- [40] Wechuysen, B.M., *In-situ spectroscopy of Catalysts*, American Scientific Publishers, CA, USA, **2004**.

- [41] Aiken III J.D., Finke R.G., *J.Mol. Catal. A: Chem.*, **1999**, 145, 1- 44
- [42] (a) Rothenberg, G. *Catalysis: Concepts and Green Applications*, Wiley-VCH, Weinheim, **2008**. (b) Smith, G.V., Notheisz, F., *Heterogeneous Catalysis in Organic Chemistry*; Academic Press, San Diego, **1999**.
- [43] Gates, B.C., *Catalytic Chemistry*; Academic Press: New York, **1992**.
- [44] Thomas, J.M., Thomas, W.J., *Principles and Practice of Heterogeneous Catalysis*, VCH, New-York, **1997**.
- [45] Anthonsen, T., *Reactions Catalyzed by Enzymes In Applied Biocatalysis*, 2. Harwood Academic Publishers, UK, **1999**.
- [46] Özkar S., *Appl. Surf. Sci.*, **2009**, 256,1272.
- [47] Richards, R.M., *Surface and Nanomolecular Catalysis*, Taylor & Francis, Boca Raton, **2006**.
- [48] Klabunde, K.J., Stark, J., Koper, C., Park, D., *J. Phys. Chem.*, **1996**, 100, 12142.
- [49] Schmid, G., *Endeavour*, **1990**, 14, 172.
- [50] Energy Information Administration, Annual Energy Outlook 2005 With Projections To 2025, [www.eia.doe.gov/oiaf/aeo/pdf/0383\(2005\).pdf](http://www.eia.doe.gov/oiaf/aeo/pdf/0383(2005).pdf), February, **2005**.
- [51] U. S. Department of Energy, Basic Research Needs For the Hydrogen Economy, Report of the Basic Energy Sciences Workshop on Hydrogen Production, Storage and Use , www.sc.doe.gov/bes/hydrogen.pdf May 13-15, **2003**.

- [52] (a) Schlapbach, L., Züttel, A., *Nature*, **2001**, 414, 353; (b) Orimo, S., Nakamori, Y., Eliseo, J. R., Züttel, A., Jensen, C.M., *Chem. Rev.* **2007**, 107, 4111.
- [53] (a) Sandrock, G., Suda, S., Schlapbach, L., *Hydrogen in Intermetallic Compounds II, Topics in Applied Physics*, Springer, Verlag, Vol. 67, p 197, **1992**; (b) Sandrock, G., Yurum, Y., *Hydrogen Energy Systems: Production and Utilization of Hydrogen and Future Aspects*, NATO ASI Series, Kluwer Academic Publishers, **1994**.
- [54] Rosi, N.L., Eckert, J., Eddaoudi, M., Vodak, D.T., Kim, J., O'Keeffe, M., *Science*, **2003**, 300, 1127.
- [55] (a) Dillion, A.C., Jones, K.M., Bekkedahl, T.A., Kiang, C.H., Bethune, D.S., Heben, M., *Nature*, **1997**, 386, 377; (b) Park, C., Anderson, P.E., Chambers, A., Tan, C.D., Hidago, R., Rodriguez, N.M., *J. Phys. Chem. B*, **1999**, 103, 10572; (c) Liu, C., Fan, Y.Y., Liu, M., Wei, Y.L., Lu, M.Q., Cheng, H.M., *Science*, **1999**, 286, 1127; (d) Nikitin, A., Ogasawara, H., Mann, D., Denecke, R., Zhang, Z., Dai, H., Cho, K., Nilsson, A., *Phys. Rev. Lett.* **2005**, 95, 225507.
- [56] (a) Marrero-Alfonso, Y.E., Beard, A.M., Davis, T.A., Matthews, M.A., *Ind. Eng. Chem. Res.*, **2009**, 48, 3703; (b) Umegaki, T., Yan, J-M., Zhang, Z-B., Shioyama, H., Kuriyama, N., Xu, Q., *Int. J. Hydrogen Energy* **2009**, 34, 2303.
- [57] Züttel, A., *Mater. Today*, **2003**, 6, 24.
- [58] (a) Liu, B.H., Li, Z.P., *J. Power Sources*, **2009**, 187, 527. (b) Metin, Ö., Özkar, S., *Int. J. Hydrogen Energy*, **2007**, 32, 1707. (c) Metin, Ö., Özkar, S., *Energy&Fuels*, **2009**, 23, 3517. (d) Zahmakıran, M., Özkar, S., *Langmuir* **2009**, 25, 2667. (e) Rakap, M., Özkar, S., *Appl. Catal. B: Env.*, **2009**, 91, 21.

- (f) Metin, Ö., Özkar, S., *J. Mol. Catal. A: Chem.*, **2008**, 295, 39. (g) Cakanyildirim, C., Gürü, M., *Int. J. Hydrogen Energy*, **2008**, 33, 4634.
- [59] (a) Amendola, S.C., Janjua, J.M., Spencer, N.C., Kelly, M.T., Petillo, P.J., Sharp-Goldman, S.L., Binder, M., *Int. J. Hydrogen Energy*, **2000**, 25, 969. (b) Lee, J.Y., Lee, H.H., Lee, J.H., Kim D.M., Kim J.H., *J. Electrochem. Soc.*, **2002**, 149(5), A 603.
- [60] (a) Levy A., Brown J.B, Lyons C.J., *Ind. Eng. Chem.*; **1960**, 52, 211. (b) Kaufman C.M, Sen B., *J. Am. Chem. Soc. Dalton Trans.*; **1985**, 307. (c) Brown H.C, Brown C.A., *J. Am. Chem. Soc.*; **1962**, 84, 1493.
- [61] James B.D, Wallbridge MGH., *Prog. Inorg. Chem.*; **1970**, 11, 99-231.
- [62] Aicillo R, Sharp J.H, Matthews M.A., *Int. J. Hydrogen Energy*, **1999**, 24, 1123.
- [63] Davis W.D, Mason L.S, Stegaman G., *J. Am. Chem. Soc.*, **1949**, 71, 2775.
- [64] (a) Marder, T.B., *Angew. Chem. Int. Ed.*, **2007**, 46, 8116. (b) Chen, Y.S., Fulton, J.L., Linehan, Y.C., Autrey, T., *J. Am. Chem. Soc.*, **2005**, 127, 3254. (c) Gutowska, A., Li, L.Y., Shin, Y.S., Wang, C.M.M., Li, X.H.S., Linehan, J. C.; Smith, R.S.; Kay, B.D.; Schmid, B.; Shaw, W.; Gutowski, M., Autrey, T., *Angew. Chem. Int. Ed.*, **2005**, 44, 3578. (b) Stephens, F.H., Pons, V., Baker, R.T., *Dalton Trans.*, **2007**, 25, 2613, and references therein.
- [65] Ramachadran, P.V.; Gagare, P.D., *Inorg. Chem.*, **2007**, 46, 7810.
- [66] Klooster, W.T., Koetzle, T.F., Siegbahn, P.M., Richardson, T.B., Crabtree, R.H., *J. Am. Chem. Soc.*, **1999**, 121, 6337.
- [67] Richardson, T.B., de Gala, S., Crabtree, R.H., *J. Am. Chem. Soc.*, **1995**, 117, 12785.

- [68] (a) Baitalow, F., Baumann, J., Wolf, G., Jaenicke, K., Leitner, G., *Thermochim. Acta*, **2002**, 391, 159. (b) Wolf, G., Baumann, J., Baitalow, F., Hoffman, F.P., *Thermochim. Acta*, **2000**, 343, 19.
- [69] Chandra, M., Xu, Q., *J. Power Sources*, **2006**, 156, 190.
- [70] Metin, Ö. *Synthesis and characterization of hydrogenphosphate stabilized nickel(0) nanoclusters as catalyst for the hydrolysis of sodium borohydride*, MS thesis, Ankara, May, **2006**. (b) Metin, Ö., Özkar, S., *Int. J. Hydrogen Energy*, **2007**, 32, 1707.
- [71] Zhang, J., Zheng, Y., Gore, J.P., Fisher, T.S., *J. Power Sources*, **2007**, 165, 844.
- [72] Schmid, G. *Nanoparticles: From Theory To Application*, Wiley-VCH, Weinheim, **2004**.
- [73] Mayer, A.B.R., *Polym. Adv. Technol.*, **2001**, 12, 96.
- [74] Vu, Y.T., Mark, J.E., *Colloid Polym. Sci.*, **2004**, 282, 603.
- [75] Metin, Ö.; Özkar, S., *J. Mol. Catal. A: Chem.*, **2008**, 295, 39.
- [76] Hirai, H., Chawanya, H., Toshima, N., *Bull.Chem.Soc. Jpn.* **1985**, 58, 682.
- [77] Hirai, H., Nakao, Y., Toshima, N., Adachi, K., *Chem. Lett.*, **1976**, 5, 905.
- [78] Hirai, H., Chawanya, H., Toshima, N., *Reactive Polym.*, **1985**, 3,127.
- [79] Kwon, S.G., Hyeon, T., *Acc. Chem. Res.*, **2008**, 41, 1696.
- [80] International XPS Spectral Data Processors, www.xpsdata.com. (Last Access date: 09.11.2010)

- [81] Tan, B.J., Klabunde, K.J., Sherwood, P.M., *J. Am. Chem. Soc.* **1991**, 113, 855.
- [82] McIntyre, N.S., Cook, M.G., *Anal.Chem.*, **1975**, 47, 2208.
- [83] (a) Schlesinger, H.I., Brown, H.C., Finholt, A.E., Gilbreath, J.R., Hockstrue, H.R., Hye, E.K., *J. Am. Chem. Soc.*, **1953**, 75, 215. (b) Glavee, G.N., Klabunde, K.J., Sarensen, M., Hajapanayis, G.C., Langmuir, **1992**, 8, 771. (c) Walter, J.C., Zrawski, A., Montgomery, D., Thornburg, M., Revankar, S.J., *J. Power Sources*, **2008**, 179, 335.
- [84] (a) Creighton, J.A., Eadon, D.G., *J. Chem. Soc. Faraday Trans.*, **1991**, 87, 3881. (b) Wilcoxon, J.P., Abrams, B.L., *Chem.Soc.Rev.*, **2006**, 35, 1162-164.
- [85] Yan, J.M., Zhang, X.B., Han, S., Shioyama, H., Xu, Q. *J. Power Sources*, **2010**, 195, 1091.
- [86] Chen ,W, Davies, J.R., Ghosh, D., Tong, M.C., Konopelski, J.P., Chen, S., *Chem. Mater.*, **2006**, 18, 5253.
- [87] Chen W, Ghosh, D., Sun, J., Tong, M.C., Deng, F., Chen. S., *Electrochem. Acta*, **2007**, 53, 1150.
- [88] Jiang, Y-X.,Weng, W-Z., Si, D., Sun, S-G., *J. Phys. Chem. B*, **2005**, 109, 7637.
- [89] Clune, M.W.F., *Powder Diffraction File Alphabetical Index Inorganic Phase, JCPPDS*, Swarthmore, PA, **1980**.
- [90] Watts, J.F., Wolstenholme, J., *An introduction to surface analysis by XPS and AES*, John Wiley & Sons Ltd., West Sussex, England, **2003**.
- [91] Dmowski, W., Egami, T., Swider-Lyons, K.E., Love, C.T., Rolison, D.R. *J. Phys. Chem. B*, **2002**, 106, 12677.

- [92] Kim, H.S., Kim, Y.J., Kim, J.J., Lee, S.D., Kang, Y.S., Chin, C.S., *Chem. Mater.*, **2001**, 13, 1720.
- [93] Laidler, K.J., *Chemical Kinetics*; Third Ed.; Benjamin-Cummings, **1997**.
- [94] (a) Evans, M.G., Polanyi M., *Trans. Faraday Soc.*, **1935**, 31, 875. (b) Eyring, H., *J. Chem. Phys.*, **1935**, 3, 107. (c) Eyring, H., Polanyi M., *Z. Phys. Chem. Abt. B*, **1931**, 12, 279.
- [95] Kaufman, C.M., Sen, B., *J. Chem. Soc. Dalton. Trans.*, **1985**, 83, 307.
- [96] Davis, R.E., Swain, C.G., *J. Am. Chem. Soc.*, **1960**, 82, 5950.
- [97] Chandra, M., Xu, Q., *J. Power Sources*, **2006**, 163, 364.
- [98] Basu, S., Brockman, A., Gagore, P., Zheng, Y., Ramachandran, P.V., Delgass, W.N., *J. Power Sources*, **2009**, 188, 238.
- [99] Mesmer, R.E.; Jolly, W.L. *Inorg. Chem.* **1962**, 1, 608-612.
- [100] Amendola, S.C., Janjua, J.M., Spencer, N.C., Kelly, M.T., Petillo, P.J., Sharp-Goldman, S.L., Binder, M., *J. Power Sources*, **2000**, 85, 186.
- [101] (a) Lee, J., Kong, K.Y., Jung, C.R., Cho, E., Yoon, S.P., Han, J., Lee, T.G., Nam, S.W., *Catal. Today*, **2007**, 120, 305. (b) Ye, W., Zhang, H., Xu, D., Ma, L., Baolian, B., *J. Power Sources*, **2007**, 32, 4711. (c) Garron, A., Swierczynski, D., Bennici, S., Auroux, A., *Int. J. Hydrogen Energy*, **2009**, 34, 1185.
- [102] Jeong, S.U., Kim, R.K., Cho, E.A., Kim, H.J., Nam, S.W., Oh, I.H., Hong, S.A., Kim, S.H., *J. Power Sources*, **2005**, 144, 129.
- [103] Holbrook, K.A., Twist, P.J., *J. Chem. Soc. A.*, **1971**, 15, 890.
- [104] Zahmakiran, M., Özkar, S., *J. Mol. Catal. A*, **2006**, 258, 95.

- [105] Amendola, S.C., Janjua, J.M., Spencer, N.C., Kelly, M.T., Petillo, P.J., Sharp-Goldman, S.L., Binder, M., *Int. J. Hydrogen Energy*, **2000**, 25, 969.
- [106] Kaufman, C.M., Sen, B., *J. Chem. Soc. Dalton. Trans.*, **1985**, 83, 307.
- [107] Schreiner, P., Schaefer, H., Schleyer, P. V., *J. Chem. Phys.*, **1994**, 101, 7625.
- [108] Mesmer, R. E., Jolly, W. L., *Inorg. Chem.*, **1962**, 1, 608.
- [109] (a) Chatenet, M., Micoud, F., Roche, I., Chainet, E., *Electrochim. Acta*, **2006**, 51, 5459. (b) Guella, G., Zanchetta, C., Patton, B., Miotello, A., *J. Phys. Chem. B*, **2006**, 110, 17024. (c) Zhang, H., Yi, B., Wu, C., *Catal. Today*, **2004**, 93, 477. (d) Ingersoll, J. C., Mani, N., Thenmozhiyal, J. C., Muthaiah, A., *J. Power Sources*, **2007**, 173, 450. (e) Walter, J. C., Zurawski, A., Montgomery, D., Thomburg, M., Pevankar, S., *J Power Sources*, **2008**, 179, 335.
- [110] Amendola, S. C., Janjua, J. M., Spencer, N. C., Kelly, M. T., Petillo, P. J., Sharp-Goldman, S. L., Binder, M., *J. Power Sources*, **2000**, 85, 186.
- [111] Ingersoll, J. C., Mani, N., Thenmozhiyal, J. C., Muthaiah, A., *J. Power Sources*, **2007**, 173, 450.
- [112] Dai, H. B., Liang, Y., Wang, P., Chang, H. M. *J. Power Sources*, **2008**, 177, 17.
- [113] Hanxi, Y., Hua, D., Xinping, A., Chuansin, C., *Int. J. Hydrogen Energy*, **2003**, 28, 1095.
- [114] Lee, J., Kong, K. Y., Jung, C. R., Cho, E., Yoon, S. P., Han, J., Lee, T.-G., Nam, S. W., *Catal. Today*, **2007**, 120, 305.
- [115] Demirci, U. B., Garin, F., *J. Mol. Catal. A Chem.*, **2008**, 279, 57.

- [116] Zhao, J., Ma, H., Chen, J., *Int. J. Hydrogen Energy*, 2007, 32, 4711.
- [117] Patel, N., Patton, B., Zanchetta, C., Fernandes, R., Guella, G., Kale, A., Miotello, A., *Int. J. Hydrogen Energy*, **2008**, 33, 287.
- [118] Zhang, Q., Wu, Y., Sun, X., Ortega, J., *Ind. Eng. Chem. Res.*, **2007**, 46, 1120.
- [119] Mitov, M., Rashkov, R., Atanassov, N., Zielonka, A., *J. Mater. Sci.*, **2007**, 42, 3367.
- [120] Zhang, Z. S., Delgass, W. N., Fisher, T. S., Gore, J. P., *J. Power Sources*, **2007**, 164, 772.
- [121] Alonso, R. P., Sicurelli, A., Callone, E., Carturan, G., Raj, R., *J. Power Sources*, **2007**, 165, 315.
- [122] Dai, A. B., Liang, Y., Wang, P., Yao, X. D., Rufford, T., Lu, M., Cheng, H. M., *Int. J. Hydrogen Energy*, **2008**, 33, 4405.
- [123] Metin, Ö.; Özkar, S. *Energy&Fuels*, **2009**, 23, 3517.
- [124] Knecht, M.R., Garcia-Martinez, J.C., Crooks, R.M., *Chem. Mater.*, **2006**, 18, 5039.
- [125] Wilcoxon, J.P., Abrams, B.L., *Chem. Soc. Rev.*, **2006**, 35, 1162.
- [126] Watzky, M.A., Finke, R.G., *J. Am. Chem. Soc.*, **1997**, 119, 10382.
- [127] Kalidindi, S.D., Indirani, M., Jagirdar, B.R., *Inorg. Chem.*, **2008**, 47, 7424.
- [128] (a) Yan, J.M., Zhang, X.B., Han, S., Shioyama, H., Xu, Q. *J Power Sources*, **2010**, 195, 1091. (b) Yan, J.M., Zhang, X.B., Han, S., Shioyama, H., Xu, Q., *J. Power Sources*, **2009**, 194, 478. (c) Jiang, H.L., Umegaki, T., Akita, T., Zhang, X.B., Haruta, M., Xu, Q., *Chem. Eur. J.*, **2010**, 16, 3132. (d) Metin, Ö., Mazumder, V., Özkar, S., Sun, S., *J. Am. Chem. Soc.*, **2010**, 132, 1468. (e)

Yan, J.M., Zhang, X.B., Han, S., Shioyama, H., Xu, Q., *Inorg. Chem.*, **2009**, 48, 7389. (f) Umegaki, T., Yan, J.M., Zhang, X.B., Shioyama, H., Kuriyama, N., Xu, Q., *Int J Hydrogen Energy*, **2009**, 34, 3816. (g) Cheng, F., Ma, H., Li, Y., Chen, J., *Inorg. Chem.*, **2007**, 46, 788. (h) Yan, J.M., Zhang, X.B., Han, S., Xu Q., *Angew. Chem. Int. Ed.*, **2008**, 47, 2287. (i) Rakap, M., Ozkar, S., *Int. J. Hydrogen Energy*, **2010**, 35, 3341 (j) Chandra, M., Xu, Q., *J. Power Sources* **2006**, 163, 364. (k) Chandra, M., Xu, Q., *J. Power Sources*, **2007**, 168, 135. (m) Kalidindi, S.D., Sayal, U., Jagirdar, B.R., *Phys Chem Chem Phys.* **2008**, 10, 5870.

[129] Dmowski, W., Egami, T., Swider-Lyons, K.E., Love, C.T., Rolison, D.R. *J. Phys. Chem. B*, **2002**, 106, 12677.

APPENDIX A

TABLES

Table A1. The values of rate constant (k_{app}) for the sole catalytic hydrolysis starting with a solution of 150 mM NaBH₄ and 1.4 mM PVP stabilized nickel(0) nanoclusters at different temperatures, calculated from the hydrogen volume versus time data corrected by subtracting the volume of hydrogen generated from the self hydrolysis of sodium borohydride.

Temperature (K)	Rate Constant, k_{app} $\text{mol H}_2 \cdot (\text{mol Ni})^{-1} \cdot \text{s}^{-1}$
298	0.170
303	0.240
308	0.326
313	0.436
318	0.579

Table A2. The values of rate constant (k_{app}) for the catalytic hydrolysis of ammonia borane starting with a solution of 100 mM H_3NBH_3 and 1.4 mM PVP stabilized nickel(0) nanoclusters at different temperatures, calculated from the hydrogen volume versus time data.

Temperature (K)	Rate Constant, k_{app} $mol H_2.(mol Ni)^{-1}.s^{-1}$
293	0,0008
298	0,0013
303	0,0018
308	0,0030
313	0,0037

Table A3. The values of rate constant (k_{app}) for the sole catalytic hydrolysis starting with a solution of 150 mM $NaBH_4$ and 1.5 mM PVP stabilized cobalt(0) nanoclusters at different temperatures, calculated from the hydrogen volume versus time data corrected by subtracting the volume of hydrogen generated from the self hydrolysis of sodium borohydride

Temperature (K)	Rate Constant, k_{app} for hydrolysis of $NaBH_4$ in aqueous medium $mol H_2.(mol Co)^{-1}.(mol NaBH_4)^{-1}.s^{-1}$
293	0.021
298	0.034
303	0.055
308	0.080
313	0.108

Table A4. The values of rate constant (k_{app}) for the catalytic hydrolysis of ammonia borane starting with a solution of 100 mM H_3NBH_3 and 2.0 mM PVP stabilized cobalt(0) nanoclusters at different temperatures, calculated from the hydrogen volume versus time data.

Temperature (K)	Rate Constant, k_{app} for hydrolysis of H_3NBH_3 $mol H_2.(mol Co)^{-1}.s^{-1}$
293	0.277
298	0.376
303	0.496
308	0.626
313	0.763

Table A5. The values of rate constant (k_{app}) for the catalytic hydrolysis of sodium borohydride (150 mM) catalyzed by PVP stabilized cobalt(0) nanoclusters (1.5 mM Co) in 5 wt% NaOH solution at different temperatures, calculated from the hydrogen volume versus time data.

Temperature (K)	Rate Constant, k_{app} for hydrolysis of $NaBH_4$ in basic medium $mol H_2.(mol Co)^{-1}.s^{-1}$
293	0.277
298	0.376
303	0.496
308	0.626
313	0.763

Table A6. The values of rate constant (k_{app}) for the sole catalytic hydrolysis starting with a solution of 150 mM NaBH₄ and 0.45 mM PVP stabilized ruthenium(0) nanoclusters at different temperatures, calculated from the hydrogen volume versus time data corrected by subtracting the volume of hydrogen generated from the self hydrolysis of sodium borohydride

Temperature (K)	Rate Constant, k_{app} for hydrolysis of NaBH ₄ in aqueous solution mol H ₂ .(mol Ru) ⁻¹ .s ⁻¹
298	0,266
303	0,508
308	0,704
313	0,904
318	1,208

Table A7. The values of rate constant (k_{app}) for the catalytic hydrolysis of sodium borohydride (150 mM) catalyzed by PVP stabilized ruthenium(0) nanoclusters (0.45 mM Ru) in 5 wt% NaOH solution at different temperatures, calculated from the hydrogen volume versus time data.

Temperature (K)	Rate Constant, k_{app} for hydrolysis of NaBH ₄ in basic medium mol H ₂ .(mol Ru) ⁻¹ .s ⁻¹
288	0.178
293	0.221
298	0.280
303	0.340
308	0.440

Table A8. The values of rate constant (k_{app}) for the catalytic hydrolysis of ammonia borane starting with a solution of 100 mM H_3NBH_3 and 0.35 mM PVP stabilized ruthenium(0) nanoclusters at different temperatures, calculated from the hydrogen volume versus time data.

Temperature (K)	Rate Constant, k_{app} for hydrolysis of H_3NBH_3 $mol H_2.(mol Ru)^{-1}.s^{-1}$
288	0.717
293	0.897
298	1.254
303	1.551
308	2.031

Table A9. The values of rate constant (k_{app}) for the catalytic hydrolysis of ammonia borane starting with a solution of 100 mM H_3NBH_3 and 2.0 mM PSSA-co-MA stabilized nickel(0) nanoclusters at different temperatures, calculated from the hydrogen volume versus time data.

Temperature (K)	Rate Constant, k_{app} for hydrolysis of H_3NBH_3 $mol H_2.(mol Ni)^{-1}.s^{-1}$
288	0.061
293	0.083
298	0.100
303	0.123
308	0.151

Table A10. The values of rate constant (k_{app}) for the catalytic hydrolysis of ammonia borane starting with a solution of 100 mM H_3NBH_3 and 2.0 mM PSSA-co-MA stabilized cobalt(0) nanoclusters at different temperatures, calculated from the hydrogen volume versus time data.

Temperature (K)	Rate Constant, k_{app} for hydrolysis of H_3NBH_3 mol H_2 .(mol Co) ⁻¹ .s ⁻¹
288	0.116
293	0.148
298	0.192
303	0.238
308	0.293

Table A11. The values of rate constant (k_{app}) for the catalytic hydrolysis of ammonia borane starting with a solution of 100 mM H_3NBH_3 and 0.55 mM PSSA-co-MA stabilized ruthenium(0) nanoclusters at different temperatures, calculated from the hydrogen volume versus time data.

Temperature (K)	Rate Constant, k_{app} for hydrolysis of H_3NBH_3 mol H_2 .(mol Ru) ⁻¹ .s ⁻¹
288	1.444
293	2.171
298	3.127
303	4.703
308	6.256

CURRICULUM VITAE

Name : Önder METİN
Date of Birth : September 10, 1981
Place of Birth : Adana/TURKEY
Status : Married

Education:

September 2006- Present **PhD in Chemistry (Inorganic Chemistry) (GPA: 4.0/4.0)**
Department of Chemistry, Middle East Technical
University, Ankara, TURKEY
Thesis Title: Synthesis and Characterization of Water-
Soluble Polymer-Stabilized Transition Metal(0)
Nanoclusters as Catalystin Hydrogen Generation from the
Hydrolysis of Sodium Borohydride and Ammonia Borane
Supervisor: Prof. Dr. Saim Özkar

September 2004-June 2006 **MS in Chemistry, (Inorganic Chemistry) (GPA: 3.6/4.0)**
Department of Chemistry, Middle East Technical
University, Ankara, TURKEY
Thesis Title: ‘Synthesis and Characterization of
Hydrogenphosphate-stabilized Nickel(0) Nanoclusters as
Catalysts for the Hydrolysis of Sodium Borohydride ’
Supervisor: Prof. Dr. Saim Özkar

September 1998-July 2002 **BS in Chemistry (GPA: 3.2/4.0, the second honor degree)**
Faculty of Arts and Sciences Çukurova University, Adana,
Turkey

Positions

- 2004-2005 Teaching Assistant In General Chemistry Laboratory, METU, Turkey
- 2005-2007 Teaching Assistant In Analytical Chemistry Laboratory, METU, Turkey
- 2007-2010 Teaching Assistant In Inorganic Chemistry, METU, Turkey
- 2009-2010 Visiting Researcher in Sun Research Group at Department of Chemistry, Brown University, Providence, RI, USA.
(Host Scientist: *Prof. Dr. Shouheng Sun*)
- July-October 2010 Visiting Researcher in Anorganische Chemie Research Group at Department of Chemistry, Technical University of Darmstadt (TUD) Darmstadt, Germany.
(Host Scientists: *Prof. Dr. Jörg J. Schneider*)

Awards

- 2002** The Second Undergraduate Student of Department of Chemistry, Çukurova University, Adana, Turkey.
- 2008** The Best PhD Student of Graduate School Natural And Applied Sciences METU, Turkey
- 2009** **The Best Poster Prize ‘ 24th National Chemistry Conference’** 16-20 June 2009, Sivas, Turkey.

Publications:

17- Dinç, M.; **Metin, Ö.**; Özkar, S. Water Soluble Polymer Stabilized Iron(0) Nanoclusters: A Cost-Effective and Magnetically Recoverable Catalyst for Hydrogen Generation from the Hydrolysis of Sodium Borohydride and Ammonia Borane, *Appl. Catal. B: Env.*, **2010**, submitted.

- 16- Metin, Ö.;** Dinç, M.; Eren, Z.S.; Özkar, S. Silica Embedded Cobalt(0) Nanoclusters: Efficient, Stable and Cost-Effective Catalyst for Hydrogen Generation from the Hydrolysis of Ammonia Borane, *Catalysis Today*, **2010**, under review.
- 15- Metin, Ö.;** Koçak, E.; Özkar, S. Effect of Stabilizer Type on the Activity of Cobalt(0) Nanoclusters as Catalyst in Hydrogen Generation from the Hydrolysis of Sodium Borohydride, *J. Mol. Catal. A: Chem.*, **2010**, under review.
- 14- Metin, Ö.;** Durap, F.; Aydemir, M.; Ün, S. S.; Özkar, S. Palladium(0) Nanoclusters Stabilized by Poly(4-styrenesulfonic acid-co-maleic acid): Superb Catalyst in Suzuki Cross-Coupling Reactions in Water, *J. Mol. Catal. A: Chem.*, **2010**, under review.
- 13- Erdogan, H.;** **Metin, Ö.;** Özkar, S. In-Situ Generated Polymer Stabilized Ruthenium(0) Nanoclusters: An Effective Catalyst in the Hydrogen Generation from the Methanolysis of Ammonia Borane, *Catalysis Today*, **2010**, in press.
- 12- Metin, Ö.;** Özkar, S. Nickel(0) and Cobalt(0) Nanoclusters Stabilized by Poly(4-styrenesulfonic acid-co-maleic acid) as Highly Active Catalysts in Hydrolytic Dehydrogenation of Ammonia Borane, *Int. J. Hyd. Energy*, **2010**, in press.
- 11- Metin, Ö.;** Özkar, S.; Sun, S. Monodisperse Nickel Nanoparticles Support on SiO₂ as an Effective Catalyst for the Hydrolysis of Ammonia Borane, *Nano Research*, **2010**, 3, 676-684.
- 10- Metin, Ö.;** Mazumder, V.; Özkar, S.; Sun, S. Monodisperse Nickel Nanoparticles and Their Catalysis in Hydrolytic Dehydrogenation of Ammonia Borane, *J. Am. Chem. Soc.*, **2010**, 32, 1468-1469.
- 9- Metin, Ö.;** Özkar, S. Water-soluble Poly(4-styrenesulfonic acid-co-maleic acid)-stabilized Nickel(0) and Cobalt(0) Nanoclusters as Highly Active Catalysts in Hydrogen Generation from the Hydrolysis of Ammonia borane, *Mater. Res. Soc. Symp. Proc.* **2010**, 1217, Y-08-14.
- 8- Durap, F.;** **Metin, Ö.;** Aydemir, M.; Özkar, S. New Route to Synthesis of PVP stabilized Palladium(0) Nanoclusters and Their Enhanced Catalytic Activity in Heck and Suzuki Cross-Coupling Reactions, *Appl. Organometal. Chem.* **2009**, 23, 498-503.

- 7- Erdogan, H.; **Metin, Ö.**; Özkar, S. In-situ Generated PVP stabilized Palladium(0) Nanocluster Catalyst in Hydrogen Generation From the Methanolysis Of Ammonia borane, *Phys. Chem. Chem. Phys.*, **2009**, *11*, 10519-10525.
- 6- **Metin, Ö.**; Sahin, S.; Özkar, S. Water-soluble Poly(4-styrenesulfonic acid-co-maleic acid)-stabilized Ruthenium(0) and Palladium(0) Nanoclusters as Highly Active Catalysts in Hydrogen Generation from the Hydrolysis of Ammonia borane, *Int. J. Hydrogen Energy*, **2009**, *34*, 6304-6313.
- 5- **Metin, Ö.**; Özkar, S. Hydrogen Generation from the Hydrolysis of Ammonia borane and Sodium Borohydride Using Water-soluble Polymer-Stabilized Cobalt(0) Nanoclusters Catalyst, *Energy&Fuels*, **2009**, *23*, 3517-3525.
- 4- **Metin, Ö.**; Özkar, S.; Synthesis and Characterization Of Poly(N-Vinyl-2-pyrrolidone)-Stabilized Water-Soluble Nickel(0) Nanoclusters as Catalyst for The Hydrolysis of Sodium Borohydride, *J. Mol. Catal. A: Chem.*, **2008**, *295*, 39-46.
- 3- Pitcher, M.W.; Arslan, Y.; Edinç, P.; Kartal, M.; Maşjedi, M.; **Metin, Ö.**; Şen, F.; Türkarşlan, Ö.; Yiğitsoy, B. Recent Advances in The Synthesis and Applications of Inorganic Polymers, *Phosphorous, silicon, sulfur and related elements*, **2007**, *182*, 2861-2880.
- 2- **Metin, Ö.**; Yıldırım, L.T.; Özkar, S. Synthesis, Characterization and Crystal Structure of Bis(acetylacetonato)dimethanolnickel(II): [Ni(acac)₂(MeOH)₂], *Inorg. Chem. Commun.* **2007**, *10*, 1121-1123.
- 1- **Metin, Ö.**; Özkar, S. Hydrogen Generation From The Hydrolysis Of Sodium Borohydride By Using Water-dispersible Hydrogenphosphate-stabilized Nickel(0) Nanoclusters As Catalyst, *Int. J. Hydrogen Energy*, **2007**, *32*, 1707-1715.

International Symposiums:

9. **Metin, Ö.**; Özkar, S.; Sun, S. Monodisperse Nickel Nanoparticles on SiO₂ as an Effective Catalyst in the hydrolysis of Ammonia Borane, *11st International Chemistry Conference and Exhibition in Africa (11 ICCA)*, November 20-23, 2010, Luxor, Egypt. (Oral Presentation)
8. **Metin, Ö.**; Mazumder, V.; Özkar, S.; Sun, S. Monodisperse Nickel Nanoparticles and Their Catalysis in Hydrolytic Dehydrogenation of Ammonia Borane, *1st*

International Conference on Materials for Energy, July 4-8, 2010, Karlsruhe, Germany. (Oral Presentation)

7. Metin, Ö.; Özkar, S. Water-soluble Poly(4-styrenesulfonic acid-co-maleic acid)-stabilized Nickel(0) and Cobalt(0) Nanoclusters as Highly Active Catalysts in Hydrogen Generation from the Hydrolysis of Ammonia borane, *Mater. Res. Soc. 2009 Fall Meeting*, November 30 - December 4, 2009, Boston, USA.

6. Ün, S.S.; **Metin, Ö.;** Özkar, S. Water-soluble Poly(4-styrenesulfonic acid-co-maleic acid)-stabilized Ruthenium(0) and Palladium(0) Nanoclusters as Highly Active Catalysts in Hydrogen Generation from the Hydrolysis of Ammonia borane, *13th European Conference on Applications of Surface and Interface Analysis (ECASIA-09)*, October 18-23, 2009, Antalya/TURKEY.

5. Ünel, E.; **Metin, Ö.;** Özkar, S. Synthesis and Characterization of Water-Soluble Polymer-Stabilized Ruthenium(0) Nanoclusters as Catalyst in Hydrogen Generation from the Hydrolysis of Sodium Borohydride, *13th European Conference on Applications of Surface and Interface Analysis (ECASIA-09)*, October 18-23, 2009, Antalya/TURKEY.

4. Erdogan, H.; **Metin, Ö.;** Özkar, S.; Hydrogen Generation from the Methanolysis of Ammonia Borane Catalyzed by In Situ Generated PVP Stabilized Palladium(0) Nanoclusters. *13th European Conference on Applications of Surface and Interface Analysis (ECASIA-09)*, October 18-23, 2009, Antalya/TURKEY.

3. Metin, Ö.; Özkar, S. Synthesis and Characterization Of Poly(N-Vinyl-2-pyrrolidone)-Stabilized Water-Soluble Nickel(0) Nanoclusters as Catalyst for The Hydrolysis of Sodium Borohydride, *10th Young Chemist Conference on Chemistry*, March 27-29, 2008, Rostock/Germany.

2. Metin, Ö.; Özkar, S. Hydrogen Generation From The Hydrolysis Of Sodium Borohydride By Using Nickel(0) Nanoclusters as Catalyst, *3rd International Boron Symposium*, November 02-04, 2006, Ankara/TURKEY (Oral Presentation)

1. Metin, Ö.; Özkar, S. Synthesis and Characterization of Water-Dispersible Nickel(0) Nanoclusters As Catalyst For The Hydrolysis Of Sodium Borohydride, *International Workshop on Nanostructured Materials (NANOMAT)*, June 21-23, 2006, Antalya/TURKEY

National Symposiums:

6. Durap, F., **Metin, Ö.**, Aydemir, M., Özkar, S. Polimer ile Kararlılaştırılmış Paladyum(0) Nanokümelere: Sentezi, Tanımlanması ve Sulu Ortam Suzuki Tepkimelerinde Olağanüstü Katalitik Etkinliği, 24. Ulusal Kimya Kongresi, 28 Haziran-02 Temmuz 2010, Zonguldak. (Sözlü sunum)
5. **Metin, Ö.**; Sun, S.; Özkar, S. Tekdüze Parçacık Boyutuna Sahip Nikel(0) Nanokümelere: Hazırlanması, Tanımlanması ve Amonyak Boranın Hidrolizinde Katalitik Etkinliği, 24. Ulusal Kimya Kongresi, 28 Haziran-02 Temmuz 2010, Zonguldak. (Sözlü sunum)
4. Durap, F., **Metin, Ö.**, Aydemir, M., Özkar, S. Polimer ile Kararlılaştırılmış Paladyum(0) Nanokümelere: Hazırlanması, Tanımlanması, Heck ve Suzuki Reaksiyonlarındaki Katalitik Etkinliği, 23. Ulusal Kimya Kongresi, 16-20 Haziran 2009, Sivas. (Poster Sunum- En iyi poster ödülü)
3. **Metin, Ö.**; Özkar, S. Polimer ile Kararlılaştırılmış Suda-Çözünür Nikel(0) Nanokümelere: Hazırlanması, Tanımlanması ve Amonyak-Boranın Hidrolizinde Katalitik Etkinliği. II. Ulusal Anorganik Kimya Kongresi, 16-19 Mayıs, 2009, Elazığ (Sözlü Sunum)
2. **Metin Ö.**, Özkar S, Nikel(0) Nanokümelereinin Eldesinde Metal Tuzu Olarak Nikel(II) Asetilasetonatın Sodyum Borhidrür İle İndirgenmesinin Kinetiği, I. Ulusal Anorganik Kimya Günleri, 20-23 Nisan, 2007, Balcalı/ADANA, (Poster Sunum)
1. **Metin Ö.**, Özkar S, Suda Çözünür Nikel(0) Nanokümelereinin Sentezi, Tanımlanması Ve Katalitik Etkinliği, XIX. Ulusal Kimya Kongresi, 2005, Kuşadası/İZMİR, (Poster Sunum)